D2.6

ACCURATE MEASUREMENTS OF THE THERMAL CONDUCTIVITY OF LIQUIDS

A thesis submitted to the University of London
for the degree of Doctor of Philosophy

by

JULIAN MENASHE
B.Sc.(Eng), A C G I

Department of Chemical Engineering and Chemical Technology
Imperial College of Science and Technology
London SW7

November 1980

A B S T R A C T

The thesis describes the design, construction, and use of an apparatus of the transient hot wire type which enables the accurate measurement of the thermal conductivity of liquids. The design of the instrument has been such as to permit operation over the pressure range 0.1 to 700 MPa and the temperature range 300 to 500K. When operating within this range, the precision of the thermal conductivity measurements thus obtained is estimated to be one of $\pm$ 0.2%.

Because most liquids absorb and reemit electromagnetic radiation, the effect of radiative heat transfer through a participating medium, during measurement on a transient hot wire apparatus, has been investigated. As a result, a method of correcting for the systematic effects of radiative heat transfer has been found, so improving the absolute accuracy obtainable for thermal conductivity measurements on a liquid.

Experimental data are reported for the thermal conductivity of n-Heptane, n-Nonane, and n-Undecane, in the temperature range 308.15K to 363.15K and the pressure range 50 to 500 MPa. The accuracy of these measurements is slightly worse than their precision due to the uncertainty in the optical properties of the liquids at elevated pressures. As a result of this uncertainty, only approximate corrections for the effect of radiative heat transfer could be applied to the results and their accuracy is therefore estimated to be between $\pm$ 0.5% and $\pm$ 0.8% depending, primarily, upon the absolute temperature at which a measurement was performed.

From investigation of these thermal conductivity data a method has been found and tested for extrapolating the liquid thermal conductivity data of an odd numbered n-Alkane. This enables the prediction of thermal conductivities outside the range for which measurements are available.

ACKNOWLEDGEMENTS

The Author wishes to express his sincere gratitude to Dr. W.A. Wakeham for his excellent counsel and guidance during the course of this work. His proffered advice on many aspects of the production of this thesis has also been invaluable. The Author also wishes to extend his appreciation to Dr. M.J. Assael for his suggestions, constant encouragement, and companionship. Special thanks are also due to Mr. A. Lucas for his help in designing, manufacturing, and maintaining the mechanical components of the measuring apparatus and to Mr. M.J. Dix and Mr. R. Wood for their design of, and help with, the electronic components. Thanks are also due to Dr. H.J. Michels, Dr. K.E. Bett, and Mr. I. Drummond for the loan of auxiliary equipment and to Mr. V. Vesovic for his assistance about the laboratory.

Finally, the Author wishes to thank his parents for their encouragement and financial support without which this work would not have been possible. The Author also extends extra special gratitude to his wife for her patience, support and also for the effort required in typing this thesis.

C O N T E N T S

INTRODUCTION

A critical survey of the results of measurements of the thermal conductivity of liquids by Jamieson et al [122] revealed the scarcity of reliable experimental data. It was estimated that even the results obtained from the most precise and carefully executed measurements, of which there are very few, had, at best, an uncertainty of ± 2%, and that most data on liquid thermal conductivities were probably burdened with an uncertainty of at least ± 5% and in certain cases a great deal more. Furthermore, the thermodynamic range covered by the experimental data was small and generally restricted to temperatures near ambient and pressures near the saturation vapour pressure. During the past decade, development of the transient hot wire technique for thermal conductivity measurement [56,57,58,68] has made possible the determination of the thermal conductivity of gases to an accuracy of ± 0.2% [41], while the recent application of the technique to the measurement of liquid phase thermal conductivities at the saturation vapour pressure and over a modest temperature range was reported by Castro et al [123,124] . The accuracy of the preliminary thermal conductivity data as reported by Castro et al was estimated to be one of ± 0.6% but this estimate has since been revised.

The principal advantages of the transient hot wire technique of measuring the thermal conductivity of a fluid are two-fold. Firstly, it provides an absolute method of measuring the thermal conductivity and secondly, the measurements obtained are devoid of the effects of convective heat transfer which are thought to be present in most of the alternative methods of measuring fluid thermal conductivities. Moreover, when performing measurements on fluids which are not transparent to electromagnetic radiation the technique has an additional advantage in that the effects of radiative heat transfer are smaller than they are for steady state methods [71,72,73] .

The objective of the work undertaken for this thesis has been to develop the apparatus, and where necessary, the theory of the transient hot wire technique, so as to enable the accurate measurement of liquid thermal conductivities at pressures elevated above atmospheric and over a moderate temperature range above ambient. The work is required to enable the gathering of accurate liquid thermal conductivity data. It is envisaged that the data thus obtained will be used both to examine liquid phase thermal conductivity theories, which have been developed and will be developed in the future, and also for the direct application in predicting thermal conductivities of pure liquids and mixtures of liquids at thermodynamic states for which measurements are unavailable.

CHAPTER 1

Review of Experimental Methods of Thermal Conductivity Measurement

1.1 Introduction

The Thermal Conductivity of an isotropic fluid is formally defined by the Fourier equation of conductive heat transfer:-

$$\vec{Q} = -\lambda \nabla T \qquad \text{.....(1.1)}$$

Where λ is the thermal conductivity, $\vec{Q}$ is the three-dimensional heat flux, and T the local fluid temperature. By convention λ is a positive quantity and as heat transfer through a medium occurs in the direction of decreasing temperature, this necessitates the -ve sign in equation (1.1).

Generally the transfer of heat through a fluid occurs by simultaneous conduction, convection and radiation. Conduction is the transmission of heat through a medium by intermolecular forces, vibrational or rotational field interaction, or random diffusion. Radiative heat transfer is the transfer of heat energy by the emission, absorption and scattering of electromagnetic radiation. Finally, convective heat transfer occurs by the bulk transfer of elements of a fluid due to velocity fields within the fluid medium.

If the thermal conductivity of a fluid is to be obtained experimentally, because the three mechanisms of heat transfer within a fluid are inseparable, the measurements must be performed on apparatus which either compensates for, or renders negligible the effects due to radiative and convective heat transfer.

This chapter briefly, as an introduction to the subject, is a resumé of the important methods of thermal conductivity measurement and illustrates the process by which the transient hot-wire technique evolved. The review will be confined to direct methods of thermal conductivity measurement, as opposed to indirect measurements, whereby the thermal conductivity can be determined

from quantities like for instance the thermal diffusivity or Prandtl number. This is both in the interest of brevity and also because, as in the example of thermal diffusivity, the properties involved with the thermal conductivity in the measured quantity, (specific heat capacity and density in the case of thermal diffusivity) are for most fluids at most thermodynamic states unknown to the degree of accuracy required. The latter reason being even more relevant in regard to liquid thermal conductivity measurements.

In this chapter the discussion is kept to the general case of fluid thermal conductivity measurement, rather than restricting it to the liquid case. This is for the sake of completeness as the principles of the methods are essentially the same whether it is a gas or liquid upon which the experiments are to be performed.

The methods of fluid thermal conductivity measurement generally fall into two different catagories which reveal their different approaches, namely steady state, or stationary methods and time dependent or transient methods. The stationary methods can be subdivided into three subsections based on the geometry of the apparatus used namely parallel plate (planar geometry) methods, concentric cylinders (cylindrical geometry) methods, and concentric spheres (spherical geometry) methods. Under the transient measurement catagory the only method requiring serious consideration is the transient hot wire technique although other methods have been attempted with varying degrees of success.

1.2 Steady State Methods

The principles involved in the steady state measurement of fluid thermal conductivity are in essence relatively simple. It is possible to solve equation (1.1) in either plane, cylindrical polar or spherical polar, coordinate systems subject to simple boundary conditions. If the fluid under investigation is placed in a vessel of known geometry, a constant heat flux is applied at the boundary of the fluid, and the system is left to attain

equilibrium, then a steady state temperature profile will be established within the fluid. The thermal conductivity can then be calculated, as a consequence of the solution of equation (1.1), knowing the heat flux, the temperature gradient in the fluid and the geometry of the vessel.

1.21 Parallel Plate Methods

The parallel plate method was the first method used for measuring the thermal conductivity of fluids, and was first used by Murry, Nicholson, Thomson & Rumford [1,2,3,4] . A vertical column of fluid was contained between two horizontal flat plates and to reduce the effects due to convection (convection was recognised as a major source of error even in the earliest methods) the heat flux was applied from above by heating the top plate. Following Biot's [5] formulation of a law of conduction, measurements of thermal conductivities were made by Depritz [6] , Paalzov [7] and others using similar techniques employing as a working equation the planar solution to (1.1):-

$$\lambda = \frac{Qd}{(T_1 - T_2)} \qquad \text{.....(1.2)}$$

where Q is the heat flux across the plates separated by a distance d, and $(T_1 - T_2)$ is the steady state temperature difference between the two plates.

The method was developed, to suppress convection and reduce heat losses to the sides, by using thin layer techniques [8,9] where the ratio of the horizontal extent of the fluid to its vertical extent was of the order of one hundred. Towards the end of the 19th century guard rings were first used [10] to ensure that all the heat passed vertically through the fluid layer and so eliminated heat losses to the sides of the apparatus. Christiansen [11], Hennenberg [12], Jäger [13] and others made measurements relative to air by using alternate layers of air and test fluid separated by horizontal plates to try and overcome

inherent errors, but the technique was better suited to absolute measurements [14].

Bates [15,16] argued in favour of increasing the fluid layer thickness due to the difficulty in measuring small plate separations to the required accuracy and reported on apparent temperature jumps at the liquid/copper plate interface of his apparatus. Similar arguments were put forward later by Sakiadis & Coates [17,18] who used a horizontal liquid layer contained between the flat, chromed and polished ends of two steel bars, six inches in diameter. The bars and liquid were surrounded by a glass tube and incorporated guard heaters. The driving force for heat transfer was applied by circulating water at the upper and lower ends of the bars.

The heat flowed through the liquid and then through a length of the steel bars in which thermocouples were evenly spread. The heat flux was calculated from the thermocouple readings and the conductivity of the steel. The resistance contribution, due to the steel and interfaces, was calculated with the bars in direct contact and subtracted from the overall resistance. The results obtained were four to five percent higher than those obtained from thin layer equipment using plate temperatures. This method has not been generally adopted by later workers.

Probably the best parallel plate method apparatus was that described by Michels and Botzen [19] and later improved by Michels, Sengers and Van der Gulik [20] which used the guarded thin layer technique and provided measurements of thermal conductivities of gases up to 300 MPa. A diagram of the apparatus is shown, see fig. (1.1). The apparatus consists of an upper, Ⓤ, and a lower, Ⓛ, plate both made out of copper enclosing platinum wires which were used both as heaters and as resistance thermometers. The upper plate Ⓤ is enveloped by a guard ring, Ⓖ, which contains a similar heating, temperature measuring platinum wire, separated from each other by 1.4 mm glass spacers and screwed together by

insulated copper screws. This assembly was finally covered by an insulating cap (I). The upper surface consisting of plate (U) and guard ring (G) and the lower surface, consisting of lower plate, (L), between which the test gas resided, were machined flat to within a micron. The plates were then separated by a set of three glass washers which were either one, one and a half, or two and a half millimeters in thickness depending on the test fluid thickness required.

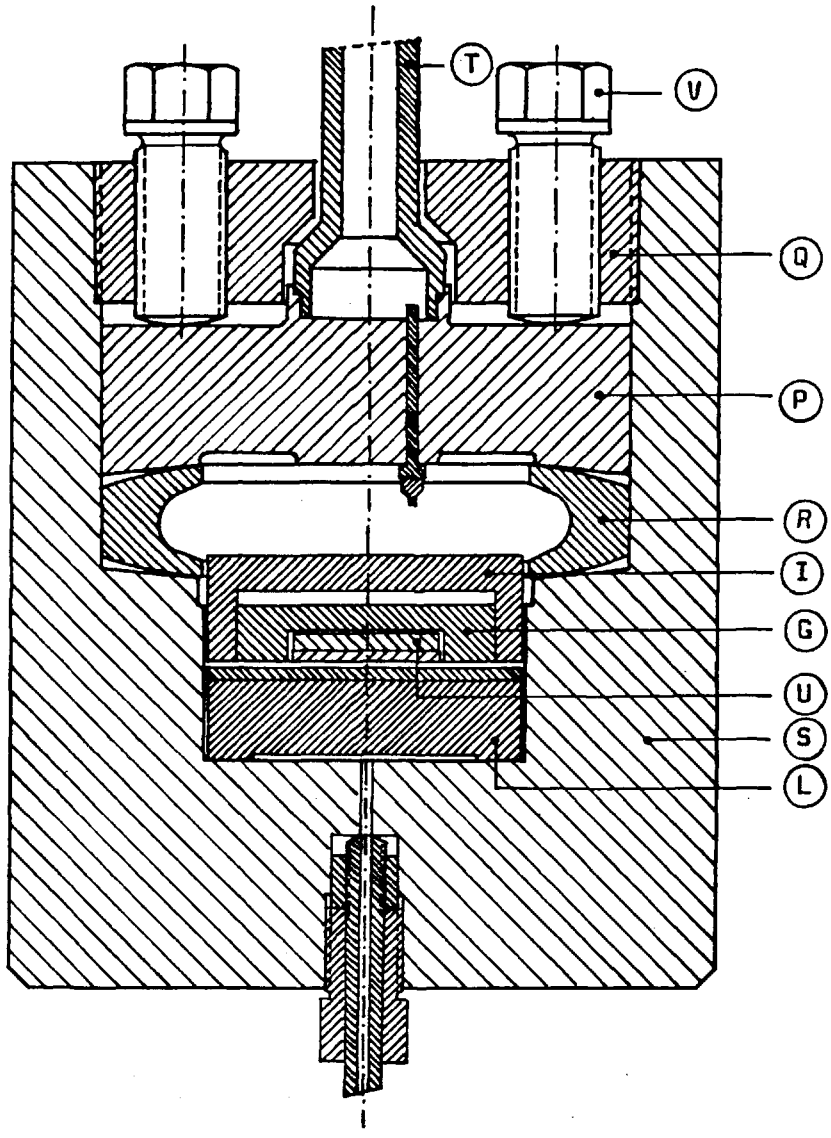

Fig. (1.1) Apparatus used by Michels & Botzen.

The washers were polished to be equal to each other's thickness within one micron and through them passed an insulated guide rod. The two halves of the cell were bolted together using insulated copper bolts. The cell was then hung from the lid (P) of the high pressure reservoir by three telescopic studs which ensured the cell rested properly on the bottom of the pressure vessel. The vessel was sealed using the lens ring (R), the thrust ring (Q) and eight bolts (V). Twelve pressure tight insulated terminals were located in the lid through which electrical contact was made between the cell and the measuring equipment. The accuracy of the measurements made on this apparatus was estimated as $\pm$ 1%.

Fritz & Poltz [21] used a similar apparatus to measure fluid thermal conductivities and to determine the dependence of the contribution of convection and radiation to the total heat transfer upon plate separation.

1.22 Concentric Cylinders Methods

The principle of the concentric cylinders method is similar to that of the flat plate methods. Consider a test fluid contained between two concentric cylinders with heat being supplied to one of them (the emitter) at a constant rate while the other is kept at a constant temperature. Assume the system has been left to attain a thermal equilibrium and the heat dissipation to the fluid per unit length of the emitter as well as the dimensions of the cylinders are known. If the temperature difference across the fluid can be measured, and provided effects due to convection and radiation were eliminated or rendered negligible, then the thermal conductivity of the fluid can be calculated by solving equation (1.1) for a cylindrical geometry, subject to the appropriate boundary condition. From the solution one obtains:-

$$\lambda = \frac{q}{2\pi(T_1 - T_2)} \operatorname{Ln}\left[\frac{r_2}{r_1}\right] \qquad \text{.....(1.3)}$$

where q is the heat dissipation to the fluid per unit length of emitter, r_1 & r_2 are the radii of the emitter and receiver respectively and $(T_1 - T_2)$ is the temperature difference across the fluid. The system just described provides the basis for the concentric cylinders methods.

The method was first used by Bridgman [22] as an alternative to the parallel plate instruments which were elaborate and required the use of guard rings which made them cumbersome and bulky. The apparatus used by Bridgman to investigate the effect of pressure on liquid thermal conductivity, consisted of two concentric cylinders $1\frac{1}{4}$ ins in height held together by german-silver end rings. The external diameter of the inner cylinder was $^3/_8$ ins, the internal diameter of the outer cylinder was $^{13}/_{32}$ ins and the $^1/_{64}$ ins thick annulus between the two cylinders contained the test fluid.

Although Bridgman realised that a driving force for convection would always be present in his apparatus, he believed that by using a small temperature difference across the liquid, the viscous forces in the relatively thin liquid layer would suppress, or render negligible, the effect. The results obtained from this apparatus are considered to be high [23] which is largely due to inadequate compensation for conduction through the connecting rings holding the two cylinders apart.

The apparatus was significantly improved upon by Schmidt & Sellschop [24] who completely surrounded the central cylindrical emitter with fluid and used quartz spacers to position the outer cylinder. A geometric constant was obtained from the electrical capacitance of the cell and a correction was applied for the existance of ends to the cylinders.

Inevitably, as in the evolution of parallel plate methods, guard heaters were used on the emitters to eliminate end effects [25] . These were separately heated cylindrical sections added to the ends of the emitters and were controlled to ensure that the temperatures

of the emitter and guard heaters were the same.

At about the same time Kraussold [26] and Schmidt & Milverton [27] produced correlations of convective heat transfer as a function of the Rayleigh number. It is on this work that subsequent workers relied to determine the maximum thicknesses of fluid layers allowable in their apparati before the debilitating effects of natural convection became significant.

Ziebland, Burton & Needham [28,29,30,31] have performed measurements on a number of fluids in the temperature range 100 - 700K and at pressures up to 50 MPa with essentially the same apparatus. A diagram of the thermal conductivity cell and autoclave used by Ziebland & Burton [30] for the measurement of the thermal conductivity of heavy water is shown in fig. (1.2).

The emitter cylinder ① and the two guard heaters ② and ③, made of a high conductivity copper alloy, were mounted on a stainless steel sheath ④ and heated by independently controlled constantan wire heaters ⑤ on a glass former ⑥. The guard heaters were separated from the emitter cylinder by 1 mm thick mica washers ⑦ and ⑧, and the emitter cylinder and guard heaters were arranged coaxially within an outer receiving cylinder ⑨, using mica leaves, held in place by grub-screws, so forming an annulus 0.2 mm in width. Stainless steel sheathed thermocouples were placed in holes drilled through the emitting and receiving cylinders, and the whole conductivity cell was placed within a Monel autoclave ⑩. To reduce convection, the free space was filled with fired pyrophillite and the autoclave was filled with liquid through the connection in the lid ⑫.

The autoclave was placed in a heavy gauge steel tube ⑬ which carried on its external surface an electric heater. This heater in conjunction with a controller, which used the platinum resistance thermometer ⑪ within the wall of the pressure vessel as a sensing element, regulated the temperature of the system.

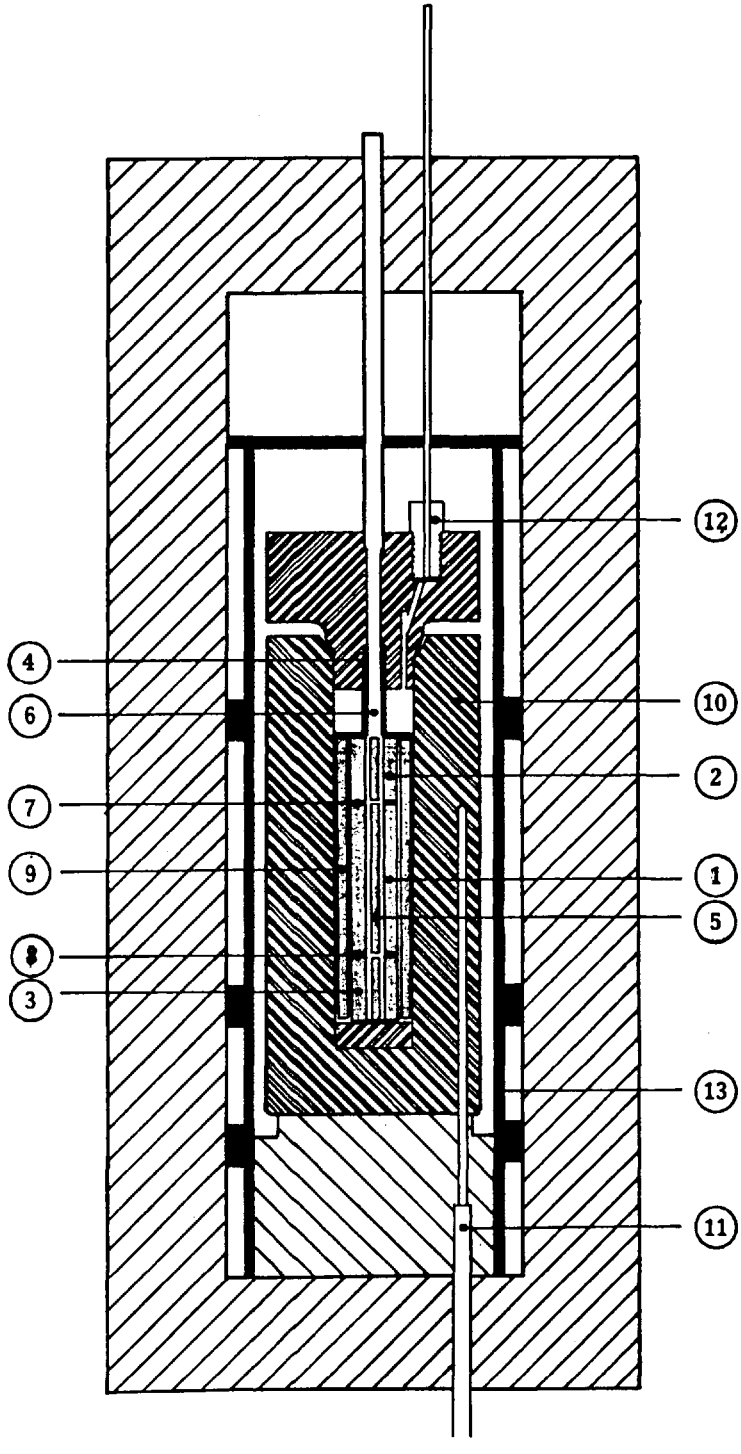

Fig. (1.2) Cell and Autoclave used by Ziebland & Burton.

Aluminium powder was used to fill the space between the heating tube and the autoclave, thus ensuring good thermal contact whilst providing for the differential thermal expansion. Additional heaters were fitted to the top and bottom of the heating tube to compensate for end losses.

The effect of radiation was treated by ignoring absorption and measuring transfer through the evacuated cell. Convective effects were presumed to be negligible if the Rayleigh number was kept below 1000 and additional checks were made by using different emitter powers. The accuracy of the reported data for liquids and dense gases was estimated as $\pm$ 1.5% and for low pressure gas and in the critical region as $\pm$ 2%.

A major advancement in the concentric cylinders method was the introduction of an electrically heated wire as the emitter. This innovation is acredited to Schliermacher [32] who attempted to avoid end effects by using potential leads to measure the power dissipation and average temperature over the central section of the wire. The wire is used simultaneously as the central cylinder (emitter) in the concentric cylinders method and as a resistance thermometer.

Measurements on dilute gases to a stated accuracy of 0.5% were performed by Taylor & Johnston [33] on a piece of apparatus incorporating a 0.025 cm diameter platinum hot wire tensioned by an 18 gm weight. Effects due to temperature jumps; axial heat flow in the hot wire and potential leads; geometrical constants; and radiation were calculated. Temperature differences of up to 26K were used and it was claimed that convective effects were negligible due to the low pressures used.

Another major advancement is acredited to Goldschmidt [34] who proposed the use of two wires one long and one short, their resistances being compared in a Wheatstone Bridge. The difference

in resistance should then be equivalent to that of a finite segment, whose length is equal to the difference in lengths of the long and short wires, of an infinitely long wire. An analysis of the problem of how much the middle section of a hot wire differs from a segment from an infinite wire was later given by Blackwell [35] and more recently alternative analyses were given by Haarman [68] and Healy et al [57], results of which are used in §2.334 of this work.

1.23 Concentric Spheres Method

Consider a test fluid contained between two concentric spheres with heat being applied to the emitter (inner) sphere at a constant rate while the outer (receiving) cylinder is held at a constant temperature. Assume the system has reached thermal equilibrium and the temperature drop across the fluid, as well as the power dissipated into the fluid by the emitter and also the dimensions of the spheres are known. By solving equation (1.1) for a spherical geometry subject to the constant boundary condition; and provided effects due to convection and radiation can be ignored; then the thermal conductivity of the fluid is calculated as:-

$$\lambda = \frac{q(r_2-r_1)}{4\pi(T_1-T_2)r_1r_2} \qquad \text{.....(1.4)}$$

where q is the power dissipated by the emitter to the fluid, r_2 and r_1 are the radii of the emitter and receiver spheres and $(T_1 - T_2)$ is the temperature drop across the fluid. The system just described forms the basis of the Concentric Spheres Method for thermal conductivity measurement with equation (1.4) as its working equation.

The method was used in order to avoid edge effects which occur in parallel plate and concentric cylinder based designs. Reidel [36]

constructed a cell consisting of a spherical copper emitter, 28 mm in diameter, containing a heater and a resistance thermometer, supported within a spherical receiver containing another resistance thermometer. Careful alignment was necessary in order to ensure the spheres were concentric. The results obtained using this apparatus agreed to within 1% of his measurements using parallel plate and concentric cylinder cells.

Schrock & Starkman [37] used a similar cell, to that used by Riedel, on measurements of hydrocarbons and water from 200 - 300K. They attempted to demonstrate the absence of convection by showing the linearity of a plot of the emitter power versus the temperature drop across the test layer. Accuracy was claimed to be $\pm$ 1.7% and results on water agreed to within 0.3% of those measured by Riedel.

Richter & Sage [38] using a concentric spheres apparatus for measurements on methane and nitrogen with temperature drops in the range of 2 to 4K, found the measured thermal conductivity to be dependent on heat input to the emitter, even when the Rayleigh number was below 1000. They also observed an uneven temperature distribution over the surface of the emitter believed to be due to convective currents in the fluid.

1.24 Inadequacies of Stationary Methods

The biggest error incurred in using stationary methods for the measurement of the thermal conductivity of fluids is believed to be due to convection currents. These currents are caused by the steady temperature differences required by the methods and by non-uniformities in the emitter. Convection currents when set up within the apparatus during a measurement provide another mechanism for heat transfer through the fluid, other than by pure conduction and so introduce errors in thermal conductivity measurements. In order to minimise the errors incurred due to convection, smaller thicknesses of fluid layers have been employed in steady state equipment

in an attempt to dampen convective currents. As a result of this the errors incurred in measuring the thicknesses of the fluid layers, used in steady state apparati, have become more significant as has the uniformity of the boundary surfaces.

The other main source of error occurs due to the radiative contribution to the heat transferred through the fluid during measurement. Unfortunately surface emissivities and absorbtivities are not accurately known and, for some fluids, their extinction coefficients, over most of their thermodynamic states, can only be estimated to approximate orders of magnitudes and, in the majority of cases, can be in error by more than 25%. This means that, even if it were possible to exactly solve the mathematical model for radiative heat transfer through the measuring apparatus, the effect due to radiation, if significant, would still not be accurately accounted for. However, non-steady state methods are, owing to approximate analyses, believed to be subject to smaller inherent errors, brought about by radiative heat transfer. Another inadequacy of steady state methods is that they often use measurements of heat losses in evacuated cells to determine emissivities and absorbtivities of the materials used in the cells. But, especially when the refractive index of the test fluid is significantly different from unity, these measurements often give erroneous results. [39]

From the kinetic theory of gases, a relationship between the thermal conductivity and viscosity of monatomic gases was obtained thus enabling the examination of the accuracy of thermal conductivity measurements using viscosity data. [40] The relationship obtained for monatomic gases involved the Eucken factor:-

$$Eu = \frac{\lambda^{\circ}(T)\, M}{C_v \mu^{\circ}(T)\, F(T)} = 2.5000 \qquad \text{.....(1.5)}$$

where $\lambda^{\circ}(T)$, $\mu^{\circ}(T)$, are the thermal conductivity and viscosity of

the gas at temperature T, extrapolated to their hypothetical values at vanishingly small density, (zero density) respectively; C_v is the molar heat capacity of the monatomic gas at constant volume; M is the molecular weight of the gas; and F(T) is a factor close to unity which can be calculated by evaluating corrections to the Chapman-Enskog expressions used to derive (1.5). The method for calculating these corrections to any required order has been detailed by Assael. [41]

The inability of steady state method based equipment to produce data which satisfy equation (1.5) to the expected accuracy, corresponding to that estimated for the absolute thermal conductivities as measured on these apparati, has led to the belief that inherent errors exist even in the most sophisticated and carefully used steady state equipment. These errors, which limit the accuracy of the method, are believed to be due to convection, radiation, and perhaps other errors as yet unaccounted for. An error in the latter context may be due, for instance, to the experimental arrangement being too far removed from the theoretical treatment.

As a result, emphasis has been placed on transient techniques which, as in the case of the transient hot wire technique based equipment have been able to produce data satisfying equation (1.5) to the expected accuracy [42] and do not seem to have the same limitations.

1.3 Transient Methods

Transient methods for the measurement of thermal conductivity were developed to overcome the inadequacies in steady state methods primarily due to convection. They were also thought to reduce errors due to radiation effects which, on the basis of approximate analyses or arguments (as a rigorous treatment, of the type given in chapter 3, had not as yet been possible) were thought to be larger for measurements performed on steady state equipment.

They are derived from:-

$$\frac{DT}{Dt} = k \nabla^2 T \qquad \text{.....(1.6)}$$

which mathematically describes the transient conductive and convective flow of heat through an isotropic medium whose physical properties are independent of time or temperature. The essence of transient methods is that it is found that under certain conditions the convective terms contained in the substantial derivative in equation (1.6) can be neglected resulting in:-

$$\frac{\partial T}{\partial t} = k \nabla^2 T \qquad \text{.....(1.7)}$$

and it is upon the solution of (1.7) that the transient methods have been based.

1.31 Transient Hot Wire Technique

The method is based on the solution of equation (1.7) in cylindrical geometry for the initiation of a constant heat flux, supplied at time t=0, to an infinitely long line heat source, in a fluid of infinite extent, initially at constant temperature. The solution is of the form [43] :-

$$\Delta T\,(r,t) = \frac{q}{4\pi\lambda} \operatorname{Ln}\left[\frac{4kt}{r^2 C}\right] \qquad \text{.....(1.8)}$$

subject to $$\frac{a^2}{4k} \ll t \qquad \text{.....(1.9)}$$

where; $\Delta T(r,t)$ is the local temperature rise of the fluid at time t, and at radial position r; q is the heat emitted to the fluid per unit length of the line heat source; k is the thermal diffusivity of the fluid and C is the exponent of Euler's Constant.

In the transient hot wire technique, a thin electrically heated platinum wire takes the place of the line heat source and the resistance, corresponding to the wire's temperature rise, as a function of time, is measured and recorded following the instantaneous initiation of the heat flux. The thermal conductivity of the fluid is then obtained, as a consequence of equation (1.8) from the gradient of the measured temperature rise of the fluid at radial position a (the surface of the wire) versus the logarithm of time since the initiation of the heat flux in the wire.

The technique was first used by Stalhane & Pyk [44] to measure the thermal conductivity of powders. Stalhane & Pyk empirically obtained the relationship for the temperature rise of a fine straight wire subjected to a step change in the heat input to the wire. They found that, after a short interval proceding the initiation of the step change, the following relationship could be used to describe the system:-

$$\Delta T = A \frac{q}{\lambda} \text{Ln} \left[\frac{a^2}{t} + B \right] \qquad \text{.....(1.10)}$$

The constants were found using fluids of "known" conductivity.

The mathematical derivation of equation (1.8) was later formulated by Van der Held and Pfriem [45] developed the technique to obtain absolute values of the thermal conductivity. Weishaupt [46] used a 10 cm, 70 μm diameter gold wire in one arm of a Wheatstone Bridge and photographed the spot from a galvanometer to record the bridge's imbalance as a function of time. The onset of convection was discussed in terms of modified Grashof numbers. Consideration was given to the errors due to the finite heat capacity and dimensions of the wire as well as to those errors incurred because of axial conduction at the wire ends.

The effects of the fluid not being infinite in extent, and the wire's temperature rise not being constant across its diameter were also considered. The apparatus unfortunately had no potential leads and large end effects were inevitably present.

Van der Held & Van Drunen [47] in order to attempt to eliminate effects due to 3-dimensional heat flow at the ends of the wire, and to reduce the variation in the power dissipation from the hot wire, used a copper/constantan thermocouple at the centre of a manganin wire heater. The thermocouple and manganin wire were enclosed in a thin glass tube to insulate the mangainin wire from the test fluid. This was claimed to prevent problems due to the bare wire being in electrical contact with the fluid, also the intention was to develop an apparatus capable of enabling measurements to be performed on all fluids including acids. The temperature rise during a measurement, typically 5 seconds in duration, was recorded by connecting the thermocouple output leads to a Mollgalvanometer and photographing the movement of the light spot. It was later shown [48] that the effect of the heat capacity of the heater and thermocouple enclosed in the glass tube was not negligible as thought.

Gillam, Romben, Nisson & Lamm [49] used a bare 0.1 mm diameter platinum wire with two potential leads 10 cm apart in an out of balance Kelvin Bridge to measure fluid thermal conductivities and derived a correction to account for the change in power during a measurement. This change in power was caused by the variation in resistance of the platinum wire.

An interesting variation of the transient hot wire technique was described by Hill [50] who developed a method using a thermocouple formed from wire alloys, having the same resistivity. The thermocouple was then drawn to a uniform diameter and heated by radio frequency alternating current. Unfortunately, the accuracy was low, $\pm$ 10%.

Turnbull [51] made absolute measurements on molten salts using an apparatus in which a single platinum wire was divided into a long and short section by a single potential lead, the two sections were then connected into opposite arms of a Wheatstone Bridge. This had the effect of "subtracting" the ends from the long section and so one was essentially performing the experiment for the middle portion of the long section, thus eliminating end effects. The imbalance of the bridge was recorded using a chart recorder to which corrections for recorder response times and current variations were applied, the accuracy of the results was believed to be $\pm$ 3%.

Horrocks & McLoughlin [52] developed the transient hot wire technique further and describe an apparatus they used to measure the thermal conductivity of liquid benzene, toluene, diphenyl and terphenyl to examine the relationship between the thermal conductivity and the coefficient of thermal expansion. The apparatus consisted of a platinum wire, 25 μm in diameter, used as a four terminal resistance thermometer in order to correct for end effects caused by the wire not being infinite in length. Times of up to 30 seconds were used and accuracies of $\pm$ 0.25% were quoted although this is generally considered to be an overestimate of the accuracy. Based on this work, Pittman [53] and Kandiyoti [54] designed instruments to measure the thermal conductivity of liquids and gases over large pressure and temperature ranges. Kandiyoti [54] measured the thermal conductivity of toluene up to 600 MPa using apparatus similar to that used by McLoughlin. The apparatus consisted of a 25 μm diameter platinum wire, used as a four terminal resistance thermometer as well as a heat source, held vertically within the test fluid. The offset voltage from a potentiometer (see fig. (1.3)) was recorded following the initiation of a current through the platinum wire. Times of between 20 and 30 seconds and accuracies of $\pm$ 5% were estimated over the pressure range.

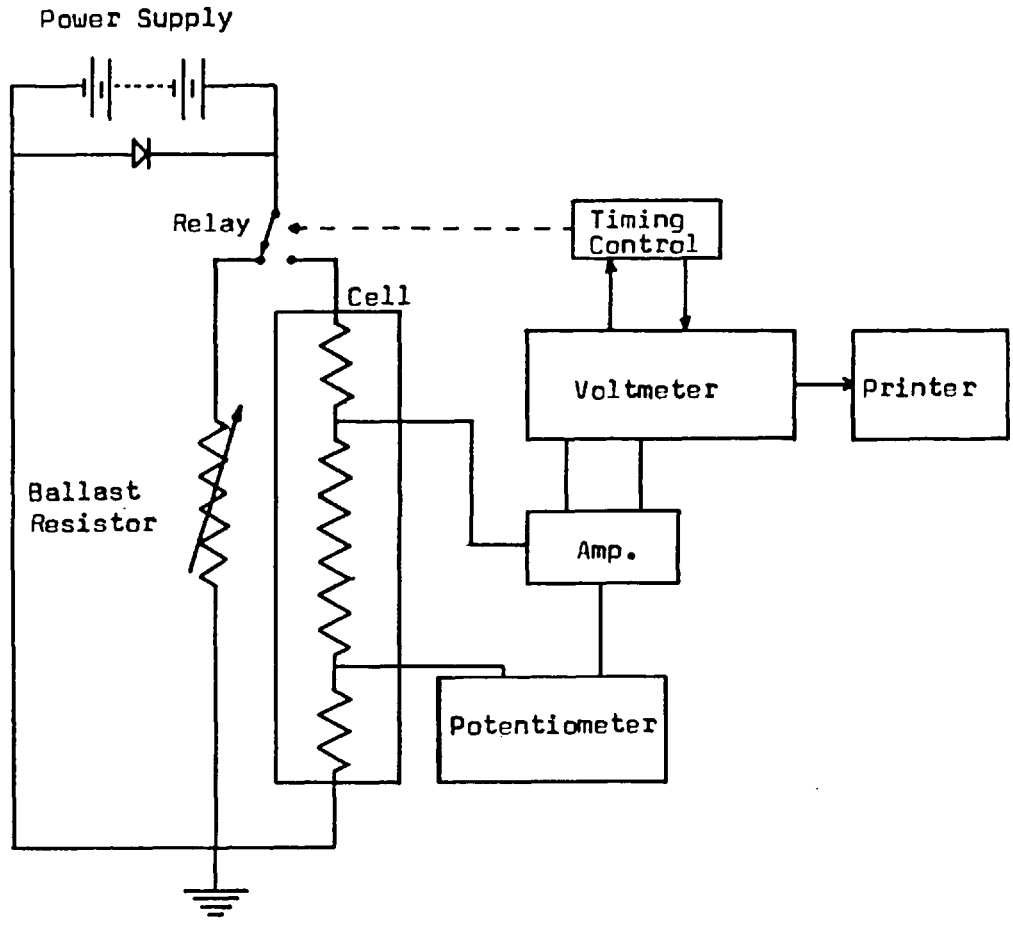

Fig. (1.3) Diagram of electrical circuit used by Kandiyoti.

A major advancement occured as a result of the work by Haarman [55] who first introduced the concept of and used an automatic bridge to measure resistances. Great improvements in the performance of the instrument were achieved using the newly available high speed electronic switches and counters. The times at which the resistance of the hot wire attained predetermined values were recorded instead of indirectly measuring the temperature rise of the wire with time. This new bridge made possible a ten-fold reduction in the duration of an experiment, enabling the complete elimination of effects due to convection and greatly reducing other time dependent errors (see § 2.3). In the last ten years, work by de Groot, Healy, Kestin & Wakeham [56,57,58] on the theory of

the method has recently enabled the measurement by Assael [42], and de Groot, Kestin & Sookiazian [56], of the thermal conductivity of a large number of gases and gas mixtures at 303K and up to 10 MPa to an accuracy of $\pm$ 0.2%.

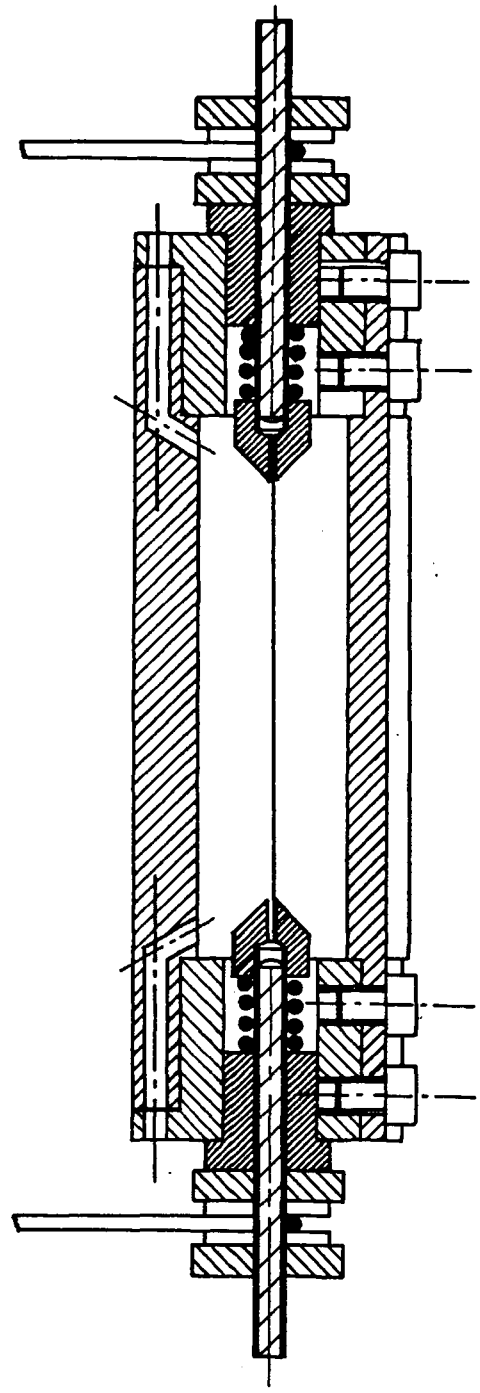

Fig. (1.4) Measurement cell used by Castro & Wakeham.

In the liquid phase the best available measurements using the technique are probably those by Castro & Wakeham [59]. In their apparatus an automatic bridge similar to that used in the present work (see § 4.41), was used to perform measurements on toluene and several n-alkanes over a temperature range 275K - 330K, at their saturated vapour pressure. Two 10 μm diameter wires were used as heat sources, and to eliminate end effects, (as explained in § 2.334) were mounted vertically and fixed between two terminals as shown in fig. (1.4). Times of up to 2 seconds were used for the duration of a measurement and relatively high temperature rises of up to 15K were obtained. The accuracy of the results obtained was estimated to be one of $\pm$ 0.5%.

1.32 Other Transient Methods

Although the most widely used transient method adopted has been that using the hot wire, in order to encompass the entire range of methods used for direct thermal conductivity measurement, it should be mentioned that other non steady state methods have been used.

Most of this work has been performed by Russian scientists such as Danilov [60] and Petruchov & Ragulin [61] who performed measurements on concentric spheres apparati and Golubev [62] on a cooling concentric cylinders apparatus.

CHAPTER 2

Theory of the Transient Hot Wire Technique

2.1 Introduction

In the transient hot wire method of measuring the thermal conductivity of a fluid, the temporal temperature rise of a thin platinum wire immersed in a test fluid, initially at thermal equilibrium, is observed following the application of a step voltage across the wire. The platinum wire acts as a heat source and produces a time dependent temperature field within the fluid. To a good approximation, the temperature rise of the wire, ΔT, can be expressed as:-

$$\Delta T(a,t) = -\frac{q}{4\pi\lambda} E_i\left(-\frac{a^2}{4kt}\right) \qquad \ldots\ldots\ldots\ldots\ldots(2.1)$$

or:-

$$\Delta T(a,t) = \frac{q}{4\pi\lambda} \mathrm{Ln}\left[\frac{4kt}{a^2 C}\right] \qquad \ldots\ldots\ldots\ldots\ldots(2.2)$$

Provided that:-

$$\frac{a^2}{4kt} \ll 1 \qquad \ldots\ldots\ldots\ldots\ldots(2.3)$$

In equations (2.1) and (2.2); q is the heat per unit length emitted from the wire; a is the diameter of the wire; k is the thermal diffusivity of the test fluid; λ is the thermal conductivity of the test fluid; t is the time lapse since the initial application of the step voltage across the wire and E_i is the exponential integral.

The wire, which is used simultaneously as a heat source and as a thermometer, forms part of an automatic bridge (described in § 4.41). The bridge is used to record the times at which the temperature rise of the wire attains several predetermined values.

Each time recorded corresponds to the occurrance of a bridge balance condition and therefore to the time at which the wire attains a preset resistance associated with a known temperature rise.

As implied by equation (2.2) the plot of the temperature rise of the wire, ΔT, versus the logarithm of the time lapse since the step voltage initiation, Lnt, would result in a straight line, the gradient of which is inversely proportional to the thermal conductivity. In practice, the physical model of the transient hot wire does not correspond exactly to the mathematical model used to derive equation (2.1). However the model is sufficiently close to it that, by applying corrections (detailed later in this chapter) to the observed temperature rise of the wire, the physical system can, within the required accuracy, be reduced to the mathematical model. What this in effect means is that provided the geometry of the hot wire cell as well as the physical properties of the fluid and platinum wire (other than the thermal conductivity of the fluid) are known then the thermal conductivity of the test fluid can be determined. This is done by correcting the observed temperature rise of the wire to its idealised temperature rise from which the thermal conductivity of the fluid can be calculated using:-

$$\lambda = \frac{q}{4\pi \left\{ \frac{\partial \Delta T_{id}}{\partial Lnt} \right\}} \qquad \text{.....(2.4)}$$

where ΔT_{id} is the idealised temperature rise as defined by equation (2.4).

The rest of the chapter details the mathematical model used and the corrections to the observed temperature rise of the wire required to enable the use of equation (2.4) for the measurement of the thermal conductivity of a fluid. The discussion of the corrections is kept to fluids in general, as most of the corrections

are independent of whether the fluid under consideration is gaseous or liquid, but where this is not so the corrections are treated separately and for completeness, both are included.

Most of the corrections detailed in § 2.3 are based on work which was available prior to the designing of the apparatus. The analyses used were originally developed for measurements on gases and where necessary they have been extended to include fluids in the liquid phase. The purpose of the correction analyses are two fold. Firstly, they provide, quantitatively, methods of correcting observed experimental quantities to those required for the determination of the thermal conductivity of a test fluid. Secondly, as the analyses are often approximate, and the corrections obtained are subject to their own errors, these corrections must therefore be kept small to minimise the error incurred in the absolute measurement of the thermal conductivity. The analyses are therefore used in the design of the apparatus, to ensure that these corrections and therefore the error in the thermal conductivities measured are kept to a minimum.

Unfortunately, the results of the work described in chapter 3 concerning the effect of radiative heat transfer on the thermal conductivity of a fluid, as measured on transient hot wire apparatii, were not available prior to the apparatus construction and therefore could not be used as a basis for its design.

2.2 The Idealised Mathematical Model

Consider a section of a hypothetical infinitely long line heat source (no ends) immersed in an isotropic fluid of infinite extent. Assume the density and heat capacity of the fluid are independent of temperature, also that heat transfer through the fluid can only occur by conduction and let the system be in thermal equilibrium at temperature T_o. A step function in the heat emitted by the line source to the fluid is applied at time t=0, resulting in a constant power per unit length of the line source being supplied after this time.

The system can be represented by the following mathematical model using equation (1.7) in a cylindrical polar coordinate system:-

$$\frac{\partial T}{\partial t} = \frac{k}{r}\frac{\partial}{\partial r}\left(r\frac{\partial T}{\partial r}\right) \qquad \text{.....(2.5)}$$

with initial condition:-

$$\Delta T\ (0 \leqslant r \leqslant \infty,\ t \leqslant 0) = 0 \qquad \text{.....(2.6)}$$

and boundary conditions:-

i) $$\lim_{r\to\infty} \Delta T(r,\ t \geqslant 0) = 0 \qquad \text{.....(2.7)}$$

ii) $$\lim_{r\to 0}\left[r\frac{\partial T}{\partial r}\right] = -\frac{q}{2\pi\lambda} = \text{constant},\ t \geqslant 0 \qquad \text{.....(2.8)}$$

where:-

$$\Delta T(r,t) = T(r,t) - T_0 \qquad \text{.....(2.9)}$$

The solution is [43]:-

$$\Delta T(r,t) = -\frac{q}{4\pi\lambda}\ E_i\left(-\frac{r^2}{4kt}\right) \qquad \text{.....(2.10)}$$

where $E_i(x) = \int_x^{\infty}\frac{e^{-x}}{x}\,dx = -\gamma - \ln x + x + O\{x^2\}$ .....(2.11)

and γ is Euler's constant (0.5772156649...).

At a distance r=a into the fluid (the position the surface of a wire would occupy were the line source replaced by a wire),

equation (2.10) yields equation (2.1) and therefore, subject to:-

$$t \gg \frac{a^2}{4k} \qquad \text{.....(2.12)}$$

$$\Delta T\,(a,t) = \frac{q}{4\pi\lambda}\ \mathrm{Ln}\left\{\frac{4kt}{a^2 C}\right\} + O\left\{\frac{a^2}{4kt}\right\} \qquad \text{.....(2.13)}$$

which by truncation yields the working equation:-

$$\Delta T_{id}\ (a,t) = \frac{q}{4\pi\lambda}\ \mathrm{Ln}\left\{\frac{4kt}{a^2 C}\right\} \qquad \text{.....(2.14)}$$

This is the model upon which the transient hot wire technique is based and all corrections due to the physical system and ideal system not being identical are applied to the observed temperature rises in the real physical system in order to obtain the hypothetical idealised temperature rises from which using equation (2.4) the thermal conductivity can be calculated.

2.3 Corrections

In this section the ways in which the real physical system deviates from the idealised mathematical model are examined in detail. The effects of these deviations are quantified and those contributing errors of less than 0.01% in ΔT_{id} are deemed negligible and ignored, while those constituting more than 0.01% in ΔT_{id} are examined to ascertain how mathematically an observed temperature rise ΔT can be corrected, for these effects, to the idealised temperature rise ΔT_{id} . It has been assumed that, because the required corrections to ideality are small, the combined effect can be taken to be additive.

Hence:- $$\Delta T_{id} = \Delta T + \sum_i \delta T_i \qquad \text{.....(2.15)}$$

where δT_i is a temperature correction due to the physical system in one aspect being non-ideal.

The discussion of the effects is presented under three subsections, namely for, those effects entirely eliminated, those effects which constitute a negligible correction in ΔT, and those effects for which a correction to ΔT is required.

2.31 Effects Entirely Eliminated

The major advantage of the transient hot wire technique is that effects due to convection, the major source of error in steady state methods for thermal conductivity measurements, can be entirely eliminated using this technique.

It is necessary to distinguish between two essentially different types of convection occurring in thermal conductivity measurement equipment. The first is due to gradients in the equipment even prior to measurement. This is caused by uneven temperature control of the apparatus whereby the volume of test fluid in a lower region of the apparatus is warmer and therefore less dense than that in an upper region, resulting in a velocity field within the fluid. This type of convection can and must be avoided by careful design of equipment and by setting up a small temperature gradient in the apparatus which opposes convection. This was implemented in the apparatus used by the indirect heating of the top of the pressure vessel containing the measurement cell (see § 4.23). This type of convection if present in the test fluid would exist whether or not a measurement was being performed and therefore whether or not heat was supplied to the emitter.

The other type of convection occurs due to the fluid being heated by the emitter and therefore occurs only during measurement. The mechanism is best explained by considering what happens in the case of the hot wire apparatus. Consider an infinitely long, perfectly straight wire immersed vertically in a fluid of infinite extent down which there is a small externally applied temperature gradient which opposes convection. This means that at any constant radial distance into the fluid the temperature of the fluid increases with increase in the vertical direction. Thus, the system is in a

stable state which would not support convection. Now let a constant heat flux be emitted from the wire surface into the fluid and, assuming there to be no convective heat transfer, consider the hypothetical steady state the system would attain.

The expected steady state temperature field in the fluid is shown in the pseudo-three dimensional (isometric) drawing fig.(2.1).

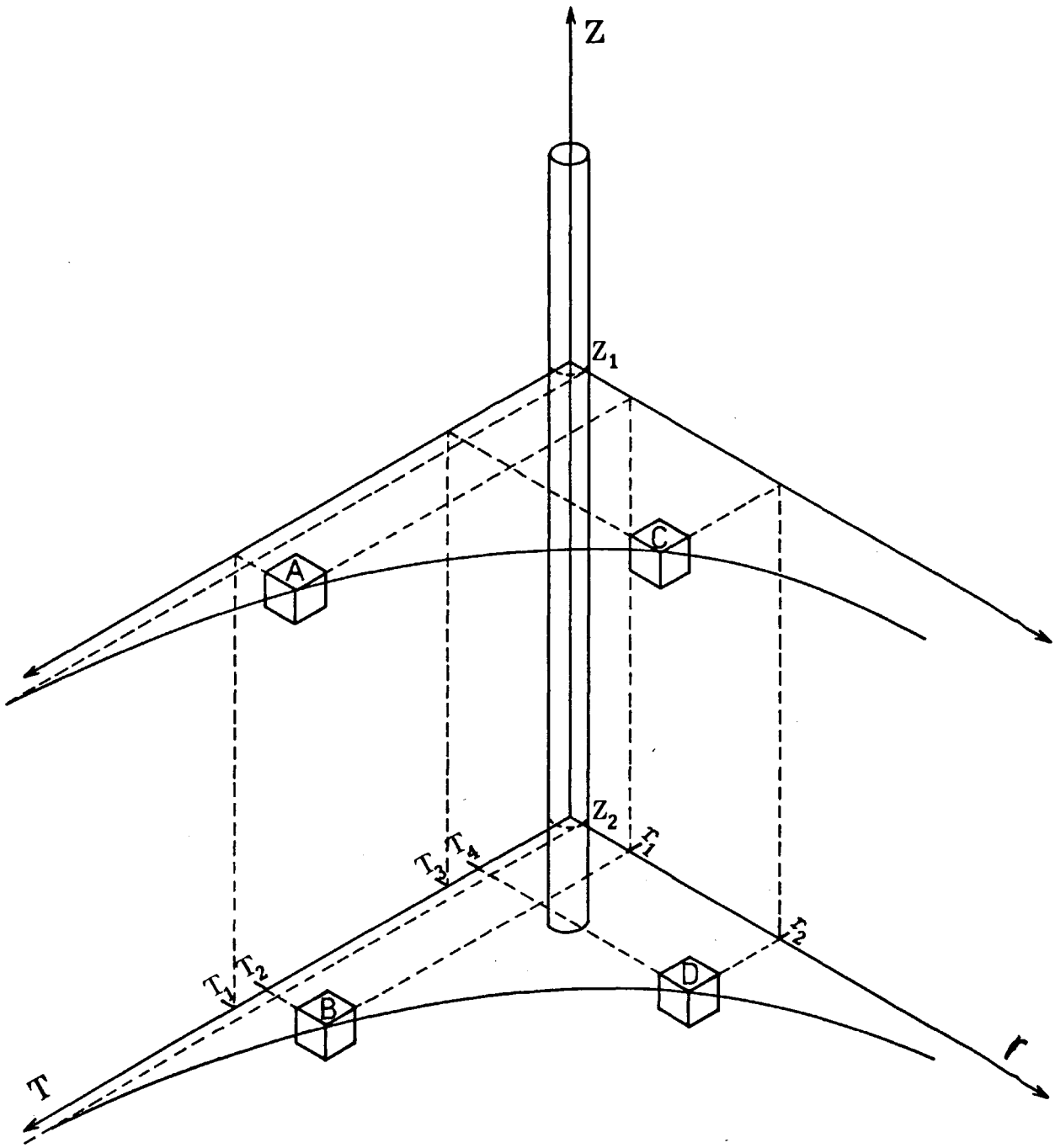

Fig.(2.1) Hypothetical steady state temperature field surrounding a hot wire.

Consider the local temperatures T_1 and T_2 of two elements of fluid, A and B, close to and at the same radial distance, r_1, from the wire, but at different vertical heights, z_1 and z_2, respectively. Temperature T_1 is greater than temperature T_2 and therefore there is no driving force for convection between elements A and B. The same can be said about elements C and D, two elements further away from the wire surface, at radial distance r_2, temperatures T_3 and T_4 and vertical heights z_1 and z_2 respectively. But the temperature T_2 of element B is greater than that, T_3, of element C and, because the vertical height, z_1, of element C is greater than that, z_2, of element B, there is a driving force for convection between elements B and C.

Initially, the argument made use of the assumption that there was no convective heat transfer. But, based on this assumption, as has just been proven, convection would occur and therefore the assumption of there being no convective heat transfer is false. This proves that there is always a driving force for convection in a hot wire or by the same argument concentric cylinder arrangement at steady state not withstanding claims to the contrary. It should be noted here that by moving the wire from the vertical, using similar arguments as detailed above, the situation is aggravated and the driving forces for convection become larger.

Consider also the case of a horizontal flat plate in contact with a fluid to which it supplies heat from above (to reduce convection). Assume there to be an inhomogeneity in the plate heater such that at one point it is slightly cooler than over the rest of the surface of the plate. The temperature field around the inhomogeneity will have the form shown in fig. (2.2).

Element A at height z_1 is at the same temperature as element C at height z_3 and so there is no driving force for convection between fluid elements A and C. But, element A at height z_1 is at a lower temperature than element B at height z_2; therefore a driving force for convection exists and convection will occur as long as the

depicted regime is in existance. Since in practice a heating surface can never be perfectly homogeneous, by using the argument just prescribed it can be seen that there will always be convection in flat plate apparati used at steady state.

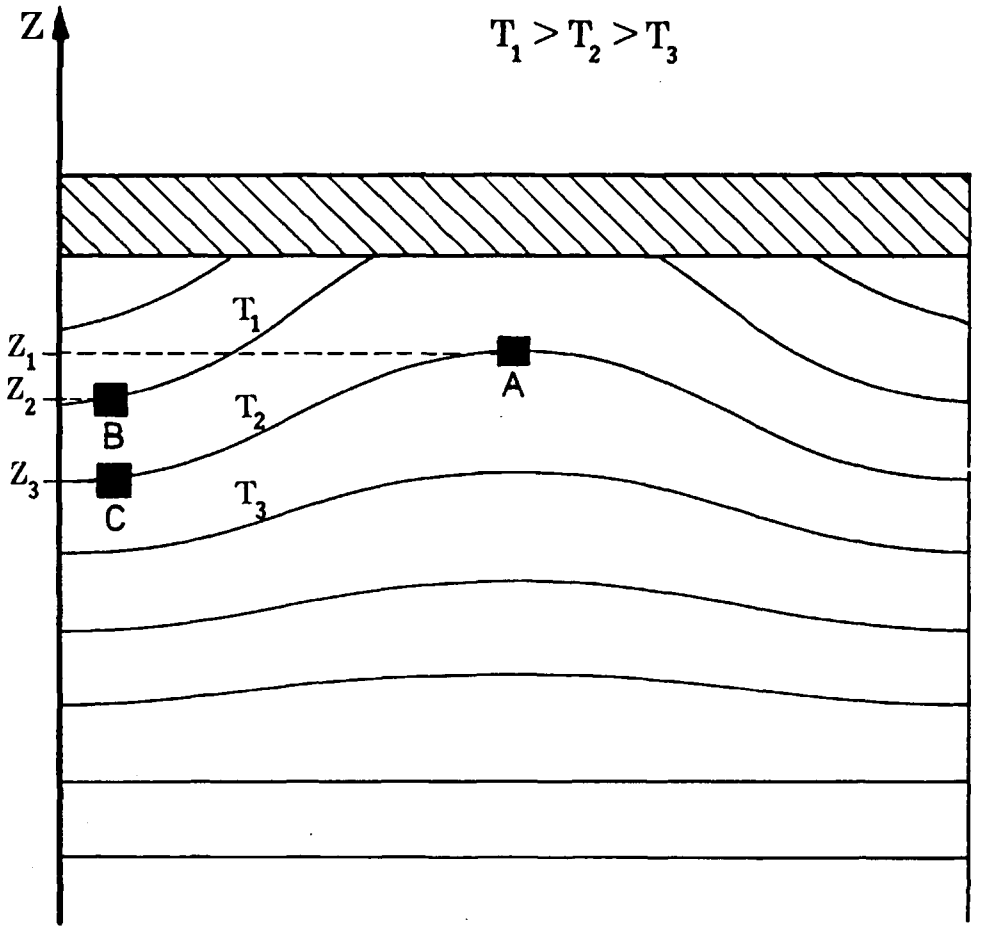

Fig. (2.2) Temperature field around an inhomogeneity in a heating surface.

In order to eliminate this second mechanism of convection, the transient hot wire technique relies on the fact that, due to inertial and viscous forces within real fluids, there is a

characteristic time before the buoyancy forces, which cause convection, can accelerate the fluid sufficiently to cause an appreciable effect on the rate of heat transfer through the fluid. By suitable arrangement of the apparatus, the characteristic time can be made large enough to be greater than the time required to perform the experiment.

The great advantage the transient hot wire technique has over other methods of fluid thermal conductivity measurement is that, convection if present can be immediately detected. This occurs because, after applying the necessary corrections to the raw experimental data, obtained during a run on the apparatus, when the resulting temperature rises are plotted versus Ln t, then the expected temperature rise of the fluid versus Ln t has the form shown in fig. (2.3).

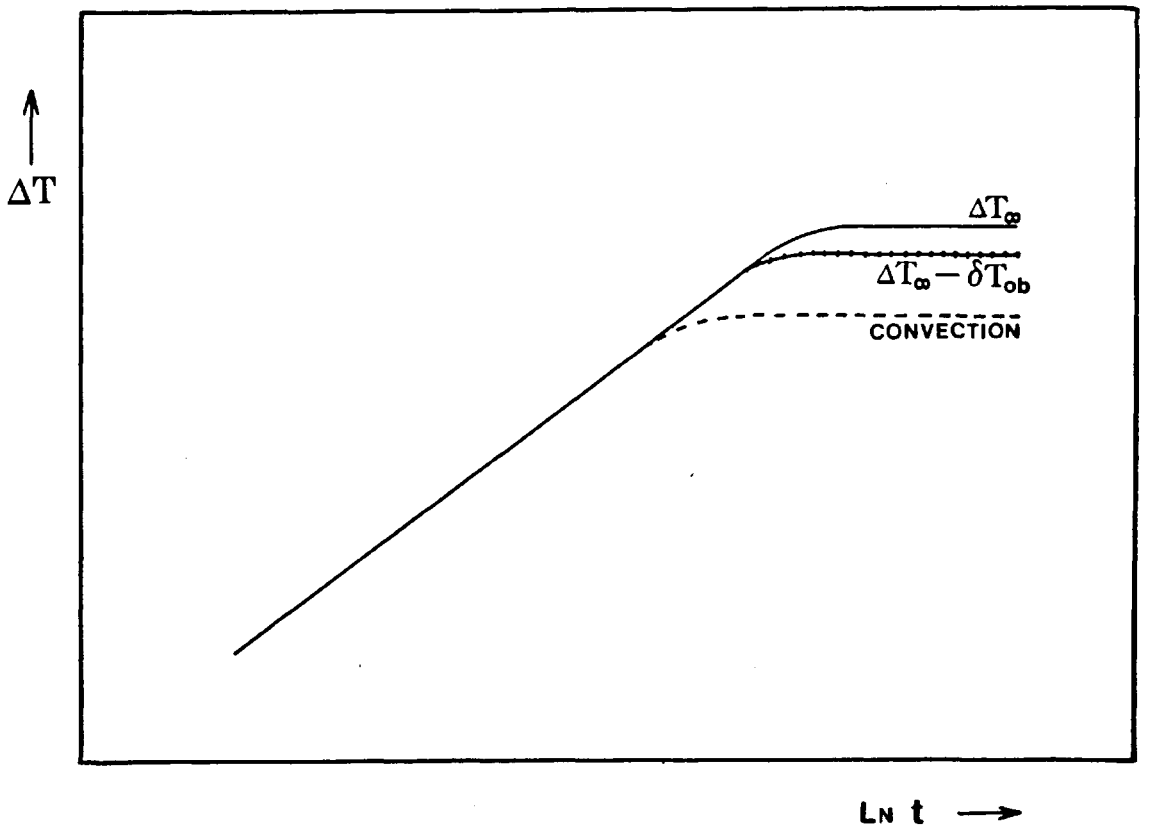

Fig. (2.3) Effect of convection on the temperature rise of the wire.

In practice because of the existance of an outer boundary the plateau occurs at $\Delta T_{\infty} - \delta T_{ob}$ (see § 2.333). Where convective heat transfer occurs together with conduction then the plateau occurs at a significantly lower temperature rise because there is another mechanism for heat transfer. If the apparent thermal conductivity is observed during a run in which convection is believed to occur, then at first the apparent thermal conductivity is independent of time but after a characteristic time (dependent on apparatus and fluid measured) the apparent thermal conductivity is seen to increase dramatically with increasing time. The observed deviations from the straight line ΔT versus Ln t (see fig. (2.4)) are seen to be significantly larger than normal (cf. fig. (4.15)) and exhibit a systematic curvature.

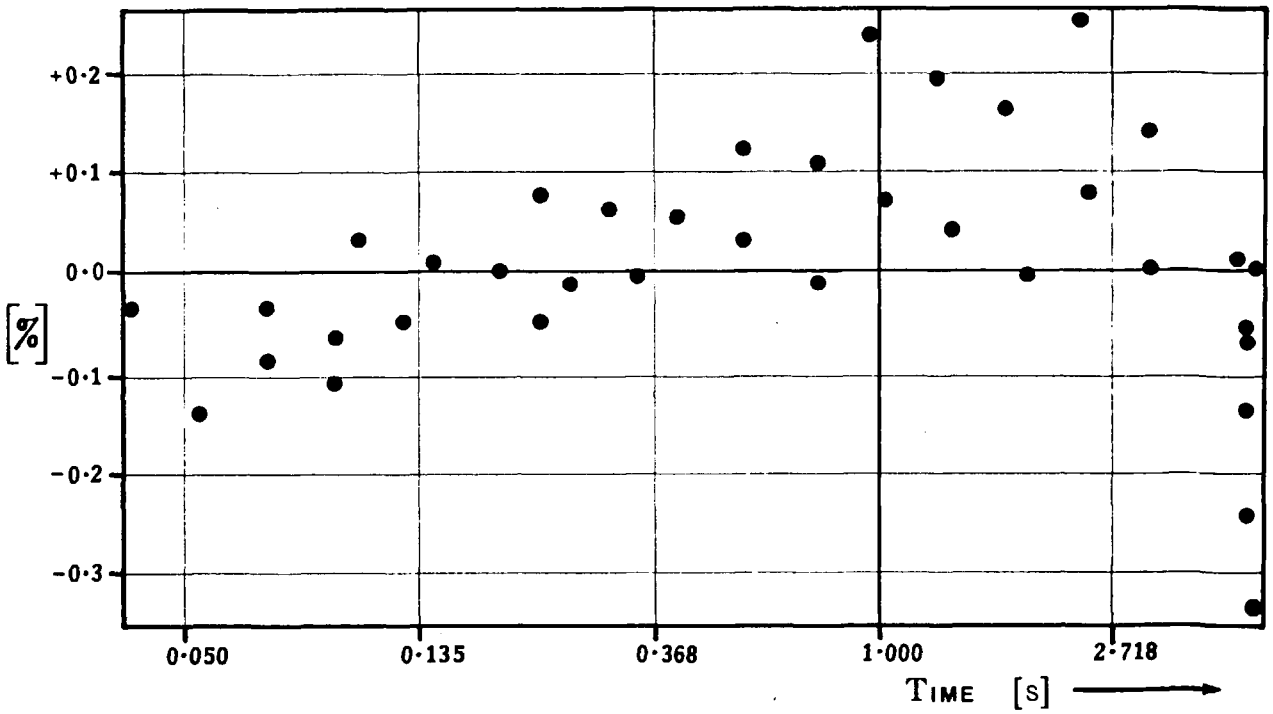

Fig. (2.4) Deviations from the straight line ΔT versus Ln t (N-Undecane at 170 MPa and 300K)

It should be mentioned here that only the second mechanism of convection can be detected, where initially convection is absent but starts following the initiation of an experiment. It is not certain whether a steady state convection field within the apparatus can be detected.

2.32 Effects Made Negligible

This subsection quantitatively examines effects that either by suitable design of the apparatus or by their very nature contribute errors of less than 0.01% to the idealised temperature rise, ΔT_{id} . This examination is performed to determine the conditions under which these effects are negligible, thus justifying their exclusion from consideration.

2.321 Truncation Error

The working equation (2.14) is a truncation of equation (2.13) and the error incurred is of order a^2/kt . The major part of the error is contained in the first neglected term and to make the error negligible therefore requires:-

$$10^{-4}\,\Delta T_{id} \geqslant \frac{q}{4\pi\lambda}\left(\frac{a^2}{4kt}\right) \qquad \text{.....(2.16)}$$

or

$$10^{-4} \geqslant \left|\frac{a^2}{4kt\ \mathrm{Ln}\left\{\frac{4kt}{a^2c}\right\}}\right| \qquad \text{.....(2.17)}$$

which is satisfied for $70\ \mathrm{ms} \lesssim t \lesssim 1\mathrm{s}$ and $6 \times 10^{-8} \lesssim k \lesssim 10^{-7}$, by choosing a wire of radius $a \approx 3.5\ \mu\mathrm{m}$.

2.322 Finite Wire Diameter

As in practice a heat source of finite diameter is used instead of a line source, the boundary condition (2.8) requires modification to:-

$$a\left(\frac{\partial T}{\partial r}\right)_{r=a} = -\frac{q}{2\pi\lambda} \qquad \text{.....(2.18)}$$

and therefore, by the solution of equation (2.5) subject to (2.6), (2.7) and (2.18), the temperature rise of the wire is found [63]

to be:-

$$\Delta T(r<a,t) = -\frac{q}{\pi^2 a\lambda}\int_0^{\infty}(1 - e^{-ku^2t})\left[\frac{J_o(ur)Y_1(ua) - Y_o(ur)J_1(ua)}{u^2\left[J_1^2(ua) + Y_1^2(ua)\right]}\right]du \qquad \ldots\ldots\ldots\ldots(2.19)$$

which for $\frac{4kt}{r^2} \gg 1$ reduces to:-

$$\Delta T(r,t) = \frac{q}{4\pi\lambda}\ln\left[\frac{4kt}{r^2C}\right] + O\left(\frac{r^2}{kt}\right) \qquad \ldots\ldots\ldots\ldots\ldots\ldots(2.20)$$

and at (r=a) equation (2.13) is recovered.

2.323 Radiation (Transparent Media)

In deriving the working equation (2.14) it was assumed that heat transfer occurred purely by conduction. In practice, however, simultaneous conductive and radiative heat transfer occurs through the test fluid, but, provided the fluid is transparent and the temperature rise of the wire is small ($\sim$5K), then the error incurred due to radiation can be shown to be negligible.

Assuming the fluid to be transparent, the radiative heat flux at the surface can be represented as:-

$$Q_R = A_a E_a F_{ab} - \alpha A_b E_b F_{ba} \qquad \ldots\ldots\ldots\ldots\ldots\ldots(2.21)$$

Using reciprocity the view factor F_{ba} is found as:-

$$F_{ba} = \frac{A_a}{A_b}F_{ab} = \frac{A_a}{A_b} \qquad \ldots\ldots\ldots\ldots\ldots\ldots(2.22)$$

resulting in:-

$$Q_R = A_a(E_a - \alpha E_b) \qquad \ldots\ldots\ldots\ldots\ldots\ldots(2.23)$$

or:-

$$q_R = 2\pi a(\epsilon\sigma T_a^4 - \alpha\sigma T_b^4) \qquad \text{.....(2.24)}$$

If we assume:-

$$\epsilon \approx \alpha \qquad \text{.....(2.25)}$$

then:-

$$q_R = 2\pi a\epsilon\sigma(T_a^4 - T_b^4) \qquad \text{.....(2.26)}$$

$$\approx 8\pi a\epsilon\sigma T_o^3 \Delta T(a,t) \qquad \text{.....(2.27)}$$

and from equation (2.14):-

$$\frac{\delta T_R}{\Delta T} = \frac{q_R}{q} = \frac{8\pi a\epsilon\sigma T_o^3}{q} \Delta T(a,t) \qquad \text{.....(2.28)}$$

The resulting correction is negligible in the present apparatus which employs a 3.5 μm diameter wire; a temperature rise of less than 5K; a heat input per unit length of wire of approximately 0.7 Wm^{-1} and steady state temperature, T_o, of 363K, these conditions corresponding to the worst encountered.

For participating fluids, the full integro partial differential equation governing simultaneous conductive and radiative heat transfer requires solution and results in the prediction of an appreciable difference between the apparent thermal conductivity (that calculated from equation (2.14) assuming there only to be conductive heat transfer) and the actual thermal conductivity.

In the case of these fluids which may absorb and re-emit radiation, there has been until now no exact solution of the integro partial differential equation governing simultaneous conduction and radiation. However, there have been a number of approximate treatments of the problem which indicate that the effects due to radiation are smaller in transient measurement apparati than in those operated at steady state. In transient measurement apparati the effects due to radiation

are believed to contribute an error of a few percent which is small but not insignificant. Since the purpose of the present work is to perform thermal conductivity measurements with an accuracy of a fraction of 1%, it is clear that these approximate analyses are inadequate for the present purposes. Consequently, the next chapter is entirely devoted to a new comprehensive numerical treatment of the problem of simultaneous conduction and radiation for the purposes of interpretating the present measurements. Meanwhile, the approximate analyses are used merely as a guide to the design of an instrument.

2.324 Knudsen Effect

The Knudsen effect is due to a temperature jump existing at the surface of the wire. This occurs when the diameter of the wire becomes of the same order of magnitude as the mean free path of a molecule of the fluid under observation, and results in the temperature of the fluid at r=a being less than the temperature of the wire surface.

Because the mean free path of a molecule of a liquid is never of the same order of magnitude as that of the platinum wire diameter (7 μm) this effect does not present itself and is only applicable to gases at low densities, and its inclusion is purely for completeness.

The temperature jump at the wire surface can be described by the Smoluchowski equation [64,65] as:-

$$T_w(a,t) - T(a,t) = - g_1 \left(\frac{\partial T}{\partial r}\right)_{r=a} \qquad \text{.....(2.29)}$$

where g_1 is an impirical factor proportional to the mean free path of the fluid. Now by solving equation (2.5) subject to equations (2.6),(2.7), and (2.18) using equation (2.29) one obtains:-

$$\Delta T_w(a,t) = \Delta T(a,t) + T_w(a,t) - T(a,t) \qquad \text{.....(2.30)}$$

where:-

$$\Delta T_w(a,t) = \frac{q}{4\pi\lambda}\left[\left(\frac{2g_1}{a}\right) + \mathrm{Ln}\left[\frac{4kt}{a^2C}\right] + O\left[\frac{a^2}{kt}\right]\right] \quad \ldots\ldots\ldots\ldots(2.31)$$

or:-

$$\delta T_k = \frac{q}{4\pi\lambda}\left\{\frac{2g_1}{a}\right\} \quad \ldots\ldots\ldots\ldots\ldots\ldots\ldots\ldots(2.32)$$

To a good first approximation, the temperature jump is independent of time and although g_1 is not known its magnitude is not required for the calculation of the thermal conductivity because of the way in which the thermal conductivity is calculated. From equation (2.4) because the Knudsen effect does not change the gradient of $\Delta T(a,t)$ versus Lnt, it just shifts the line, we find that the value of the thermal conductivity obtained is unaltered.

To a higher order approximation, it can be shown [57] that the effect of the temperature jump at the wire surface produces a temperature correction δT_k of the form:-

$$\frac{\delta T_k}{\Delta T} = \frac{q\Lambda}{2\pi\lambda a T_o} \quad \ldots\ldots\ldots\ldots\ldots\ldots\ldots\ldots(2.33)$$

where Λ is the mean free path of a molecule in the fluid.

By a suitable choice of the radius of the platinum wire, a, (3.5 μm) at most temperatures, T_o, and for all but very low pressures the effect can be rendered negligible.

2.325 Viscous Heating and Reversible Work of Compression

As explained previously (§ 2.31) the temperature field set up in the fluid during a measurement by the transient hot wire apparatus is conducive to the consequent formation of a velocity field within the fluid. This velocity field causes viscous dissipation in the fluid which results in local temperature increases within the fluid and hence a reduction in the heat emitted from the hot wire.

In order to determine the correction due to viscous heating, what is required is the simultaneous solution of the equations of continuity:-

$$\frac{\partial \rho}{\partial t} + \frac{1}{r}\frac{\partial(\rho r V_r)}{\partial r} = 0 \qquad \text{.....(2.34)}$$

momentum in the radial, r, direction:-

$$\frac{\partial V_r}{\partial t} + V_r \frac{\partial V_r}{\partial r} = -\frac{1}{\rho}\frac{\partial p}{\partial r} + \frac{4}{3}\frac{\mu}{\rho}\left\{\frac{1}{r}\frac{\partial V_r}{\partial r} + \frac{\partial^2 V_r}{\partial r^2} + \frac{V_r}{r^2}\right\} \qquad \text{.....(2.35)}$$

momentum in the vertical, z, direction:-

$$\frac{\partial V_z}{\partial t} + V_r \frac{\partial V_z}{\partial r} = -\frac{1}{\rho}\frac{\partial p}{\partial z} + \frac{\mu}{\rho}\left\{\frac{1}{r}\frac{\partial V_z}{\partial r} + \frac{\partial^2 V_z}{\partial r^2}\right\} + g \qquad \text{.....(2.36)}$$

and Energy:-

$$\frac{\partial T}{\partial t} + V_r \frac{\partial T}{\partial r} = k\left\{\frac{1}{r}\frac{\partial T}{\partial r} + \frac{\partial^2 T}{\partial r^2}\right\} + \frac{1}{\rho C_p}\left\{\frac{\partial p}{\partial t} + V_r \frac{\partial p}{\partial r}\right\} + \frac{4}{3}\frac{\mu}{\rho C_p}\left\{\left(\frac{\partial V_r}{\partial r}\right)^2 + \left[\frac{V_r}{r}\right]^2 - \frac{V_r}{r}\frac{\partial V_r}{\partial r} + \frac{3}{4}\left(\frac{\partial V_z}{\partial r}\right)^2\right\} \qquad \text{...(2.37)}$$

Subject to the initial and boundary conditions:-

$$T(r,t) = T^{(o)};\ \rho(r,z,t) = \rho^{(o)}(z);\ p(r,z,t) = p^{(o)} \text{ at } t \leqslant 0 \qquad \text{..(2.38)}$$

$$\frac{\partial T}{\partial r} = -\frac{q}{2\pi\lambda a};\quad V_r(r,t) = V_z(r,t) = 0, \text{ at } r=a \text{ and any } t>0 \qquad \text{...(2.39)}$$

$$V_r(r,t) = V_z(r,t) = 0 \text{ and } T(r,t) = T^{(o)}, \text{ at } r=\infty \text{ and } t>0 \qquad \text{...(2.40)}$$

As the simultaneous solution of the partial differential equations, subject to the initial conditions, boundary conditions and an

equation of state for the fluid, is difficult, if not impossible to obtain and, as the effect is believed to be small, what is required is a first approximation to the solution similar to that obtained earlier for gases [57].

A first order estimate of the temperature field can be obtained by ignoring the convective, dissipative, and reversible work terms in the energy equation, yielding:-

$$\frac{\partial T^{(1)}}{\partial t} = k^{(o)} \left\{ \frac{1}{r} \frac{\partial T^{(1)}}{\partial r} + \frac{\partial^2 T^{(1)}}{\partial r^2} \right\} \qquad \ldots\ldots\ldots\ldots\ldots\ldots\ldots\ldots (2.41)$$

where the superscripts (o) and (1) denote the Zeroth (equilibrium), and first itteration respectively.

The solution of (2.41) as for the solution of equation (2.5) results in:-

$$\frac{T^{(1)} - T^{(o)}}{T^{(o)}} = \bar{q} \, \mathrm{Ln} \, \bar{\alpha} \qquad \ldots\ldots\ldots\ldots\ldots\ldots\ldots\ldots (2.42)$$

for $\bar{\alpha} \gg 1$ $\qquad \ldots\ldots\ldots\ldots\ldots\ldots\ldots\ldots (2.43)$

where $\bar{\alpha} = \frac{4kt}{r^2 C}$, $\bar{q} = \frac{q}{4\pi\lambda T^{(o)}}$ $\qquad \ldots\ldots\ldots\ldots\ldots\ldots\ldots\ldots (2.44)$

Because the fluid is almost infinite in extent, then to a very good first approximation, the change in pressure in the radial direction can be neglected. We therefore assume:-

$$P(r,t) = P(t) = p^{(o)} \qquad \ldots\ldots\ldots\ldots\ldots\ldots\ldots\ldots (2.45)$$

and that:-

$$\rho^{(1)} = \rho^{(o)} \left(1 - \frac{\beta \Delta T}{T^{(o)}}\right) \qquad \ldots\ldots\ldots\ldots\ldots\ldots\ldots\ldots (2.46)$$

which in practice is a good approximation provided $\frac{\Delta T}{T^o} \ll 1$.

Now implementing equation (2.42) in (2.46) one obtains:-

$$\rho^{(1)} = \rho^{(o)}(1 - \beta\bar{q}\,\mathrm{Ln}\bar{\alpha}) \quad \text{for} \quad \beta\bar{q}\,\mathrm{Ln}\bar{\alpha} \ll 1 \qquad \ldots\ldots\ldots\ldots(2.47)$$

which used with equation (2.34) enables the radial velocity $V_r^{(1)}$ to be found as:-

$$V_r^{(1)} \approx \frac{\beta\bar{q}r}{2t}\left(1 - \left\{\frac{a}{r}\right\}^2\right)(1 + \beta\bar{q}\,\mathrm{Ln}\bar{\alpha}) \qquad \ldots\ldots\ldots\ldots\ldots\ldots(2.48)$$

and using equation (2.35) results in:-

$$\frac{1}{\rho}\frac{\partial p}{\partial r} = \frac{\beta\bar{q}k}{tr}\left\{1 - \left\{\frac{a}{r}\right\}^2\right\}\left\{\frac{8}{3}\beta\bar{q}\{Pr\} + O(\bar{a})^{-1}\right\} \qquad \ldots\ldots\ldots\ldots(2.49)$$

where:-

$$\{Pr\} = \frac{\mu}{\rho k} = \text{Prandtl No.} \qquad \ldots\ldots\ldots\ldots\ldots\ldots\ldots\ldots(2.50)$$

From equations (2.49) and (2.47) we find that:-

$$\frac{1}{p}\frac{\partial p}{\partial r}\Big/\frac{1}{\rho}\frac{\partial \rho}{\partial r} \sim O\left(\frac{k\beta\bar{q}}{pt}\right) \ll 1 \qquad \ldots\ldots\ldots\ldots\ldots\ldots\ldots\ldots(2.51)$$

for the experimental condition important here, so that the assumption of constant pressure in equation (2.45) is justified.

By using the Boussinesq approximation that the variable density is only important in the buoyancy term of equation (2.36) one obtains:-

$$\frac{\partial V_z}{\partial t} \approx \frac{\mu}{\rho}\left(\frac{1}{r}\frac{\partial V_z}{\partial r} + \frac{\partial^2 V_z}{\partial r^2}\right) + \frac{g\beta\Delta T}{T^{(o)}} \qquad \ldots\ldots\ldots\ldots\ldots\ldots(2.52)$$

which to a first approximation [66] for $r \leqslant 10^3 a$ gives:-

$$V_z^{(1)} = \bar{q}\beta g t \, \mathrm{Ln}\left\{\frac{r}{a}\right\}^2 \Big/ \mathrm{Ln}\left\{\frac{4kt}{C^2 a^2}\right\} \qquad \ldots\ldots\ldots\ldots\ldots\ldots (2.53)$$

For the times used in practice 70 ms $< t <$ 1 sec. it can be seen that:-

$$V_z \gg V_r \quad \text{and} \quad V_r \frac{\partial V_z}{\partial r} \ll \frac{\partial V_z}{\partial t} \qquad \ldots\ldots\ldots\ldots\ldots\ldots (2.54)$$

as is required by the need for consistency following the neglection of the convective term in equation (2.52).

If the thermal conductivity and specific heat of the fluid are assumed constant then from equation (2.46) one finds the first itteration expression for the thermal diffusivity:-

$$k^{(1)} = k^{(o)} (1 + \beta \bar{q} \, \mathrm{Ln}\bar{\alpha}) \qquad \ldots\ldots\ldots\ldots\ldots\ldots\ldots\ldots (2.55)$$

For the second itteration on the temperature rise from equation (2.37) using (2.53) we obtain:-

$$\frac{\partial T^{(2)}}{\partial t} - k^{(o)}\left\{\frac{1}{r}\frac{\partial T^{(2)}}{\partial r} + \frac{\partial^2 T^{(2)}}{\partial r^2}\right\} = k^{(o)}\beta\bar{q} \, \mathrm{Ln}\,\bar{\alpha}\left\{\frac{1}{r}\frac{\partial T^{(1)}}{\partial r} + \frac{\partial^2 T^{(1)}}{\partial r^2}\right\}$$

$$- V_r^{(1)}\frac{\partial T}{\partial r} + \frac{4\mu}{3\rho^{(o)}t_p}\left\{\left(\frac{\partial V_r^{(1)}}{\partial r}\right)^2 + \left(\frac{V_r^{(1)}}{r}\right)^2 - \frac{V_r^{(1)}}{r}\frac{\partial V_r^{(1)}}{\partial r} + \right.$$

$$\left. + \frac{3}{4}\left(\frac{\partial V_z^{(1)}}{\partial r}\right)^2\right\} + \frac{1}{\rho^{(o)}t_p}\left\{\frac{\partial p^{(1)}}{\partial t} + V_r^{(1)}\frac{\partial p}{\partial r}\right\} \qquad \ldots\ldots\ldots (2.56)$$

where the terms on the right side of equation (2.56) refer to corrections for; the variation in thermal diffusivity; radial convection; viscous dissipation and reversible work of compression. As these corrections are small, they can therefore be assumed

additive to within adequate accuracy.

The viscous dissipation term can be split into two parts, one for radial dissipation of the form:-

$$\frac{\beta^2\bar{q}^2}{t^2}\ \frac{\mu}{\rho C_p}\left\{\ \frac{1}{3}\left[1+\left(\frac{a}{r}\right)^4\right]\right\} \qquad \ldots\ldots\ldots\ldots\ldots\ldots\ldots\ldots(2.57)$$

and the other for vertical dissipation in the form:-

$$\frac{\beta^2\bar{q}^2}{t^2}\ \frac{\mu}{\rho C_p}\left[\frac{2gt^2}{r\ \mathrm{Ln}\left[4kt/(Ca)^2\right]}\right]^2 \qquad \ldots\ldots\ldots\ldots\ldots\ldots\ldots\ldots(2.58)$$

of which the term for vertical dissipation is by far the greater at r=a, 70 ms$<$t$<$1s.

The temperature correction due to viscous dissipation is obtained by solving:-

$$\frac{\partial T^{(2)}}{\partial t} - k^{(o)}\left\{\frac{1}{r}\frac{\partial T^{(2)}}{\partial r} + \frac{\partial^2 T^{(2)}}{\partial r^2}\right\} \approx \frac{\bar{q}^2\{Pr\}k^{(o)}}{C_p}\left[\frac{2\beta gt}{r\ \mathrm{Ln}\ (4kt/C^2a^2)}\right]^2$$

$$\ldots\ldots\ldots\ldots\ldots(2.59)$$

from which is obtained [63] the second itteration for the temperature rise at r=a:-

$$\frac{T^{(2)}-T^{(o)}}{T_o} = \bar{q}\ \mathrm{Ln}(\bar{\alpha})\left[1+\frac{\bar{q}^2\{Pr\}\beta^2g^2t^2}{2C_pT_o\mathrm{Ln}\,\bar{\alpha}}\right] \qquad \ldots\ldots\ldots\ldots\ldots(2.60)$$

and so an expression for the temperature correction due to viscous heating:-

$$\frac{\delta T_{Visc}}{T_o} = \frac{\bar{q}^2\{Pr\}\beta^2g^2t^2}{2C_pT_o} \qquad \ldots\ldots\ldots\ldots\ldots\ldots\ldots\ldots(2.61)$$

or:-

$$\delta T_{Visc} = \frac{(q/4\pi\lambda)^2 \{Pr\}\beta^2 g^2 t^2}{2\, T_o^{\,2} C_p} \qquad \ldots\ldots\ldots\ldots\ldots\ldots\ldots\ldots (2.62)$$

For liquids where $Pr \sim 10$, $\lambda \approx 0.15$ W/m/K and $C_p \approx 2000$ J/Kg/K, it is easily shown that for the experimental conditions employed in transient hot wire measurements, $q \simeq 0.5$ W/m, $t \simeq 1$s and $T_o \simeq 350$K, this correction amounts to less than 0.01% of the temperature rise and is therefore negligible.

The last term in equation (2.56) is due to the reversible work of compression resulting from the temperature rise in the fluid during a measurement. Using equations (2.48) and (2.49) the term reduces to:-

$$\frac{\beta^2 \bar{q}^2}{t^2} \frac{\mu}{\rho C_p} \left[\frac{4\beta\bar{q}}{3} \left(1 - \left\{ \frac{a}{r} \right\}^2 \right)^2 \right] \left[1 + \beta\bar{q}\, Ln\bar{\alpha} \right] \qquad \ldots\ldots\ldots\ldots (2.63)$$

which is even smaller than the viscous dissipation term and as a result the error due to the reversible work of compression is also negligible.

Of course the validity of the entire analysis rests on assumption (2.46), but for the small temperature rises employed in the measurements, $\Delta T \sim 3$K, the assumption of a linear temperature variation of the density is a good approximation.

2.33 Significant Corrections

In this subsection, the significant errors (those amounting to greater than 0.01% ΔT_{id}) are examined, and using mathematical models are quantified so as to enable their use with the observed temperature rises in order to obtain the thermal conductivity of the test fluid. In practice one of the criteria used for the apparatus design is that

none of these errors should ever contribute more than 1% in ΔT_{id} thus limiting inaccuracies due to the sometimes approximate error analyses used.

2.331 Variable Fluid Properties

This correction occurs owing to the fact that the density and thermal conductivity of the fluid vary with temperature. This results in the observed temperature rises differing from their ideal values, since in the ideal model the fluid properties are considered constant.

The thermal conductivity of a test fluid is obtained from the slope of a plot of ΔT versus Ln t and in the present work the time domain within which measurements are recorded is between 70 ms - 1s and the change in the temperature rise during this time is less than 2K. Because the change in thermal conductivity during this period is less than 0.5% it is small enough to enable the use of the analysis given by Healy, de Groot, & Kestin [57]. It is found using this analysis that the temperature rise has the form:-

$$\Delta T(t) = \Delta T_{id} - \tfrac{1}{2}\chi(\Delta T)^2 + \left\{\frac{q}{4\pi\lambda_o}\right\}^2 (\chi - \phi)\,\mathrm{Ln}\,4 \qquad \ldots\ldots\ldots(2.64)$$

where by definition $\lambda(T,\rho) = \lambda_o(1 + \chi\Delta T)$ $\ldots\ldots\ldots(2.65)$

$$\rho C_p = \rho_o C_p(1 + \phi\Delta T) \qquad \ldots\ldots\ldots(2.66)$$

The last term in equation (2.64) is time independent and does not influence the slope of ΔT versus Ln t and is therefore ignored. Now considering the temperature rise at either end of the range of measurement times $\Delta T(t_1)$ and $\Delta T(t_n)$ (corresponding to the first and last bridge balance conditions, see § 4.41) from their difference we find:-

$$\Delta T(t_n) - \Delta T(t_1) = \frac{q\,\mathrm{Ln}\left[t_n/t_1\right]}{4\pi\lambda_o\left\{1 + \tfrac{1}{2}\chi\left[\Delta T(t_1) + \Delta T(t_n)\right]\right\}} \qquad \ldots\ldots\ldots(2.67)$$

which using (2.65) is identical in form to the idealised temperature rise with the properties evaluated at:-

$$T_r = T_o + \delta T_{fp} \qquad \text{.....(2.68)}$$

$$= T_o + \tfrac{1}{2}\left\{\Delta T(t_1) + \Delta T(t_n)\right\} \qquad \text{.....(2.69)}$$

$$\rho = \rho(T_r, P_o) \qquad \text{.....(2.70)}$$

It is therefore implied that the fluid thermal conductivity obtained from the slope of the measured ΔT versus $\ln t$ line corresponds to the thermal conductivity at temperature T_r and density $\rho_r(T_r, P_o)$ as we have demonstrated the pressure to be invariant.

2.332 Composite Cylinders

In the mathematical model from which the idealised temperature rise of the fluid is calculated, heat is assumed to be emitted from a line source whereas in practice a hot wire with finite, non-zero physical properties different from those of the fluid is used thus incurring an error. To account for the error one requires the solution of coupled equations for the composite cylinder system (hot wire and fluid). The equations requiring solution are, for the wire:-

$$(\rho C_p)_w \frac{\partial T_w}{\partial t} = \lambda_w \nabla^2 T_w - \frac{q}{\pi a^2} \qquad 0 \leq r \leq a \qquad \text{.....(2.71)}$$

for the fluid:-

$$\rho C_p \frac{\partial T}{\partial t} = \lambda \nabla^2 T \qquad r > a \qquad \text{.....(2.72)}$$

and by continuity we require:-

$$T_w(a,t) = T(a,t) \; ; \; \lambda_w \left(\frac{\partial T_w}{\partial r}\right)_{r=a} = \lambda \left(\frac{\partial T}{\partial r}\right)_{r=a} \qquad \text{.....(2.73)}$$

The initial condition is:-

$$T_w(r, t<0) = T(r, t<0) = T_o \qquad \text{all } r \qquad \text{.....(2.74)}$$

and the boundary conditions are:-

$$\left(\frac{\partial T_w}{\partial r}\right)_{r=0} = 0 \qquad t \geqslant 0 \qquad \text{.....(2.75)}$$

$$T(r \rightarrow \infty, t) = T_o \qquad t \geqslant 0 \qquad \text{.....(2.76)}$$

$$\left(\frac{\partial T}{\partial r}\right)_{r=a} = -\frac{q}{2\pi\lambda a} \qquad t \geqslant 0 \qquad \text{.....(2.77)}$$

The solution at large values of $4kt/r^2$ is found [P347 of 43] to be:-

$$\Delta T_w(r,t) = \frac{q}{4\pi\lambda}\left\{\left[1 - a^2\left((\rho C_p)_w - \rho C_p\right)/2\lambda t\right] \; \mathrm{Ln}\left[\frac{4kt}{r^2 C}\right] + \left[\frac{a^2}{2kt}\right] - \left[\frac{a^2}{8k_w t}\right]\right\} + \frac{q}{4\pi\lambda_w}\left[\left(1 - \frac{r^2}{a^2}\right)\left(1 - \frac{a^2\lambda_w}{4k_w\lambda t}\right)\right] \qquad \text{.....(2.78)}$$

During measurements on a fluid what is measured in the hot wire method, using the hot wire as a thermometer, is the average temperature over the wire diameter as defined by:-

$$\Delta T_w(t) = \frac{\int_o^a \Delta T_w(r,t) r dr}{\int_o^a r dr} \qquad \text{.....(2.79)}$$

$$\Delta T_w(t) = \frac{q}{4\pi\lambda} \ln\left\{\frac{4kt}{a^2 C}\right\}\left(1 - a^2 \frac{\{(\rho c_p)_w - \rho c_p\}}{2\lambda t}\right)$$

$$+ \frac{q}{4\pi\lambda}\left(\frac{a^2}{2kt} - \frac{a^2}{4k_w t} + \frac{\lambda}{2\lambda_w}\right) \qquad \text{.....(2.80)}$$

It should be noted that the second term, including the reference temperature shift, $q/8\pi\lambda_w$, is negligible and therefore ignored, so resulting in the correction due to the finite physical properties of the hot wire being:-

$$\delta T_{cc} = a^2\left(\frac{(\rho c_p)_w - (\rho c_p)}{2\lambda t}\right) \Delta T_{id} \qquad \text{.....(2.81)}$$

It should also be noted here that the error is largest at small times, decreases with increasing time and it accounts not only for the wire having finite physical properties but also for the averaging process used to obtain the wire temperature.

2.333 Outer Boundary Correction

The mathematical model used to obtain the idealised temperature rise of the fluid as a function of time, assumes the fluid to be infinite in extent. However this is not the case and an outer concentric cylindrical boundary at r = b exists due to the need to contain the fluid.

The existence of this outer boundary will modify the temperature field in the fluid and a correction to the measured temperature rise is required in order to recover the necessary idealised temperature rises, through which the thermal conductivity is calculated. It is expected that the correction due to the outer boundary will be small since $b/a > 1000$ and will increase with time. This is because, in the idealised model, at small times the temperatures of elements of the fluid, at the position which would be occupied by the outer boundary in the real system will be very close to the initial temperature of the fluid. The real and idealised models would therefore

be very similar at small times but, as these same elements in the idealised model increase in temperature with time, the effect is expected to increase.

To obtain the deviation due to the outer boundary equation, (2.5) must be solved subject to initial condition (2.6) and boundary conditions (2.8) and

$$\Delta T(r_b, t \geqslant 0) = 0 \qquad \ldots\ldots\ldots\ldots\ldots\ldots\ldots\ldots (2.82)$$

The second boundary condition implies that the outer boundary is kept at the initial condition. In practice, the boundary cylinder is relatively massive and made of a metal with a large thermal conductivity, so making this an acceptable and valid approximation.

The asymptotic form of the solution as derived by Fischer [67] is:-

$$\Delta T(a,t) = \frac{q}{4\pi\lambda}\left\{ 2\,\mathrm{Ln}\left\{\frac{b}{a}\right\} - \sum_{\upsilon=0}^{\infty} e^{-g_\upsilon{}^2 kt/b^2}\left[\prod_{\upsilon} Y_o(g_\upsilon)\right]^2 \right\} \ldots\ldots (2.83)$$

$$\text{subject to } \frac{b}{a} \gg 1 \text{ and } \frac{4kt}{a^2} \gg 1 \qquad \ldots\ldots\ldots\ldots\ldots\ldots\ldots\ldots (2.84)$$

which results in a correction, δT_{OB} , to the idealised temperature rise of:-

$$\delta T_{OB} = -\frac{q}{4\pi\lambda}\left\{ \mathrm{Ln}\left\{\frac{4kt}{b^2 C}\right\} + \sum_{\upsilon=0}^{\infty} e^{-g_\upsilon{}^2 kt/b^2}\left[\prod_{\upsilon} Y_o(g_\upsilon)\right]^2 \right\} \ldots (2.85)$$

which in the present apparatus when performing measurements on liquid alkanes, as expected increases in magnitude with time, but amounts to no more than 0.1% in ΔT_{id} .

2.334 End Effects

The mathematical model, used to obtain the idealised temperature rise of the transient hot wire, is based on conductive transfer of

heat emitted by a segment of an infinitely long line heat source. In practice, a hot wire is used which does not correspond sufficiently closely to a line heat source, as it has a finite radial extent and a finite heat capacity and thermal conductivity. (The effects of these discrepancies have already been examined in § 2.322 and § 2.332.) But, since the hot wire requires electrical contacts and physical support it cannot be infinitely long and this departure from ideality must also be accounted for.

Approximate analyses for the departures from ideality have been provided by Haarman [68] & J.H. Blackwell [69]. The latter predicts the factor, δ, by which the slope, in the middle (z=0) section of a wire, of length L, departs from that in an infinitely long wire as defined by:-

$$\delta = 1 - \frac{4\pi\lambda}{q} \frac{\partial[T(a,t)]}{\partial[\ln(4kt/a^2C)]} \qquad \ldots\ldots\ldots\ldots\ldots\ldots\ldots\ldots\ldots(2.86)$$

$$= \frac{e^{-L^2/16kt}}{\pi} \left\{ \frac{\sqrt{16kt}}{L} + \frac{L}{a}\left[\frac{\lambda_w}{\lambda} - \frac{(\rho C_p)_w}{\rho C_p}\right]\left[\frac{\ln\left[\frac{4kt}{a^2C}\right]}{\left(\frac{4kt}{a^2}\right)^{3/2}}\right]\right\} \ldots\ldots(2.87)$$

The apparatus used employs two wires which are constructed so as to be as near identical (apart from their lengths) as is practically possible. The shorter wire is constructed to be of such a length that at the centre of the wire, δ, obtained from equation (2.86) is of the order of 10^{-4} (corresponding in practice to a length of $\gtrsim$4 cm). Consider now the situation when the two wires are immersed in the same fluid, under identical thermodynamic conditions, and when during measurements the same current passes through both of the wires, emitting the same heat per unit length from each of the wires. The difference in resistance of the two wires then, to within the required accuracy, gives a measurement of the temperature of a hypothetical finite segment of an infinitely long wire, the length of the segment being equal to the difference in lengths of the two wires. Thus the end effects of the wires have been eliminated

by a practical cancellation.

This cancellation requires that apart from their lengths the two wires be identical which in practice is impossible as due to the method of manufacture of the wires their diameter is subject to variation over their lengths. It is also not possible to exactly duplicate solder joints and connections to the wire ends thus introducing further dissimilarities. However, provided the resistances per unit length of the two wires differ from each other by less than a few percent, then an analysis given by Kestin & Wakeham [58] can be used. From the analysis the measured temperature rise of the middle section of the long wire can be calculated. This temperature rise is shown by Kestin & Wakeham to correspond, within the required accuracy, to the temperature rise of the middle segment of an infinitely long, long wire. The length of the segment is equal to the difference in lengths between the long and short wires. The means whereby this is achieved is delayed to a later section (§ 4.53).

2.335 Radiation (Absorbing Media)

In real fluid systems heat transfer occurs through radiation as well as by conduction and convection (the effects due to convection have already been considered in § 2.31 and § 2.325). The effect due to radiative heat transfer through a transparent medium has already been quantified (§ 2.323) and found to be negligible. When the fluid medium under consideration absorbs and reemits heat, in the form of electromagnetic radiation, the effect is often not negligible and requires consideration. This is necessary because the additional mechanism for heat transfer destroys the ideal conductive temperature field within the fluid and alters the form of the temperature rise of the hot wire as a function of time, moving it away from ideality.

To obtain the effect due to radiation, the full conduction - radiation problem requires solution. The problem is defined via a

Basic Equation:-

$$\frac{\partial^2 T}{\partial r^2} + \frac{1}{r}\frac{\partial T}{\partial r} = \frac{1}{k}\frac{\partial T}{\partial t} + \frac{1}{\lambda}\frac{\partial \dot{Q}_R}{\partial r} + \frac{\dot{Q}_R}{\lambda r} \qquad \text{.....(2.88)}$$

with Initial Conditions:-

$$T = T_o \; ; \; \dot{Q}_R = 0 \qquad (t=0,\ a<r<\infty) \qquad \text{.....(2.89)}$$

and Boundary Conditions:-

$$-\lambda\frac{\partial T}{\partial r} + \dot{Q}_R = \frac{q}{2\pi a} \qquad (t>0\ ,\ \ r=a) \qquad \text{.....(2.90)}$$

$$\lim_{r\to\infty} T(r,t) = T_o \; ; \; \dot{Q}_R = 0 \quad (t>0) \qquad \text{.....(2.91)}$$

where $\dot{Q}_R$ is the radiative heat flux.

In the same fashion as for other corrections using:-

$$T - T_o = -\frac{q}{4\pi\lambda} E_i\left(-\frac{r^2}{4kt}\right) + \delta T_R \qquad \text{.....(2.92)}$$

$$= \Delta T_{id} + \delta T_R \quad \text{when} \quad \frac{r^2}{4kt} \ll 1 \qquad \text{.....(2.93)}$$

from (2.92) one obtains:-

$$\frac{\partial^2(\delta T_R)}{\partial r^2} + \frac{1}{r}\frac{\partial(\delta T_R)}{\partial r} = \frac{1}{k}\frac{\partial(\delta T_R)}{\partial t} + \frac{1}{\lambda}\frac{\partial \dot{Q}_R}{\partial r} + \frac{\dot{Q}_R}{\lambda r} \qquad \text{.....(2.94)}$$

with Initial Conditions:-

$$\delta T_R = 0, \quad \dot{Q}_R = 0, \qquad t = 0, \qquad a<r<\infty \qquad \text{.....(2.95)}$$

and Boundary Conditions:-

$$-\left(\frac{\partial \delta T_R}{\partial r}\right) + \dot{Q}_R = 0 \qquad (t\ 0 \quad r=a) \qquad \text{.....(2.96)}$$

$$\delta T_R = 0, \quad \frac{\partial \delta T_R}{\partial r} = 0, \quad \dot{Q}_R = 0, \quad t \geqslant 0 \qquad \text{.....(2.97)}$$

What is required is an analytic solution to equation (2.94) for, $\delta T_R(a,t)$, the temperature rise correction due to radiation, this can then be applied to the measured temperature rise of the wire to obtain the idealised temperature rise of the wire from which the fluid thermal conductivity is obtained.

Unfortunately, as yet, there is no available analytical solution to the problem and a numerical solution is found which could, in principle, be used in its place. But, as the solution requires an enormous amount of computing time and expense, a different technique must be used, implementing a newly developed analysis which is given in Chapter 3. The analysis is delayed to a later chapter due to the enormity of the task required in order to obtain the correction.

2.336 Summary of Corrections

The transient hot wire technique is based on the idealised solution for the temperature rise of a fluid of infinite extent initially at thermal equilibrium through which heat is conducted from an infinitely long line heat source within the medium. The solution at a distance a (the diameter of the hot wire) into the fluid, after truncation, supplies the working equation from which the thermal conductivity is calculated:-

$$\Delta T_{id} = \frac{q}{4\pi\lambda(T_r)} \operatorname{Ln}\left[\frac{4k_o t}{a^2 C}\right] \qquad \text{.....(2.98)}$$

From measurements on the hot wire apparatus the temperature rises of the wire, $\Delta T(t)$, at a number of times, following the initiation of the heat dissipation to the fluid, are found. From these experimentally measured temperature rises the corresponding idealised temperature rise ΔT_{id} must be calculated in order to use (2.98) to calculate $\lambda(T_r)$. As stated previously it has been assumed that because the error corrections involved, in transforming the measured temperature rises to idealised temperature rises, are small their combined effect is additive. The idealised temperature rise is therefore obtained by summing the experimental temperature rise and individual temperature corrections:-

$$\Delta T_{id}(t) = \Delta T(t) + \sum_i \delta T_i \qquad \ldots\ldots\ldots\ldots\ldots\ldots\ldots (2.99)$$

Similarly the reference temperature T_r at which the thermal conductivity is measured is obtained:-

$$T_r = T_o + \sum_i \delta T_i^* \qquad \ldots\ldots\ldots\ldots\ldots\ldots\ldots (2.100)$$

Limiting the inclusion of errors which contribute temperature corrections of greater than 0.01% in ΔT_{id} results in:-

$$\Delta T_{id} = \Delta T(t) + \delta T_{cc} + \delta T_{08} \qquad \ldots\ldots\ldots\ldots\ldots\ldots\ldots (2.101)$$

where from (§ 2.332):-

$$\delta T_{cc} = \frac{a^2}{2\lambda T}\left[(\rho C_p)_w - (\rho C_p)\right] \Delta T_{id} \qquad \ldots\ldots\ldots\ldots\ldots\ldots\ldots (2.102)$$

and from (§ 2.333):-

$$\delta T_{08} = -\frac{q}{4\pi\lambda}\left\{ \mathrm{Ln}\left\{\frac{4kt}{b^2 C}\right\} + \sum_{\upsilon=0}^{\infty} e^{-g_\upsilon{}^2 kt/b^2}\left[\prod_\upsilon Y_o(g_\upsilon)\right]^2\right\} \ldots (2.103)$$

The reference temperature to which the thermal conductivity calculated from (2.102) corresponds, is obtained from § 2.331 as:-

$$T_r = T_o + \delta T^*_{FP} \qquad \text{.....(2.104)}$$

where

$$\delta T^*_{FP} = \tfrac{1}{2} \left\{ \Delta T(t_1) + \Delta T(t_2) \right\} \qquad \text{.....(2.105)}$$

and the reference density is:-

$$\rho_r = \rho(T_r, p_o)$$

CHAPTER 3

Simultaneous Conduction and Radiation

3.1 Introduction

As shown in § 2.335 the effect of radiative heat transfer on the measured thermal conductivity of a fluid as obtained by transient hot wire experiments is negligible provided the fluid can be treated as a transparent medium. If the fluid cannot be treated as transparent, the temperature field set up within the fluid is significantly perturbed from the corresponding temperature field for heat transfer by pure conduction. The purpose of this chapter is to calculate this perturbation.

Estimates for the difference between the absolute, 'true', thermal conductivity and the apparent thermal conductivity (that obtained from measurement assuming heat transfer occurs entirely by conduction) have until recently been restricted to steady state transfer between infinite parallel plates at small temperature differences. Leidenfrost [70] estimated that during measurements on toluene radiative transfer could give rise to errors of about 2 per cent depending on emissivities and wall temperatures. A few years later, Poltz & Jugel [71,72,73] concluded that the effect of radiation on the apparent thermal conductivity of toluene measured on steady state parallel plate equipment could be as high as a few per cent even at room temperature and suggested that errors of the same order of magnitude would be expected in measurements by the hot wire technique.

The optically thick approximation has been treated by Diessler [74] and Grief & Clapper [75] using the Rosseland diffusion approximation [76]. In this approximation radiation is treated as a diffusion process in which the radiative heat flux is assumed to have the form:-

$$Q_R = -\lambda_r \frac{\partial T}{\partial r} = \frac{16\, n^2 \sigma T^3}{3K} \frac{\partial T}{\partial r} \qquad \text{.....(3.1)}$$

This approximation is valid provided that the following condition on the optical thickness, KL, of the system holds true:-

$$KL \gg 1 \qquad \ldots\ldots\ldots\ldots\ldots\ldots\ldots\ldots\ldots\ldots (3.2)$$

In equation (3.2) K is the mean extinction coefficient as defined by the absorption low for radiative transfer through an absorbing medium:-

$$I = I_o e^{-KL} \qquad \ldots\ldots\ldots\ldots\ldots\ldots\ldots\ldots\ldots\ldots (3.3)$$

where I_o is the incident radiative flux at $l = 0$, I is the radiative flux at a distance, $l = L$, and L is some characteristic length.

The application of such an approximation is not valid for the present work because close to the hot wire, used in the apparatus, for typical extinction coefficients of the fluids under measurement ($K \approx 1000\ m^{-1}$) the system is optically thin:-

$$Kr \ll 1 \qquad \ldots\ldots\ldots\ldots\ldots\ldots\ldots\ldots\ldots\ldots (3.4)$$

and at the outer cell boundary the system is optically thick:-

$$Kr \gg 1 \qquad \ldots\ldots\ldots\ldots\ldots\ldots\ldots\ldots\ldots\ldots (3.5)$$

and somewhere inbetween the intermediate state exists:-

$$Kr \approx 1 \qquad \ldots\ldots\ldots\ldots\ldots\ldots\ldots\ldots\ldots\ldots (3.6)$$

As all three regimes, optically thin, intermediate, and optically thick exist within the apparatus used, it seems unlikely that a solution to the problem, based on an approximation valid for any single regime, will yield usable results. For this reason, Saito, Mani, & Venart [77] proposed an approximate, combined, finite - difference and integral technique in which the fluid around the hot wire is

subdivided into three regions, one for each of the afore mentioned regimes.

The method preferred for the present work involves a numerical solution to an approximate form of the full integro partial differential equation for simultaneous conductive and radiative heat transfer through an absorbing emitting medium contained within the annulus formed by the hot wire and the outer boundary of the measurement cell. This approach has the advantage that it is generally applicable and eliminates the artificial discontinuities at boundaries in the fluid created by the model adopted by Saito et al.

As for the other corrections (see § 2.33) the effect of the error due to this other mechanism of heat transfer, is assumed, additive and its effect on the observed temperature rise can be accounted for, along with the other non negligible errors, using equation (2.99). What is therefore needed is a solution to equation (2.94) for simultaneous conductive and radiative heat transfer from a line heat source into an infinite absorbing, reemitting medium, following a step heat emission from the line source. The form of solution required is:-

$$\Delta T(a,t) = \Delta T_{id}(t) + \delta T_R(t) \qquad \text{.....(3.7)}$$

It is difficult, and sometimes, as in this case, undesirable to numerically solve partial differential equations with boundary conditions at zero and infinity in one of the independent variables. For this reason the approximate numerical solution of equation (2.94) is obtained for an infinitely long hot wire (of radius a) concentrically mounted within an outer cylinder of radius b (the radius of the measurement cell). The numerical solution obtained can then be written in the form:-

$$\Delta T(a,t) = \Delta T_{id}(t) + \delta T_{ob}(t) + \delta T_R(t) \qquad \text{.....(3.8)}$$

subject to:-

$$b/a \gg 1 \qquad \text{..............................(3.9)}$$

and

$$kt/a^2 \gg 1 \qquad \text{..............................(3.10)}$$

The conditions, (3.9) and (3.10), on equation (3.8) are due to the restrictions imposed by the solutions of the problems involving finite boundaries (see § 2.322 and § 2.333), and are not imposed to obtain a solution for the correction due to radiation.

Having obtained a numerical solution, then using it in conjunction with equations (3.8), (2.14) and (2.85) the temperature rise correction for radiative heat transfer, $\delta T_R(t)$, can be obtained which in principle can be used to correct the observed temperature rises to the required idealised temperature for evaluation of the absolute thermal conductivity. The derivation of the governing equations; a detail of the method by which a numerical solution was obtained; as well as the use made of the numerical solution, now follows.

3.2 Derivations of the Equations

The formulation of the integro partial differential equation and relevant initial and boundary conditions for simultaneous radiative and conductive heat transfer through an absorbing medium bounded by concentric cylinders, is presented in this section.

The fundamental equations requiring solution have been made as general as possible and during their derivation, approximations have been used and detailed as and when required to enable their solution. This has been implemented to enable the further development of the method using the same technique if or when better approximations to the real physical system are available and required.

3.21 Energy balance over elemental volume dV_i

Consider an element of fluid dV_i within the annulus formed by fluid contained between two concentric cylinders (see fig.(3.1)). Let the inner (emitting) cylinder be of radius r_1 and the outer (receiving) cylinder be of radius r_2 and let both cylinders be infinite in length (no ends). Assume the fluid is isotropic, grey, diffusely emitting and non-scattering and its physical properties are temperature independent. Also assume; the system to be in a state of local thermodynamic equilibrium; the validity of Kirchhoff's Law for emission and absorption of radiated energy by the fluid medium and surfaces; and the additivity of conductive and radiative heat fluxes.

By using an energy balance over elemental volume, dV_i, within the fluid, we derive the equation:-

$$dV_i\,(\rho C_p)\,\frac{\partial T}{\partial t} = dV_i\,\lambda\nabla^2 T + Q_{V\rightleftharpoons dV_i}\,dV_i + Q_{A_1\rightleftharpoons dV_i}\,dV_i + Q_{A_2\rightleftharpoons dV_i}\,dV_i \quad ..(3.11)$$

Where the first term of equation (3.11) is due to conduction; the second, third and fourth terms account for the two way radiative transfer between dV_i, and; the rest of the fluid volume; the inner cylinder and the outer cylinder respectively. Equation (3.11) may be more conveniently written in terms of one way flux gradients by introducing the total outgoing radiative heat flux E_i in the form:-

$$\rho C_p\,\frac{\partial T}{\partial t} = \lambda\nabla^2 T + Q_{V\rightarrow dV_i} + Q_{A_1\rightarrow dV_i} + Q_{A_2\rightarrow dV_i} - 4K_i E_i \quad ....(3.12)$$

The second, third and fourth terms of equation (3.12) account for the one way transfer of radiation to dV_i by the fluid volume, the inner and the outer cylinders respectively and the final term accounts for the emission of radiation by dV_i to the surroundings (into 4π steradians). Subscript 'o' refers to equilibrium conditions; '1' and '2' refer to conditions at the inner and outer cylinder surfaces; i refers to conditions in the fluid at the position of volume element dV_i; and j refers to conditions in the fluid at the position of a second volume element dV_j.

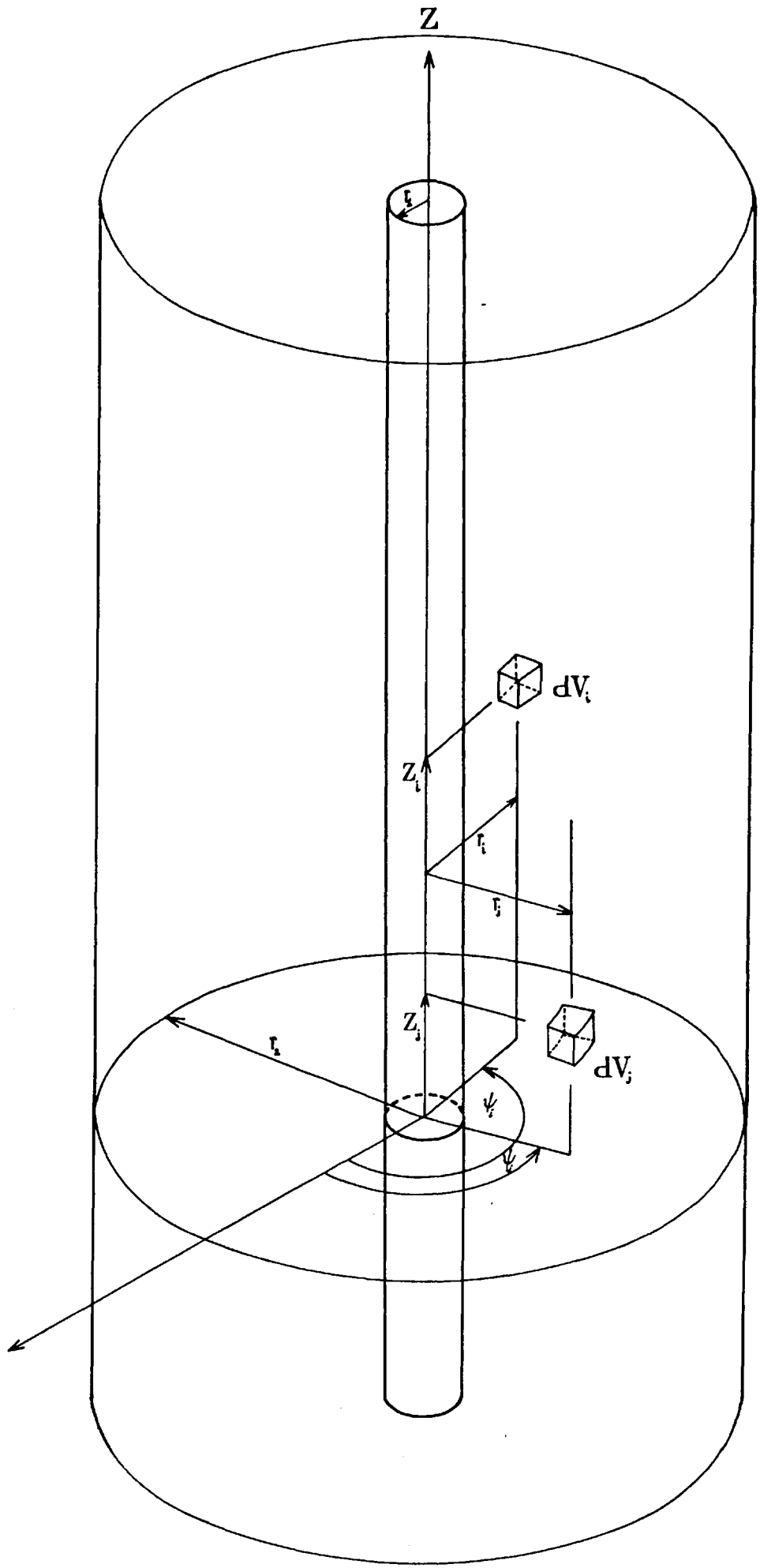

Fig. (3.1) The Cylindrical Polar Coordinate System

3.22 Boundary and Initial Conditions

For the solution of equation (3.12) which is parabolic in form, two boundary conditions and one initial condition are required. The first boundary condition is obtained via an energy balance at the surface of the inner, emitting cylinder.

Consider an element of surface dA_1 on the surface of the inner cylinder, then:-

$$\frac{dA_1 q}{2\pi r_1} = - dA_1 \lambda\left(\frac{\partial T}{\partial r}\right)_{r=r_1} + {}^{Q}dA_1 \rightleftharpoons A_2 \, dA_1 + {}^{Q}dA_1 \rightleftharpoons V \, dA_1 \quad \ldots\ldots\ldots(3.13)$$

$$\frac{q}{2\pi r_1} = - \lambda\left(\frac{\partial T}{\partial r}\right)_{r=r_1} - \alpha_1 {}^{Q}A_2 \rightarrow dA_1 - \alpha_1 {}^{Q}V \rightarrow dA_1 + \epsilon_1 n^2 \sigma T^4 \quad \ldots.(3.14)$$

where as before the second and third terms of equation (3.13) account for the two way transfer of radiation between the surface element dA_1 and the outer cylinder and between dA_1 and the fluid volume respectively. In equation (3.14) the second and third terms account for the one way transfer of radiation from the outer cylinder and fluid volume to surface element dA_1 while the last term accounts for radiative energy emitted from the surface element.**

The second boundary condition is imposed assuming the heat capacity and thermal conductivity of the outer cylinder to be infinite, and can be taken to remain at a constant temperature, therefore:-

$$T(r_2, 0 \leq t \leq \infty) = T(r_2) = T_o \quad \ldots\ldots\ldots\ldots\ldots(3.15)$$

**Note the difference between ${}^{Q}A_2 \rightarrow dA_1$ and ${}^{Q}A_2 \rightarrow dV_i$ (used earlier) which are notationally similar, but the former has dimensions of a a heat flux $\left[W/m^2\right]$ and the latter a flux gradient $\left[W/m^3\right]$.

which is exactly the condition imposed in obtaining the finite outer boundary correction in § 2.333 .

The initial condition used the stipulation that at $t \leq 0$ the system be at thermal equilibrium and therefore:-

$$T(r_1 \leq r \leq r_2, t \leq 0) = T_o \qquad \text{.....(3.16)}$$

3.23 Evaluation of terms due to radiative transfer

In order to solve equation (3.12) the one way transfer terms in equations (3.12) and (3.14) require evaluation and in the following subsection the results for each term are presented in turn. The more detailed algebra leading to final equations is placed in Appendix 1 to preserve continuity of the discussion.

3.231 The One-Way radiation heat fluxes

By considering the energy radiated from volume element dV_j to surface element dA_1 (see fig. (3.2)).

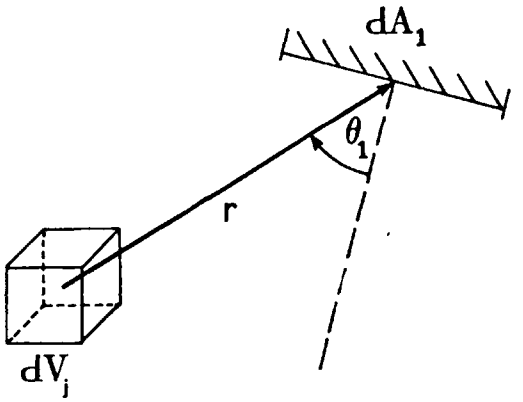

Fig. (3.2) Heat transfer between fluid volume and surface elements.

It may be shown that [78] :-

$$dQ_{dV_j \rightarrow dA_1} = \underbrace{E_j 4K_j \, dV_j}_{\text{emission by } dV_j \text{ into } 4\pi \text{ steradians}} \quad \underbrace{\frac{dA_1 \cos\theta_1}{4\pi r^2}}_{\text{fraction directed towards } dA_1} \quad \underbrace{\tau(r)}_{\text{fraction transmitted}} \qquad \text{.....(3.17)}$$

and so we find the heat flux $Q_{V \rightarrow dA_1}$ to be:-

$$Q_{V \rightarrow dA_1} = \int dQ_{dV_j \rightarrow dA_1} = \int_V \frac{E_j \tau(r) K_j \cos\theta_1}{\pi r^2} \, dV_j \qquad \text{.....(3.18)}$$

where $\tau(r) = \exp(-Kr)$ .....(3.19)

Consideration of the energy radiated from surface element dA_2 on the surface of the outer cylinder to dA_1 on the inner cylinder, see fig. (3.3),

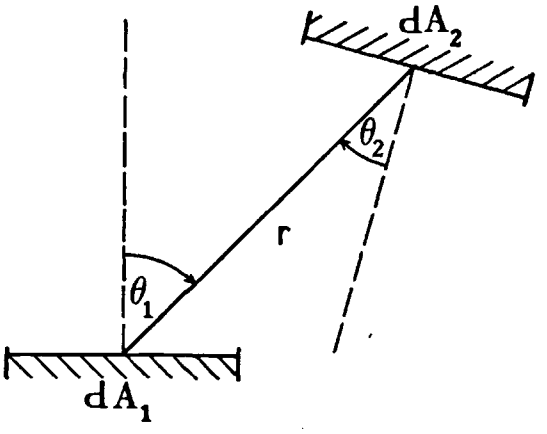

Fig. (3.3) Heat transfer between surface elements.

leads to the result that:-

$$dQ_{dA_2 \rightarrow dA_1}^{dA_1} = \underbrace{\frac{(E_2 + \tilde{R}_2)\, dA_2 \cos\theta_2}{\pi}}_{\text{emission by } dA_2 \text{ in direction } \theta_2 \text{ per unit solid angle}} \quad \underbrace{\frac{dA_1 \cos\theta_1}{r^2}}_{\text{solid angle subtended by } dA_1 \text{ at } dA_2} \quad \underbrace{\tau(r)}_{\text{fraction transmitted}} \qquad \text{.....(3.20)}$$

where $\tilde{R}_2$ is the fraction of the energy flux falling on surface dA_2 that is not absorbed. And therefore, the heat flux, $Q_{A_2 \rightarrow dA_1}$, is found as:-

$$Q_{A_2 \rightarrow dA_1} = \int dQ_{dA_2 \rightarrow dA_1} = \int_{A_2} \frac{(E_2 + \tilde{R}_2)\cos\theta_1 \cos\theta_2\, \tau(r) dA_2}{\pi r^2} \qquad \text{.....(3.21)}$$

3.232 The One-Way radiation heat flux gradients

From consideration of the energy radiated from fluid volume element dV_j to element dV_i (see fig. (3.4) we find that:-

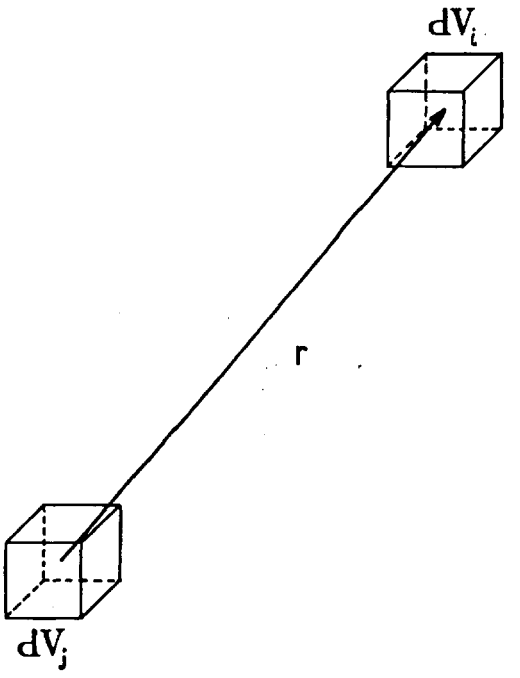

Fig. (3.4) Heat transfer between fluid volume elements.

$$dQ_{dV_j \rightarrow dV_i dV_i} = \frac{K_i K_j dV_i dV_j \tau(r) E_j}{\pi r^2} \qquad \text{.....(3.22)}$$

(see appendix 1.1)

and therefore the flux gradient $Q_{V \rightarrow dV_i}$ is obtained as:-

$$Q_{V \rightarrow dV_i} = \int dQ_{dV_j \rightarrow dV_i} = \int_V \frac{K_i K_j \tau(r) E_j dV_j}{\pi r^2} \qquad \text{.....(3.23)}$$

Similarly from the energy radiation from the surface element, dA_1, on the surface of the inner cylinder, to the fluid volume element dV_i (see fig. (3.5)) we find that:-

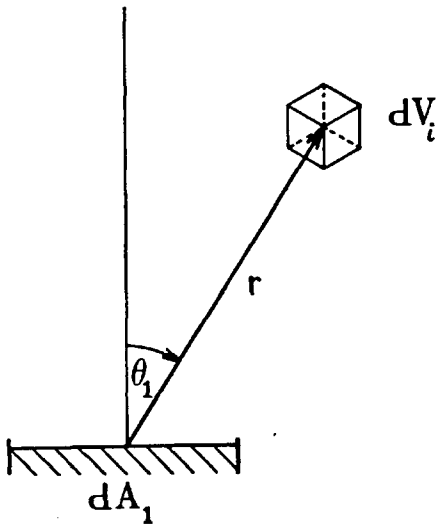

Fig. (3.5) Heat transfer between surface and fluid volume elements.

$$dQ_{dA_1 \rightarrow dV_i dV_i} = \frac{(E_1 + \tilde{R}_1)\, dA_1 \cos\theta_1\, dV_i\, \tau(r) K_i}{\pi r^2} \qquad \text{.....(3.24)}$$

and therefore obtain the flux gradient, $Q_{A_1 \rightarrow dV_i}$, as:-

$$Q_{A_1 \rightarrow dV_i} = \int dQ_{dA_1 \rightarrow dV_i} = \int_{A_1} \frac{K_i (E_1 + \tilde{R}_1)\cos\theta_1 \, \tau(r) dA_1}{\pi r^2} \qquad \text{.....(3.25)}$$

As before from the energy radiated from surface element, dA_1, on the surface of the inner cylinder, to fluid volume element dV_i we find immediately from equation (3.25) the flux gradient $Q_{A_2 \rightarrow dV_i}$ as:-

$$Q_{A_2 \rightarrow dV_i} = \int_{A_2} \frac{K_i (E_2 + \tilde{R}_2)\cos\theta_2 \, \tau(r) dA_2}{\pi r^2} \qquad \text{.....(3.26)}$$

Using these one way transfer terms in equations (3.12) and (3.14) enables their representation as:-

$$\rho C_p \frac{\partial T}{\partial t} = \lambda \nabla^2 T + \int_V \frac{K_i K_j \, \tau(r) E_j dV_j}{\pi r^2} + \int_{A_1} \frac{K_i (E_1 + \tilde{R}_1)\cos\theta_1 \, \tau(r) dA_1}{\pi r^2}$$

$$+ \int_{A_2} \frac{K_i (E_2 + \tilde{R}_2)\cos\theta_2 \, \tau(r) dA_2}{\pi r^2} - 4K_i E_i \qquad \text{.....(3.27)}$$

and the boundary condition as:-

$$\frac{q}{2\pi r_1} = -\lambda\left(\frac{\partial T}{\partial r}\right)_{r=r_1} - \alpha_1 \int_{A_2} \frac{(E_2 + \tilde{R}_2)\cos\theta_1\cos\theta_2\, \tau(r)dA_2}{\pi r^2}$$

$$- \alpha_1 \int_{V} \frac{E_j\, \tau(r)K_j\cos\theta_1 dV_j}{\pi r^2} + \epsilon_1 n^2\sigma T^4 \quad \ldots\ldots\ldots\ldots\ldots(3.28)$$

3.24 The Simplifying Approximations

In order to proceed certain approximations have been introduced which greatly simplify the solution of the simultaneous conduction and radiation problem, these are:-

1) The extinction coefficient is independent of the temperature of the fluid and therefore:-

$$K(r,t) = K = \text{Constant} \quad \ldots\ldots\ldots\ldots\ldots\ldots\ldots(3.29)$$

This approximation is used since it is in the spirit of a first order analysis and because the temperature differences involved are small ($\lesssim 5K$).

2) The outer cylinder surface is black and therefore:-

$$\epsilon_2 = \alpha_2 = 1 \quad \ldots\ldots\ldots\ldots\ldots\ldots\ldots(3.30)$$

resulting in:-

$$\tilde{R}_2 = 0 \quad \ldots\ldots\ldots\ldots\ldots\ldots\ldots(3.31)$$

and also:-

$$\tilde{R}_1 = (1 - \alpha_1) \left\{ Q_{V \rightarrow dA_1} + Q_{A_2 \rightarrow dA_1} \right\} \quad \text{.....(3.32)}$$

This approximation is thought to introduce a negligibly small error because near the outer cylinder's surface the fluid temperature is close to that at equilibrium and most of the energy radiated by the hot wire and fluid is absorbed before reaching the surface of the outer cylinder. If it is thought necessary the measurement cells used in the transient hot wire apparatus can be blackened to reduce this error but this has not been thought necessary for the present cell.

3) The absorbtivity and emissivity of the inner cylinder are equal and temperature independent and so:-

$$\epsilon_1 = \alpha_1 = \epsilon \quad \text{.....(3.33)}$$

Introducing the simplifying assumption in the one way radiative transfer terms we obtain:-

1) $$Q_{V \rightarrow dA_1} = \frac{K}{\pi} \int_V \frac{E_j \tau(r) \cos\theta_1 \, dV_j}{r^2} \quad \text{.....(3.34)}$$

2) $$Q_{A_2 \rightarrow dA_1} = \frac{1}{\pi} \int_{A_2} \frac{E_2 \cos\theta_1 \cos\theta_2 \, \tau(r) dA_2}{r^2} \quad \text{.....(3.35)}$$

3) $$Q_{V \rightarrow dV_i} = \frac{K^2}{\pi} \int_V \frac{E_j \tau(r) dV_j}{r^2} \quad \text{.....(3.36)}$$

$$4)\quad Q_{A_1 \rightarrow dV_i} = \frac{K}{\pi}\int_{A_1} \frac{\left[E_1 + (1-\epsilon)\left\{Q_{V \rightarrow dA_1} + Q_{A_2 \rightarrow dA_1}\right\}\right] \cos\theta_1\, \tau(r)\, dA_1}{r^2} \qquad \text{.....(3.37)}$$

$$5)\quad Q_{A_2 \rightarrow dV_i} = \frac{K}{\pi}\int_{A_2} \frac{E_2 \cos\theta_2\, \tau(r)\, dA_2}{r^2} \qquad \text{.....(3.38)}$$

Defining spherical coordinate axes with reference direction the normal to elemental area dA_1 on the surface of the inner cylinder and the reference plane parallel to the Z axis, normal to the reference direction and containing dA_1 (see fig. (3.6)).

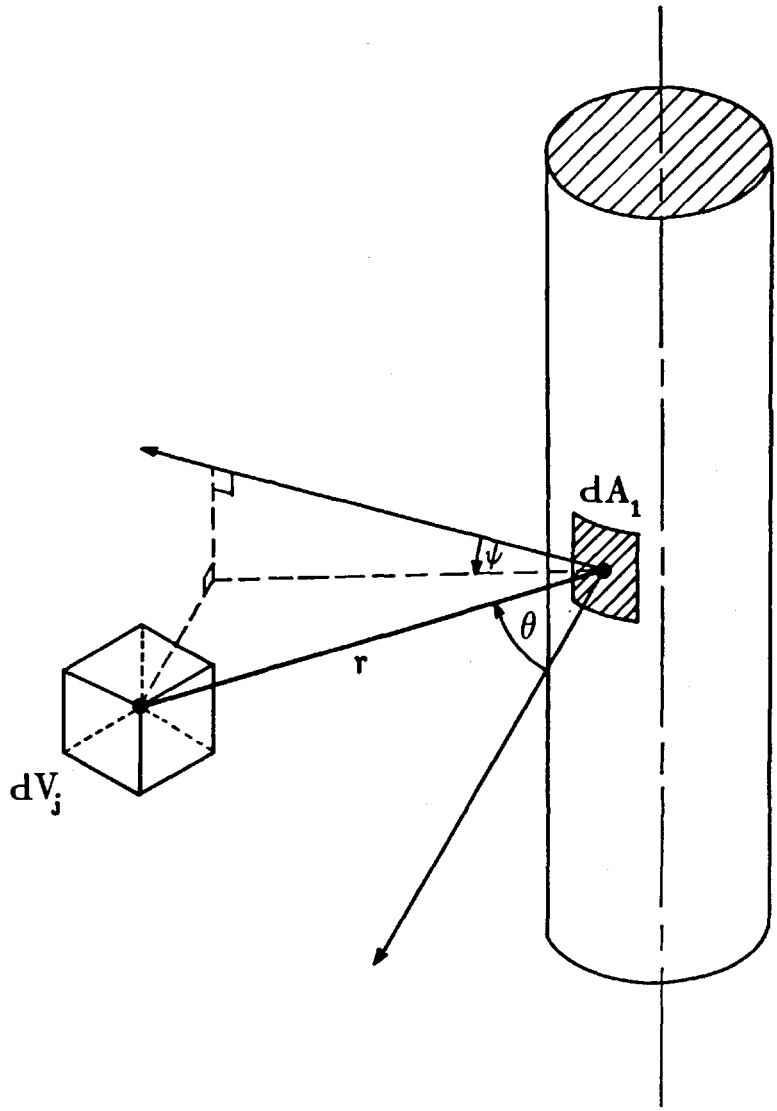

Fig. (3.6) Diagram defining spherical coordinates.

Equation (3.34) may now be written:-

$$Q_{V\rightarrow dA_1} = \frac{K}{\pi}\iiint_V \varepsilon_j\,\tau(r)\cos\theta_1\sin\theta_1\,d\theta_1\,d\psi\,dr \qquad \text{.....(3.39)}$$

In the cylindrical coordinate system about the axis through the centre of the inner cylinder and applying a shift in the azimuthal and vertical coordinates:-

$$\Phi = \psi_j - \psi_1 \;;\; Z = z_j - z_1 \qquad \text{.....(3.40)}$$

we then find (see appendix 1.2) that equation (3.39) may be written as:-

$$Q_{V\rightarrow dA_1} = \frac{K}{\pi}\iiint_V \frac{\varepsilon_j\,\tau(r)\cos\theta_1\sin\theta_1\,r_j\,dr_j\,d\Phi\,dZ}{r\sqrt{r_j^2\sin^2\Phi + Z^2}} \qquad \text{.....(3.41)}$$

$$= \frac{K}{\pi}\iiint_V \frac{\varepsilon_j(r_j\cos\Phi - r_1)r_j\exp(-Kr)\,dr_j\,d\Phi\,dZ}{r^3} \qquad \text{.....(3.42)}$$

$$= \frac{4K}{\pi}\int_0^{\infty}\int_0^{\cos^{-1}\left(\frac{r_1}{r_j}\right)}\int_{\frac{r_1}{\cos\Phi}}^{r_2} \frac{r_j\varepsilon_j(r_j\cos\Phi - r_1)\exp(-Kr)\,dr_j\,d\Phi\,dZ}{r^3} \qquad \text{.....(3.43)}$$

or finally:-

$$Q_{V\rightarrow dA_1} = \frac{4K}{\pi}\int_0^{\infty}\int_{r_1}^{r_2}\int_0^{\cos^{-1}\left(\frac{r_1}{r_j}\right)} \frac{r_j\varepsilon_j(r_j\cos\Phi - r_1)\exp(-Kr)\,d\Phi\,dr_j\,dZ}{r^3} \qquad \text{.....(3.44)}$$

where:-

$$r = \sqrt{r_j^2 + r_1^2 - 2r_1r_j\cos\Phi + Z^2} \qquad \text{.....(3.45)}$$

The limits of integration are indicated in fig. (3.7) where the integral occurs over the shaded volume.

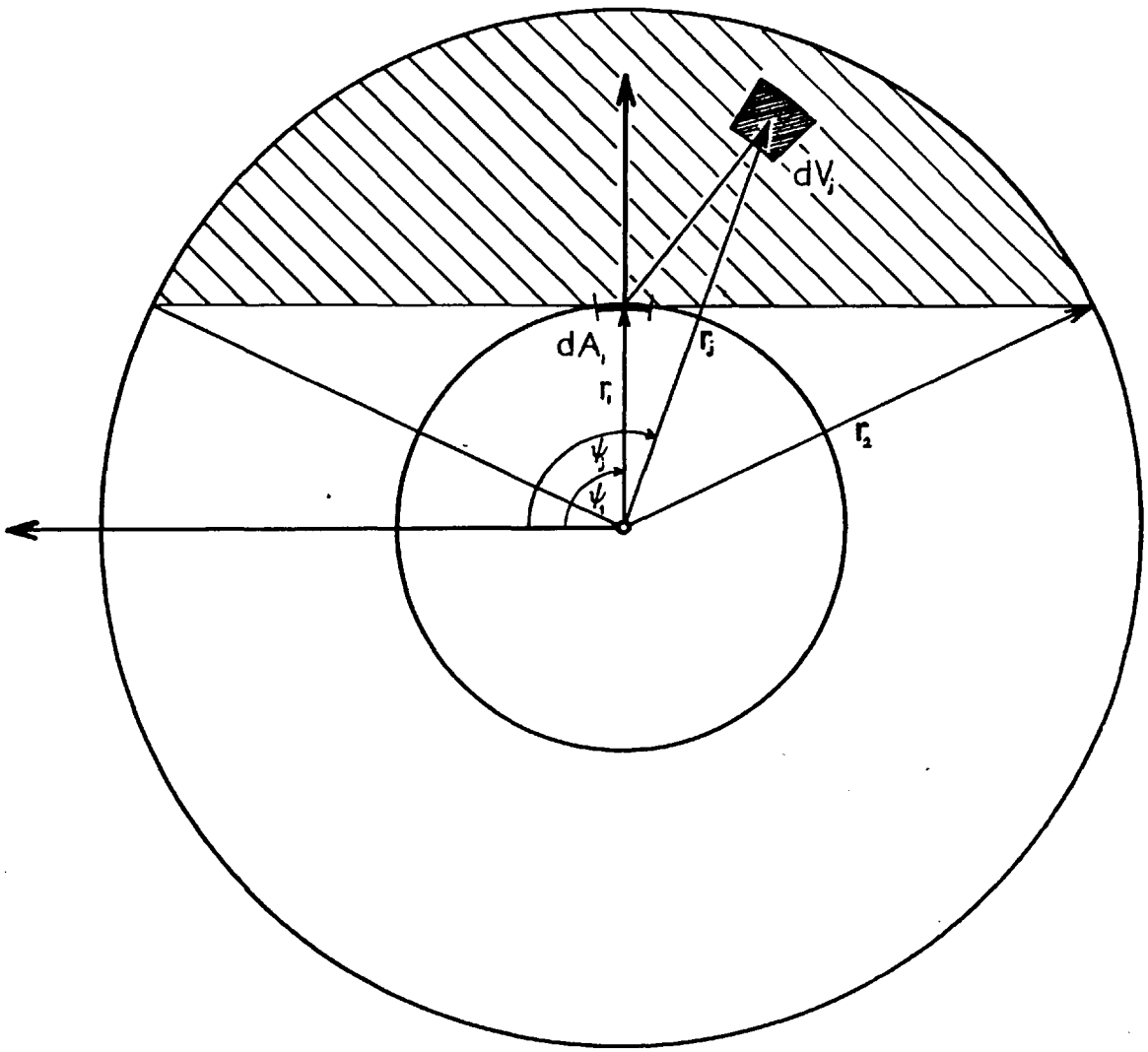

Fig. (3.7) Diagram indicating integration limits for $Q_{V\rightarrow dA_1}$

In a similar manner to that used to evaluate $Q_{V\rightarrow dA_1}$ we find that:-

$$Q_{A_2\rightarrow dA_1} = \frac{E_2 r_2}{\pi} \iint_{A_2} \frac{\cos\theta_1 \cos\theta_2 \exp(-Kr)\, d\psi_2 dZ_2}{r^2} \qquad \text{.....(3.46)}$$

In the shifted cylindrical polar coordinates about the centre of the inner cylinder with:-

$$\Phi = \psi_2 - \psi_1 \; ; \; Z = z_2 - z_1 \qquad \text{.....(3.47)}$$

we may write:-

$$Q_{A_2 \rightarrow dA_1} = \frac{E_2 r_2}{\pi} \iint_{A_2} \frac{(r_2 \cos\Phi - r_1)(r_2 - r_1 \cos\Phi)\exp(-Kr)\,d\Phi\,dZ}{r^4}$$

$$\text{.....(3.48)}$$

$$= \frac{4E_2 r_2}{\pi} \int_0^{\infty} \int_0^{\cos^{-1}\left(\frac{r_1}{r_2}\right)} \frac{(r_2 \cos\Phi - r_1)(r_2 - r_1 \cos\Phi)\exp(-Kr)\,d\Phi\,dZ}{r^4}$$

$$\text{.....(3.49)}$$

where:-

$$r = \sqrt{r_2^2 + r_1^2 - 2r_1 r_2 \cos\Phi + Z^2} \qquad \text{.....(3.50)}$$

and integration occurs over the area indicated in fig. (3.8).

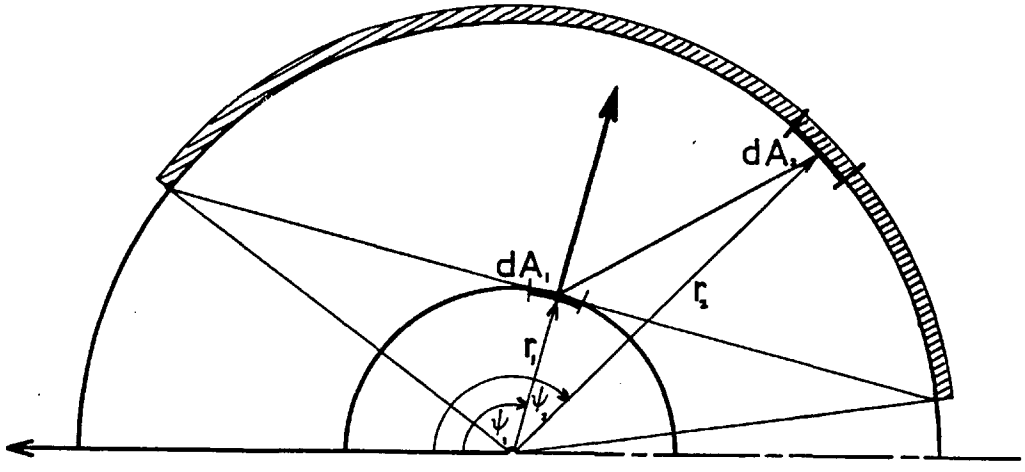

Fig. (3.8) Diagram indicating integration limits for $Q_{A_2 \rightarrow dA_1}$

Defining spherical polar coordinates around dV_i, equation (3.36) may be written in the form:-

$$Q_{V\rightarrow dV_i} = \frac{K^2}{\pi}\iiint_V E_j\,\tau(r)\sin\theta\,d\theta\,d\psi\,dr \qquad \text{.....(3.51)}$$

Now, by a transformation to cylindrical polar coordinates about the axis through the centre of the inner cylinder and using the shift:-

$$\Phi = \psi_j - \psi_i \;;\; Z = z_j - z_i \qquad \text{.....(3.52)}$$

it follows that:- (see appendix 1.2)

$$Q_{V\rightarrow dV_i} = \frac{K^2}{\pi}\iiint_V \frac{E_j\,\tau(r)\sin\theta\,r_j\,dr_j\,d\Phi\,dZ}{r\sqrt{r_j^2\sin^2\Phi + Z^2}} \qquad \text{.....(3.53)}$$

$$= \frac{4K^2}{\pi}\int_0^{\infty}\int_0^{\cos^{-1}\left(\frac{r_1}{r_i}\right)}\int_{r_1}^{r_2}\frac{E_j\,r_j\exp(-Kr)\,dr_j\,d\Phi\,dZ}{r^2}$$

$$+ \frac{4K^2}{\pi}\int_0^{\infty}\int_{\cos^{-1}\left(\frac{r_1}{r_i}\right)}^{\cos^{-1}\left(\frac{r_1}{r_i}\right)+\cos^{-1}\left(\frac{r_1}{r_2}\right)}\int_{\frac{r_1}{\cos\left[\Phi-\cos^{-1}\left(\frac{r_1}{r_i}\right)\right]}}^{r_2}\frac{E_j\,r_j\exp(-Kr)\,dr_j\,d\Phi\,dZ}{r^2} \qquad \text{.....(3.54)}$$

or finally:-

$$Q_{V\rightarrow dV_i} = \frac{4K^2}{\pi}\int_0^{\infty}\int_{r_1}^{r_2}\int_0^{\cos^{-1}\left(\frac{r_1}{r_i}\right)+\cos^{-1}\left(\frac{r_1}{r_j}\right)}\frac{E_j\,r_j\exp(-Kr)\,d\Phi\,dr_j\,dZ}{r^2}$$

.....(3.55)

where:-

$$r = \sqrt{r_j^2 + r_i^2 - 2r_i r_j \cos\Phi + Z^2} \qquad \text{.....(3.56)}$$

The limits of integration are indicated in fig.(3.9) in which the integration occurs over the shaded volume.

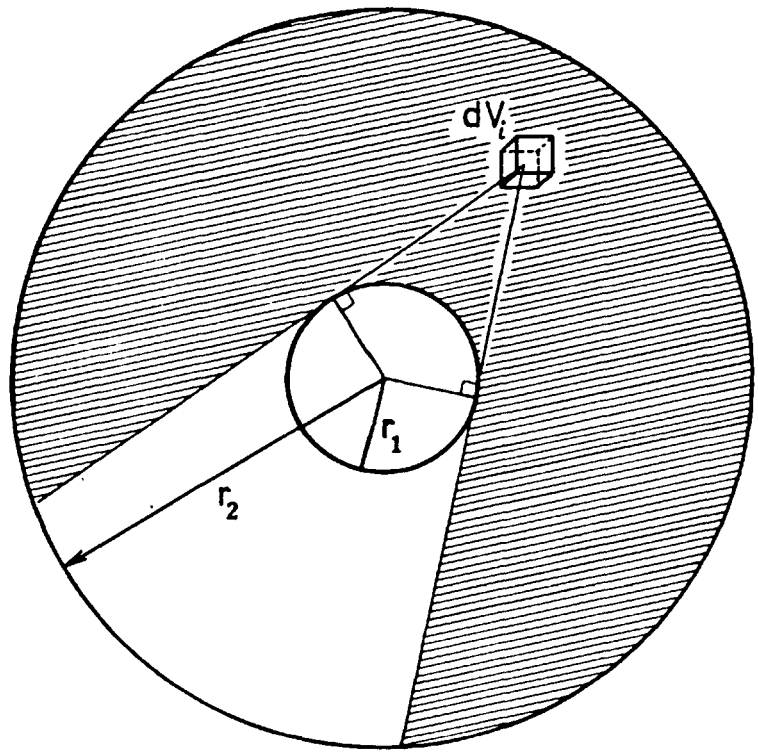

Fig. (3.9) Diagram indicating integration limits for $Q_{V\rightarrow dV_i}$

Using a similar technique to that used to obtain $Q_{V\rightarrow dV_i}$ from equation (3.37) we obtain the expression for $Q_{A_1\rightarrow dV_i}$ as:-

$$Q_{A_1\rightarrow dV_i} = \frac{K}{\pi}\left[E_1 + (1-\epsilon)\left\{Q_{V\rightarrow dA_1} + Q_{A_2\rightarrow dA_1}\right\}\right] r_1 \iint_{A_1} \frac{\cos\theta_1\, \tau(r)\, d\psi_1\, dZ_1}{r^2}$$

.....(3.57)

In cylindrical polar coordinates about the axis through the centre of the inner cylinder, using the shift in azimuthal and vertical coordinates:-

$$\Phi = \psi_1 - \psi_i \quad ; \quad Z = z_1 - z_i \qquad \text{.....(3.58)}$$

we obtain:-

$$Q_{A_1 \rightarrow dV_i} = \frac{Kr_1}{\pi}\left[E_1+(1-\epsilon)\left\{Q_{V\rightarrow dA_1} + Q_{A_2\rightarrow dA_1}\right\}\right]\iint_{A_1}\frac{(r_i\cos\Phi - r_1)\exp(-Kr)d\Phi\ dZ}{r^3}$$

$$\text{.....(3.59)}$$

$$= \frac{4Kr_1}{\pi}\left[E_1+(1-\epsilon)\left\{Q_{V\rightarrow dA_1} + Q_{A_2\rightarrow dA_1}\right\}\right]\int_0^{\infty}\int_0^{\cos^{-1}\left(\frac{r_1}{r_i}\right)}\frac{(r_i\cos\Phi - r_1)\exp(-Kr)d\Phi\ dZ}{r^3}$$

$$\text{.....(3.60)}$$

where:-

$$r = \sqrt{r_i^{\,2} + r_1^{\,2} - 2r_i r_1\cos\Phi + Z^2} \qquad \text{.....(3.61)}$$

The limits of integration are indicated in fig. (3.10) in which integration occurs over the indicated surface.

Finally, from equation (3.38) we find that:-

$$Q_{A_2\rightarrow dV_i} = \frac{K}{\pi}E_2 r_2\iint_{A_2}\frac{\cos\theta_2\,\tau(r)d\psi_2 dZ_2}{r^2} \qquad \text{.....(3.62)}$$

$$= \frac{4K}{\pi}E_2 r_2\int_0^{\infty}\int_0^{\cos^{-1}\left(\frac{r_1}{r_i}\right)+\cos^{-1}\left(\frac{r_1}{r_2}\right)}\frac{(r_2 - r_i\cos\Phi)\exp(-Kr)d\Phi\ dZ}{r^3}$$

$$\text{.....(3.63)}$$

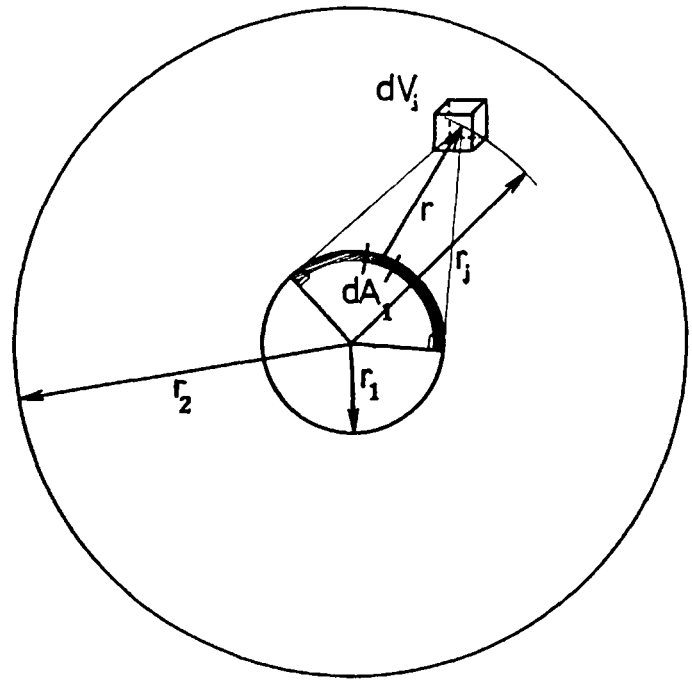

Fig. (3.10) Diagram indicating integration limits for $Q_{A_1 \rightarrow dV_i}$

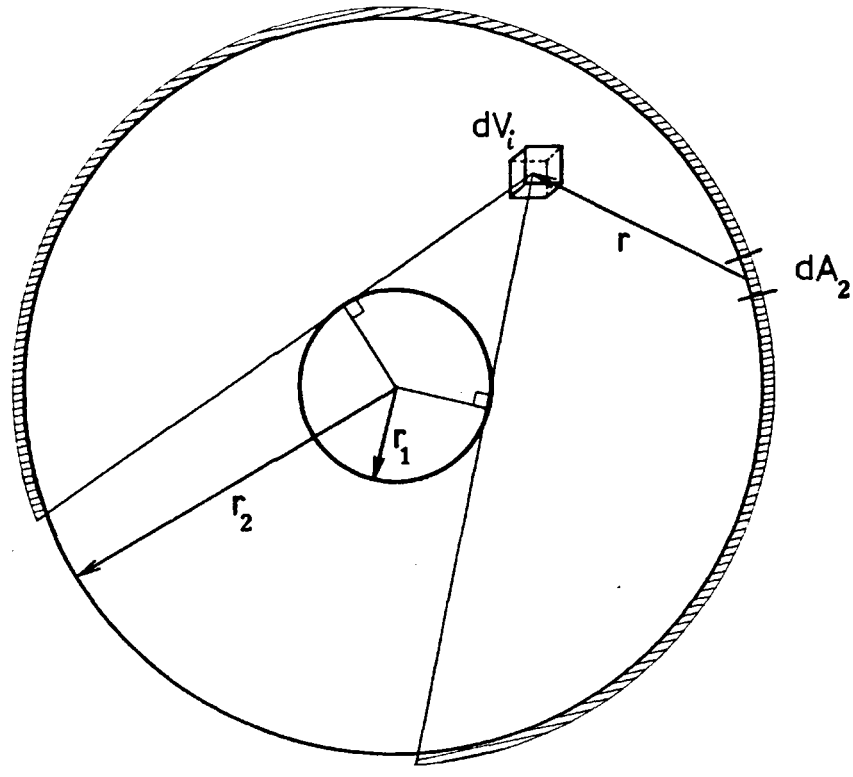

Fig. (3.11) Diagram indicating integration limits for $Q_{A_2 \rightarrow dV_i}$

where:-

$$r = \sqrt{r_i^2 + r_2^2 - 2r_i r_2 \cos\Phi + Z^2} \qquad \text{.....(3.64)}$$

The limits of integration are indicated in fig. (3.11) in which, once more, integration occurs over the indicated surface.

3.25 The Integro-Partial Differential Equation

Using the derived integral forms of the one way radiative transfer terms, $Q_{V\rightarrow dA_1}$, $Q_{A_2\rightarrow dA_1}$, $Q_{V\rightarrow dV_i}$, $Q_{dA_1\rightarrow dV_i}$, & $Q_{dA_2\rightarrow dV_i}$ in equations (3.12) and (3.14), results in the approximate integro-partial differential equation for simultaneous conductive and radiative heat transfer between concentric cylinders, containing an absorbing, emitting, non scattering grey medium. The equation is therefore:-

$$\rho C_p \frac{\partial T}{\partial t}(r_i,t) = \nabla^2 T(r_i,t) + Q_{V\rightarrow dV_i} + Q_{A_1\rightarrow dV_i} + Q_{A_2\rightarrow dV_i} - 4Kn^2\sigma T^4$$

.....(3.65)

with boundary conditions:-

1) $$\frac{q}{2\pi r_1} = -\lambda\left(\frac{\partial T}{\partial r}\right)_{r=r_1} - \epsilon Q_{V\rightarrow dA_1} - \epsilon Q_{A_2\rightarrow dA_1} + \epsilon n^2\sigma T^4 \qquad \text{.....(3.66)}$$

2) $$T(r_2, 0\leq t\leq\infty) = T_o \qquad \text{.....(3.67)}$$

and initial condition:-

$$T(r_1\leq r\leq r_2, t\leq 0) = T_o \qquad \text{.....(3.68)}$$

where:-

$$Q_{V\rightarrow dA_1} = \frac{4Kn^2\sigma}{\pi}\int_0^{\infty}\int_{r_1}^{r_2}\int_0^{\cos^{-1}\left(\frac{r_1}{r_j}\right)} \frac{r_j T(r_j,t)^4 (r_j\cos\phi - r_1)\exp(-Kr_a)}{r_a^3}\, d\phi\, dr_j\, dZ$$

.....(3.69)

$$Q_{A_2\rightarrow dA_1} = \frac{4r_2 n^2\sigma T(r_2,t)^4}{\pi}\int_0^{\infty}\int_0^{\cos^{-1}\left(\frac{r_1}{r_2}\right)} \frac{(r_2\cos\phi - r_1)(r_2 - r_1\cos\phi)\exp(-Kr_b)}{r_b^4}\, d\phi\, dZ$$

.....(3.70)

$$Q_{V\rightarrow dV_i} = \frac{4K^2n^2\sigma}{\pi}\int_0^{\infty}\int_{r_1}^{r_2}\int_0^{\cos^{-1}\left(\frac{r_1}{r_i}\right)+\cos^{-1}\left(\frac{r_1}{r_j}\right)} \frac{T(r_j,t)^4 r_j \exp(-Kr_c)}{r_c^2}\, d\phi\, dr_j\, dZ$$

.....(3.71)

$$Q_{A_1\rightarrow dV_i} = \frac{4Kr_1}{\pi}\left[E_1 + (1-\epsilon)\left\{Q_{V\rightarrow dA_1} + Q_{A_2\rightarrow dA_1}\right\}\right]\int_0^{\infty}\int_0^{\cos^{-1}\left(\frac{r_1}{r_i}\right)} \frac{(r_i\cos\phi - r_1)}{r_d^3} \times$$

$$\times \exp(-Kr_d)\, d\phi\, dZ \qquad .....(3.72)$$

$$Q_{A_2\rightarrow dV_i} = \frac{4Kr_2 n^2\sigma T(r_2,t)^4}{\pi}\int_0^{\infty}\int_0^{\cos^{-1}\left(\frac{r_1}{r_i}\right)+\cos^{-1}\left(\frac{r_1}{r_2}\right)} \frac{(r_2 - r_i\cos\phi)\exp(-Kr_e)}{r_e^3}\, d\phi\, dZ$$

and:- .....(3.73)

$$r_a = \sqrt{r_j^2 + r_1^2 - 2r_1 r_j\cos\phi + Z^2} \qquad .....(3.74)$$

$$r_b = \sqrt{r_2^2 + r_1^2 - 2r_1 r_2\cos\phi + Z^2} \qquad .....(3.75)$$

$$r_c = \sqrt{r_j^2 + r_i^2 - 2r_i r_j\cos\phi + Z^2} \qquad .....(3.76)$$

$$r_d = \sqrt{r_1^2 + r_i^2 - 2r_1 r_i \cos\phi + Z^2} \qquad \ldots\ldots\ldots\ldots(3.77)$$

$$r_e = \sqrt{r_2^2 + r_i^2 - 2r_2 r_i \cos\phi + Z^2} \qquad \ldots\ldots\ldots\ldots(3.78)$$

3.3 Transformation of the Equations for Numerical Solution

The integro partial differential equation derived in the previous section and detailed in equations (3.65) to (3.78) is parabolic, non linear and has as yet no analytical solution. For the reasons discussed in § 3.1 approximate solutions based on optical thicknesses are thought to be too far removed from the real physical situation. Thus, the only alternatives remaining are to find some other method of accounting for the error to the measured temperature rises induced by radiative heat transfer or to solve the equations numerically. As an alternative method for accounting for the error has not as yet been found the numerical solution approach must be adopted.

Before a numerical solution can be attempted, equations (3.65) to (3.78) are normalised and the terms requiring integration are transformed into converging series (mechanical quadrature). This section details these operations.

3.31 Normalisation and use of Quadratures

Defining the dimensionless forms of the fluid temperature and position

$$\Theta = \frac{T}{T_o} \qquad R = \frac{r}{r_1} \qquad \ldots\ldots\ldots\ldots\ldots\ldots(3.79)$$

The equation of heat transfer becomes:-

$$\frac{\partial\Theta}{\partial t} = \frac{\lambda}{\rho C_p r_1^2}\left[\frac{\partial^2\Theta}{\partial R^2} + \frac{1}{R}\frac{\partial\Theta}{\partial R}\right] + \frac{1}{T_o \rho C_p}\left[Q_{V\rightarrow dV_i} + Q_{A_1\rightarrow dV_i} + Q_{A_2\rightarrow dV_i} - 4Kn^2\sigma T_o^4 \Theta(R_i)^4\right] \qquad \ldots\ldots\ldots\ldots(3.80)$$

with boundary conditions:-

$$\frac{q}{2\pi T_o} = -\lambda\left(\frac{\partial\Theta}{\partial R}\right)_{R=1} - \frac{\epsilon r_1}{T_o}\left[Q_{V\rightarrow dA_1} + Q_{A_2\rightarrow dA_1}\right] + \epsilon n^2\sigma r_1 T_o^{\,3}\Theta(1)^4 \qquad \text{.....(3.81)}$$

$$\Theta(R_2, 0\leqslant t\leqslant\infty) = 1 \qquad \text{.....(3.82)}$$

and initial condition:-

$$\Theta(1\leqslant R\leqslant R_2, t\leqslant 0) = 1 \qquad \text{.....(3.83)}$$

In these equations:-

$$Q_{V\rightarrow dA_1} = \frac{4n^2\sigma K T_o^{\,4}}{\pi}\underset{C_1\rightarrow\infty}{\text{Lim}}\int_0^{C_1}\int_1^{R_2}\int_0^{\cos^{-1}\left(\frac{1}{R_j}\right)}\frac{R_j\Theta(R_j)^4\left[R_j\cos\phi - 1\right]}{R_a^{\,3}} \times$$

$$\times \exp(-KR_a r_1)\,d\phi\, dR_j dZ \qquad \text{....(3.84)}$$

which through changing the limits of integration using:-

$$2Z = C_1 M + C_1 \qquad \text{.....(3.85)}$$

can be written as:-

$$Q_{V\rightarrow dA_1} = \underset{C_1\rightarrow\infty}{\text{Lim}}\frac{2n^2\sigma K T_o^{\,4} C_1}{\pi}\int_{-1}^{1}\int_1^{R_2}\int_0^{\cos^{-1}\left(\frac{1}{R_j}\right)} f_1\left\{\phi, R_j, \frac{C_2 M + C_1}{2}\right\} d\phi\, dR_j dM$$

$$\text{.....(3.86)}$$

By employing the Gaussian Quadrature formula [79]:-

$$\int_{-1}^{1} f(x)dx = \sum_{j=1}^{n} H_j f(a_j) \qquad \text{.....(3.87)}$$

where a_j are the abscisae and H_j are the weighting coefficients, equation (3.86) becomes:-

$$Q_{V\rightarrow dA_1} = \lim_{\substack{C_1\rightarrow\infty \\ n_1\rightarrow\infty}} \frac{2n^2\sigma KT_o{}^4C_1}{\pi} \sum_{j=1}^{n_1} H_j \int_1^{R_2}\int_0^{\cos^{-1}\frac{1}{R_j}} f_1\left\{\phi, R_j, \frac{C_1a_j + C_1}{2}\right\} d\phi\, dR_j \qquad \ldots\ldots\ldots(3.88)$$

Similarly using:-

$$2R_j = (R_2 - 1)N + R_2 + 1 \qquad \ldots\ldots\ldots(3.89)$$

as before we obtain:-

$$Q_{V\rightarrow dA_1} = \lim_{\substack{C_1\rightarrow\infty \\ n_1\rightarrow\infty \\ n_2\rightarrow\infty}} \frac{2n^2\sigma KT_o{}^4C_1}{\pi} \sum_{j=1}^{n_1} \frac{H_j(R_2-1)}{2} \sum_{k=1}^{n_2} H_k \times \int_0^{\cos^{-1}\left(\frac{2}{(R_2-1)a_k+R_2+1}\right)} f_1\left\{\phi, \frac{(R_2-1)a_k+R_2+1}{2}, \frac{C_1a_j+C_1}{2}\right\} d\phi \qquad \ldots\ldots\ldots(3.90)$$

and finally:-

$$Q_{V\rightarrow dA_1} = \lim_{\substack{C_1\rightarrow\infty \\ n_1,n_2,n_3\rightarrow\infty}} \frac{2n^2\sigma KT_o{}^4C_1}{\pi} \sum_{j=1}^{n_1} \frac{H_j(R_2-1)}{2} \sum_{k=1}^{n_2} \frac{H_k\cos^{-1}\left(\frac{2}{(R_2-1)a_k+R_2+1}\right)}{2} \times \sum_{l=1}^{n_3} H_l g_1(a_l, a_k, a_j) \qquad \ldots\ldots\ldots(3.91)$$

where:-

$$g_1(a_1,a_k,a_j)= f_1\left\{\frac{\left[\cos^{-1}\left(\frac{2}{(R_2-1)a_k+R_2+1}\right)\right]a_1+\cos^{-1}\left(\frac{2}{(R_2-1)a_k+R_2+1}\right)}{2}, \frac{(R_2-1)a_k+R_2+1}{2}, \frac{C_1 a_j+C_1}{2}\right\}$$

.....(3.92)

$$f_1(\phi,R_j,Z) = \frac{R_j\Theta(R_j)^4(R_j\cos\phi -1)\exp(-KR_a r_1)}{R_a^3} \quad .....(3.93)$$

and:-

$$R_a = \sqrt{R_j^2 + 1 - 2R_j\cos\phi + (Z/r_1)^2} \quad .....(3.94)$$

In a similar manner equation (3.70) becomes:-

$$Q_{A_2\rightarrow dA_1} = \lim_{\substack{C_2\rightarrow\infty \\ n_1,n_2\rightarrow\infty}} \frac{2R_2 n^2\sigma T_o^4\Theta(R_2)^4 C_2}{\pi r_1}\sum_{j=1}^{n_1}\frac{H_j\cos^{-1}\left(\frac{1}{R_2}\right)}{2}\sum_{k=1}^{n_2} H_k g_2(a_1,a_k) \quad ...(3.95)$$

where:-

$$g_2(a_1,a_k) = f_2\left\{\frac{\left[\cos^{-1}\left(\frac{1}{R_2}\right)\right]a_k + \cos^{-1}\left(\frac{1}{R_2}\right)}{2}, \frac{C_2 a_j + C_2}{2}\right\} \quad .....(3.96)$$

$$f_2(\phi,Z) = \frac{(R_2\cos\phi -1)(R_2-\cos\phi)\exp(-Kr_1R_b)}{R_b^4} \quad .....(3.97)$$

and:-

$$R_b = \sqrt{R_2^2 + 1 - 2R_2\cos\phi + (Z/r_1)^2} \quad .....(3.98)$$

Likewise, equation (3.71) can be transformed to:-

$$Q_{V\rightarrow dV_i} = \lim_{\substack{C_3\rightarrow\infty \\ n_1,n_2,n_3\rightarrow\infty}} \frac{2K^2n^2\sigma T_o^4 C_3}{\pi}\sum_{j=1}^{n_1}\frac{H_j(R_2-1)}{2}\sum_{k=1}^{n_2}\frac{H_k\left[\cos^{-1}\left(\frac{1}{R_i}\right)+\cos^{-1}\left(\frac{2}{(R_2-1)a_k+R_2+1}\right)\right]}{2} \times$$

$$\times \sum_{l=1}^{n_3} H_l g_3(a_l,a_k,a_j) \quad \ldots\ldots\ldots(3.99)$$

where:-

$$g_3(a_l,a_k,a_j) = f_3\left\{\frac{\left[\cos^{-1}\left(\frac{1}{R_i}\right)+\cos^{-1}\left(\frac{2}{(R_2-1)a_k+R_2+1}\right)\right]a_l+\cos^{-1}\left(\frac{1}{R_i}\right)+\cos^{-1}\left(\frac{2}{(R_2-1)a_k+R_2+1}\right)}{2},\right.$$

$$\left.\frac{(R_2-1)a_k+R_2+1}{2},\ \frac{C_3a_j+C_3}{2}\right\} \quad \ldots\ldots\ldots\ldots\ldots\ldots(3.100)$$

$$f_3(\phi,R_j,Z) = \frac{\Theta(R_j)^4 R_j \exp(-Kr_1R_C)}{R_C^2} \quad \ldots\ldots\ldots\ldots\ldots\ldots(3.101)$$

and:-

$$R_C = \sqrt{R_j^2 + R_i^2 - 2R_jR_i\cos\phi + (Z/r_1)^2} \quad \ldots\ldots\ldots(3.102)$$

Also, transforming equation (3.72) we obtain:-

$$Q_{A_1\rightarrow dV_i} = \lim_{\substack{C_4\rightarrow\infty \\ n_1,n_2\rightarrow\infty}} B_1\sum_{j=1}^{n_1}\frac{H_j\cos^{-1}\left[\frac{1}{R_i}\right]}{2}\sum_{k=1}^{n_2}H_k g_4(a_k,a_j) \quad \ldots\ldots\ldots(3.103)$$

where:-

$$g_4(a_k, a_j) = f_4\left\{\frac{\left[\cos^{-1}\left[\frac{1}{R_i}\right]\right]a_k + \cos^{-1}\left[\frac{1}{R_i}\right]}{2}, \frac{C_4 a_j + C_4}{2}\right\} \quad \text{.....(3.104)}$$

$$B_1 = \frac{2KC_4\left\{\epsilon n^2 \sigma T_o{}^4 \Theta(1)^4 + (1-\epsilon)\left[Q_{V\rightarrow dA_1} + Q_{A_2\rightarrow dA_1}\right]\right\}}{r_1 \pi} \quad \text{.....(3.105)}$$

$$f_4(\phi, Z) = \frac{(R_i \cos\phi - 1)\exp(-KR_d r_1)}{R_d{}^3} \quad \text{.....(3.106)}$$

and:-

$$R_d = \sqrt{R_i{}^2 + 1 - 2R_i \cos\phi + (Z/R_1)^2} \quad \text{.....(3.107)}$$

Finally, equation (3.73) can be transformed to:-

$$Q_{A_2\rightarrow dV_i} = \lim_{\substack{C_5\rightarrow\infty \\ n_1, n_2\rightarrow\infty}} \frac{2Kn^2\sigma T_o{}^4 \Theta(R_2)^4 R_2}{\pi r_1} \sum_{j=1}^{n_1} H_j \frac{\cos^{-1}\left[\frac{1}{R_i}\right] + \cos^{-1}\left[\frac{1}{R_2}\right]}{2} \sum_{k=1}^{n_2} g_5(a_k, a_j)$$

.....(3.108)

where:-

$$g_5(a_k, a_j) = f_5\left\{\frac{\left\{\cos^{-1}\left[\frac{1}{R_i}\right] + \cos^{-1}\left[\frac{1}{R_2}\right]\right\}a_k + \cos^{-1}\left[\frac{1}{R_i}\right] + \cos^{-1}\left[\frac{1}{R_2}\right]}{2}, \frac{C_5 a_j + C_5}{2}\right\}$$

.....(3.109)

$$f_5(\phi,Z) = \frac{(R_2 - R_i\cos\phi)\exp(-Kr_1R_e)}{R_e^3} \qquad \text{.....(3.110)}$$

and:-

$$R_e = \sqrt{R_2^2 + R_i^2 - 2R_2R_i\cos\phi + \left[\frac{Z}{r_1}\right]^2} \qquad \text{.....(3.111)}$$

3.32 Linearisation of Equations

As presented in the previous section, the integro-partial differential equation is non linear and requires a routine that is able to solve non linear partial differential equations. Routines of this type are available but require significantly more computing time to solve non linear partial differential equations than linear equations, as additional itterations over the non linear terms are often required. For this reason and because the temperature rise during experiments is less than 2% of the equilibrium absolute temperature, T_o , before implementing the previous derived equations they are first linearised. This approach is again consistent with the attempt at a first order treatment of the problem.

Linearisation is performed using:-

$$\Theta = \frac{T - T_o}{T_o} = \frac{\Delta T}{T_o} = \Theta - 1 \qquad \text{.....(3.112)}$$

The energy balance equation from equation (3.80) becomes:-

$$\frac{\partial\Theta}{\partial t} = \frac{\lambda}{\rho C_p r_1^2}\left[\frac{\partial^2\Theta}{\partial R^2} + \frac{1}{R}\frac{\partial\Theta}{\partial R}\right] + \frac{1}{\rho C_p T_o}\left[\tilde{Q}_{V\rightarrow dV_i} + \tilde{Q}_{A_1\rightarrow dV_i} + \tilde{Q}_{A_2\rightarrow dV_i} - 16Kn^2\sigma T^4\Theta(R_i)\right]$$

.....(3.113)

With boundary conditions:-

$$\text{i)}\quad \frac{q}{2\pi T_o} = -\lambda\left(\frac{\partial\Theta}{\partial R}\right)_{R=1} - \frac{\epsilon r_1}{T_o}\left[\tilde{Q}_{A_2\rightarrow dA_1} + \tilde{Q}_{V\rightarrow dA_1}\right] + 4\epsilon n^2\sigma r_1 T_o^3\Theta(1) \qquad \text{.....(3.114)}$$

$$\text{ii)}\quad \Theta(R_2, 0\leqslant t\leqslant\infty) = 0 \qquad \text{.....(3.115)}$$

and initial condition:-

$$\Theta(1\leqslant R\leqslant R_2, t\leqslant 0) = 0 \qquad \text{.....(3.116)}$$

The linearised one way perturbation heat fluxes are now:-

$$\tilde{Q}_{V\rightarrow dA_1} = \lim_{\substack{C_1\rightarrow\infty \\ n_1,n_2,n_3\rightarrow\infty}} \frac{8n^2\sigma K T_o^4 C_1}{\pi}\sum_{j=1}^{n_1}\frac{H_j(R_2-1)}{2}\sum_{k=1}^{n_2}\frac{H_k\cos^{-1}\left[\frac{2}{(R_2-1)a_k+R_2+1}\right]}{2} \times \sum_{l=1}^{n_3} H_l G_1(a_l, a_k, a_j) \qquad \text{.....(3.117)}$$

where:-

$$G_1(a_l, a_k, a_j) = E_1\left\{\frac{\left[\cos^{-1}\left\{\frac{2}{(R_2-1)a_k+R_2+1}\right\}\right]a_l + \cos^{-1}\left\{\frac{2}{(R_2-1)a_k+R_2+1}\right\}}{2}, \frac{(R_2-1)a_k+R_2+1}{2}, \frac{C_1 a_j + C_1}{2}\right\} \qquad \text{.....(3.118)}$$

$$E_1(\phi, R_j, Z) = \frac{R_j\Theta(R_j)(R_j\cos\phi - 1)\exp(-KR_a r_1)}{R_a^3} \qquad \text{.....(3.119)}$$

and:-

$$R_a = \sqrt{R_j^2 + 1 - 2R_j\cos\phi + \left(\frac{Z}{r_1}\right)^2} \qquad \text{.....(3.120)}$$

Of course, we then find that by definition:-

$$\tilde{Q}_{A_2 \rightarrow dA_1} = 0 \qquad \text{.....(3.121)}$$

The linearised one way perturbation heat flux gradients are:-

$$\tilde{Q}_{V \rightarrow dV_i} = \lim_{\substack{C_3 \rightarrow \infty \\ n_1, n_2, n_3 \rightarrow \infty}} \frac{8K^2 n^2 \sigma T_o^4 C_3}{\pi} \sum_{j=1}^{n_1} \frac{H_j (R_2 - 1)}{2} \sum_{k=1}^{n_2} H_k \frac{\left\{ \cos^{-1}\left[\frac{1}{R_i}\right] + \cos^{-1}\left[\frac{2}{(R_2-1)a_k + R_2 + 1}\right] \right\}}{2} \times$$

$$\times \sum_{l=1}^{n_3} H_l G_3(a_l, a_k, a_j) \qquad \text{.....(3.122)}$$

where:-

$$G_3(a_l, a_k, a_j) = E_3 \left\{ \frac{\left[\cos^{-1}\left\{\frac{1}{R_i}\right\} + \cos^{-1}\left\{\frac{2}{(R_2-1)a_k + R_2 + 1}\right\} \right] a_l + \cos^{-1}\left\{\frac{1}{R_i}\right\} + \cos^{-1}\left\{\frac{2}{(R_2-1)a_k + R_2 + 1}\right\}}{2}, \right.$$

$$\left. , \frac{(R_2-1)a_k + R_2 + 1}{2} , \frac{C_3 a_j + C_3}{2} \right\} \qquad \text{.....(3.123)}$$

$$E_3(\phi, R_j, Z) = \frac{\Theta(R_j) R_j \exp(-K r_1 R_C)}{R_C^2} \qquad \text{.....(3.124)}$$

and:-

$$R_C = \sqrt{R_j^2 + R_i^2 - 2R_i R_j \cos\phi + \left\{\frac{Z}{r_1}\right\}^2} \qquad \text{.....(3.125)}$$

Similarly:-

$$\tilde{Q}_{A_1 \rightarrow dV} = \lim_{\substack{C_4 \rightarrow \infty \\ n_1, n_2 \rightarrow \infty}} B_2 \sum_{j=1}^{n_1} \frac{H_j \cos^{-1}\left\{\frac{1}{R_i}\right\}}{2} \sum_{k=1}^{n_2} G_4(a_k, a_j) \qquad \text{.....(3.126)}$$

where:-

$$B_2 = \frac{2KC_4}{r_1\pi}\left\{4\epsilon n^2\sigma T_o^4\Theta(1) + (1-\epsilon)\left\{\tilde{Q}_{V\rightarrow dA_1} + \tilde{Q}_{A_2\rightarrow dA_1}\right\}\right\} \quad \ldots\ldots(3.127)$$

$$G_4(a_k,a_j) = E_4\left\{\frac{\left[\cos^{-1}\left\{\frac{1}{R_i}\right\}\right]a_k + \cos^{-1}\left\{\frac{1}{R_i}\right\}}{2}, \frac{C_4 a_j + C_4}{2}\right\} \quad \ldots\ldots(3.128)$$

$$E_4(\phi,Z) = \frac{(R_i\cos\phi - 1)\exp(-KR_d r_1)}{R_d^3} \quad \ldots\ldots(3.129)$$

and:-

$$R_d = \sqrt{R_i^2 + 1 - 2R_i\cos\phi + \left\{\frac{Z}{r_1}\right\}^2} \quad \ldots\ldots(3.130)$$

And finally by definition:-

$$\tilde{Q}_{A_2\rightarrow dV} = 0 \quad \ldots\ldots(3.131)$$

3.4 The Numerical Solution

3.41 Introduction

In order to obtain the temperature correction due to the additional, radiative mechanism of heat transfer through the fluid medium, what is required is a solution to the equations derived in the previous subsection. These linearised, normalised equations (equations (3.112) to (3.131)) are an approximate mathematical representation of the real physical system encountered in transient hot wire apparati.

At present no analytical solution to these equations has been found, and one has to resort to a numerical solution. The "Method of Lines" was implemented to obtain this numerical solution as it was the only method tried, which was able to solve the problem to the required accuracy.

3.42 The Method of Lines

The method of lines [80] involves the conversion of partial differential equations to systems of ordinary differential equations. To briefly explain the method, consider the equation:-

$$\frac{\partial U}{\partial t} - \Phi(s,t,\frac{\partial U}{\partial s}, \frac{\partial^2 U}{\partial s^2} \cdots\cdots \text{ etc.}) = 0 \qquad \text{.....(3.132)}$$

where s is a spatial variable. This equation has the same form as the energy equation, equation (3.113) which is to be solved numerically. Representing the function U at N points, across the spatial domain, by a series of approximating Lagrange polynomials in the spatial coordinate, $L_i(s)$, results in:-

$$U_a(s,t) = \sum_{i=1}^{m} L_i(s)\, U_i(t) \qquad \text{.....(3.133)}$$

where (m-1) is the order of the polynomial and $m<N$. The spatial derivatives U' and U" $\left(\frac{\partial U}{\partial s}, \frac{\partial^2 U}{\partial s^2}\right)$ in equation (3.132) can now be replaced by expressions derived from differentiating equation (3.133); namely:-

$$U'(s,t) = \sum_{i=1}^{m} L'_i(s) U_i(t) \qquad \text{.....(3.134)}$$

$$U''(s,t) = \sum_{i=1}^{m} L''_i(s) U_i(t) \qquad \text{.....(3.135)}$$

Using equations (3.133) to (3.135), the partial differential equation (3.132) can be converted into a set of coupled ordinary differential equations, which can then be integrated in the time domain.

In the specific application of the method of lines technique, involved in the numerical solution of the problem of simultaneous conduction and radiation, given a set of data points, $(r_1,f_1(t)),(r_2,f_2(t))\cdots\cdots(r_m,f_m(t))$, (these data points describing the temperature profile of the test fluid contained between concentric cylinders) the $(m-1)$th degree polynomial through the points is given by:-

$$P_{m-1}(r,t) = \sum_{i=1}^{m} L_i(r) f_i(t) \qquad \cdots\cdots\cdots\cdots\cdots\cdots (3.136)$$

where:-

$$L_i(r) = \frac{(r-r_1)\cdots\cdots(r-r_{i-1})(r-r_{i+1})\cdots(r-r_m)}{(r_i-r_1)\cdots\cdots(r_i-r_{i-1})(r_i-r_{i+1})\cdots(r_i-r_m)} \qquad \cdots\cdots (3.137)$$

$$= \frac{\prod_{j=1}^{m}(r-r_j)}{\prod_{j=1}^{m}(r_i-r_j)}, \quad j \neq i \qquad \cdots\cdots\cdots\cdots\cdots\cdots (3.138)$$

Since $L_i(r_i) = 1$ and $L_i(r_j) = 0$, $j \neq i$, $r_j \neq 0$, then $P_{m-1}(r_i,t) = f_i(t)$ and the polynomial passes through the given data points. An important point to notice from equation (3.137) is that the points r_i need not be equidistant in the spatial domain.

$P_{m-1}(r,t)$ may therefore be used as an approximation to the unknown function $f(r,t)$ defining the data points. Similarly, the derivatives of $f(r,t)$ may be approximated by the derivatives of the polynomial at the approximate spatial station i, as:-

$$\left(\frac{\partial f}{\partial r}\right)_i \simeq \left(\frac{\partial p}{\partial r}\right) = \sum_{i=1}^{m} L'_i(r) f_i(t) \qquad \text{.....(3.139)}$$

$$= \sum_{i=1}^{m} f_i(t) \frac{\sum_{j=1}^{m} \prod_{k=1}^{m} (r - r_k)}{\prod_{j=1}^{m} (r - r_j)} \quad \begin{matrix} j \neq i \\ k \neq i, j \end{matrix} \qquad \text{.....(3.140)}$$

and:-

$$\left(\frac{\partial^2 f}{\partial r^2}\right)_i \simeq \left(\frac{\partial^2 p}{\partial r^2}\right) = \sum_{i=1}^{m} f_i(t) \frac{\sum_{j=1}^{m} \sum_{k=1}^{m} \prod_{l=1}^{m} (r - r_l)}{\prod_{j=1}^{m} (r - r_j)} \quad \begin{matrix} j \neq i \\ k \neq i, j \\ l \neq i, j, k \end{matrix} \qquad \text{....(3.141)}$$

These equations just derived for the approximate forms of the unknown function $f(r,t)$ and its derivatives are used, at the N spatially discretised points, to transform the partial differential equation (3.113) into N coupled ordinary differential equations. These ordinary differential equations when integrated in the time domain provide the temperature field in an absorbing, emitting fluid through which simultaneous conductive and radiative heat transfer occur. From the calculated temperature rise of the fluid at the surface of the hot wire the temperature rise correction due to radiation, $\delta T_R(t)$, as defined by equation (3.8), can be calculated.

The coupled ordinary differential equations obtained by the transformation just described are stiff and are therefore solved using an algorithm developed by Gear [81] and Hindmarsh [82] . The algorithm has the advantage over usual predictor - corrector methods in that the formulation allows variable order and step size integration.

The algorithm used for the integration of a stiff set of equations of the form:-

$$\vec{\Theta}'(t) = \vec{F}(\vec{\Theta}, t) \qquad \text{.....(3.142)}$$

consists of the following predictor - corrector set for each dependent variable:-

$$\Theta_{n+1,i} = \alpha_1 \Theta_{n,i} + \cdots\cdots + \alpha_k \Theta_{n-k+1,i} + \beta_1 h \Theta'_{n,i} \qquad \text{....(3.143)}$$

$$\Theta_{n+1,i} = a_1 \Theta_{n,i} + \cdots\cdots + a_k \Theta_{n-k+1,i} + \beta_o h \Theta'_{n+1,i} \qquad \text{...(3.144)}$$

where; $\Theta_{n,i}$ is in the present application the reduced temperature rise of the fluid at a spatial station i , a distance r_i into the fluid. The values of the constants $\alpha_1 - - - \alpha_k$, $a_1 - - - a_k$ and β_o, β_1 are dependent upon the order of the integration used and are found by the method of undetermined coefficients, while h is the incremental time step length.

Convergence is ensured using the Newton - Raphson method which requires that for the (m+1)th correction itteration in Θ_i :-

$$\Theta_{(m+1),i} = \Theta_{m,i} - \left[W^{-1}\right] g_n(\Theta_{m,i}) \qquad \text{.....(3.145)}$$

where $g(\Theta_n)$ is a linear function found by writing the correction equation in the form:-

$$g_n = h \beta_o F(t_{n+1}, \Theta_{n+1}) - \Theta_{n+1,i} \qquad \text{.....(3.146)}$$

and W^{-1} is the inverse of matrix W where:-

$$W = \left(I + h \beta_o \frac{\partial \vec{F}}{\partial \vec{\Theta}} \right) \qquad \text{.....(3.147)}$$

I is the identity matrix and $\frac{\partial \vec{F}}{\partial \vec{\Theta}}$ is the jacobian formed by the elements $\frac{\partial f_i}{\partial \Theta_i}$ resulting from the solution of the set of ordinary differential equations. Fortunately the method is strongly convergent and W^{-1} does not need to be known with much accuracy so its updating is therefore not performed very frequently. In this context, because W^{-1} is not required to great accuracy, an approximate matrix inversion technique developed by Curtis & Reid [83] is used to speed up integration.

3.43 Accuracy of the Numerical Solution

In order to account for radiative heat transfer being present, during transient hot wire thermal conductivity measurements, on radiation absorbing, reemitting fluids, corrections to the fluids' measured temperature rises or the fluids' apparent thermal conductivities (those obtained neglecting effects due to radiation) are required. These corrections are to be obtained from numerical solutions to the previously defined (see § 3.22) radiation problem for sumultaneous conductive and radiative heat transfer from a hot wire through a participating medium.

In order to establish confidence in the numerical procedure described above, one would like some assurance that the numerical solution, from which the corrections are found, was sufficiently accurate to result in these corrections being non-spurious. What is required therefore is a method of checking the numerical solution to determine its accuracy. An absolute check is, of course, not possible as that would require another method of solving the radiation problem. Therefore a problem is required, similar to the full radiation problem, but for which an accurately known solution exists. The problems which immediately spring to mind are the optically thin and optically thick approximations to the full radiation problem. Unfortunately, there is no readily available solution for the optically thin case [84] and for the optically thick approximation to be valid for the experimental arrangement used, the extinction coefficient of the fluid must be of the order of 3×10^7 m^{-1}. This results in the radiative contribution to

the thermal conductivity, λ_r, which using the Rosseland approximation analysis [76] , is found to be:-

$$\lambda_r \approx \frac{16}{3} \frac{n^2 \sigma T_o^3}{K} \qquad \text{.....(3.148)}$$

having a value of approximately 7×10^{-7} $W/m^2/K$. This value is small when compared with the thermal conductivities of the test fluids on which measurements are to be performed, their thermal conductivities being of the order of 1.5×10^{-1} $W/m^2/K$. This small contribution to the observed thermal conductivities would therefore result in an indiscernibly small temperature difference between the pure conductive temperature profile in a fluid and that incurred due to the additional mechanism of heat transfer. The only usable readily available solution is that for pure conduction through a fluid contained between concentric cylinders (see equations (2.78) and (2.83)).

There are a number of factors which contribute to the accuracy of the numerical solution. The accuracy is governed by the number of spatial divisions used in reducing partial differential equation (3.113) to a system of ordinary differential equations (see § 3.42) and their distribution in the fluids' radial domain. The accuracy is also influenced by the order of the spatial coupling (degree of approximating Lagrange polynomials used) and the integration algorithm truncation limit used.

Because of the expected fluid temperature profile which will be obtained from the numerical solution, the spatial distribution of the N points in the radial domain was chosen such that:-

$$R_i = \left[\frac{r_b}{r_a}\right]^{\frac{i-1}{N-1}} \qquad \text{.....(3.149)}$$

where R_i is the reduced radial position of station i and (r_b/r_a) is the ratio of the radii of the outer and inner cylinders containing the fluid.

This distribution ensures that there are more points in the vicinity of the inner cylinder (wire) where the radial gradient of the temperature rise of the fluid $\frac{\partial \Theta}{\partial R}$ is greater, and few points further out into the fluid where this gradient is a lot smaller. Increasing the number of spatial divisions, N, and the order of coupling will in general increase the accuracy of the numerical solution as will the reduction of the algorithm truncation limit used. Unfortunately, increasing the number of spatial divisions will increase the stiffness of the resulting set of ordinary differential equations thus requiring smaller integration time steps, as will the reduction of the truncation limit. Increasing the coupling on the other hand increases the time steps permissable but requires more computation for each time step.

Reducing the truncation limit below 10^{-7} is not recommended as problems due to rounding errors can occur as a result and the limit is therefore set to 10^{-6}. Having set the truncation limit one has to decide whether to increase the number of spatial divisions or the order of coupling. Normally when solving parabolic problems increasing the coupling is preferable to increasing the number of spatial divisions, but for the present problem it was found better to increase the number of spatial divisions. This conclusion was obtained by comparing pairs of numerical solutions to the pure conduction problem requiring essentially the same computing time, one using a higher order coupling and fewer spatial points; the other using a lower order coupling and using a larger number of points.

Fig. (3.12) shows the numerical solutions to the pure conduction problem for transfer through a hypothetical fluid, whose physical properties are similar to those of n-heptane at atmospheric pressure and at 300K, contained within concentric cylinders. The numerical solutions obtained used third and fifth order couplings and between 30 and 200 spatial divisions. The solution using a third order coupling and 200 spatial divisions virtually superimposes the analytical solution. From fig. (3.12) one can see it is preferable to use larger numbers of points and third order couplings and it has been assumed

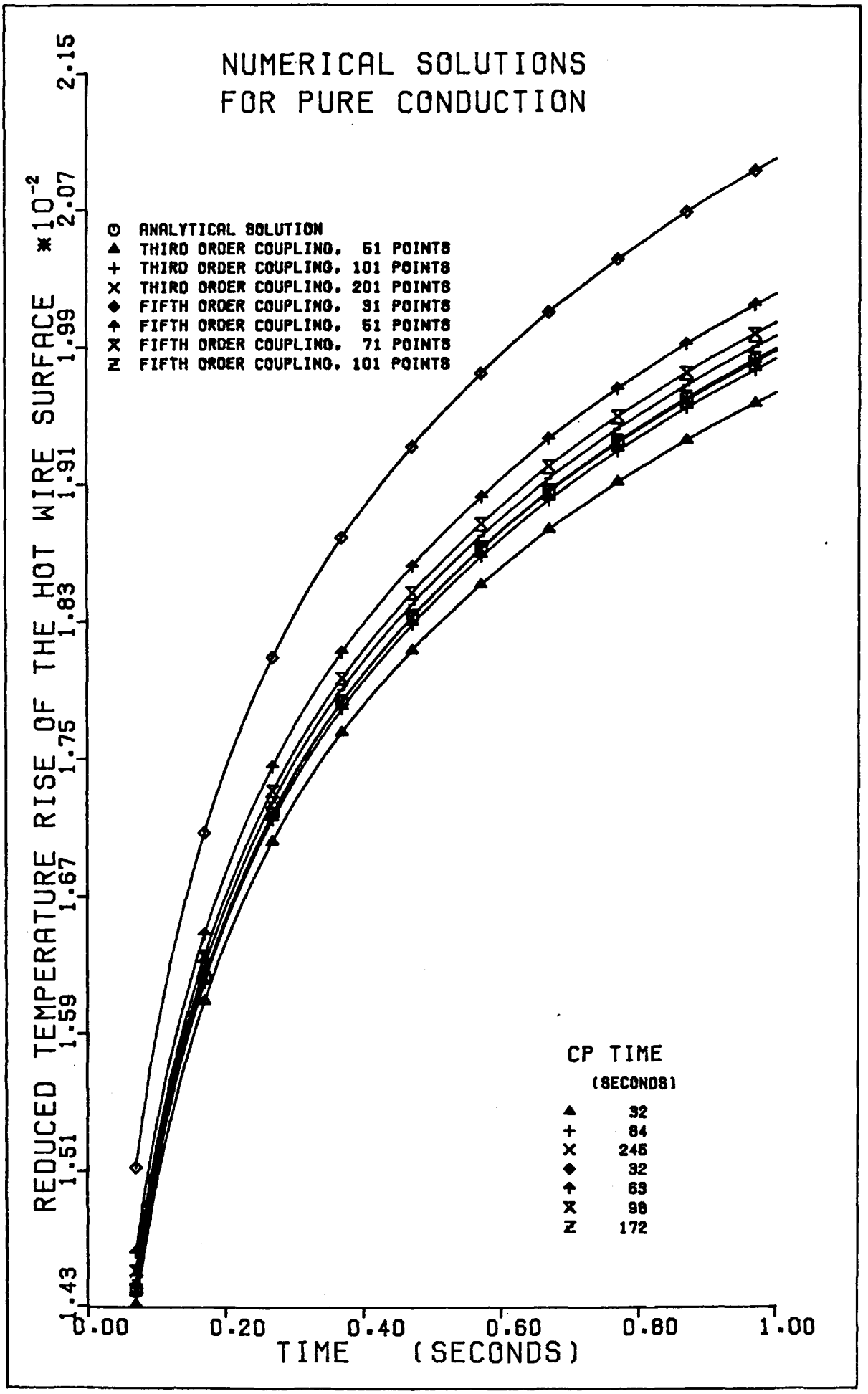
NUMERICAL SOLUTIONS
FOR PURE CONDUCTION
ANALYTICAL SOLUTION
THIRD ORDER COUPLING, 51 POINTS
THIRD ORDER COUPLING, 101 POINTS
THIRD ORDER COUPLING, 201 POINTS
FIFTH ORDER COUPLING, 31 POINTS
FIFTH ORDER COUPLING, 51 POINTS
FIFTH ORDER COUPLING, 71 POINTS
FIFTH ORDER COUPLING, 101 POINTS
CP TIME
(SECONDS)
32
84
245
32
63
98
172
REDUCED TEMPERATURE RISE OF THE HOT WIRE SURFACE *10^-2
1.43
1.51
1.59
1.67
1.75
1.83
1.91
1.99
2.07
2.15
0.00
0.20
0.40
0.60
0.80
1.00
TIME (SECONDS)

Fig. (3.12)

that this conclusion will be valid for the solution of the conduction-radiation problem.

Solution of the full integro-partial differential equation defining the radiation problem is, because of the above reasoning and assumptions, solved using the method of lines with 301 spatial points and a third order spatial coupling. The comparison between the theoretically and numerically obtained solutions for pure conduction of heat through a liquid is given in fig. (3.13). It can be seen that the numerical solution for the reduced temperature rise of the wire is accurate to within $\pm$ 0.07% of the analytical solution over the time range within which experiments are performed (Approx. 0.1 - 1.0 secs.).

The solution for the pure conduction problem was obtained from the program used to solve the simultaneous conduction and radiation problem by setting the emissivity of the platinum wire and the mean extinction coefficient of the liquid, both equal to very small values (1×10^{-40} m^{-1}). The solution of the pure conduction problem was therefore obtained using the identical algorithm as that which was used for the solution of the simultaneous conduction and radiation problem. For this reason the accuracy of the solution to the conduction - radiation problem is believed to be of the same order as that for the pure conduction solution.

Distinction must be made between the accuracy of the numerical solution to the conduction - radiation problem and the accuracy of the temperature rise corrections obtained from this numerical solution. The latter being dependent on the former as well as on how closely the mathematical model describes the behaviour of the real physical system and how accurately the physical constants of the system are known. This topic is dealt with later when estimating the accuracy of the absolute thermal conductivities obtained using the transient hot wire apparatus, but the distinction should be made here.

Problem requiring solution

Conservation of Energy:- $$\frac{\partial\Theta}{\partial t} = \frac{\lambda}{\rho C_p r_1^2}\left[\frac{\partial^2\Theta}{\partial R^2} + \frac{1}{R}\frac{\partial\Theta}{\partial R}\right]$$

Boundary Conditions i):- $$\frac{q}{2\pi T_o} = -\lambda\left(\frac{\partial\Theta}{\partial R}\right)_{R=1}$$

ii):- $$\Theta(R_2,\ 0\leqslant t) = 0$$

Initial Condition:- $$\Theta(1\leqslant R\leqslant R_2,\ t\leqslant 0) = 0$$

The analytical solution is:- (see § 2.322 & § 2.333) $$\Theta(1,t) = \frac{\Delta T_{id}}{T_o} + \frac{\delta T_{OB}}{T_o}$$

subject to:- $R_2 \gg 1$ and $\frac{4kt}{r_1^2} \gg 1$

Comparison of the Solutions

Time [s]	$\Theta(1,t)$ Analytical Solution $\times 10^{-2}$	$\Theta(1,t)$ Numerical Solution $\times 10^{-2}$
0.10	1.5128	1.5138
0.15	1.5967	1.5973
0.20	1.6562	1.6566
0.25	1.7024	1.7026
0.30	1.7401	1.7402
0.35	1.7720	1.7720
0.40	1.7996	1.7995
0.45	1.8240	1.8238
0.50	1.8458	1.8456
0.55	1.8655	1.8653
0.60	1.8835	1.8832
0.65	1.9001	1.8998
0.70	1.9154	1.9151
0.75	1.9297	1.9293
0.80	1.9431	1.9426
0.85	1.9556	1.9552
0.90	1.9674	1.9670
0.95	1.9786	1.9781
1.00	1.9892	1.9887

Values of the physical properties and variables required for the solutions

λ = 0.1282 W/m/K

T_o = 300K

R_2 = 1357

r_1 = 3.5×10^{-6} m

q = 1.0 W/m

C_p = 2252 J/kg/K

ρ = 697 kg/m^3

Fig. (3.13) Comparison of Numerical and Analytical Solutions

3.44 Use of the Numerical Solution

The numerical solution to obtain $\delta T_R(t)$ for n-heptane at an initial temperature, T_o, of 308.15K and under 500 MPa hydrostatic pressure is given in fig. (3.14). From the solution, corrections can now, in principle, be made to the measured temperature rise of the wire recorded during measurements on n-heptane under the above thermodynamic conditions. These temperature rise corrections would have to be made in the computer program used to analyse the experimental data (see § 4.61) and as this program requires an itterative procedure, a second numerical solution for $\delta T_R(t)$ under slightly different conditions may be required. The acquisition of a numerical solution to the conduction - radiation problem is in computational terms very expensive (a single solution requires $\pm$ 750 cp secs and $\pm$ 100 thousand words of storage on a CDC 7600 machine) and different solutions are required for each thermal conductivity measurement. This method of correcting for the effects of radiation on the measurement of the thermal conductivity by the transient hot wire method although possible is not feasible.

The numerical solution can, however, be used to demonstrate that the effects of radiation on the thermal conductivity as measured by the transient hot wire technique increase with the time duration of an experiment. Neglecting the correction term $\delta T_{OB}(t)$ from equation (3.8) as this term is only significant at relatively long times (when $\frac{4kt}{a^2} \gg 1$), one obtains:-

$$\Delta T(a,t) = \Delta T_{id}(a,t) + \delta T_R(a,t) \qquad \text{.....(3.150)}$$

where $\Delta T(a,t)$ is the temperature rise of the fluid at radial position, a, that would be obtained by measurement on the hypothetical system whose mathematical model can be described by equations (3.64) to (3.77). Now defining the apparent thermal conductivity by:-

$$\lambda_{app} = \frac{q}{4\pi\left(\frac{\partial \Delta T}{\partial \ln t}\right)_{r=a}} \qquad \text{.....(3.151)}$$

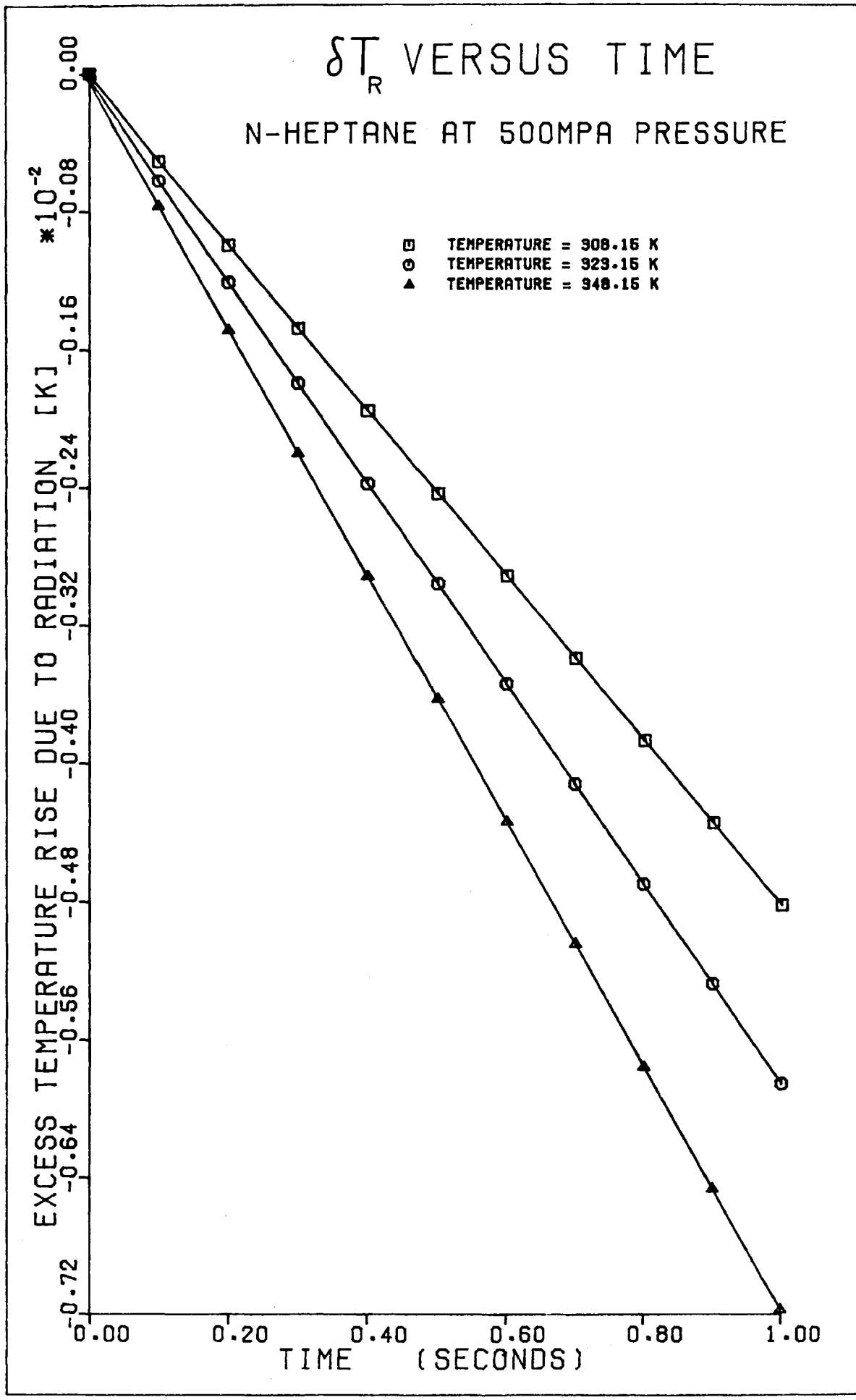
δT_R VERSUS TIME
N-HEPTANE AT 500MPA PRESSURE
TEMPERATURE = 308.15 K
TEMPERATURE = 323.15 K
TEMPERATURE = 348.15 K
EXCESS TEMPERATURE RISE DUE TO RADIATION [K] *10^-2
0.00
-0.08
-0.16
-0.24
-0.32
-0.40
-0.48
-0.56
-0.64
-0.72
0.00
0.20
0.40
0.60
0.80
1.00
TIME (SECONDS)

FIG. (4.14)

then for small values of $\frac{a^2}{4kt}$ we find from equations (3.151) and (3.150) that:-

$$\frac{\lambda}{\lambda_{app}} = 1 + \frac{4\pi\lambda}{q}\left(\frac{\partial \delta T_R}{\partial \mathrm{Ln}\, t}\right)_{r=r_1} \qquad \text{.....(3.152)}$$

The ratio of thermal conductivities λ/λ_{app} as obtained from equation (3.152) is, of course, time dependent and a plot of λ/λ_{app} versus time is given for n-heptane at 500 MPa in fig. (3.15).

The functions λ/λ_{app} are smooth, approximately linear in the region close to time t=0 and pass through 1.0 at t=0. When neglecting effects due to radiation on the thermal conductivity, the thermal conductivities of fluids as measured on transient hot wire apparati are not absolute but apparent. However, it can be seen that the absolute thermal conductivity can be obtained by extrapolating the plot of the apparent thermal conductivity versus time back to zero time.

It is also immediately apparent from fig. (3.15) that transient hot wire experi ments performed using shorter run time durations incur smaller errors in their measured thermal conductivities than those requiring longer time durations.

As it is not practicable to solve the radiation problem for each measurement performed on the transient hot wire apparatus, another method for correcting for the effects of radiation is required. We define a radiation defect in the thermal conductivity as:-

$$\xi' = \frac{\lambda_{app}(t) - \lambda(t)}{\lambda(t)} = -\frac{4\pi\lambda_{app}(t)}{q}\left(\frac{\partial \delta T_R}{\partial \mathrm{Ln}\, t}\right)_{r=a} \qquad \text{.....(3.153)}$$

where generally:-

$$\xi' = \xi'(t, T_o, q, n, \lambda_{app}, K, \rho, C_p, a, b, \epsilon \ldots\ldots) \qquad \text{.....(3.154)}$$

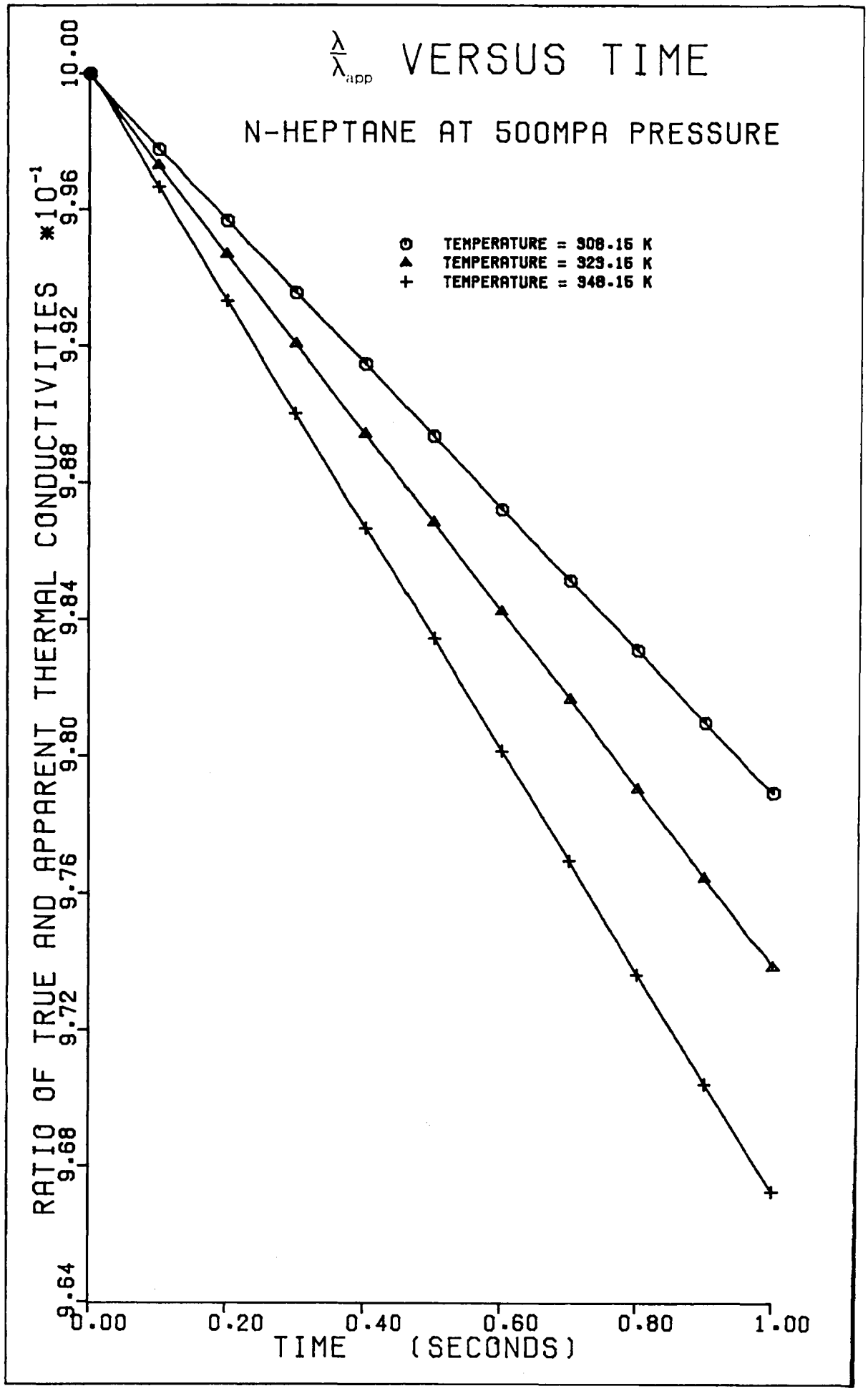
λ/λapp VERSUS TIME
N-HEPTANE AT 500MPA PRESSURE
TEMPERATURE = 308.15 K
TEMPERATURE = 323.15 K
TEMPERATURE = 348.15 K
RATIO OF TRUE AND APPARENT THERMAL CONDUCTIVITIES *10⁻¹
10.00
9.96
9.92
9.88
9.84
9.80
9.76
9.72
9.68
9.64
0.00
0.20
0.40
0.60
0.80
1.00
TIME (SECONDS)

Fig. (7.15)

However, for experiments performed on liquids using the same piece of apparatus, the factor ξ' is dependent upon far fewer quantities and for a particular apparatus is:-

$$\xi'' = \xi''(t, T_o, q, n, \lambda_{app}, K, \rho, C_p) \qquad \text{.....(3.155)}$$

In the present work, measurements on a liquid are performed along isotherms, but, unfortunately there is no information available about the variation of the extinction coefficient, refractive index and specific heat capacity of the liquid with pressure. Consequently, it has been necessary to assume all of these quantities are pressure independent, and equal to their atmospheric pressure values. Although this is an obvious and unquantified approximation we are forced to adopt it by the lack of any better information. In this case the radiation defect ξ'' is a function of an even smaller set of variables i.e.:-

$$\xi'' \approx \xi''(t, q, \lambda_{app}, \rho) \qquad \text{.....(3.156)}$$

or more correctly:-

$$\xi'' \approx \xi''(t, q, \lambda_{app}) \qquad \text{.....(3.157)}$$

since for a particular fluid the apparent thermal conductivity and density are not independent of each other.

During measurements of a liquid's apparent thermal conductivity, along an isotherm and over a range of densities, the heat flux per unit length varied typically by only 1.0% (Max.) over a pressure range of 50 MPa - 500 MPa. Also, owing to the mode of bridge operation used and by performing runs within the time range 0.08 - 1.0 seconds, making sure the smallest time used is between 0.07 - 0.09 seconds and the largest time is between 0.95 - 1.1 seconds, the times at which balance conditions occur are approximately the same for all measurements along a single isotherm. For these reasons the radiation

defect, ξ'', for a particular liquid along an isotherm and in the pressure range 50 MPa - 500 MPa is to a first approximation only dependent upon the apparent thermal conductivity and so:-

$$\xi = \frac{\lambda_{app} - \lambda}{\lambda} \approx \xi''(\lambda_{app}) \qquad \text{.....(3.158)}$$

In equation (3.158) λ_{app} is the apparent thermal conductivity calculated from measurements performed on the transient hot wire apparatus and is some time scaled mean of the time dependent apparent thermal conductivity of the liquid.

In the present work the approximate effect of radiation on the measurement of liquid thermal conductivities is accounted for through the use of equation (3.158).

The required radiation defect, ξ, is calculated from numerical solutions to the mathematical model for the simultaneous conductive and radiative transfer of heat through the test fluid. The radiation defect is calculated at the extreme ends of the range of the apparent thermal conductivities over which the fluid is measured. The relevant physical properties of the fluid at these extremes are used in the mathematical model from which the defects are calculated and subsequent defects at apparent thermal conductivities within the range are estimated by a linear interpolation. The radiation defect versus apparent thermal conductivies used for n-heptane along the 3 three isotherms at which experiments were performed are shown in fig. (3.16) and those used for n-nonane and n-undecane are shown in fig. (3.17) and fig. (3.18) respectively. It can be seen from these figures that the maximum error incurred in a measurement, due to radiative transfer, is approximately 2.8%.

It has been found that, over the temperature range within which thermal conductivity measurements have been performed namely 308 - 363K, knowing the radiation defect, ξ, for one of the test liquids at a particular apparent thermal conductivity and temperature, the radiation defect at

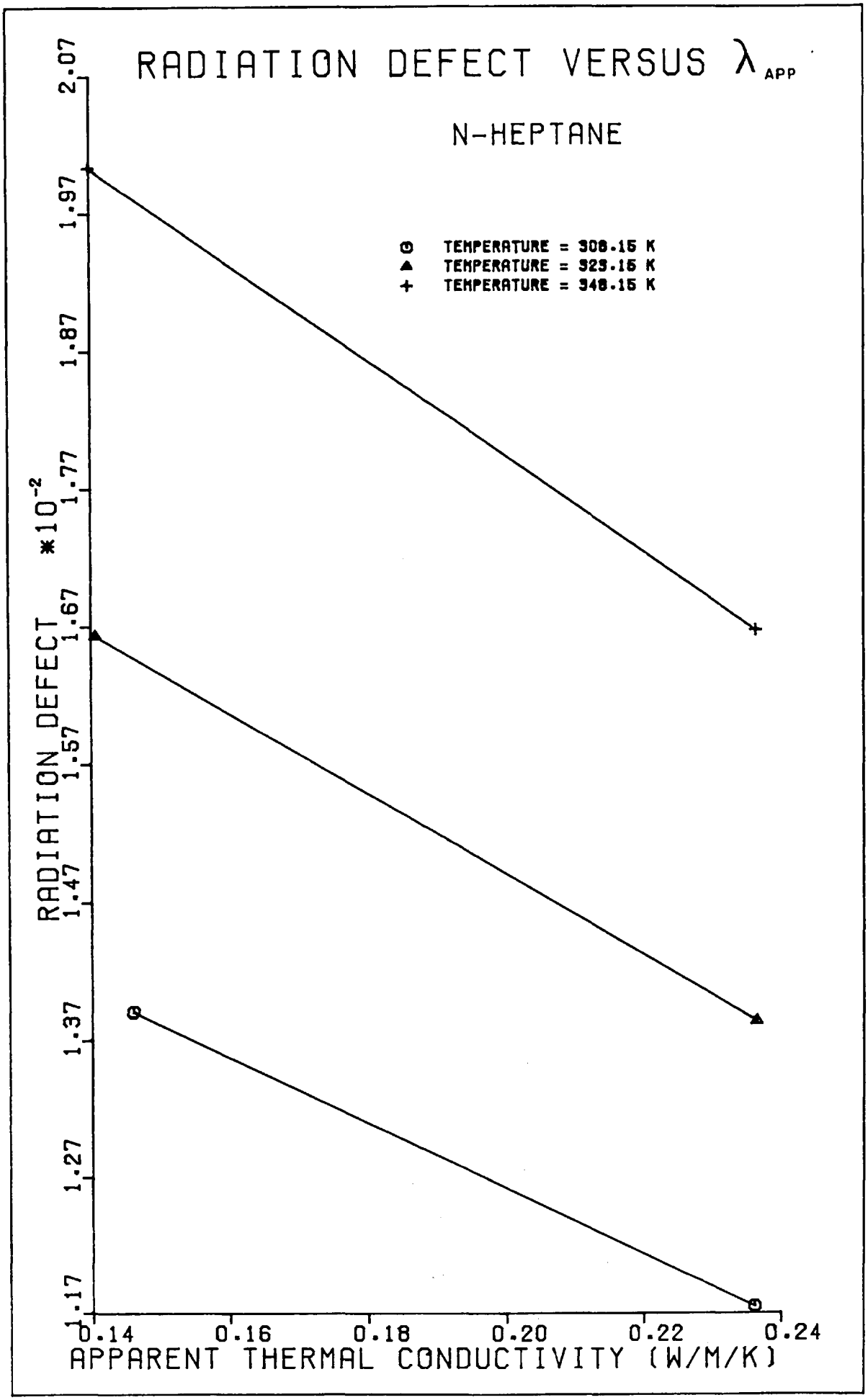
RADIATION DEFECT VERSUS λ_{APP}
N-HEPTANE
TEMPERATURE = 308.15 K
TEMPERATURE = 328.15 K
TEMPERATURE = 348.15 K
RADIATION DEFECT *10^{-2}
2.07
1.97
1.87
1.77
1.67
1.57
1.47
1.37
1.27
1.17
0.14
0.16
0.18
0.20
0.22
0.24
APPARENT THERMAL CONDUCTIVITY (W/M/K)

Fig. (7.15)

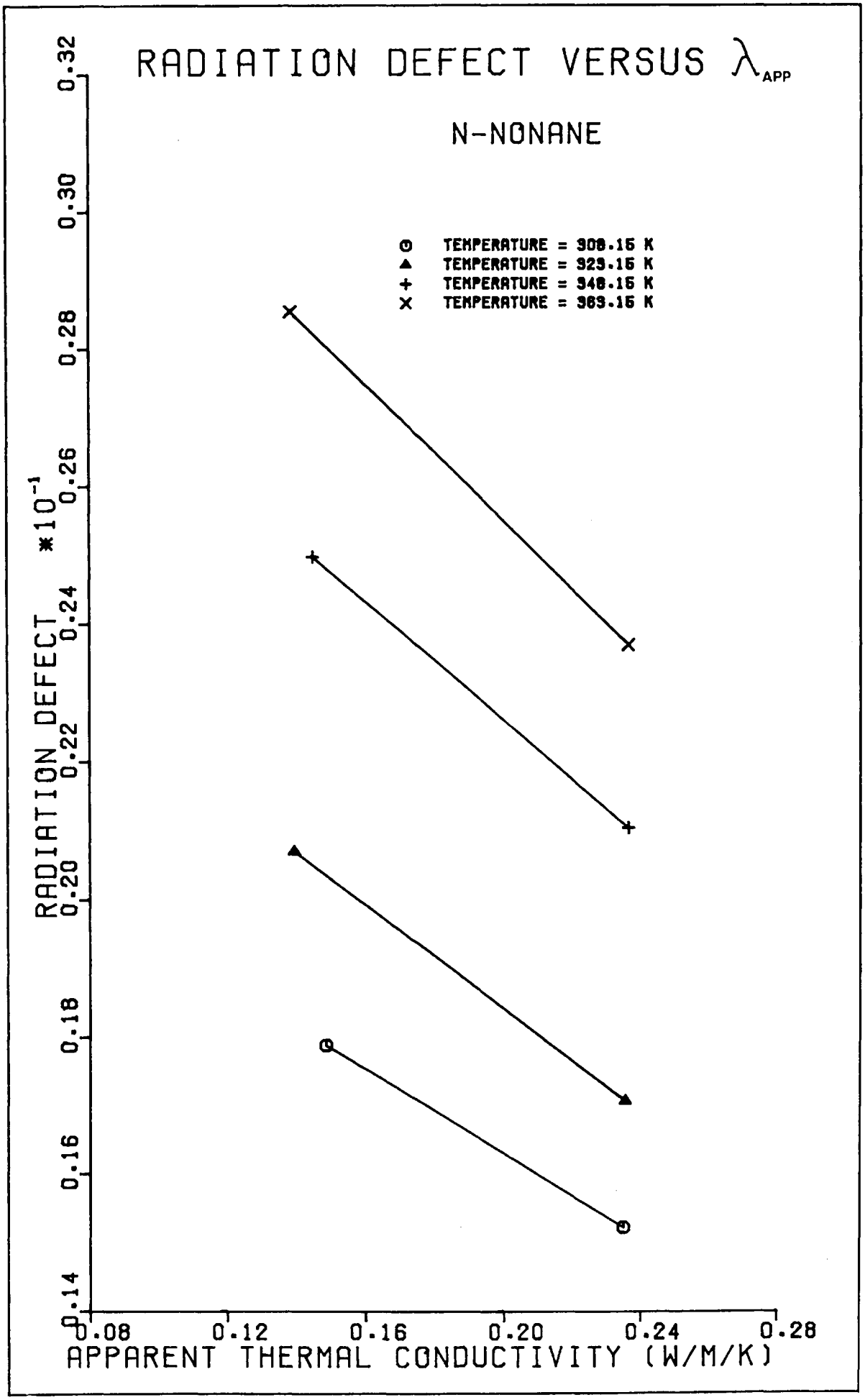
RADIATION DEFECT VERSUS λ_{APP}
N-NONANE
TEMPERATURE = 308.15 K
TEMPERATURE = 328.15 K
TEMPERATURE = 348.15 K
TEMPERATURE = 368.15 K
RADIATION DEFECT *10^{-1}
0.14
0.16
0.18
0.20
0.22
0.24
0.26
0.28
0.30
0.32
0.08
0.12
0.16
0.20
0.24
0.28
APPARENT THERMAL CONDUCTIVITY (W/M/K)

Fig. (7.17)

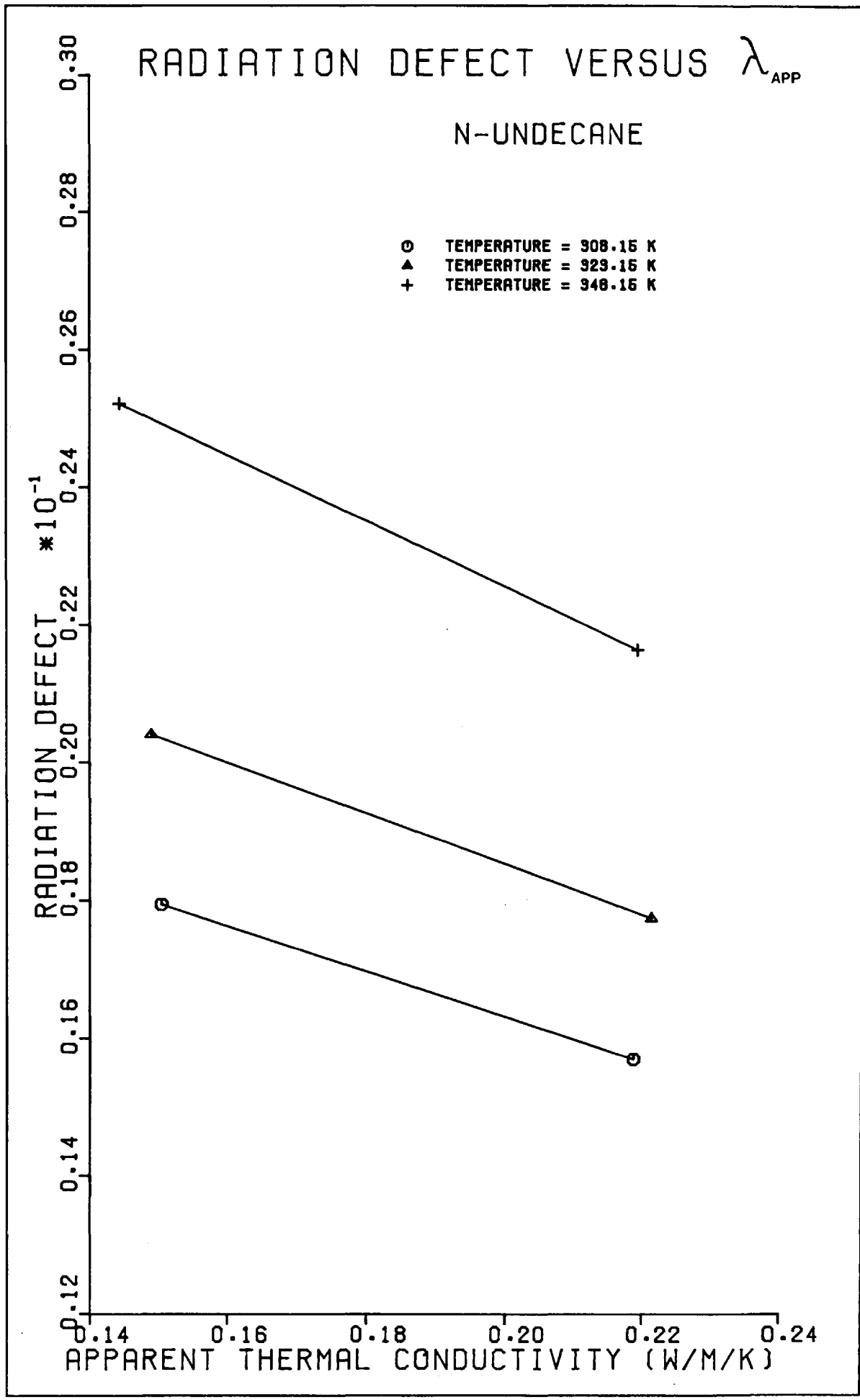
RADIATION DEFECT VERSUS λ_{APP}
N-UNDECANE
TEMPERATURE = 308.15 K
TEMPERATURE = 323.15 K
TEMPERATURE = 348.15 K
RADIATION DEFECT *10^{-1}
0.12
0.14
0.16
0.18
0.20
0.22
0.24
0.26
0.28
0.30
0.14
0.16
0.18
0.20
0.22
0.24
APPARENT THERMAL CONDUCTIVITY (W/M/K)

Fig. (7.18)

a slightly different temperature and the same apparent thermal conductivity can be found. This is done by assuming:-

$$\xi \sim T_o^3 \qquad \text{.....(3.159)}$$

The radiation defects calculated in this manner have been found to agree with those calculated from numerical solutions to the mathematical model for simultaneous conductive and radiative heat transfer to within a few percent. Similarly, the defect, ξ, has been found to have an approximately linear dependence upon the extinction coefficient. It should, however, be noted that these conclusions were drawn from a very limited number of observations as the performance of a detailed sensitivity analysis was not possible.

3.45 Accuracy of the Radiation Corrections

The accuracy of the correction made due to the extra mechanism for heat transfer through the liquid medium, namely radiation, is determined by a number of factors. These factors are; the applicability of the mathematical model used to describe the simultaneous transfer of heat by conduction and radiation; the error incurred by the numerical solution for the temperature correction due to radiation, δT_R; the inaccuracy due to errors in the physical properties of the liquid used in the mathematical model; and finally the error incurred due to the use of the radiation defect ξ.

The effect of radiation on the absolute thermal conductivity is such as to introduce a maximum error of about 2.5% in the thermal conductivity measured on the transient hot wire apparatus neglecting the effect. For this reason the accuracy of the correction has only to be to within $\pm$ 20% to incur a maximum error of $\pm$ 0.5% in the absolute thermal conductivity. It is, however, necessary to estimate the accuracy of the correction in order to determine the maximum uncertainty in the absolute thermal conductivity measurements performed on the transient hot wire apparatus.

Examining the factors contributing towards the uncertainty in turn, firstly the applicability of the mathematical model. The mathematical model, it is expected, will not produce more than a 1.0% error in the correction due to radiation ($\pm$ 0.025% in the absolute thermal conductivity). This error being due to such anomalies as the assumption of the system being in local thermodynamic equilibrium, and the liquid being non scattering, isotropic, and diffusely emitting. The error incurred by the numerical solution for the temperature correction due to radiation, δT_R, is, using the accuracy of the solution to the problem of pure conduction as a guide, likely to introduce a maximum error of approximately $\pm$ 0.05% in the absolute thermal conductivity. The error incurred due to the use of the radiation defect factor, ξ, as implemented in the present work, by calculating ξ along an isotherm at either end of the range of the apparent thermal conductivity of a particular fluid, is thought to be approximately $\pm$ 0.05% of the absolute thermal conductivity.

The final factor contributing to the uncertainty in the correction due to radiation is provided by the errors in the physical properties used to describe the system. This factor is thought to introduce the bulk of the uncertainty in the correction factor.

For the reasons indicated earlier it is not possible to estimate with any certainty the consequences of approximating the physical properties of the fluid such as the extinction coefficient, refractive index, and specific heat correction. To improve the situation it would ideally be necessary to carry out detailed studies of these quantities as a function of pressure and temperature. One would then use these experimentally determined physical properties in new numerical calculations. On the one hand the experimental effort is completely beyond this work and the computational effort entirely beyond the available computing resources.

There remain two alternative strategies, first to allow an experimental uncertainty in the 'radiation free' thermal conductivities of the magnitude of the computed radiation correction. Or secondly to obtain

a crude estimate of the likely uncertainty in this correction. Here we have adopted the latter course and based the estimate on the fact that the physical properties in question probably vary as the density of the fluid. In which case, the maximum error likely to be incurred in the correction from assuming them constant is about 20%. It therefore seems prudent to estimate the absolute accuracy of the radiation free thermal conductivity data as between $\pm$ 0.5%, for n-Heptane at 500 MPa and 308.15K, to $\pm$ 0.8% for n-Nonane at 50 MPa and 363.15K. However, it must be recognised that this estimate may need to be modified in the light of new experimental information becoming available.

CHAPTER 4

Apparatus Design and Use

4.1 Introduction

This chapter details the design, construction and use of a transient hot wire apparatus, which is suitable for the measurement of the thermal conductivity of liquids in the pressure range 0.1 - 700 MPa and temperature range 300 - 380K. The design of the equipment both mechanical and electrical has been such as to produce an apparatus which conforms as closely as possible to the mathematical model analysed in chapter 2. The resulting instrument has a precision of $\pm$ 0.2% and has been used to perform measurements on n-heptane, n-nonane, and n-undecane, the absolute thermal conductivities of which have been determined to an accuracy of between 0.5% and 0.8%.

4.2 High Pressure Equipment

This section presents the design of the equipment used to control the temperature of, and produce the high pressure in, the test fluid whose thermal conductivity is to be determined. The equipment is composed of an autoclave, pressurising system and temperature controller each of which will be discussed separately.

4.21 The Autoclave

Although first consideration being given to the pressure vessel may seem out of context, often, and as occurred in the present procedure, when designing high pressure apparatus, the first piece of equipment designed and constructed is the pressure vessel and its associated pressurising system. This is understandable since the pressure vessel is often the most expensive single piece of apparatus and its manufacture is normally externally contracted. This is, therefore, the reason for the order of the apparatus design presentation as it

emphasises that the design procedure unfortunately adds an extra constraint on the design of other apparatus. As a result, the measurement cell and bellows (described in § 4.3) must be designed to fit within the pressure vessel, rather than the pressure vessel being designed to contain the measurement cell and bellows assembly.

The pressure vessel (1) (see fig. (4.1)) used was manufactured by Pressure Products Inc. (U.K.) Limited from EN 25 stainless steel with a 39.5 mm bore and 0.305 m length, between the ends of the terminals in the plug (2) and the vessel bottom. The plug which, seals the vessel and carries the measurement cell (not shown) and bellows assembly (3) was also made of EN 25 stainless steel. It is fitted with four terminals (4) to enable electric contact to be made with the measurement cell, which during measurements is contained within the autoclave. The terminals were made of Invar and successively lapped into conical Hilumina insulators (5) (manufactured by Smith Industries, Ceramics Division) and the conical ends of passages machined into the bottom of the plug, as shown in the detail on fig. (4.1).

The vessel is sealed using the plug, the thrust nut (6) and two seals. A primary seal (7) made of PTFE seals upto ± 35 MPa by which time the secondary seal (8) made of cast, non porous, Phosphor-bronze, has taken over for the high pressure sealing. The two seals are held by a retaining ring (9) and threaded collar (10) as shown in the second detail on fig. (4.1). The dimensions of the secondary seal are shown in fig. (4.2)

The autoclave is pressurised using Shell fluid 41 (an aviation quality, non corrosive, flame retarded,hydraulic fluid) which is pumped into the autoclave from the pressurising system via the gland nut type, high pressure fitting at the bottom of the pressure vessel. The autoclave was designed for a working pressure of 700 MPa and has been tested up to 850 MPa.

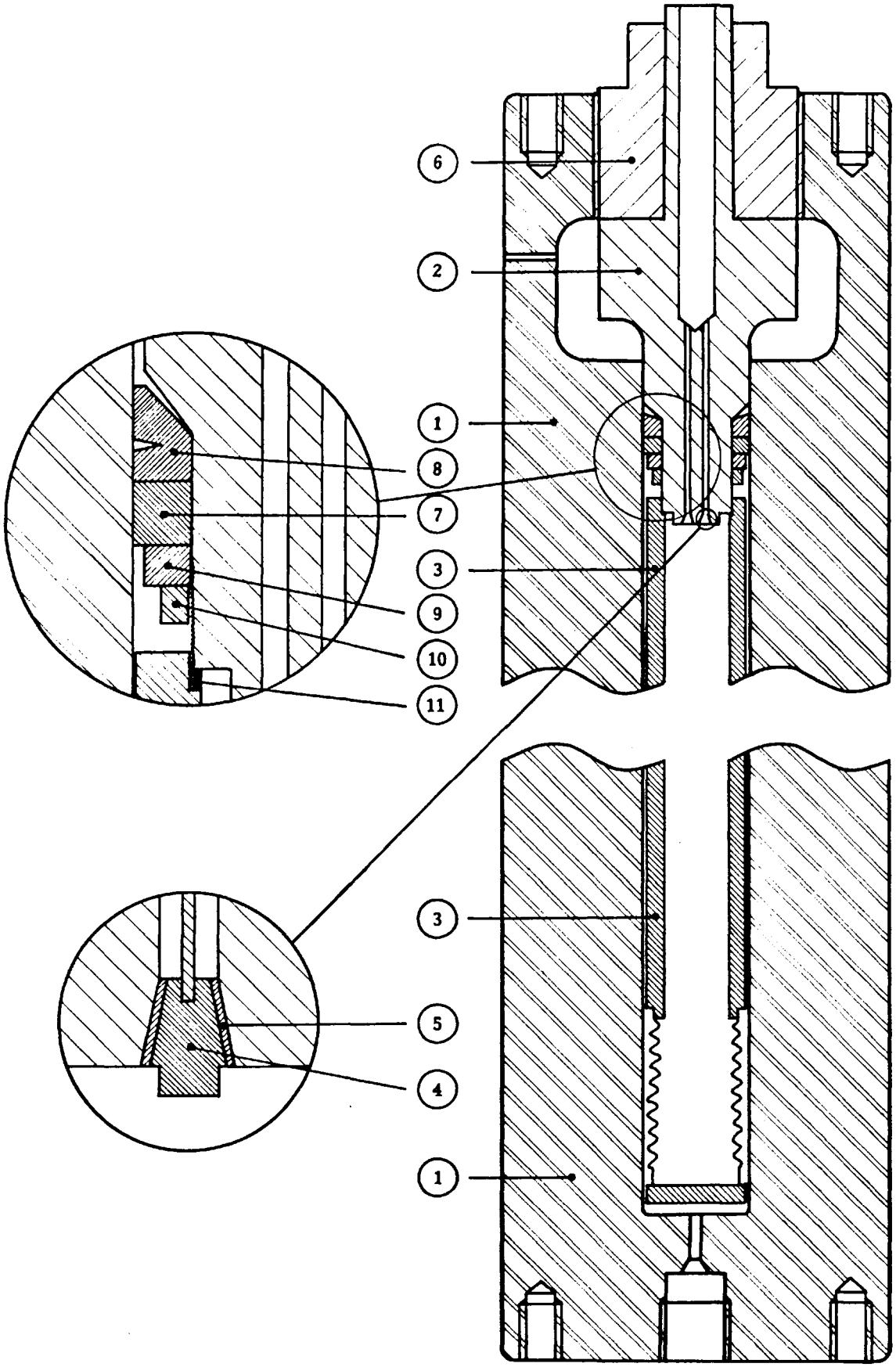

Fig. (4.1) The Autoclave (including details of the plug).

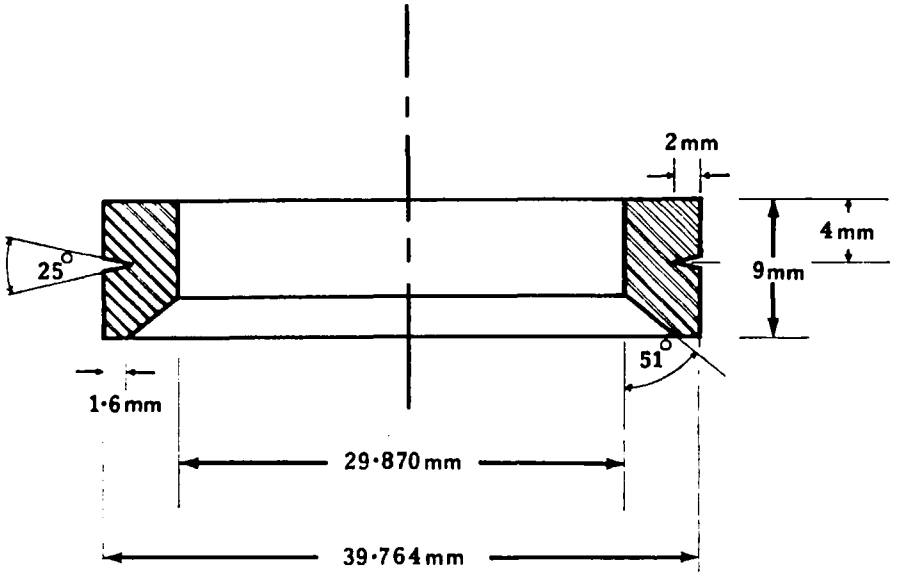

Fig. (4.2) The High Pressure Seal

4.22 The Pressurising System

The autoclave is pressurised by the pressurising system, a schematic representation of which is shown in fig. (4.3). The system consists essentially of a high and a low pressure side. The low pressure side is for pressurisation of the autoclave and high pressure side up to 200 MPa. After this initial pressurisation, the high pressure side, when isolated from the low pressure side by valve (9), pressurises the autoclave via an intensifier (6) from 200 MPa up to 700 MPa.

The specifications of the individual components of the pressurising system are listed below:-

(1) Pressure vessel (autoclave) made by Pressure Products Inc. (UK) Limited and rated to 700 MPa working pressure (see § 4.21).

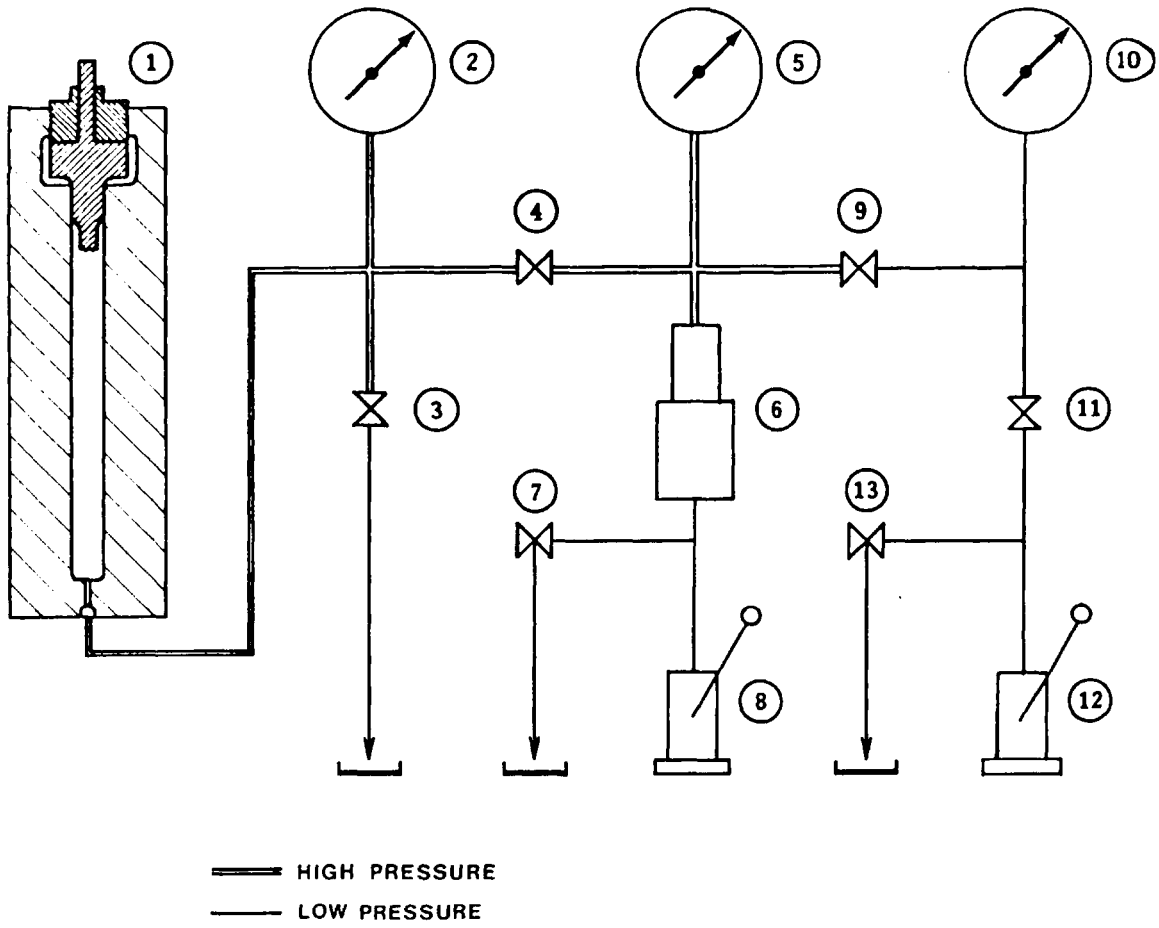

Fig. (4.3) The Pressurising System

(2) Strain Gauge made by Coleraine Instruments, Gallway, Ireland and calibrated up to 700 MPa accuracy ± 1 MPa at 700 MPa. (For calibration, see appendix 2.1.)

(3) Vent valve, non rotating spindle, model no V1-110-100, made by Pressure Products Inc. and rated to 100,000 psi (700 MPa approx.)

(4) Pressure vessel isolation valve, specifications as for (3) .

(5) 10,000 atm pressure gauge, made by Budenberg Gauge Company, accurate to ± 1% of full scale deflection (for calibration, see appendix 2.1).

(6) Intensifier, model no. A2.SJ, made by Harwood Engineering Co., U.S.A., with intensification factor of 15 and rated to 200,000 psi (1400 MPa approx.).

(7) Let down valve, non-rotating, spindle type, model no. V-110-20, made by Pressure Products Inc. Ltd. and rated to 20,000 psi (150 MPa approx.).

(8) Pressurising pump, hand-operated, stainless steel bodied, model no. HP-218, made by McCartney Manufacturing Co. U.S.A., and rated at 60,000 psi (400 MPa approx.).

(9) High pressure isolation valve, specification as for (3) .

(10) 40,000 psi Gauge, made by Budenberg Gauge Company, accurate to ± 1% of full scale deflection (for calibration see appendix 2.1).

(11) Low pressure isolation valve, non rotating, spindle type, model no. V-110-60, made by Pressure Products Inc. Ltd. and rated to 60,000 psi (400 MPa approx.).

(12) Pressurising pump, specifications as for (8) .

(13) Let down valve, specifications as for (11) .

The tubing used in the pressure lines was originally $\frac{1}{4}$" O.D. 1/32" I.D. type 304 stainless steel tubing supplied by Tube Sales Ltd. But as the tubing had a rating of only 400 MPa it often burst at the higher pressures used. It was subsequently replaced by 5/16" O.D., 1/32" I.D. type 304 stainless steel seamless tubing also supplied by Tube Sales Ltd., as and when the $\frac{1}{4}$" tubing sections ruptured.

The entire pressurising system, apart from the hand-operated pumps (8) and (12) , is enclosed within, but electrically insulated from, a steel cabinet with $\frac{1}{4}$" thick mild steel plate sides. The reason for the system being insulated from the enclosing cabinet is that the electrical apparatus (described later, see § 4.4) is sensitive to electrical noise induced by earth loops which would have otherwise occurred.

The apparatus is pressurised by initially pumping on the low pressure side pressurising pump (12) until about 200 MPa pressure is attained within the system and autoclave. The low pressure side is then isolated using the isolation valve (9) and the further pressurisation is performed using pump (8) . A full procedure for pressurisation is detailed in (appendix 2.2).

4.23 Temperature Control

The temperature rises recorded during measurements on a fluid are between 2K and 5K, therefore the maximum allowable temperature drift tolerable inside the autoclave during measurements is 2×10^{-4}K.

Because a measurement is made up of a number of 1 second runs, separated by 60 second relaxation periods and is of approximately 5 minutes duration, the maximum allowable fluctuation within the vessel is $\simeq 3 \times 10^{-3}$K/hr.

In order to achieve the required thermal stability, the autoclave was immersed and suspended within a temperature controlled, well-stirred, oil bath, see fig. (4.4). The specifications of the individual components of the temperature control system are given below:-

(1) 15 amp variac controlled booster immersion heater, supplied by Tubalox, rated at 3KW at 230/250 volts.

(2) 2.54 cm thick blockboard case, housing vermicullite insulation.

(3) 7.6 cm thick layer of vermicullite insulation surrounding sides and bottom of the galvanised iron tank.

(4) 1/30 HP induction motors, mounted on the pressurising system's cabinet to prevent vibration of the autoclave. Motors are made by Klaxton Limited and produce 1425 r.p.m. The two motors, through a reducing gearbox, drive two stirrers, one longer than the other, incorporating 4" impellers and vertical fins mounted on a $\frac{1}{2}$" shaft.

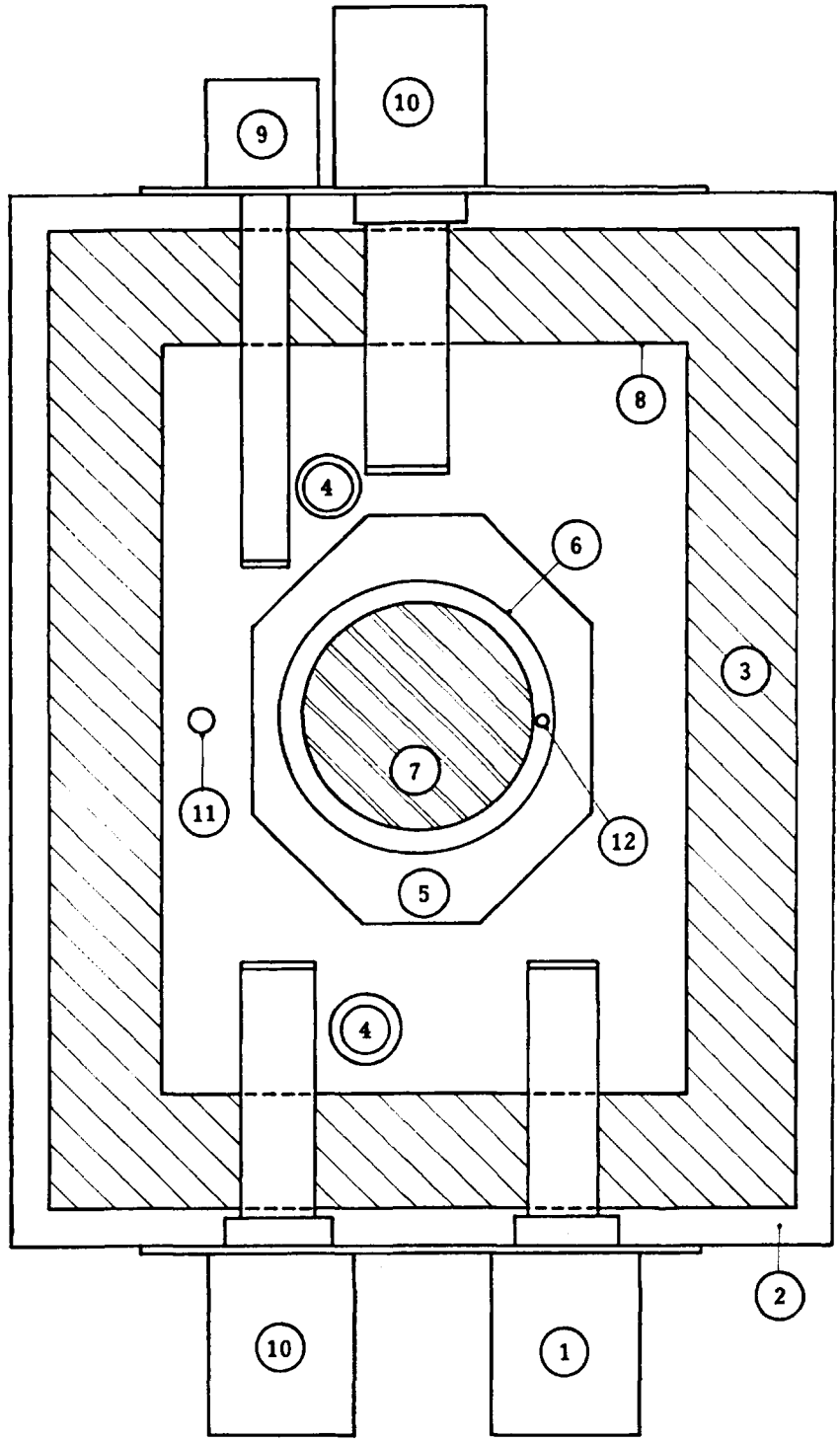

Fig. (4.4) Plan view of the Temperature Controlled Oil Bath

(5) $\frac{1}{4}$" thick mild steel plate bolted to the bottom of the pressure vessel and supporting the autoclave.

(6) 1/8" thick duraluminium sheet formed into a cylinder, providing lagging for the autoclave by trapping a 1.5 cm stagnant layer of oil between itself and the pressure vessel. A heating element 5 m long and 3 mm in diameter is wound in a bifilar position about the top 8 cms of the cylinder on its outer surface. The heater provides a temperature gradient in the outside of the pressure vessel of about 0.25K over its entire length and opposes natural convection which would otherwise occur due to cooling at the surface of the oil bath.

(7) Autoclave (see § 4.21).

(8) Oil bath, 20" long x 14" wide x 35" deep with a 4" flanged top constructed from 10 gauge galvanised iron sheeting.

(9) Control Heater, rated 230/250 volts, 500 watts, manufactured by Tubalox. The power to the heater is supplied by the temperature controller (not shown).

(10) Booster Immersion Heater, specifications as for (1).

(11) Platinum resistance thermometer, steel sheathed, manufactured by R.E.C. Ltd., model no. E666, 25 ohms nominal resistance, used as a sensing element for the temperature controller.

(12) Platinum 4 terminal class 1 resistance thermometer, manufactured by Degussa, model no. 8130 0031, 100 ohms nominal resistance, calibrated using a triple point cell (for calibration to $\pm$ 0.01K see appendix 2.3), strapped to the side of the pressure vessel and used to measure the absolute temperature of the autoclave.

4.3 Design of the Measurement Cell and Bellows Assembly

The design of the measurement cell and bellows assembly was based on experience gained through work on and the study of earlier cells used for measurements on both liquids and gases. The design incorporates the desirable aspects of earlier cells, while simultaneously

circumventing many of their undesirable features. The constraints imposed by operation up to 700 MPa and at temperatures above ambient, necessitated a somewhat different hot-wire cell design from that employed in work in the gas phase [91,85] .

4.31 The Measurement Cell

A number of criteria were used in the design of the thermal conductivity measurement cell, and these are given in their order of importance. Firstly, the assembled cell when used in the transient hot-wire apparatus must enable the thermal conductivity of the test fluid to be measured to a precision of $\pm$ 0.2% and an accuracy of $\pm$ 0.6% over the pressure range 0.1 MPa to 700 MPa, and the temperature range 300K to 400K. Secondly, the cell and bellows assembly must when assembled be able to fit and operate within the autoclave described in § 4.21 . The cell should also be easily assembled and finally, the cost of manufacture and use of the cell must be kept to a minimum.

To satisfy the first criterion, the cell must be mathematically reducible to the model upon which the transient hot wire technique is based (a description of the model is given in § 2.2), or sufficiently close to the model to enable the use of the calculable corrections (see § 2.3). In this context, by the diagramatic representation of the range of applicability of corrections and errors obtainable as a consequence of § 2.3 , (see fig. (4.5)), it is seen that the cell must enable operation within the indicated area.

One of the requirements of the mathematical model is a section of an infinitely long line heat source. As this is not physically possible, two thin wire heat sources, (the closest available substitute for line heat sources) of different lengths are used, in which the central section of the sources differ, in behaviour, from that of an infinite line source by a negligible amount. The end effects of the heat sources are "subtracted", one from the other, by a practical cancellation, resulting in the behaviour of the "remaining" segment of the long wire being sufficiently close to that of a finite

section of a heat source of infinite length. By the use of the equations given in § 2.3 , for a liquid having properties typical of those whose thermal conductivities are to be measured, it is found that the wires must be longer than about 4 cm in lenth, 10 μm or smaller in diameter, and the outer boundary of the cells must be greater than 0.6 mm in diameter [84] . The means by which the "subtraction" is invoked is presented in § 4.5 .

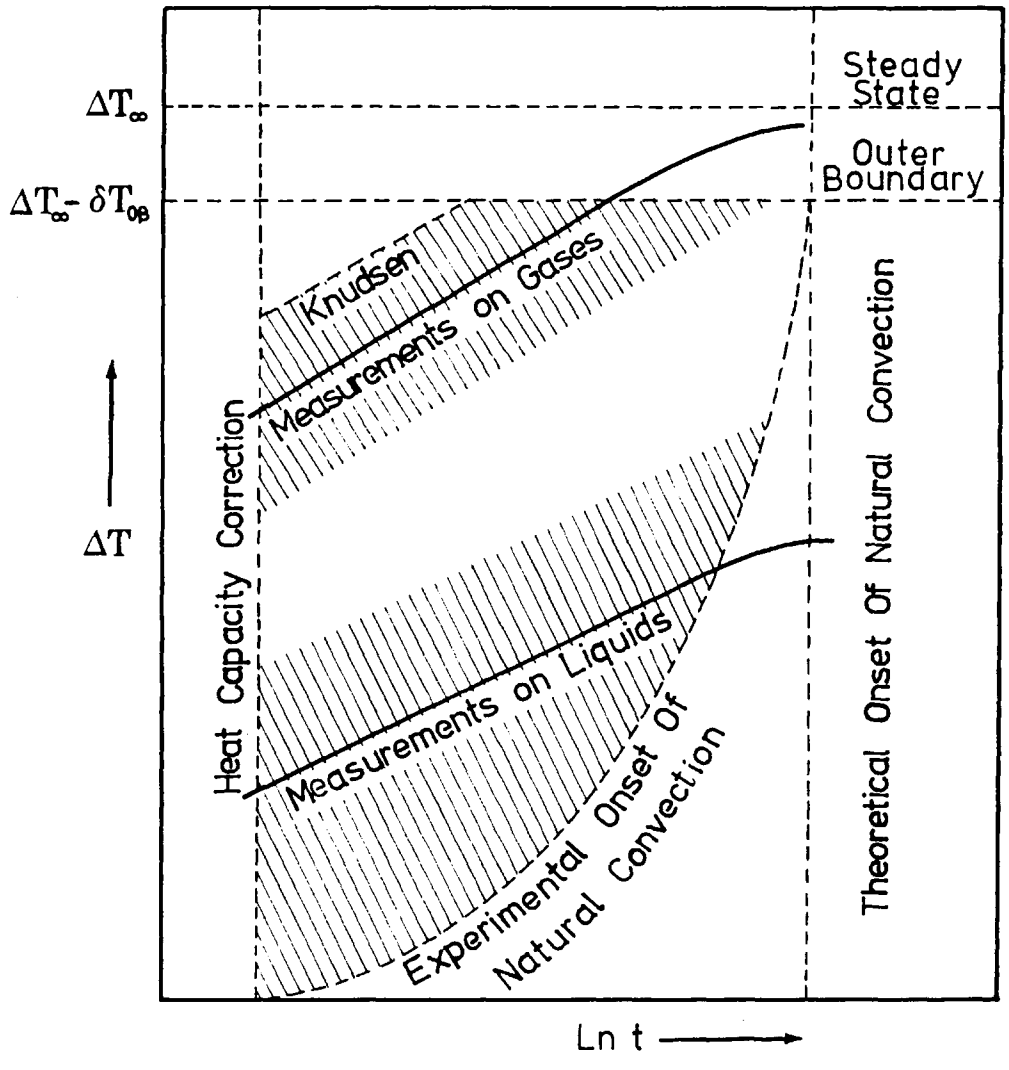

Fig.(4.5) The required operation range for a measurement cell.

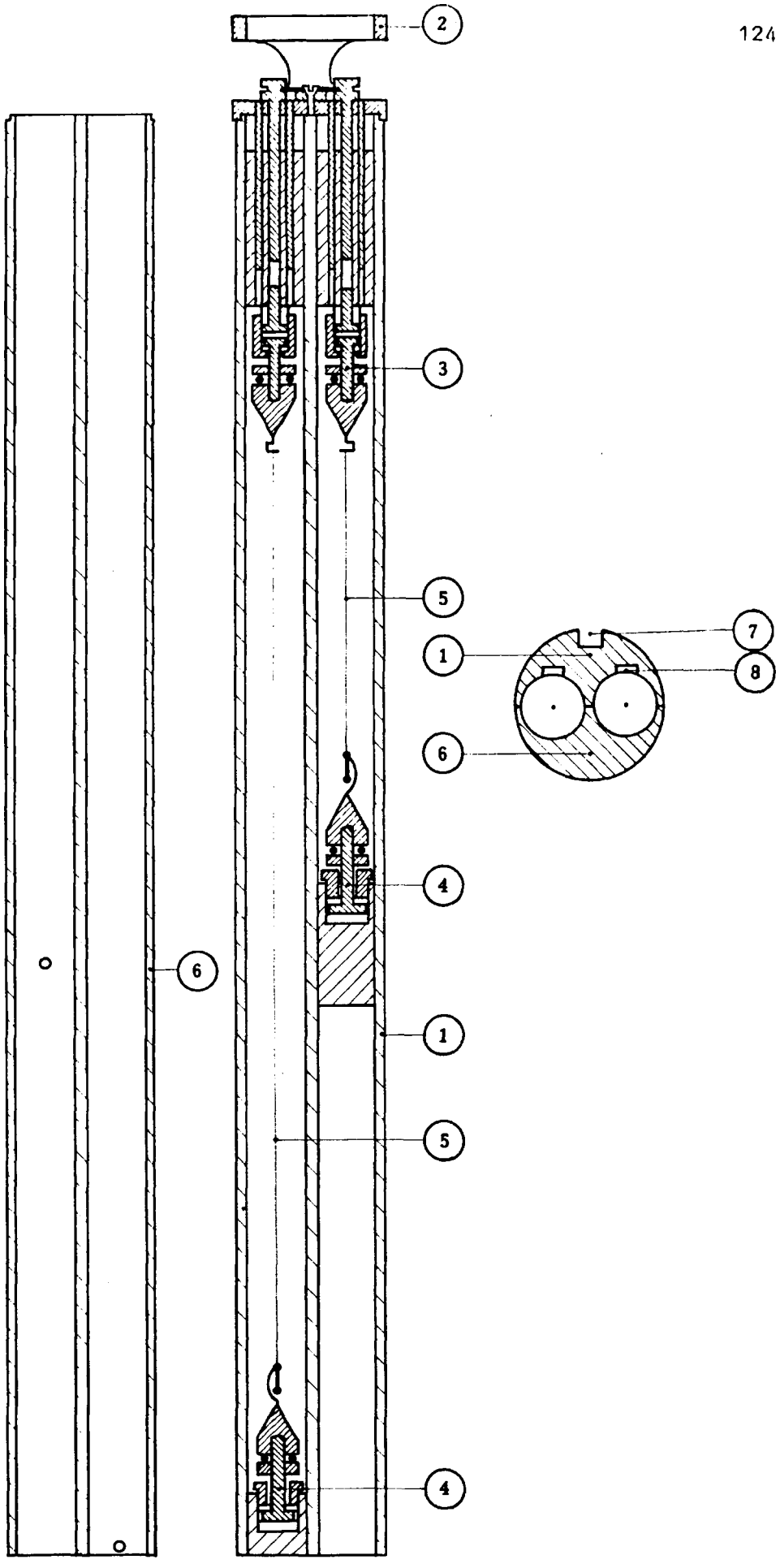

Fig. (4.6) The Measurement Cell

In the present apparatus, the cell employs two wire heat sources, differing only in length, mounted within two cylindrical compartments contained within a single stainless steel cylinder (type EN85M) The cell was made up from two hemicylindrical sections as shown in fig. (4.6), machined and lapped to form the cylinder which is 0.235 m long and 24.0 mm in diameter. Within the cylinder the compartments were formed by machining two cylindrical holes 9.5 mm in diameter, centred on the split diameter of the cylinder and parallel to its axis. The "active" half of the cylinder (1) carries; the cell top (2) which connects the cell to the pressure vessel plug; and the terminal posts (3) and (4) , which provide mechanical support for, and electrical connections to, the two platinum wires (5) of the cell. The passive half of the cell (6) forms a cover and, when fixed in position, provides a cylindrical outer surface for the two compartments of the cell. It is removable, so enabling the construction of the wire heat sources, within the two compartments. The active half also contains channels (7) and (8) down which run the 0.5 mm diameter, insulated, platinum connecting wires, which provide electrical contact with the upper terminal posts. The detail in fig. (4.6) is a crossectional view of the assembled cell and shows the positioning of the channels and compartments.

The hot wire heat source and terminal posts are shown in fig. (4.7). The lower terminal post is fixed to the cell body (1) by a screw through the stainless steel bushing (9) . The terminal connection is provided by the stainless steel screw (10) which is insulated from the bushing (9) by a 1 mm thick flat ground glass disc (11) and from the knurled threaded retaining collar (12) by a 1 mm thick flat-ground glass washer (13) . At its upper end, the terminal carries a threaded stainless steel cone (14) and a knurled lock-nut (15) which, between them secure the 0.5 mm diameter platinum wire connection lead (16) . The cone (14) is coaxial with the axis of the cell compartment and has a gold tip (17) to facilitate soldering.

The upper terminal post is constructed somewhat differently to allow for the vertical adjustment of its position. In a similar manner

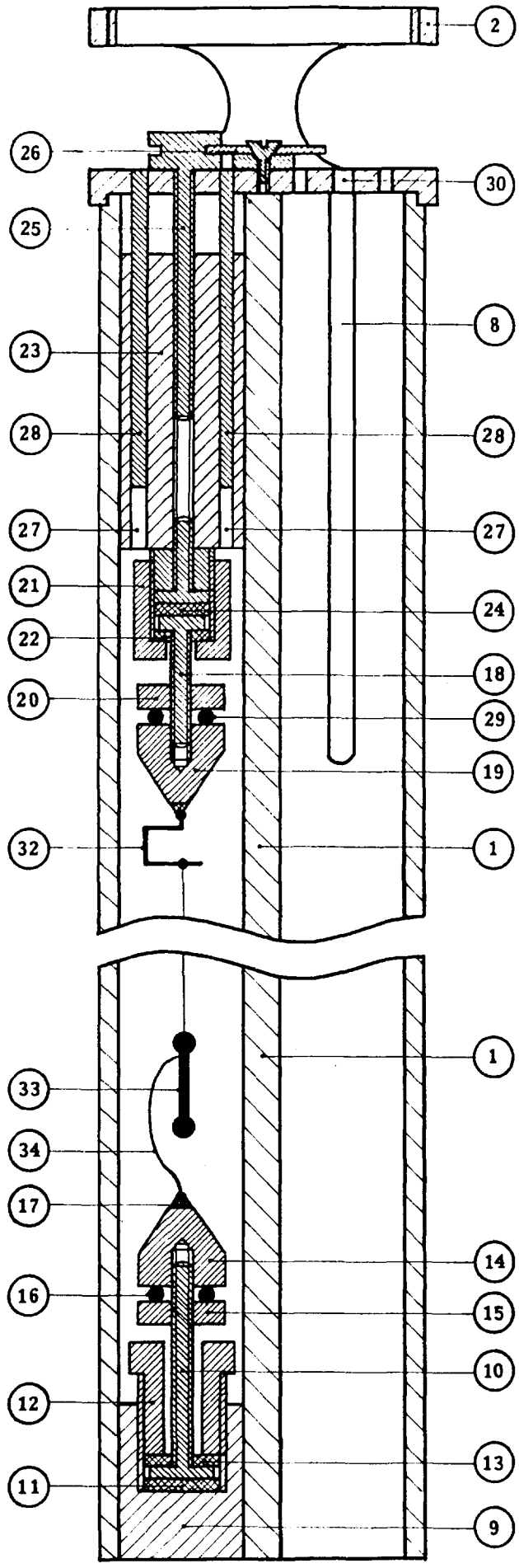

Fig. (4.7) Detail of the terminal posts.

the terminal connection screw (18) together with its gold-tipped stainless steel cone (19) and lock-nut (20) are supported in a threaded stainless steel bushing (21) , and insulated from it by a 1 mm thick, flat ground, glass washer (22) and from the stainless steel cylinder (23) by a 1 mm thick flat ground, glass disc (24). The bushing (21) is, however, free of the cell body and screwed to the stainless steel cylinder (23) , thus holding the disc (24) , washer (22) and screw (18) in position. The stainless steel cylinder (23) has a tapped hole threaded along its axis which carries an adjustment screw (25) that passes through the cell top (2) and is secured in position by means of a plate (20) . This plate fits into a groove machined in the head of the adjustment screw and is itself screwed to the cell top. The cylinder also has two guide holes (27) drilled into it which accomodate two cylindrical pins (28) fixed into the cell top (2) . The result of such a construction is that rotation of the adjustment screw (25) causes vertical movement of the terminal without its rotation and allows a total of 15 mm vertical adjustment.

The insulated platinum connection wire (29) from the upper terminal is led out of the cell through channel (8) and through a hole (30) in the cell top (2) . Whereas that from the lower terminal is run along channel (7) (in fig. (4.6)) and through another hole (not shown) in the cell top, where connection to the terminals in the pressure vessel plug occurs.

The hot wires of the cell are made of 7.78 μm(7 μm nominal) diameter platinum wire, whose purity was greater than 99.9%, as supplied by Goodfellow Metals Ltd. (The diameter reported being the average of a number of measurements on samples of the wire whose diameters were determined by electron microscope.) Fig. (4.7) shows how this wire is attached to the terminal posts. At the upper terminal a platinum hook (32) (made of 0.75 mm diameter wire) is soldered to the gold-tipped cone and the 7 μm platinum wire and is attached to it using gold as a solder. At its lower end, the 7 μm platinum wire is attached, using a gold sphere, to a cylindrical platinum weight (33) of approximately 50 mg. The upper end of the weight is electrically

connected to the lower terminal cone (14) by a loop of gold (34) attached at either end with a gold-tin solder. The loop (34) is manufactured by flattening a 2 cm piece of 0.06 mm diameter gold wire into a strip 1 mm thick followed by annealing at 1270K. In this way, a lower electrical connection of small electrical resistance (0.15 - 0.20Ω) is obtained which exerts essentially no horizontal or vertical force on the lower end of the 7 μm platinum wire. The wire, therefore, hangs vertically and is subjected to a constant tension due to the weight, this tension being virtually independent of the thermal expansion of the elements of the cell at the various experimental temperatures used. In the present measurements, the tension in the wire amounts to approximately 10% of the yield stress of platinum. Furthermore, the electrical resistance of the various components providing electrical connection to the 7 μm platinum wires amount to only 0.2 ohms, which is small by comparison with the resistances of the long and short wires ($\approx$450 ohms and $\approx$160 ohms respectively) so that a correction for this resistance may easily be applied.

After assembly of the platinum wires in the active half of the cell, the wires are annealed whilst supporting the weight, by passing an electric current through the wires, producing a power generation of approximately 85 watts/m of wire, for 1 hr followed by a show current reduction. The lengths of the two 7 μm diameter platinum wires are then very carefully measured at room temperature by means of a cathetometer. Care is needed during measurement as the % error incurred in the measured thermal conductivity due to errors in measuring the wire lengths, will be equal to the % error in the measured difference in length of the two wires. The characteristics of one of the cell constructions used in the present work to perform measurements is given in § 5.1.

The main advantage this cell design has over previous cells [41,85] is that if propertly constructed, the wires are under constant tension during measurement and do not become slack, due to differential expansion or any other reason. The weight also helps to ensure the wires

are vertical and so, to prolong the time period before the onset of convection in the test fluid during measurement.

Sample lengths of the 7 μm platinum wire were calibrated in order to determine the temperature coefficient of resistance of the wires. The details of the calibration can be found in appendix 2.4 and all that need be stated here is that the samples of wire were found to behave sufficiently closely to that of pure platinum to enable the use of the correlation quoted for pure platinum by the International Practical Temperature Scale of 1968 [86] , which can be used in the form:-

$$\frac{W(T)}{W(273.15)} = 1 + A(T-273.15) + B(T-273.15)^2 \qquad \text{.....(4.1)}$$

where:-

$$A = 3.98471 \times 10^{-3}\ K^{-1} \qquad \text{.....(4.2)}$$

$$B = -5.874557 \times 10^{-7}\ K^{-2} \qquad \text{.....(4.3)}$$

and so the latter has been adopted for the present measurements. It should be noted that, in the temperature range of interest, this correlation is insignificantly different from the correlation quoted in the International Practical Temperature Scale of 1976 [87] but is simpler to implement. The coefficients A and B in equation (4.1) and whose values are given in equations (4.2) and (4.3) refer to pure annealed platinum under no applied stresses and under atmospheric pressure conditions. The effects of tensile stresses and hydrostatic pressures are examined in § 4.521 and § 4.522 .

4.32 The Bellows Assembly

The cell which has just been described requires an enclosure inside which it and the test fluid are contained during measurement. The

enclosure is required in order to prevent contamination of the test fluid with the hydraulic fluid used to pressurise the autoclave. It must therefore be capable of transmitting the pressure to the test fluid contained within it and of accomodating for a 30% reduction in volume of the test fluid required during pressurisation. It must also fit within the autoclave described above in § 4.21 .

The bellows assembly designed and used for the present work is shown in fig. (4.8). It consists of a stainless steel tube (1), (threaded at each end) made of type EN85M stainless steel, with an inner bore of 25.4 mm and outer diameter 37 mm which at one end is connected with a lead seal (2) to the pressure vessel plug (3) and at the other to a bellows (4) and a valved end piece (5). The bellows made by Teddington Bellows Ltd., is constructed from a seamed stainless steel tube and has 19 convolutions, an inner bore of 25.4 mm, an outer bore of 35 mm and a length of 105 mm. The bellows is welded to a connector (6), which in conjunction with a lead seal (7) joins the bellows (4) to the stainless steel tube (1) The bellows is welded to the connector (6) and the valved end piece (5) using welding collars (8). The valved end piece (5) has a channel sealed by a grub screw (9), machined into it, which together with the filling holes (10) and (11) in the end piece (5) and stainless steel tube (1) are used for filling the assembly with the test fluid. The filling hole (11) is closed off with a lead seal (12) and a screw (13) after filling.

In order to prevent air being trapped in the cell and bellows the system containing the wires, which have already been assembled, is filled under vacuum. The bellows is supported mechanically during evacuation to prevent collapsing and the system is filled, from the bottom, through filling hole (10) in fig. (4.8). Once the cell and bellows have been filled, the plug on which the cell and bellows assembly are mounted is placed into the pressure vessel.

The pressure drop across the bellows during measurement is less than 0.2 MPa and contributes a negligible error in the calculation of the

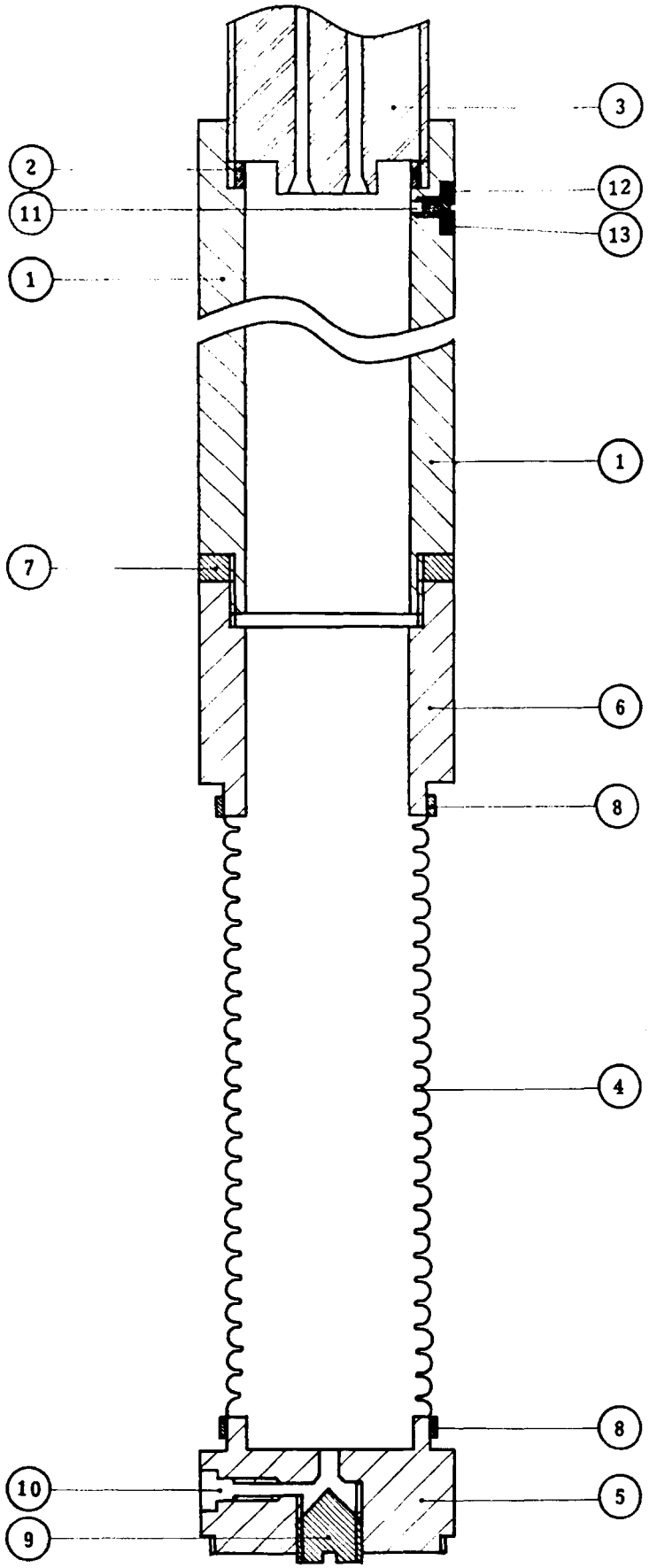

Fig. (4.8) The Bellows Assembly

test fluid density during measurement. It should also be mentioned in passing that in earlier designs of similar bellows assemblies [54] P.T.P.E. seals were used, but it was found that under high hydrostatic pressures (and independent of the differential pressure across them) these seals were compressed sufficiently to enable the hydraulic fluid to leak into the cell and contaminate the test liquid. For this reason, lead seals were used in the present work.

4.4 Electronic Apparatus

The function of the electronic apparatus is to provide the power to the hot wire heat sources and to record the times, following the initiation of this power, at which the difference in resistances between the two hot wires, immersed in the test fluid, attains certain predetermined values and so to indirectly determine the temperature rise of the middle portion of the long wire as a function of time. This section describes the components and use of the apparatus which enable these measurements to be performed.

4.41 The Automatic Bridge

The automatic bridge is based on that first used by Haarman [55] and its design and construction is detailed elsewhere [88,89] . A circuit diagram of the components is shown in fig. (4.9). The resistances of the long and short wires, mounted in the measurement cell, as described earlier (see § 4.3), are denoted by W_l and W_s respectively. Resistances are denoted using the prefix W and switches using S. The specifications of the various components used in the bridge circuit are given in Table (4.10).

Power to the bridge is supplied by two constant voltage, D.C., power supply units, type 6112A manufactured by Hewlett Packard, and arranged such that the potential of point (A) is close to earth and so keeps electrical noise, which can cause erroneous operation of the bridge, to a minimum. Changes in polarity across points (A) and (B) are detected by a high impedance, low noise level electronic comparator

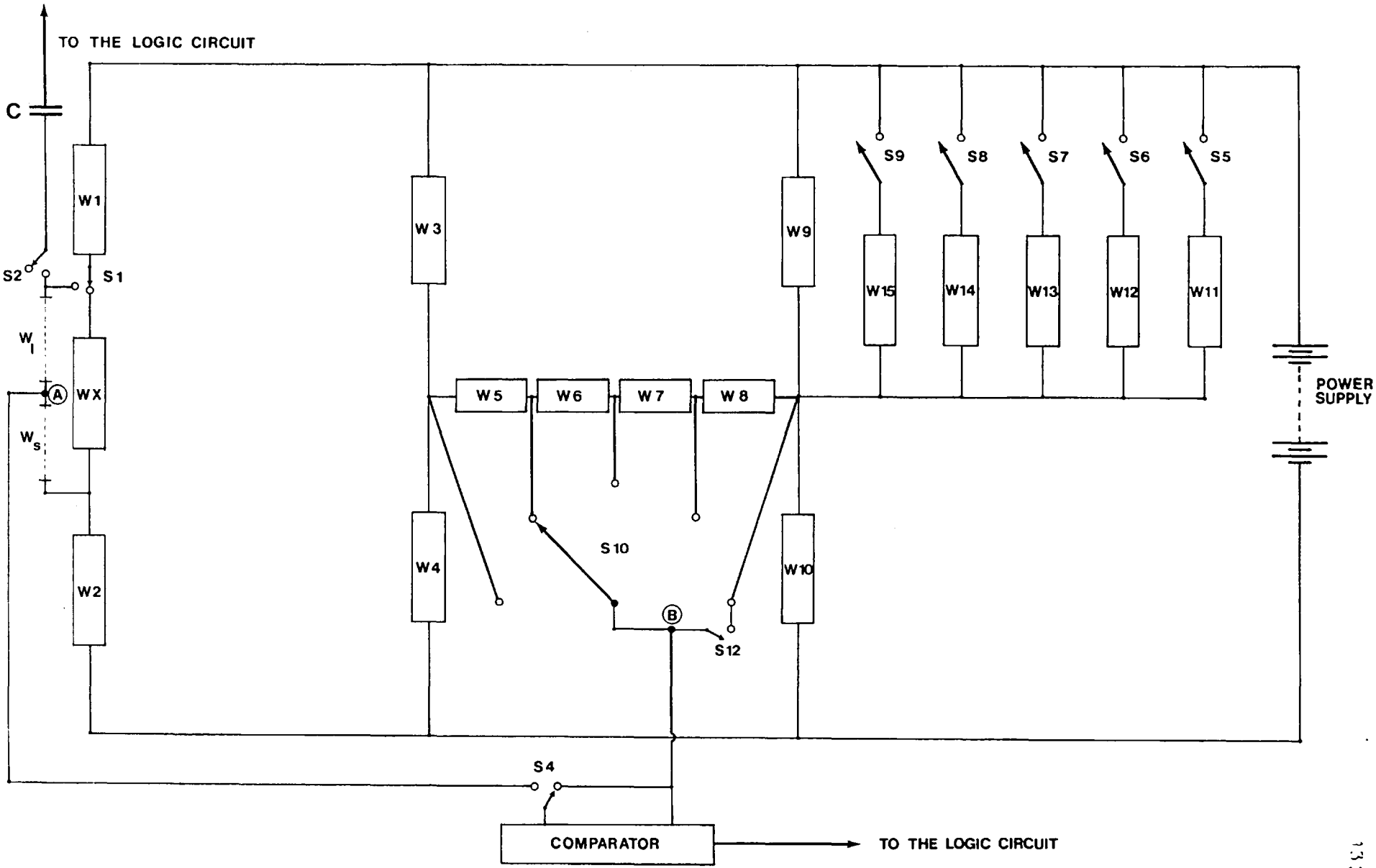

Fig. (4.9) The Automatic Bridge Circuit

BRIDGE COMPONENTS

Bridge Resistors

Resistor	Make/Model No.	Resistance Value K	Tolerance ± %	Power Dissipation W	Temperature Coefficient ppm/°C @ 20°C
W_1, W_2	Vishay 1304	10^{-5} 1	0.005	0.20	2
W_3, W_4, W_9, W_{10}	Vishay HA412	2	0.001	0.25	0
W_5	Vishay HA412	1	0.001	0.50	0
W_6	Vishay HA412	2	0.001	0.50	0
W_7	Vishay HA412	4	0.001	0.50	0
W_8	Vishay HA412	8	0.001	0.50	0
$W_{11}, W_{12}, W_{13}, W_{14}, W_{15}$	Muirhead D805 E,F,G/1	10 1100	0.001	0.50	5
WX	Muirhead D825K	10^{-4} 1	0.010	1.00	50

Switches

Switch	Switch Type
S_1	Mercury wetted reed relay
$S_2, S_5, S_6, S_7, S_8, S_9$	High speed antibalance reed relays
S_4	Single pole,single throw
S_{12}	Single pole,single throw,low contact resistance
S_{10}	Single pole,5-way,low contact resistance

Capacitor C has a capacitance of 0·1 μF

Table (4.10)

which provides the input for the controlling logic circuit (see § 4.43).

The automatic bridge operates as follows. Prior to a run, mode and selection positions (discussed later in this section) are chosen and the ballast resistor WX is set to be approximately equal to the sum of resistances of the long and short wires (this prevents current surges upon switching S1). In this "reset" position, by adjusting W_1 and W_2, to be approximately equal to the resistances of the short and long wires respectively, the bridge can be arranged such that the resistance of its upper right hand side, comprising resistors W9, and W11 to W15, is slightly in excess of that required to balance the bridge (zero voltage between (A) and (B)). The bridge is then armed, S2 is closed and the comparator is switched into the circuit using switch S4.

On firing the bridge, by switching S1, current starts flowing through the wires and simultaneously a DC signal is sent through the capacitor C, which produces a pulse that feeds the logic circuit. The logic circuit, which controls the operation of the bridge, on receiving the pulse, opens gates, between six electronic counters and a crystal controlled clock, initiating the timing sequence and reopening switch S2 after 3 ms.

The current flowing through the wires causes the wires to dissipate heat and their temperatures to increase, thus increasing their resistances. As the temperature increase in both of the wires is essentially the same, the resistance of the long wire increases by more than that of the short wire. This opposes the out of balance, caused by the resistances of the upper right hand side of the bridge, until eventually the voltage across points (A) and (B) passes through zero, indicating a balance condition. When this polarity reversal is detected by the comparators the logic circuit stops the first electronic counter and so records the time taken to reach the first balance point. It also adjusts (in a manner described later when discussing the mode switch) the right hand arm of the bridge so as to have a slightly

larger resistance than before, and thus throws the bridge out of balance again.

As the resistance of the wires continues to increase, due to their continuing increase in temperature, the bridge moves towards a further balance point. Upon reaching this second balance point, the second counter is stopped, recording the time taken to reach the second balance condition, and the resistance of the upper right hand arm is readjusted as before. The process is continued six times in total until all six counters are stopped, recording the six times at which the bridge balances. The sixth balance point occuring when all five switches in the right hand arm of the bridge S5 to S9 are "open circuit". The logic circuit then returns the bridge to the reset mode. A run, therefore, is seen to yield six times at which the resistances of the wires attain six values, predetermined by the bridge configuration. Fig. (4.11) is a plot of the voltage across points (A) and (B) versus Ln time during a run. The regular distribution in Ln time is accomplished by suitable choice of the resistors in the bridge [89] and is desirable due to the form of the working equation (2.2) from which the thermal conductivity of the test fluid is calculated.

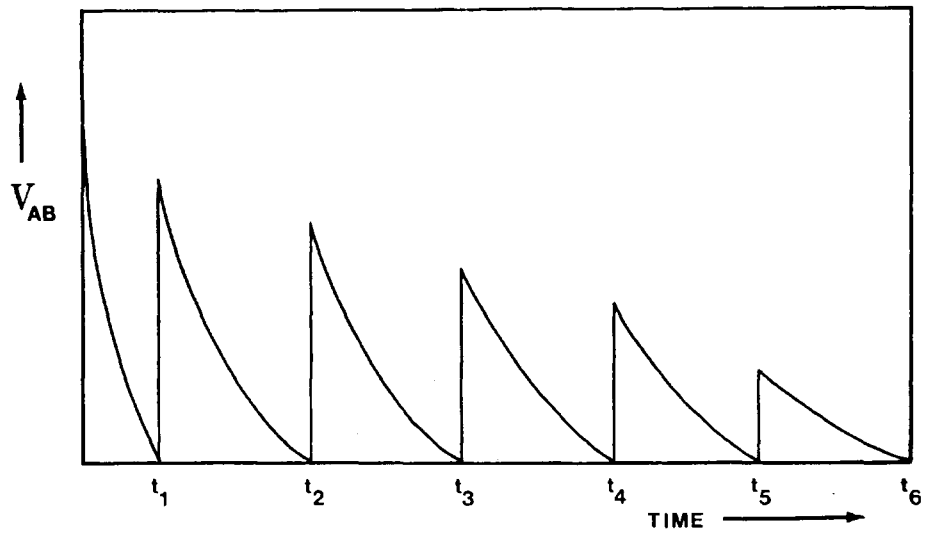

Fig. (4.11) Distribution of the balance points in time.

The logic circuit contains a mode switch which determines the manner in which the five resistors in the upper right hand side of the bridge, W11 to W15, are switched into or out of the circuit during a run. In one mode (mode A) all the resistors are initially in line (switches S5 to S9 are closed) and are switched out of circuit by sequentially opening switches S5 to S9, one at each balance point, resulting in the final balance point occuring when all the resistors are "open circuit". In the other mode (mode B) resistor W11 is initially in line and at the first balance point this is replaced by W12 and by W13 at the second and so on until for the final balance point, all the resistors are "out of circuit". The Selector switch S10 (which has five positions) and S12 alter the bridge configuration requiring different values of wire resistances W_l and W_s to produce a bridge balance. These switches increase the number of balance times obtainable by a particular bridge configuration without changing any of the individual resistance values. Moreover, as the resistances W11 to W15 are variable, decade resistors, a great deal more balance points are obtainable for a single measurement (at a particular thermodynamic state). This ensures a good distribution of points in the resulting ΔT (temperature rise) versus Ln time plot, from whose gradient the thermal conductivity of the fluid, at that particular thermodynamic state, is calculated.

It should be noted that for any bridge resistance configuration, the final (sixth) balance time in a run occurs with switches S5 to S9 open and therefore is independent of the mode of operation and selector positions and can therefore be used as a check on the bridge operation.

4.42 The Comparator

The times at which the bridge balances are determined by recording the times at which the voltage across points (A) and (B) in fig. (4.9) passes through zero. This is achieved using a comparator which is in essence a very sensitive electronic galvanometer. The circuit diagram of the comparator used is shown in fig. (4.12). It consists of two input buffer amplifiers (type 43K) which are balanced in a cross-

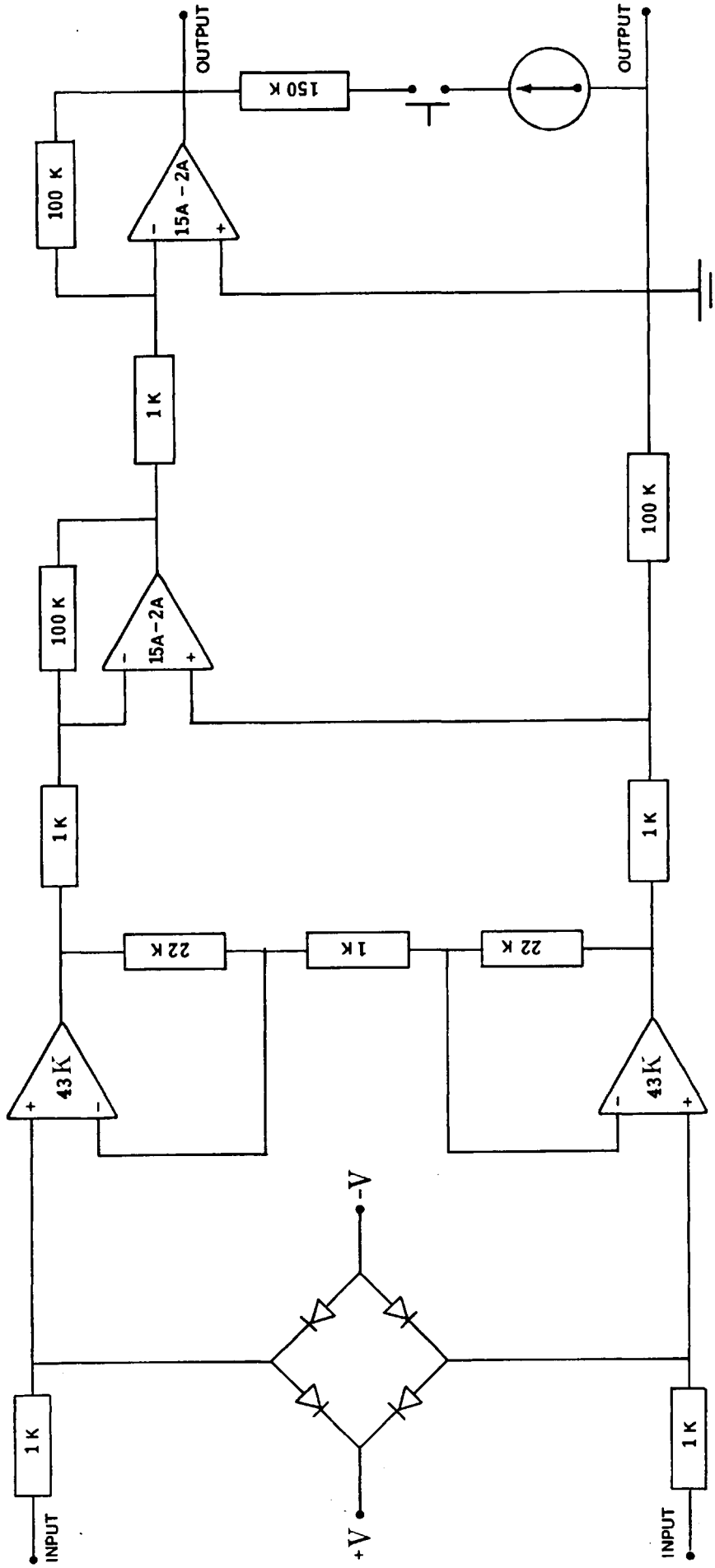

Fig. (4.12) The Comparator

coupled mode so as to achieve a very high input impedance (greater than 10^{11} ohms) and a common rejective ratio of greater than 80 db.

The crosscoupled mode implemented insures that common mode signals are passed at unit gain while differential signals are amplified. The outputs of the two buffers feed a conventional differential circuit, that is provided with a zeroing adjustment and a meter to allow offset adjustment.

In this apparatus, the specifications of the comparator are a band width of 100 KHz, a gain of 4×10^6 and a peak to peak noise level of approximately 20 μV. These parameters are consistent with the inherent noise level from the resistors used in the bridge and the time scale of the measurements.

4.43 The Controlling Logic Circuit

The operation of the automatic bridge is controlled by an electronic logic circuit which is responsible for the automatic sequencing of the resistors in the upper right hand arm of the bridge, (Resistors W11 to W15 in fig. (4.9), the gating of timing counters and the supply of power to the wires.

A circuit diagram of the apparatus used is shown in fig. (4.13). The sequencing of the bridge resistors is accomplished using a six stage shift register, clocked by signals sent from the comparator, through a 2 ms monostable. The shift register (SN74174) operates four nand gates (In mode A) or four nor gates (in mode B), depending on the mode of operation. These gates drive high speed reed relays, S5 to S9, used to switch the resistors W11 to W15 (see fig. (4.13)) into and out of the bridge circuit. The shift register also operates six nand gates which connect the quartz clock (MEON type MC105-TM) to six timing counters (each 6 X SN7490).

To initiate a run, the "Reset", "Arm", and "Start" buttons are sequentially depressed and the rest of the bridge operation is performed

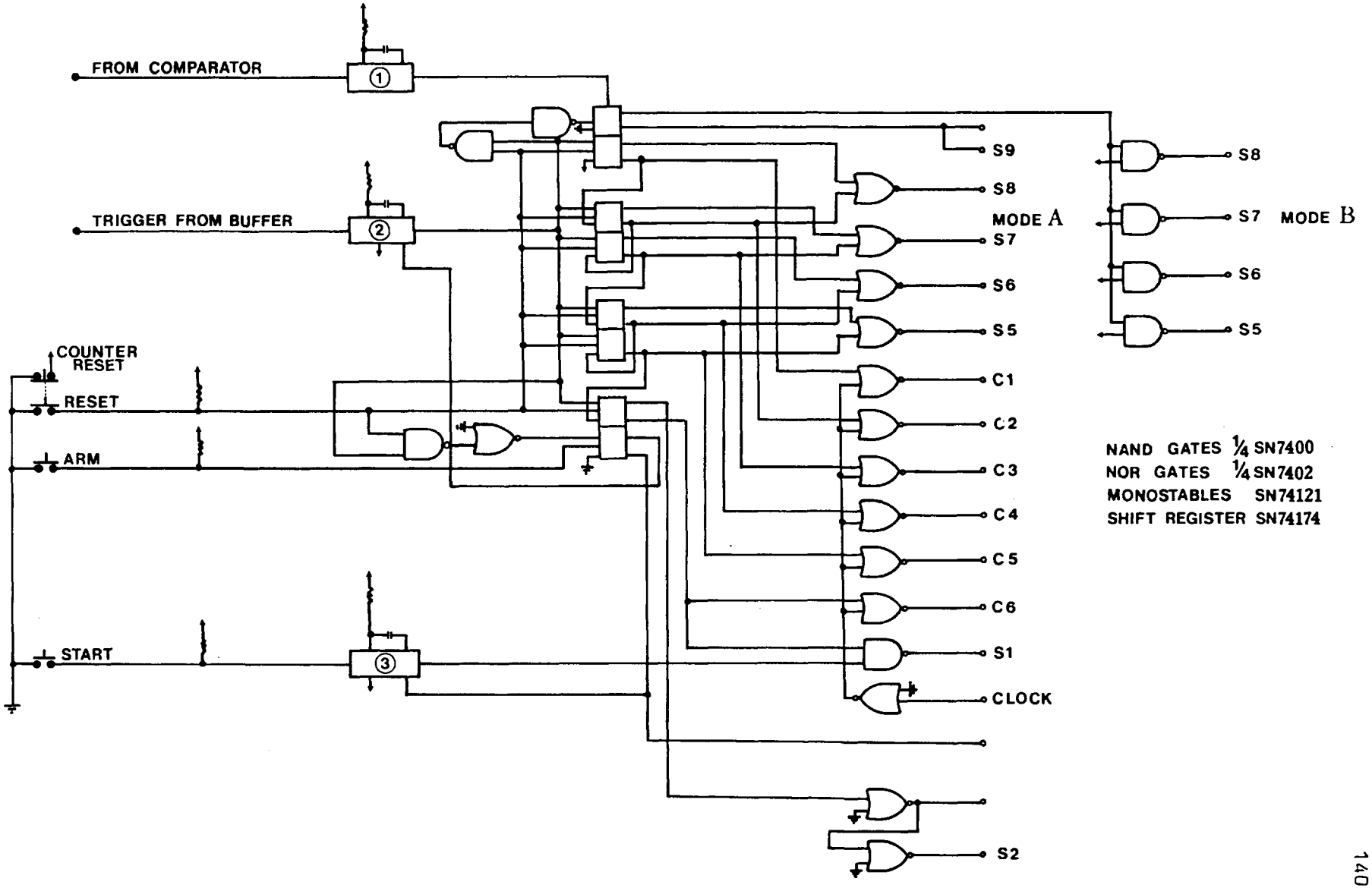

Fig. (4.13) The Bridge Control Logic Circuit

automatically by the logic circuit. The "Reset" button resets all the timing counters and loads all the bistables to logic state '1', thus gating off all the timing counters and de-energising all the reed relays, S5 to S9, disconnecting the resistors from the bridge circuit. The "Arm" button enables the Starting monostable (2) and the Triggering monostable (3) ; and energises relay S2, connecting the comparator into the circuit. On depression of the "Start" button the 30 ms Starting monostable (3) is fired, energising relay S1 and initiating the flow of current through the wires. The current flowing through the wires produces a pulse through capacitor C(in fig. (4.13), which fires the the 2 ms monostable (2) which in turn clears all the elements of the shift register setting them to logic state '0'. Should the triggering pulse not be detected, and monostable (2) not fired, then, after the 30 ms pulse, switch S1 will be deenergised thus removing the current from the wires and the system "fails safe".

Assuming mode A operation and that monostable (2) is fired, then on clearing the elements of the shift register, this energises all the reed relays S5 to S9 and connects resistors W11 to W15 into the bridge circuit. The 2 ms pulse holds the shift register clear while the relays and comparator settle, (the relays exhibit a certain amount of bouncing on operation), masking any stray signals detected by the comparator during this period.

When the first balance point is reached, the bridge polarity across (A) and (B) in fig. (4.9) is reversed and detected by the comparator which in turn fires the 2 ms monostable (1) shifting a logic state '1' to the first element of the shift register. This closes the nand gate between the clock and counter C1, so stopping this counter. With the first element of the shift register being in logic state '1' this simultaneously deenergises the relay S9 and removes resistor W15 from the circuit. During the 2 ms pulse produced by the firing of monostable (1) stray signals detected by the comparator due to relay bounce etc. are prevented from reaching the shift register because monostable (1) cannot be refired until after the pulse has subsided. For this reason the bridge is "dead" for 2 ms following

a balance condition and therefore the time between balance conditions must be made greater than 2 ms by the suitable choice of resistance values in the bridge [90] .

Resistor W15 having been removed from the circuit, the bridge moves towards a second balance point whereupon monostable (1) is again fired; in a similar manner to that described the shift register has a second element set to logic state '1'; and the second counter is stopped and W14 is removed from the circuit. This continues until all the resistors have been removed from the circuit and all the counters have been stopped. After the final (sixth) balance condition, the gates to relays S1,S2 are closed thus removing the power to the wires and then the comparator is switched out of the bridge circuit.

The prece ding description applies to mode A operation of the bridge. When operating in mode B the four nor gates between the shift register and relays S5 to S8 are replaced by the five nand gates as detailed in fig. (4.13) and the bridge on reaching balance conditions will operate by sequentially replacing resistor W15 for W14 and then for W13 and so on until for the sixth balance condition none of the resistors are in the circuit.

It should also be noted that by inhibiting the automatic operation of the bridge it is also possible to use the bridge to perform direct, steady state measurements of any resistance including that of either wire.

4.5 Working Equations

This section presents the mathematical equations used to obtain the resistance difference, between the long and short wires, at a balance point with the bridge in a particular configuration. Also included in the section are those equations used to determine the temperature rise of the middle portion of the long wire as well as the heat flux emitted from this portion to the fluid. These equations used in conjunction with the relevant physical properties and dimensions of the

platinum wire, fluid and cell enable the determination of the wire temperature rise as a function of time and so the thermal conductivity of the fluid.

4.51 The Bridge Balance Equations

The bridge is at a balance condition when the voltage between points (A) and (B) in fig. (4.9), V_{AB}, is zero. We require to know the difference in resistance between the long and short wires at balance, $W_{ls}(T)$ when the bridge is in any particular configuration.

Neglecting the tedious mathematical manipulation (which can be found elsewhere [88])required to obtain the result, the resistance difference $W_{ls}(T)$ is, for the bridge configuration shown in fig. (4.9) with switch S12 open, conveniently expressed as:-

$$W_{ls}(T) = W_l - W_s = \frac{H W_2 - W_1}{\left[\frac{W_l}{W_s} - H\right]}\left(\frac{W_l}{W_s} - 1\right) \qquad \text{.....(4.4)}$$

where:-

$$H = \frac{1 - (I + 1)/M}{(1 + I/M)} \qquad \text{.....(4.5)}$$

:- $$I = \beta\frac{W'}{W} \qquad \text{.....(4.6)}$$

:- $$M = \left\{2\,\frac{WS}{W} + 1\right\}\left\{1 + \frac{W'}{W}\right\} \qquad \text{.....(4.7)}$$

:- $$W' = W5 + W6 + W7 + W8 \qquad \text{.....(4.8)}$$

and because of the bridge design, see table (4.10):-

$$W = W3 = W4 = W9 = W10 \qquad \text{.....(4.9)}$$

$W5$ as used in the above equations is the equivalent resistance of the parallel resistors in the upper right hand arm of the bridge and is dependent upon the switch positions of S5 to S9, while β is the fraction of W' in circuit between point (B) and resistor $W3$.

Similarly, the resistance difference $W_{ls}(T)$ can also be found when switch S12 (in fig. (4.9)) is closed and results in an expression similar in form to that shown above. These expressions are to be found elsewhere[88].

In order to obtain $W_{ls}(T)$ explicitly from equations (4.4) to (4.9), all we still require is the ratio of the resistances of the two wires at equilibrium, W_l/W_s. As previously mentioned in § 4.43, when describing the automatic bridge operation, the resistances of the long and short wires at equilibrium, W_{lo} and W_{so}, can be determined directly. One can therefore write the ratio of the resistances of the wires during a measurement in the form of a perturbation as:-

$$\frac{W_l}{W_s} = \frac{W_{lo}}{W_{so}}(1 + f) \qquad \text{.....(4.10)}$$

In equation (4.10) f represents a small quantity which is only very weakly temperature dependent. To a good zeroth approximation, it may be taken to be zero and better approximations are obtained subsequently using an iterative procedure as outlined in § 4.54.

4.52 The Temperature Coefficient of Resistance

The transient hot wire technique for measuring the thermal conductivity of a fluid employs a platinum wire section which is used both as a heat source and as a thermometer. The latter function is achieved using a pseudo-linear temperature coefficient of resistance for the platinum wire to obtain its temperature rise from its resistance using the following equation:-

$$\Delta T = T - T_o = \frac{W_{ls}(T,S,P) - W_{ls}(T_o,S,P)}{\alpha'(T_o,S,P)W_{ls}(T_o,S,P)} \qquad \text{.....(4.11)}$$

In equation (4.11), $W_{ls}(T_o,S,P)$ is the resistance difference between the long and short wires at equilibrium temperature and under an axial stress S and hydrostatic pressure P.

The temperature coefficient of resistance, $\alpha'(T_o,S,P)$ is also a function of these same quantities. From equation (4.1) we see that under conditions of zero hydrostatic pressure, and axial stress, the temperature coefficient of resistance of pure platinum is:-

$$\alpha'(T_o,0,0) = \frac{A + B[(T-T_o) + 2(T_o-273.15)]}{1 + A(T_o-273.15) + B(T_o-273.15)^2} \qquad \text{.....(4.12)}$$

The above form of the temperature coefficient of resistance may be used provided that the platinum wire is always under the conditions appropriate to its calibration (zero hydrostatic pressure and axial stress). However, the cell design requires an axial tension to be imposed upon the wires which is not present during calibration and the instrument is also operated at elevated hydrostatic pressures not employed for the calibration. It is therefore necessary to investigate to what extent these effects influence the resistance temperature characteristics of the wire. Because the wire resistance itself is measured in direct, independent, measurements our only concern here need be with the effect on the temperature coefficient of resistance α'.

4.521 The Effect of Axial Tension

For the purposes of the present and some of the later analyses, it is convenient to consider the resistance difference $W_{ls}(T,S,P)$ to refer to the resistance of a segment of an infinitely long platinum wire, the length of the segment being the difference between those of the long and short wires. When therefore the hot wire is referred to, it is to be understood that it is the segment just described that is considered.

On the application of an axial stress, S, to the wire it affects both the geometry of the wire and the resistivity of the platinum from which it is made. The relationship between $W_{1s}(T,S,P)$ and $W_{1s}(T,0,P)$ can be shown to be:-

$$W_{1s}(T,S,P) = W_{1s}(T,0,P)(1+\epsilon_{1S})(1+\epsilon_{2S}) \quad \text{.....(4.13)}$$

where:-

$$\epsilon_{1S} = (1 + 2\,\nu_{pt})S/Y_{pt} \quad \text{.....(4.14)}$$

and for platinum and the relevant conditions applicable to our measurements.

$$\begin{aligned} \nu_{pt} &= \text{Poissons ratio} = 0.35 \\ Y_{pt} &= \text{Young's Modulus} = 1.6 \times 10^{5}\ \text{MPa} \\ \epsilon_{2S} &= 2.77 \times 10^{-7}\ \text{MPa}^{-1}\ [92] \end{aligned} \quad \text{.....(4.15)}$$

The present cell design results in the tension in the wire being invariant during measurement. Because of this, the resistance of the wire at the equilibrium temperature, T_o, is measured under essentially the same longitudinal stress as is present at the raised temperatures occurring during thermal conductivity measurements. Although the quantities ν_{pt}, Y_{pt}, and ϵ_{2S} are not all weakly dependent on temperature, but because the increase in resistance of the wire, due to the axial stress imposed, is less than 0.02%, we find the effect of the constant axial stress on the wire to be negligible and therefore we can write that:-

$$\alpha'(T,S = \text{constant},P) = \alpha'(T,0,P) \quad \text{.....(4.16)}$$

4.522 Effect of Hydrostatic Pressure

The effect of pressure on the coefficient of resistance of pure platinum can be expressed as (see appendix A2.4):-

$$\alpha'(T,P) = \alpha'(T,0)(1 + \epsilon_p P) \qquad \text{.....(4.17)}$$

where it has been found that:-

$$\epsilon_p \approx 1.6 \times 10^{-6} \text{ (MPa)}^{-1} \qquad \text{.....(4.18)}$$

and at the highest pressures employed during experiments constitute about 0.08% in α'.

The applicability of the form of equation (4.17) for the platinum wires used in a cell has also been tested and substantiated to within the experimental uncertainty of the automatic bridge when used to measure resistances ($\pm$ 0.1 Ω).

Equation (4.11) can now be replaced with:-

$$\Delta T = \frac{W_{ls}(T,S,P) - W_{ls}(T_o,S,P)}{\alpha'(T_o,0,0)W_{ls}(T_o,S,P)(1 + \epsilon_p P)} \qquad \text{.....(4.19)}$$

from which the temperature rise is calculated.

4.53 The Temperature Rise of the Hot Wire

The transient hot wire described and used in the present work employs two wire heat sources used in opposite arms of the automatic bridge to eliminate end effects caused by axial heat transfer through the wires to the terminals at their ends. Compensation to eliminate this effect is achieved by measuring the difference in resistance between the two wires. This would yield the temperature rise of the middle portion of the long wire, provided the wires were identical apart from their lengths. If the wires were long enough, this temperature rise would differ from that occuring in a finite segment of a hypothetical infinitely long wire by a negligible amount. (see § 2.334). Unfortunately, in practice the wires are never identical due to, among other things, non-uniformities in their radii. However, if the resistance per unit length of the two wires differ from each

other by less than a few percent, their dissimilarity can be accounted for using an analysis by Kestin & Wakeham [58] .

Ignoring all the temperature corrections arising from the non-ideal behaviour of the wires, which after all are small (see § 2.3) then the temperature rises of the long and short wire are adequately described by:-

$$(\Delta T)_1 = \frac{q_1}{4\pi\lambda} \operatorname{Ln}\left\{\frac{4kt}{a_1^2 C}\right\} \qquad \ldots\ldots\ldots\ldots\ldots\ldots\ldots\ldots\ldots\ldots(4.20)$$

and

$$(\Delta T)_s = \frac{q_s}{4\pi\lambda} \operatorname{Ln}\left\{\frac{4kt}{a_s^2 C}\right\} \qquad \ldots\ldots\ldots\ldots\ldots\ldots\ldots\ldots\ldots\ldots(4.21)$$

The subscripts 1 and s refer to the long and short wires respectively and the radii a_1 and a_s are suitable mean values for each wire.

As the temperature rise of a wire is experimentally obtained from it's measured resistance increase, an experimentally averaged temperature rise, $\overline{\Delta T}$, is defined for the long and short wires as:-

$$\overline{\Delta T}_1 = \frac{W_1 - W_{1o}}{\alpha' W_{1o}} \qquad \ldots\ldots\ldots\ldots\ldots\ldots\ldots\ldots\ldots\ldots(4.22)$$

and

$$\overline{\Delta T}_s = \frac{W_s - W_{so}}{\alpha' W_{so}} \qquad \ldots\ldots\ldots\ldots\ldots\ldots\ldots\ldots\ldots\ldots(4.23)$$

Where W_1 and W_s represent the resistances of the long and short wires at time t as would be measured during an experiment and W_{1o} and W_{so} refer to their resistances at equilibrium.

These experimentally averaged temperatures as defined by equations (4.22) and (4.23) differ from the idealised temperature rises by an amount dependent upon the heat conducted axially at the ends of the wires. Although we do not know the exact relationship between $\overline{\Delta T}_l$ and $(\Delta T)_l$ we know that their difference will increase with increase in the heat flux in the wire and decrease with increasing wire length. Therefore we write:-

$$\overline{\Delta T}_l = (\Delta T)_l - \frac{q_l}{l_l} F_l \qquad \text{.....(4.24)}$$

$$\overline{\Delta T}_s = (\Delta T)_s - \frac{q_s}{l_s} F_s \qquad \text{.....(4.25)}$$

where, F_l and F_s are functions of their respective wires' radius, thermal conductivity and thermal diffusivity; and the wires' end geometry as well as being a function of time.

Defining a further temperature rise $\Delta T'$ where:-

$$\Delta T' = \frac{(w_l - w_s) - (w_{lo} - w_{so})}{\alpha'(w_{lo} - w_{so})} = \frac{w_{ls} - w_{lso}}{\alpha' w_{lso}} \qquad \text{.....(4.26)}$$

we see that this temperature rise, $\Delta T'$, as defined by the directly measurable quantities in equation (4.26) above, is not as yet identifiable with the central portion of either wire. The object of the analysis is to relate this experimentally determinable quantity $\Delta T'$ with the hypothetical temperature rise of the middle portion of an infinitely long, long wire $(\Delta T)_l$.

Using equations (4.22) and (4.23) the temperature rise $\Delta T'$ may be expressed in terms of the temperature rises $\overline{\Delta T}_l$ and $\overline{\Delta T}_s$ as:-

$$\Delta T' = \frac{w_{lo}\,\overline{\Delta T}_l - w_{so}\,\overline{\Delta T}_s}{w_{lso}} \qquad \text{.....(4.27)}$$

After manipulation, this is seen to result in:-

$$\Delta T' = (\overline{\Delta T})_1 \left\{ 1 + \frac{W_{so}}{W_{lso}} \left[1 - \frac{(\Delta T)_s}{(\Delta T)_1} \right] - \frac{(q_1 \bar{\sigma}_1 F_1 - q_s \bar{\sigma}_s F_s)}{W_{lso}} \right\} \quad \ldots\ldots(4.28)$$

where $\bar{\sigma}_1$ and $\bar{\sigma}_s$ are equilibrium mean resistances per unit length of the wires defined by:-

$$\bar{\sigma}_1 = \frac{W_{lo}}{l_1} \quad \text{and} \quad \bar{\sigma}_s = \frac{W_{so}}{l_s} \quad \ldots\ldots\ldots\ldots\ldots\ldots(4.29)$$

It is immediately obvious from equation (4.28) that if the two wires are identical with each other, apart from their lengths, then $\Delta T'$ would be equal to $(\Delta T)_1$. In practice, this situation never exists and the general form of equation (4.28) is applicable. This equation contains two perturbation terms, the first arising due to the difference in the temperature rises between the long and short wires and the second due to the conditions of their ends not being identical. It can, however, be seen that if the resistance/unit length of the two wires differ by less than 2% then the second perturbation term is negligible as it is a second order effect. Using the fact that:-

$$\frac{(\Delta T)_s}{(\Delta T)_1} \approx \frac{1 - p_1}{1 + \left[\frac{p_1}{\text{Ln} \frac{4kt}{a_s^2 C}} \right]} \quad \ldots\ldots\ldots\ldots\ldots\ldots(4.30)$$

equation (4.28) now becomes:-

$$(\Delta T)_1 = \frac{\Delta T'}{1 + p_3} \quad \ldots\ldots\ldots\ldots\ldots\ldots(4.31)$$

where:-

$$p_1 = \left[1 - \frac{\bar{\sigma}_s}{\bar{\sigma}_1} \right] \quad \ldots\ldots\ldots\ldots\ldots\ldots(4.32)$$

$$p_2 = \frac{p_1\left[1 + \ln\left[\frac{4kt}{a_s^2 C}\right]\right]}{\ln\left[\frac{4kt}{a_s^2 C}\right]} \approx \frac{(\Delta T)_1 - (\Delta T)_s}{(\Delta T)_1} \qquad \ldots\ldots\ldots\ldots(4.33)$$

and:-

$$p_3 = \frac{w_{so} p_2}{w_{1so}} \qquad \ldots\ldots\ldots\ldots\ldots\ldots\ldots\ldots\ldots\ldots\ldots\ldots(4.34)$$

Using the bridge balance equation from § 4.51, with the zeroth order approximation that $\frac{w_1(t)}{w_s(t)} \approx \frac{w_{1o}}{w_{so}}$, enabling $w_{1s}(t)$ to be calculated and when used with the previously derived equations, the temperature rise of the middle section of the hot wire, $(\Delta T)_1$ is found.

An improvement on the zeroth order approximation for the ratio of resistances $\frac{w_1(t)}{w_s(t)}$ is now available as to a better approximation:-

$$\frac{w_1(t)}{w_s(t)} = \frac{w_{1o}}{w_{so}}\left\{1 + \alpha'\left\{(\Delta T)_1 - (\Delta T)_s\right\}\right\} \qquad \ldots\ldots\ldots(4.35)$$

which in the present ratio is:-

$$\frac{w_1(t)}{w_s(t)} = \frac{w_{1o}}{w_{so}}\left\{1 + \alpha'(\Delta T)_1 p_2\right\} \qquad \ldots\ldots\ldots\ldots\ldots(4.36)$$

and results in an itterative procedure being required to calculate $(\Delta T)_1$. In practice, it is found that the correction to the zeroth order approximation, as made through the use of equation (4.36), is under the worst condition encountered $\approx 0.03\%$ and so the convergence of the itteration procedure is rapid.

4.54 The Heat Flux from the Hot Wire

Having obtained the temperature rise of the middle portion of the long wire, the final quantity required to obtain the thermal conductivity of the test fluid is the heat flux per unit length from this portion of the wire. The bridge design shown in fig. (4.9) ensures that the same current flows through both the long and short wires. However, because the resistance per unit length of the two wires is not identical, this arrangement does not ensure that identical heat fluxes per unit length are emitted from the two wires.

Using a similar technique to that used to obtain the temperature rise, it is found that the heat flux from the middle section of the long wire is [58] :-

$$q_1 = \frac{q_{11}}{(1 - p_4)(1 + p_5)} \qquad \text{.....(4.37)}$$

where q_{11} is the heat flux obtained assuming ideal wire compensation (the wires are identical apart from their lengths) and:-

$$q_{11} = \left(\frac{V}{w_1(t) + w_s(t) + w1 + w2}\right)^2 \left[\frac{w_1(t) + w_s(t)}{(l_1 + l_s)}\right] \qquad \text{....(4.38)}$$

In terms of the resistance difference $w_{ls}(t)$, q_{11} may be expressed as:-

$$q_{11} = \frac{V^2 w_{ls}(t)/(l_1 - l_s)}{\left\{\frac{w_{ls}(t)(l_1 + l_s)}{(l_1 - l_s)} + w1 + w2\right\}^2} \qquad \text{.....(4.39)}$$

which is true provided that:-

$$\frac{w_1}{l_1} = \frac{w_s}{l_s} \qquad \text{.....(4.40)}$$

In equation (4.37):-

$$p_4 = \frac{2\,\bar{\sigma}_l p_1 l_l l_s}{(l_l - l_s)(W1+W2) + (W_l(t) - W_s(t))(l_l + l_s)} \quad \ldots\ldots\ldots\ldots (4.41)$$

also:-

$$p_5 = \frac{l_s p_1}{l_l - l_s} \quad \ldots\ldots\ldots\ldots\ldots\ldots\ldots\ldots\ldots\ldots\ldots\ldots (4.42)$$

and, p_1 is defined via (4.32); W1 and W2 are the bridge resistors set and recorded prior to measurement and V is the voltage applied across the bridge by the power supply units.

4.55 Wire Lengths

As the temperature at which measurements are performed is often significantly different from that at which the wires' lengths were measured ($\approx$295K), it is necessary to correct for this temperature difference. The correction used is:-

$$l(T_o) = l(T_m)(1 + \gamma(T_o - T_m)) \quad \ldots\ldots\ldots\ldots\ldots\ldots (4.43)$$

where γ is the temperature coefficient of expansion of platinum ($\approx 8.9 \times 10^{-6}\ K^{-1}$), T_m is the temperature at which the wires' measurements were performed, and l is the length of a wire.

Because the temperature rise during a measurement is only $\sim$5K, a further correction is not required as this causes an error of less than 0.01% in ΔT_{id}. The correction to $l(T_o)$ in practice accounts for at most (when $(T_m - T_o) \approx 70$K) for a 0.06% change in the calculated thermal conductivity.

4.56 Lead Resistances

Resistances of leads and connections are often significant in most transient hot wire apparati, and this is especially true for the present design of apparatus. The leads whose resistances are of importance are those connecting the long and short platinum wires to the bridge. In the present design, these leads include the golden loops (34) in fig. (4.7) which have a resistance of approximately 0.2Ω each. The design of the bridge is such that the effect is manifested in the calculation of the heat flux emitted from the wire but not in the measurement of its resistance. The resistances of these leads which would otherwise be included in the resistances of the platinum wires must instead be included in the resistances of the resistance boxes W1 and W2 of fig. (4.9).

4.6 Calculation of Liquid Thermal Conductivities

The previous sections have described how the instrument operates and the detailed working equations of the experimental method. In this section, the two are combined and it is shown how the thermal conductivity may be deduced from measurements with the transient hot wire technique.

4.61 Data Processing

The experimental measurements yield directly the times of bridge balances; the bridge configuration corresponding to each time; the bridge voltage used; the equilibrium resistances of the wires; the equilibrium bath temperature and the hydrostatic pressure within the measurement cell during the experiment. From these data we compute the idealised temperature rise, ΔT_{id}, of a segment of the platinum wire as a function of time, during an experiment. This, as a consequence of the working equation describing their relationship:-

$$\Delta T_{id} = \frac{q}{4\pi\lambda(T_r,P_r)} \ln\left[\frac{4k_o t}{a^2 C}\right] \qquad \text{.....(2.98)}$$

through a linear regression of Ln t on ΔT_{id}, yields the thermal conductivity of the test liquid.

The algorithm for a computer program used to process these data follows. The program accepts the raw experimental data as input and returns the thermal conductivity of the liquid $\lambda(T_r, \rho_r)$ as well as the corresponding reference temperature T_r and density ρ_r.

Algorithm for calculation of the thermal conductivity of a test liquid.

i Enter data and relevant physical properties of the wire, the measurement cell and the liquid.

ii From the bridge resistances and configurations, using the zeroth order approximation equation (4.10), calculate the resistance difference, $W_{ls}(t_i)$, corresponding to each of the balance times, t_i, (see § 4.51).

iii Calculate the temperature coefficient of resistance, α', from equation (4.17) by assuming $(T-T_o)$ in equation (4.12) to be zero.

iv Calculate the temperature rises, $\Delta T'(t_i)$, from equation (4.26) and $(\Delta T)_1$ from equation (4.31).

v Obtain the heat flux q_1 from equation (4.37).

vi Apply the temperature rise corrections to $(\Delta T)_1$, using equation (2.101), in order to obtain the idealised temperature rise, $\Delta T_{id}(t_i)$. In equation (2.101) $(\Delta T)_1$ is equal to $\Delta T(t_i)$.

vii Repeat steps ii to vi, until convergence on ΔT_{id}. (Less than $\pm$ 0.01% change in ΔT_{id} on successive itterations). Use equation (4.36) in step ii instead of equation (4.10) and $(T-T_o)$ equal to $(\Delta T)_1$ in step iii.

viii Using the idealised temperature rises $\Delta T_{id}(t_i)$ and their associated balance times, t_i, regress Ln t on ΔT_{id} and from the slope, obtain $\lambda(T_r, \rho_r)$.

ix Repeat steps vii and viii until convergence on $\lambda(T_r, \rho_r)$.

x Calculate T_r from equation (2.104) and $\rho_r(T_r, P_o)$.

The algorithm just described requires an approximate estimate for the thermal conductivity of the test liquid for use in the correction terms. This estimate can either be provided as input or obtained by neglecting those correction terms which require an approximate thermal conductivity, when first calculating the thermal conductivity. The value thus obtained after this and subsequent itterations is then used in these small correction terms.

In practice, measurements were performed on test liquids over the pressure range of 50-500 MPa at an approximately constant equilibrium bath temperatures T_o. These measurements produced liquid thermal conductivities $\lambda(T_r, \rho_r)$ at different reference densities ρ_r and slightly different reference temperatures T_r. The difference in reference temperature over the pressure range being of the order of 1.5K which is due to the pressure dependence of the physical properties of the fluid and measurement cell. In order to examine the density dependence of the thermal conductivity of a liquid, the thermal conductivity measurements were corrected to a nominal temperature T_n using the linear equation:-

$$(T_n, \rho_r) = (T_r, \rho_r) + \left(\frac{\partial \lambda}{\partial T}\right)_\rho (T_n - T_r) \qquad \text{.....(4.44)}$$

The derivative $\left(\frac{\partial \lambda}{\partial T}\right)_\rho$ in equation (4.44) is obtained by first assuming the thermal conductivity to be independent of temperature. This is done for a number of sets of measurements of thermal conductivity versus density at different equilibrium bath temperatures. From these measurements one can then obtain an estimate of $\left(\frac{\partial \lambda}{\partial T}\right)_\rho$ which is then used in equation (4.44). The Process is repeated and as convergence is rapid, usually two itterations are all that is required.

In order to examine the pressure dependence of the thermal conductivity one corrects the values of $\lambda(T_r, \rho_r)$ obtained from the measurements to a nominal temperature T_n using:-

$$\lambda(T_n,P_o) = \lambda(T_r,P_o) + \left(\frac{\partial\lambda}{\partial T}\right)_p (T_n-T_r) \qquad \text{.....(4.45)}$$

The value of $\left(\frac{\partial\lambda}{\partial T}\right)_p$ can be obtained by assuming it to be independent of pressure and using the values calculated from previous work on the thermal conductivity of the liquid at atmospheric pressure. The value of $\left(\frac{\partial\lambda}{\partial T}\right)_p$ thus obtained from literature for n-heptane is between -2.5×10^{-4} W/m/K^2 and -3.0×10^{-4} W/m/K^2; for n-nonane is between -2.5×10^{-4} W/m/K^2 and -3.5×10^{-4} W/m/K^2; and for n-undecane is between -2.0×10^{-4} W/m/K^2 and -2.5×10^{-4} W/m/K^2.

Due to the large uncertainty in the values quoted in literature and because the value of $\left(\frac{\partial\lambda}{\partial T}\right)_p$ changes by almost an order of magnitude over the pressure range in question, a different approach was adopted, which is thought to be superior. This approach makes use of the fact that we can calculate the value $\left(\frac{\partial\lambda}{\partial T}\right)_{\rho_r}$ as described above and this changes by at most a factor of two over the pressure range. We therefore use:-

$$\left(\frac{\partial\lambda}{\partial T}\right)_{P_r} = \left(\frac{\partial\lambda}{\partial\rho}\right)_{T_r}\left(\frac{\partial\rho}{\partial T}\right)_{P_r} + \left(\frac{\partial\lambda}{\partial T}\right)_{\rho_r} \qquad \text{.....(4.46)}$$

From data on the pressure and temperature dependence of test liquid's density we can find $\left(\frac{\partial\lambda}{\partial T}\right)_{P_r}$ and from the density and temperature dependence of the liquid's thermal conductivity, which we have measured, we obtain $\left(\frac{\partial\lambda}{\partial\rho}\right)_{T_r}$ and $\left(\frac{\partial\lambda}{\partial T}\right)_{\rho_r}$.

4.62 Experimental Procedure

The procedure by which the experiments are performed and the required data are obtained is briefly presented.

The measurement cell is mounted in the bellows assembly (see § 4.3) and the latter is filled with the test liquid whose thermal conductivity is to be determined. The cell and bellows, which are attached to the pressure vessel plug, are placed inside the autoclave which is then pumped up to the required pressure. The autoclave, containing the cell and test liquid, is situated within a temperature controlled oil bath and is left to attain thermal equilibrium. The time taken to reach equilibrium is of the order of 72 hours when the liquid in the cell has been changed; 24 hours when the set point on the temperature controller has been changed; and 2-3 hours when only the pressure within the autoclave has been altered.

Once the system has reached a steady temperature the equilibrium temperature of the bath, T_0, is measured using the platinum resistance thermometer which is strapped to the side of the pressure vessel. The variable resistors used in the automatic bridge are adjusted to give an approximately linear distribution in $\ln t_i$ (t_i is the time taken to balance point i) while ensuring that the final balance point during a run will not greatly exceed 1 second. The relevant bridge resistances as well as the mode and selector switch positions are recorded together with the voltage to be supplied across the bridge during a run.

A run is then performed by firing the automatic bridge and the six resulting balance times are recorded. The bridge configuration is altered by changing the mode or selection switch positions or by changing the values of the variable resistors in the upper right hand arm of the bridge (see § 4.41). The new bridge configuration is noted, a second run is initiated and the six new balance times are recorded. Subsequent runs (normally six runs being performed in total) are performed using the same routine and allowing a time lapse of 60 seconds between runs (the optimum time lapse being obtained from previous experience).

Finally, after the runs have been performed, the individual wire resistances of the long and short wires as well as their resistance difference are measured at the equilibrium bath temperature, T_o. These measurements being performed by operating the bridge in a steady state manner using several small bridge voltages and obtaining the steady state resistance at each of these voltages. The equilibrium resistance, at T_o, is then obtained by extrapolating the plot of the steady state resistance versus the square of the bridge voltage bach to zero voltage.

These experimental data are all that is required from an experiment on the test liquid at a particular thermodynamic state. These data used in conjunction with the physical properties of the liquid, cell and platinum wires (these physical properties are given in appendix 3) enable the calculation by the computer program of the liquid's thermal conductivity.

4.7 Precision, Accuracy and Performance

From the theory of the transient hot wire apparatus given in chapter 2, together with the additional information given previously in this chapter, it is seen that, if the apparatus behaves in the manner assumed by mathematical model, then the experimentally determined values of ΔT_{id} versus Ln t will lie on a perfectly straight line. However, the original mathematical model does not include the existance of radiative heat transfer which, from the work described in chapter 3, will tend to introduce a systematic curvature. But it has been found, using the method described in chapter 3 for calculating δT_R that this curvature is small and should be barely perceptible during measurements as, over most of the temperature and pressure range encountered, the curvature introduced will be within the precision of the bridge ($\pm$ 0.1% ΔT_{id}).

It therefore follows that under conditions which are unfavourable to radiative heat transfer (low values of T_o and ΔT and when measuring relatively high values of λ) the deviations of the experimentally

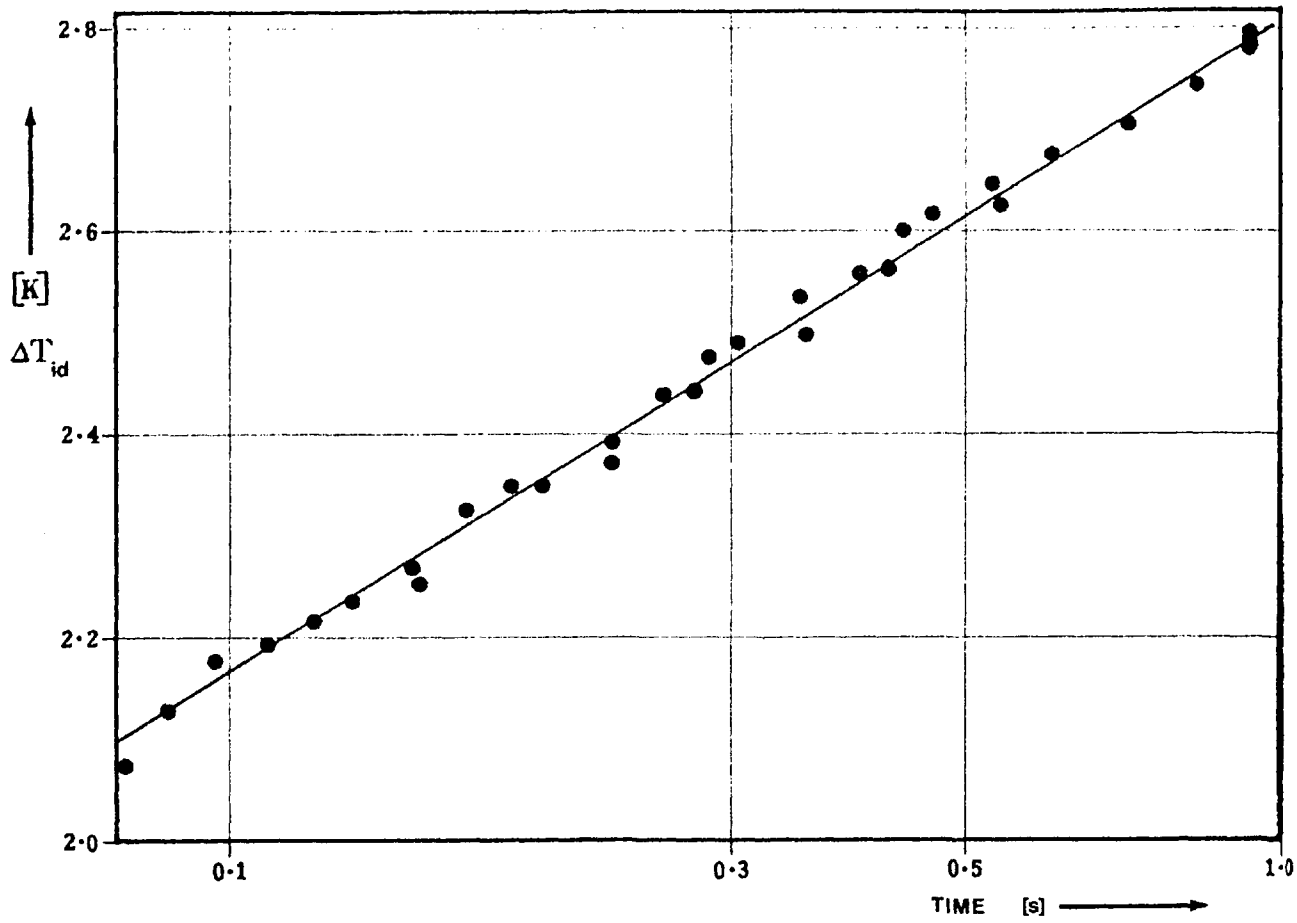

Fig. (4.14) Temperature rise of the platinum wire as a function of time. (N-Heptane at 308.15K and 230 MPa)

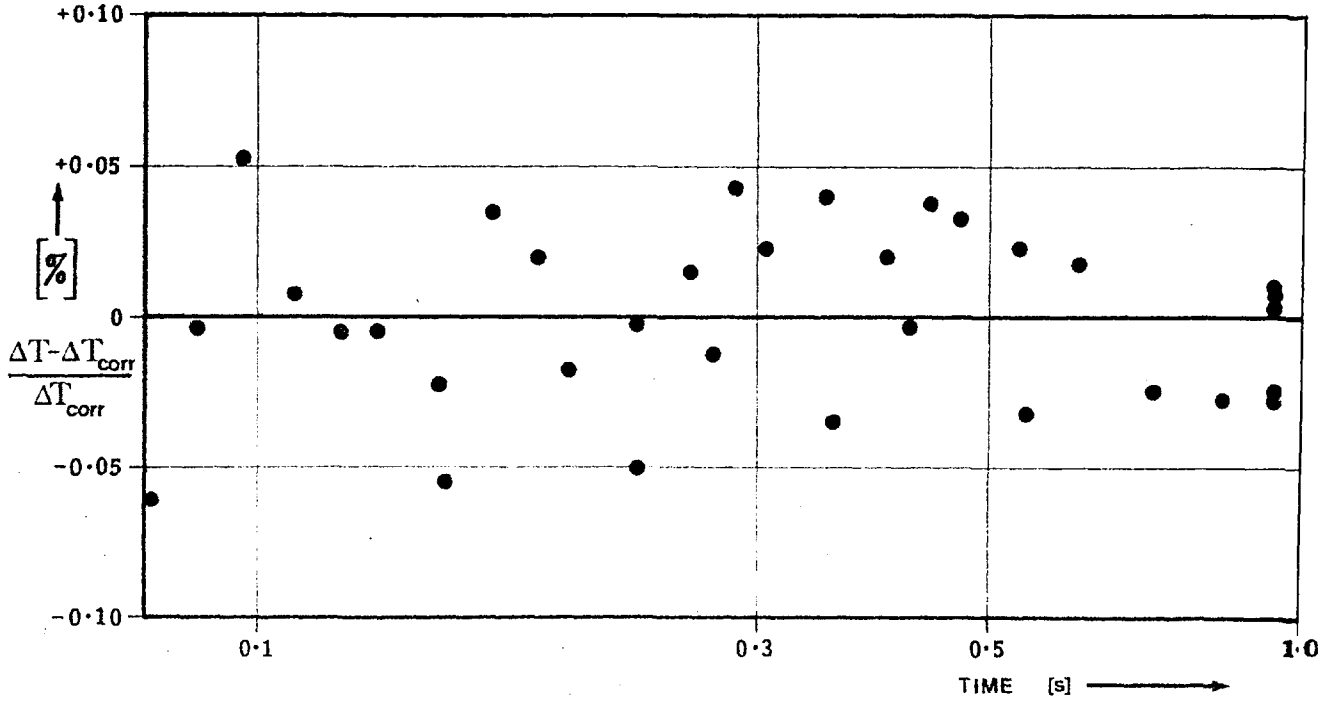

Fig. (4.15) Deviation from the fitted straight line. (N-Heptane at 308.15K and 230 MPa)

obtained values of ΔT_{id} from a straight line in Ln t should be randomly distributed and should not greatly exceed $\pm$ 0.1%. Fig. (4.14) shows a plot of the corrected temperature rise ΔT_{id} versus Ln t for an experimental run on n-Heptane at 308.15K and 230 MPa in which the above conditions are met. In order to emphasise the straightness of the line, the deviations of the points from the fitted straight line has been magnified by a factor of 20. Fig. (4.15) shows the deviation plot for the same results and shows that the deviations appear to be randomly distributed with a maximum deviation of only $\pm$ 0.06%. It has been calculated that the curvature introduced by the existance of radiative heat transfer during this measurement causes a deviation from the straight line of between -0.04% at t=0.1 s, peaking to + 0.02% at t=0.5 s and decreasing to - 0.02% at t=1 s. Thus the observed behaviour is taken as conclusive evidence of the correct operation of the apparatus.

It has been estimated that the precision of the apparatus is one of $\pm$ 0.2% which has been supported by repeating measurements under identical thermodynamic conditions but using different sets of platinum wires and different samples of the test liquid. These repeat measurements were found to repeat the original results to within 0.2%.

The absolute accuracy of the measurements, E, has been estimated using:-

$$E = E_{Pr} + E_{mm} + E_{NS} + E_{\xi} \qquad \text{.....(4.160)}$$

Where in equation (4.160) E_{Pr} is the precision of the apparatus; E_{mm} is the error introduced due to the applicability of the mathematical model; E_{NS} is the error incurred due to the numerical solution used to obtain the radiation defect; and E_{ξ} is the error introduced by the radiation defect approximation. We therefore find the accuracy to be:-

$$E = 0.3 + 20\xi \quad [\%] \qquad \text{.....(4.161)}$$

and is found to be between 0.5% and 0.8% for the measurements reported in chapter 5.

CHAPTER 5

Results

5.1 Introduction

The previous chapters have presented the theory behind the transient hot wire technique and described an apparatus which was used to perform precise, accurate measurements of liquid thermal conductivities. Using an apparatus and method based on this work, the thermal conductivity of n-Heptane, n-Nonane, and n-Undecane was measured in the pressure range 50 - 500 MPa. In this chapter, the thermal conductivity versus pressure and density is presented at 308.15K, 323.15K and 348.15K for n-Heptane [95] , n-Nonane, and n-Undecane and also at 363.15K in the case of n-Nonane. This chapter has been devoted primarily to the presentation of the results and the discussion and usage of these results is delayed until chapter 6.

The purities of each n-Alkane studied, as well as the refractive index quoted by the manufacturer, are given in Table (5.1). By means of independent measurements of the refractive index of samples of the n-Alkanes, as well as through tests on a gas chromatograph, the stated purities of the n-Alkanes were supported. In fact, and especially in the case of n-Nonane, it is thought that the purity of the samples tested were appreciably in excess of those quoted by the manufacturer.

Hydrocarbon	Purity [%]	Refractive Index @ 25°C	Extinction Coefficient [m^{-1}] @ 300K	Supplier
n-Heptane	99.5	1.3880 - 1.3885	1070	BDH
n-Nonane	98.0	1.4050 - 1.4070	1120	BDH
n-Undecane	99.0	1.4170 - 1.4180	1150	BDH

Table (5.1) Purity and optical properties of the studied hydrocarbons

The characteristics of the measurement cell and a typical set of wires are given in Table (5.2). A number of sets of wires were used during the measurements because during the changing of the test liquid, the wires often break. Repetition of the experiments with a new set of wires, give results which differed by less than ± 0.2%, thus supporting the estimate of the apparatus design (± 0.2%).

Relevant Characteristics of the Measurement Cell and a typical set of wires.		
Internal diameter of the cell	9.90 mm	± 0.01 mm
Length of the long wire @ 321K	151.63 mm	± 0.05 mm
Length of the short wire @ 321K	49.08 mm	± 0.05 mm
Long wire resistance @ 321K & 315 MPa	431.09 Ω	± 0.05 Ω
Short wire resistance @ 321K & 315 MPa	140.12 Ω	± 0.05 Ω
Platinum wire radius	3.89 μm	± 0.01 μm
Emissivity of the platinum wire	0.037	

Table (5.2)

In the case of n-Heptane and n-Nonane, the upper limit on the pressure during measurements was dictated by the available density versus pressure data as given in appendix 3. In the case of n-Undecane, the upper limit on the pressure was set to 380 MPa at T_n = 308.15K and 400 MPa at T_n = 323.15K and T_n = 348.15K. This was because n-Undecane was found to solidify at these temperatures above these pressures. It was found, to the detriment of a measurement cell, that at 304K n-Undecane freezes between 390 and 400 MPa. This finding has been supported [96] . The lower limit on the pressure range was set at approximately 50 MPa in order that on raising the temperature of the system the bellows would not expand beyond its extent when filled at room temperature as it would hit the bottom of the pressure vessel and burst. By ensuring there was at all times a minimum hydrostatic pressure of 50 MPa on the heated fluid, within the bellows, guaranteed that within the temperature range for which measurements were performed bursting would not occur.

For the purposes of correlating the experimental results, these results $\lambda(T_n,\rho_r)$ and $\lambda(T_n,P)$ were fitted to polynomials. It is thought that the measured pressure and calculated density of the hydrocarbons may be in error by as much as, if not more than, the measured thermal conductivity. This has been partially substantiated by the failure of the density versus pressure data to predict the freezing of n-Undecane at ≈400 MPa and 304K. Because of possible errors in pressures and densities, the commonly used least squares fit to the thermal conductivity, along an isotherm in ascending powers of pressure or density was thought to be unsuitable. Instead fits were used of the form:-

$$\Upsilon(\lambda,\rho) = a_o\lambda + a_1(\rho-\rho^*) + a_2(\rho-\rho^*)^2 + a_3(\rho-\rho^*)^3 \quad .....(5.1)$$

for the density dependence and:-

$$\Upsilon(\lambda,P) = a'_o\lambda + a'_1(P-P^*) + a'_2(P-P^*)^2 + a_3(P-P^*)^3 \quad .....(5.2)$$

for the pressure dependence. By setting $\Upsilon(\lambda,P)$ and $\Upsilon(\lambda,\rho)$ constant and equal to unity and minimising the square of the deviations in the direction of the two independent variables λ and P or λ and ρ, we obtain a fit which allows errors in both variables. In equations (5.1) and (5.2) P^* and ρ^* are scaling parameters and were approximately equal to the mean pressure or density over the isotherm along which measurements were performed. The coefficients a_o,a_1,a_2,a_3, and a'_o,a'_1,a'_2,a'_3 in equations (5.1) and (5.2) are determined by the regression analysis used.

The polynomials thus obtained have no physical significance as they have no theoretical basis and are merely a means of interpolating the data within the range of measurements. Because of this, care must be taken when extrapolating using these derived polynomials.

5.2 Thermal Conductivity as a function of Density

In this section the thermal conductivity data for n-Heptane, n-Nonane, and n-Undecane as a function of density are presented for each liquid and along each isotherm for which measurements were performed. Each set of results is presented in tabular form and in a graph which also contains the polynomial which was obtained by regression as indicated above. Table (5.13) at the end of this section gives the values of a_i, the coefficients pertaining to equation (5.1) for each liquid at each of the temperatures to which the data given in this section is referred, and Fig. (5.24) shows the deviation plot of the measured thermal conductivities from their correlated values (those obtained using equation (5.1)).

Table 5.3 Thermal Conductivity Versus Density
N-Heptane at T_n = 308.15K

p	T_o	ρ_o	T_r	ρ_r	$\left(\frac{\partial\lambda}{\partial T}\right)_\rho$	$\lambda_{app}(T_r, \rho_r)$	$\lambda_{app}(T_n, \rho_r)$	$\lambda(T_n, \rho_r)$
MPa	K	kg/m^3	K	kg/m^3	W/m/K^2 $\times 10^{-4}$	W/m/K	W/m/K	W/m/K
52.4	306.344	713.7	309.500	711.8	1.26	0.1406	0.1404	0.1385
61.6	307.274	718.6	310.360	716.8	1.23	0.1440	0.1437	0.1417
71.5	306.356	724.7	309.319	723.0	1.20	0.1479	0.1478	0.1457
71.5	306.351	724.7	309.318	723.0	1.20	0.1480	0.1478	0.1458
80.9	307.271	729.2	310.220	727.6	1.20	0.1507	0.1504	0.1484
91.6	306.353	735.0	309.242	733.5	1.20	0.1548	0.1546	0.1525
95.3	307.307	736.3	310.225	734.7	1.20	0.1554	0.1552	0.1531
108.8	306.360	742.9	309.193	741.4	1.22	0.1597	0.1595	0.1574
109.1	306.377	743.0	309.190	741.6	1.22	0.1600	0.1598	0.1577
121.5	306.352	748.4	309.127	747.0	1.24	0.1631	0.1630	0.1608
122.1	307.281	748.2	310.003	746.8	1.24	0.1627	0.1625	0.1603
142.9	306.346	757.0	308.993	755.8	1.30	0.1687	0.1686	0.1664
162.0	307.267	763.7	309.863	762.5	1.36	0.1733	0.1731	0.1708
167.6	307.276	765.7	309.829	764.6	1.38	0.1746	0.1744	0.1721
187.2	307.278	772.4	309.855	771.3	1.45	0.1793	0.1791	0.1767
205.5	307.274	778.3	309.794	777.2	1.51	0.1834	0.1832	0.1808
229.6	307.315	785.6	309.780	784.6	1.60	0.1885	0.1882	0.1858
253.5	307.289	792.4	310.066	791.3	1.68	0.1928	0.1925	0.1901
284.1	307.273	800.6	309.601	799.7	1.79	0.1990	0.1988	0.1963
310.9	307.280	807.2	309.535	806.4	1.87	0.2041	0.2038	0.2013
350.5	307.278	816.5	309.492	815.7	1.98	0.2110	0.2108	0.2082
405.8	307.283	828.6	309.421	827.8	2.12	0.2198	0.2195	0.2169
472.0	307.273	841.5	309.345	840.8	2.24	0.2297	0.2294	0.2267
499.6	307.282	846.5	309.307	845.8	2.28	0.2335	0.2332	0.2305

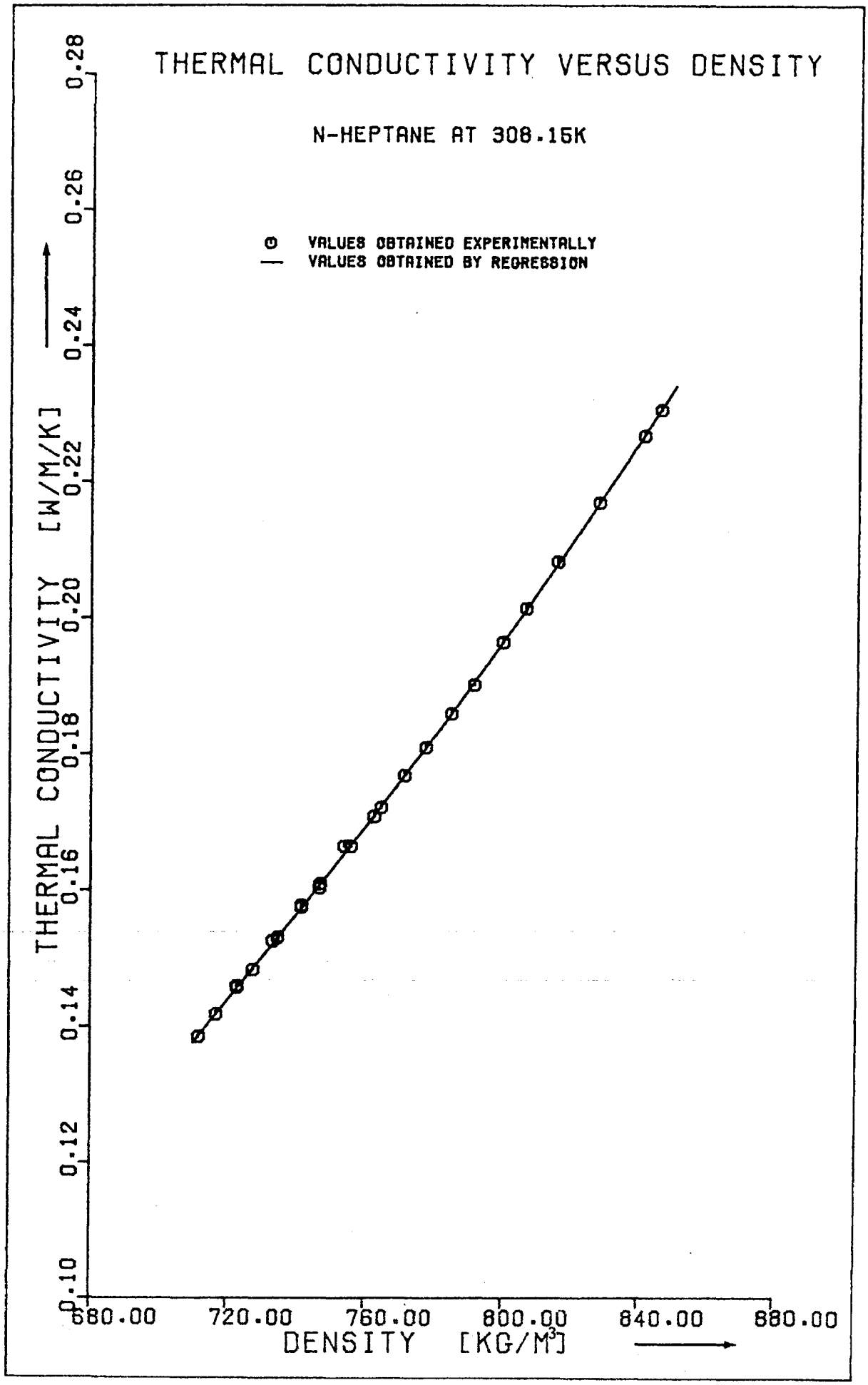
THERMAL CONDUCTIVITY VERSUS DENSITY
N-HEPTANE AT 308.15K
VALUES OBTAINED EXPERIMENTALLY
VALUES OBTAINED BY REGRESSION
THERMAL CONDUCTIVITY [W/M/K]
0.10
0.12
0.14
0.16
0.18
0.20
0.22
0.24
0.26
0.28
680.00
720.00
760.00
800.00
840.00
880.00
DENSITY [KG/M3]

Fig. (5.4)

Table 5.5 Thermal Conductivity Versus Density
N-Heptane at T_n = 323.15K

p	T_o	ρ_o	T_r	ρ_r	$\left(\frac{\partial\lambda}{\partial T}\right)_\rho$	$\lambda_{app}(T_r, \rho_r)$	$\lambda_{app}(T_n, \rho_r)$	$\lambda(T_n, \rho_r)$
MPa	K	kg/m^3	K	kg/m^3	$W/m/K^2$ $\times 10^{-4}$	W/m/K	W/m/K	W/m/K
53.2	320.897	705.4	324.028	703.5	1.34	0.1383	0.1382	0.1360
73.5	320.895	717.6	323.889	715.9	1.23	0.1454	0.1452	0.1429
108.4	320.917	735.3	323.749	733.9	1.20	0.1565	0.1564	0.1539
157.6	320.950	755.9	323.609	754.7	1.29	0.1703	0.1702	0.1676
210.2	320.956	774.1	323.392	773.1	1.47	0.1827	0.1826	0.1799
262.3	320.948	789.4	323.283	788.5	1.65	0.1937	0.1937	0.1908
310.7	320.953	801.7	323.204	801.0	1.81	0.2031	0.2031	0.2001
360.8	320.955	813.7	323.112	812.9	1.95	0.2120	0.2120	0.2090
386.5	320.931	819.4	323.068	818.7	2.02	0.2161	0.2161	0.2130
435.7	320.946	829.7	323.046	829.0	2.14	0.2239	0.2239	0.2208
499.9	320.951	842.0	322.951	841.3	2.25	0.2333	0.2333	0.2301

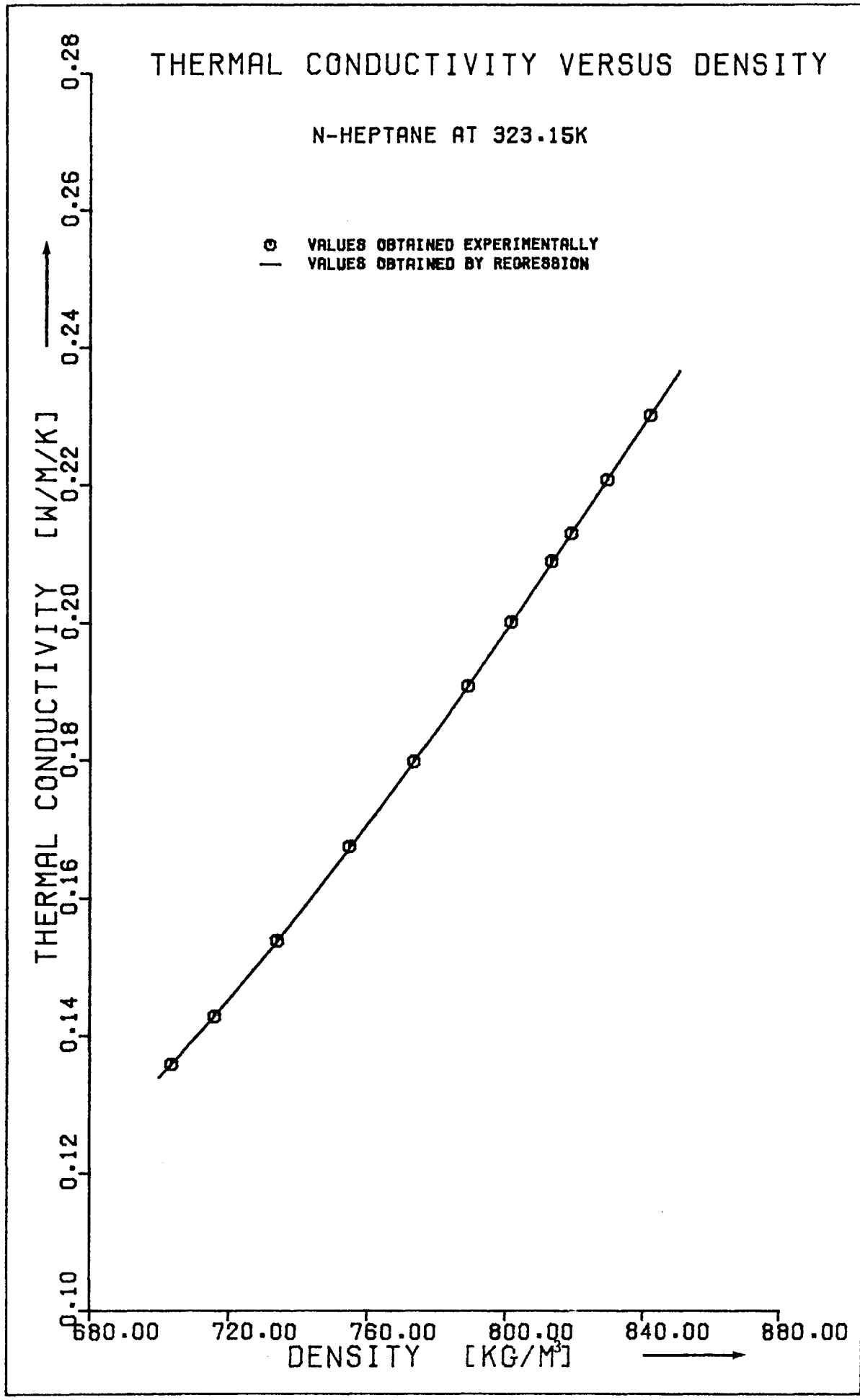
THERMAL CONDUCTIVITY VERSUS DENSITY
N-HEPTANE AT 323.15K
VALUES OBTAINED EXPERIMENTALLY
VALUES OBTAINED BY REGRESSION
THERMAL CONDUCTIVITY [W/M/K]
0.10
0.12
0.14
0.16
0.18
0.20
0.22
0.24
0.26
0.28
680.00
720.00
760.00
800.00
840.00
880.00
DENSITY [KG/M3]

Fig. (5.6)

Table 5.7 Thermal Conductivity Versus Density
N-Heptane at T_n = 348.15K

P	T_o	ρ_o	T_r	ρ_r	$\left(\frac{\partial\lambda}{\partial T}\right)_\rho$	$\lambda_{app}(T_r, \rho_r)$	$\lambda_{app}(T_n, \rho_r)$	$\lambda(T_n, \rho_r)$
MPa	K	kg/m^3	K	kg/m^3	$W/m/K^2$ $\times 10^{-4}$	W/m/K	W/m/K	W/m/K
65.1	343.479	699.8	346.512	698.1	1.42	0.1371	0.1373	0.1346
79.1	343.503	708.5	346.464	706.9	1.30	0.1424	0.1426	0.1398
111.2	343.481	725.4	346.246	724.0	1.20	0.1528	0.1530	0.1501
125.3	343.420	732.1	346.113	730.8	1.20	0.1572	0.1574	0.1544
146.7	343.438	741.4	346.071	740.3	1.21	0.1635	0.1637	0.1606
176.9	343.201	753.4	345.766	752.3	1.28	0.1713	0.1716	0.1684
203.6	343.459	762.7	345.894	761.7	1.35	0.1780	0.1783	0.1750
254.8	343.441	778.7	345.775	777.8	1.52	0.1888	0.1891	0.1857
303.4	343.447	792.0	345.696	791.2	1.68	0.1990	0.1994	0.1959
322.2	343.212	796.8	345.370	796.1	1.74	0.2029	0.2034	0.1999
360.3	343.219	806.0	345.453	805.3	1.86	0.2095	0.2100	0.2063
380.4	343.220	810.6	345.324	809.9	1.92	0.2134	0.2140	0.2103
411.9	343.204	817.5	345.364	816.9	2.00	0.2186	0.2191	0.2154
443.9	343.235	824.2	345.185	823.6	2.08	0.2238	0.2245	0.2206
499.2	343.228	834.7	345.138	834.2	2.19	0.2325	0.2331	0.2293

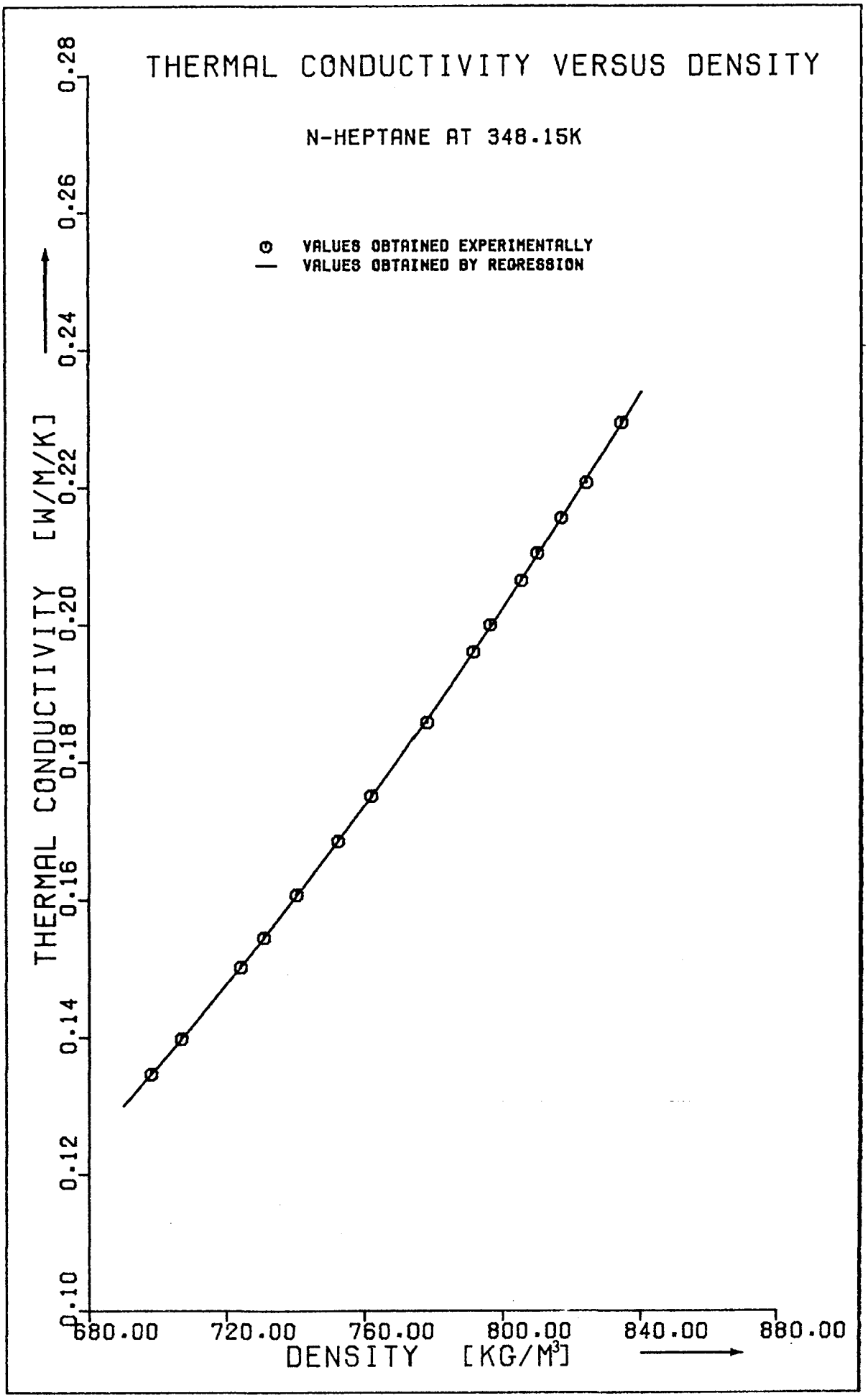
THERMAL CONDUCTIVITY VERSUS DENSITY
N-HEPTANE AT 348.15K
VALUES OBTAINED EXPERIMENTALLY
VALUES OBTAINED BY REGRESSION
THERMAL CONDUCTIVITY [W/M/K]
0.10
0.12
0.14
0.16
0.18
0.20
0.22
0.24
0.26
0.28
680.00
720.00
760.00
800.00
840.00
880.00
DENSITY [KG/M3]

Fig. (5.8)

Table 5.9 Thermal Conductivity Versus Density
N-Nonane at T_n = 308.15K

P	T_o	ρ_o	T_r	ρ_r	$\left(\frac{\partial\lambda}{\partial T}\right)_\rho$	$\lambda_{app}(T_r, \rho_r)$	$\lambda_{app}(T_n, \rho_r)$	$\lambda(T_n, \rho_r)$
MPa	K	kg/m^3	K	kg/m^3	$W/m/K^2$ $\times 10^{-4}$	W/m/K	W/m/K	W/m/K
51.6	304.145	745.3	307.137	743.5	1.29	0.1460	0.1461	0.1435
51.8	304.129	745.4	307.164	743.6	1.29	0.1461	0.1462	0.1436
52.0	304.110	745.5	307.196	743.7	1.30	0.1463	0.1464	0.1438
63.5	304.086	751.7	307.081	750.0	1.34	0.1499	0.1500	0.1474
87.1	304.116	763.3	306.977	761.8	1.41	0.1571	0.1572	0.1545
92.9	304.093	766.0	306.911	764.5	1.42	0.1583	0.1584	0.1557
112.5	304.081	774.2	306.875	772.8	1.47	0.1633	0.1635	0.1607
130.9	304.123	781.4	306.781	780.1	1.52	0.1682	0.1684	0.1655
156.3	304.122	790.6	306.714	789.3	1.58	0.1738	0.1740	0.1711
167.5	304.122	794.3	306.702	793.1	1.60	0.1764	0.1766	0.1737
190.6	304.136	801.7	306.735	800.6	1.66	0.1809	0.1812	0.1782
211.9	304.135	808.1	306.665	807.0	1.70	0.1856	0.1858	0.1827
241.0	304.132	816.2	306.596	815.2	1.77	0.1909	0.1912	0.1881
271.6	304.145	824.2	306.610	823.2	1.85	0.1967	0.1970	0.1938
309.2	304.130	833.3	306.475	832.4	1.94	0.2029	0.2032	0.2000
337.0	304.112	839.6	306.368	838.7	2.02	0.2075	0.2079	0.2046
369.2	304.118	846.6	306.348	845.7	2.11	0.2123	0.2127	0.2094
403.9	304.118	853.7	306.337	852.8	2.21	0.2175	0.2179	0.2145
435.5	304.107	859.7	306.153	859.0	2.31	0.2219	0.2224	0.2190
468.5	304.127	865.7	306.176	865.0	2.41	0.2266	0.2270	0.2236
500.1	304.147	871.2	306.120	870.5	2.51	0.2308	0.2313	0.2278

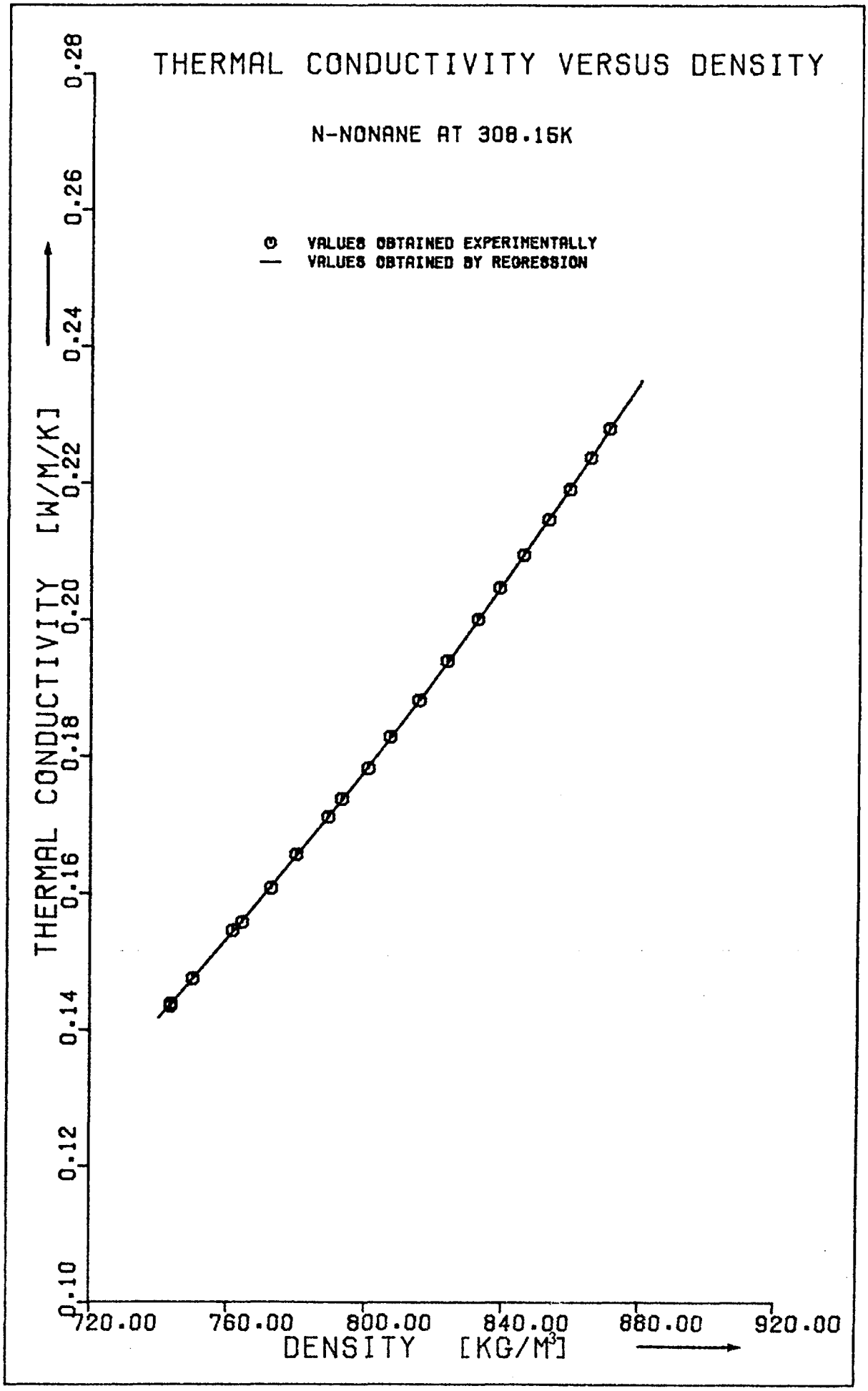
THERMAL CONDUCTIVITY VERSUS DENSITY
N-NONANE AT 308.15K
VALUES OBTAINED EXPERIMENTALLY
VALUES OBTAINED BY REGRESSION
THERMAL CONDUCTIVITY [W/M/K]
0.10
0.12
0.14
0.16
0.18
0.20
0.22
0.24
0.26
0.28
720.00
760.00
800.00
840.00
880.00
920.00
DENSITY [KG/M3]

Fig. (5.10)

Table 5.11 Thermal Conductivity Versus Density
N-Nonane at T_n = 323.15K

P	T_o	ρ_o	T_r	ρ_r	$\left(\frac{\partial\lambda}{\partial T}\right)_\rho$	$\lambda_{app}(T_r, \rho_r)$	$\lambda_{app}(T_n, \rho_r)$	$\lambda(T_n, \rho_r)$
MPa	K	kg/m^3	K	kg/m^3	W/m/K^2 $\times 10^{-4}$	W/m/K	W/m/K	W/m/K
35.3	319.685	725.8	322.858	723.8	1.11	0.1367	0.1367	0.1339
62.3	319.677	742.2	322.685	740.5	1.25	0.1466	0.1466	0.1437
85.4	319.698	754.2	322.447	752.8	1.33	0.1534	0.1535	0.1504
89.6	319.682	756.2	322.591	754.7	1.34	0.1546	0.1547	0.1516
109.7	319.711	765.1	322.523	763.7	1.40	0.1598	0.1599	0.1568
123.0	319.685	770.8	322.420	769.5	1.43	0.1636	0.1637	0.1605
139.3	319.713	777.2	322.423	775.9	1.47	0.1679	0.1680	0.1648
174.8	319.725	789.8	322.281	788.7	1.55	0.1762	0.1763	0.1730
181.0	319.690	791.9	322.216	790.8	1.56	0.1780	0.1781	0.1748
213.8	319.714	802.0	322.229	801.0	1.63	0.1846	0.1848	0.1813
249.1	319.714	811.9	322.105	811.0	1.71	0.1917	0.1919	0.1883
292.4	319.714	823.1	321.958	822.3	1.81	0.1994	0.1996	0.1960
331.2	319.702	832.2	321.949	831.4	1.90	0.2059	0.2062	0.2025
360.1	319.665	838.7	321.862	837.9	1.97	0.2105	0.2108	0.2071
412.5	319.710	849.8	321.792	849.1	2.11	0.2186	0.2189	0.2151
452.4	319.696	857.6	321.750	856.9	2.23	0.2245	0.2248	0.2209
500.5	319.698	866.4	321.712	865.7	2.42	0.2311	0.2314	0.2275

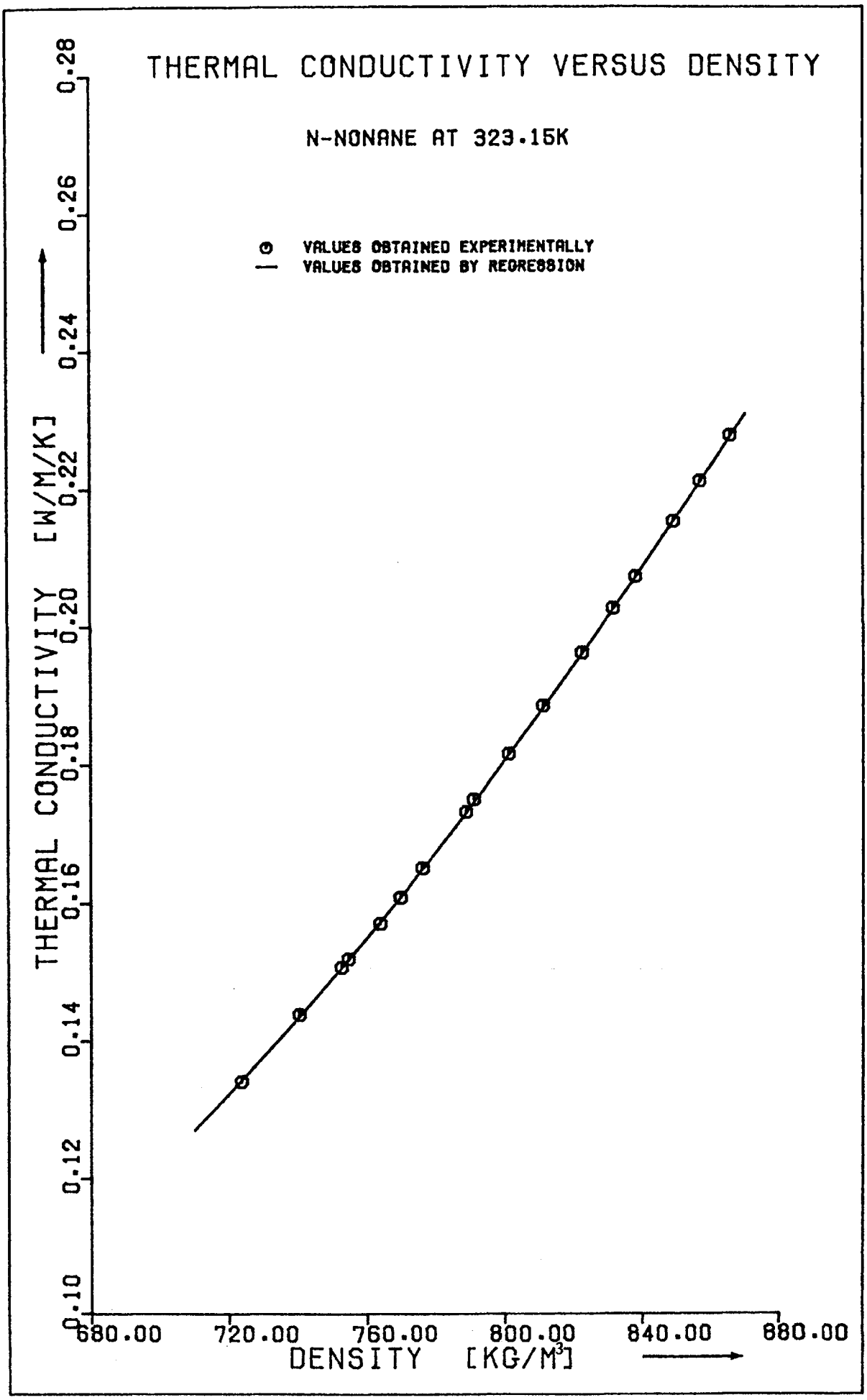
THERMAL CONDUCTIVITY VERSUS DENSITY
N-NONANE AT 323.15K
VALUES OBTAINED EXPERIMENTALLY
VALUES OBTAINED BY REGRESSION
THERMAL CONDUCTIVITY [W/M/K]
0.10
0.12
0.14
0.16
0.18
0.20
0.22
0.24
0.26
0.28
680.00
720.00
760.00
800.00
840.00
880.00
DENSITY [KG/M3]

Fig. (5.12)

Table 5.13 Thermal Conductivity Versus Density
N-Nonane at T_n = 348.15K

P	T_o	ρ_o	T_r	ρ_r	$\left(\frac{\partial\lambda}{\partial T}\right)_\rho$	$\lambda_{app}(T_r, \rho_r)$	$\lambda_{app}(T_n, \rho_r)$	$\lambda(T_n, \rho_r)$
MPa	K	kg/m^3	K	kg/m^3	$W/m/K^2$ $\times 10^{-4}$	W/m/K	W/m/K	W/m/K
63.2	344.129	729.1	347.744	727.1	1.18	0.1413	0.1413	0.1379
83.8	344.159	740.7	347.649	739.0	1.26	0.1485	0.1486	0.1450
107.3	344.175	752.3	347.520	750.7	1.34	0.1556	0.1557	0.1519
134.5	344.172	764.1	347.396	762.1	1.41	0.1632	0.1633	0.1595
169.1	344.192	777.4	347.267	776.1	1.49	0.1719	0.1721	0.1681
202.1	344.169	788.6	347.156	787.5	1.57	0.1797	0.1799	0.1758
232.3	344.179	797.8	347.060	796.7	1.63	0.1861	0.1863	0.1821
264.2	344.184	806.9	346.951	805.9	1.70	0.1924	0.1926	0.1883
303.7	344.188	817.2	346.882	816.3	1.78	0.1999	0.2000	0.1957
367.7	344.181	832.2	346.946	831.4	1.93	0.2104	0.2106	0.2061
400.2	344.184	839.3	346.669	838.6	2.02	0.2160	0.2163	0.2117
475.6	344.165	854.4	346.491	853.7	2.22	0.2277	0.2281	0.2233
502.7	344.136	859.4	346.491	858.7	2.30	0.2315	0.2319	0.2271

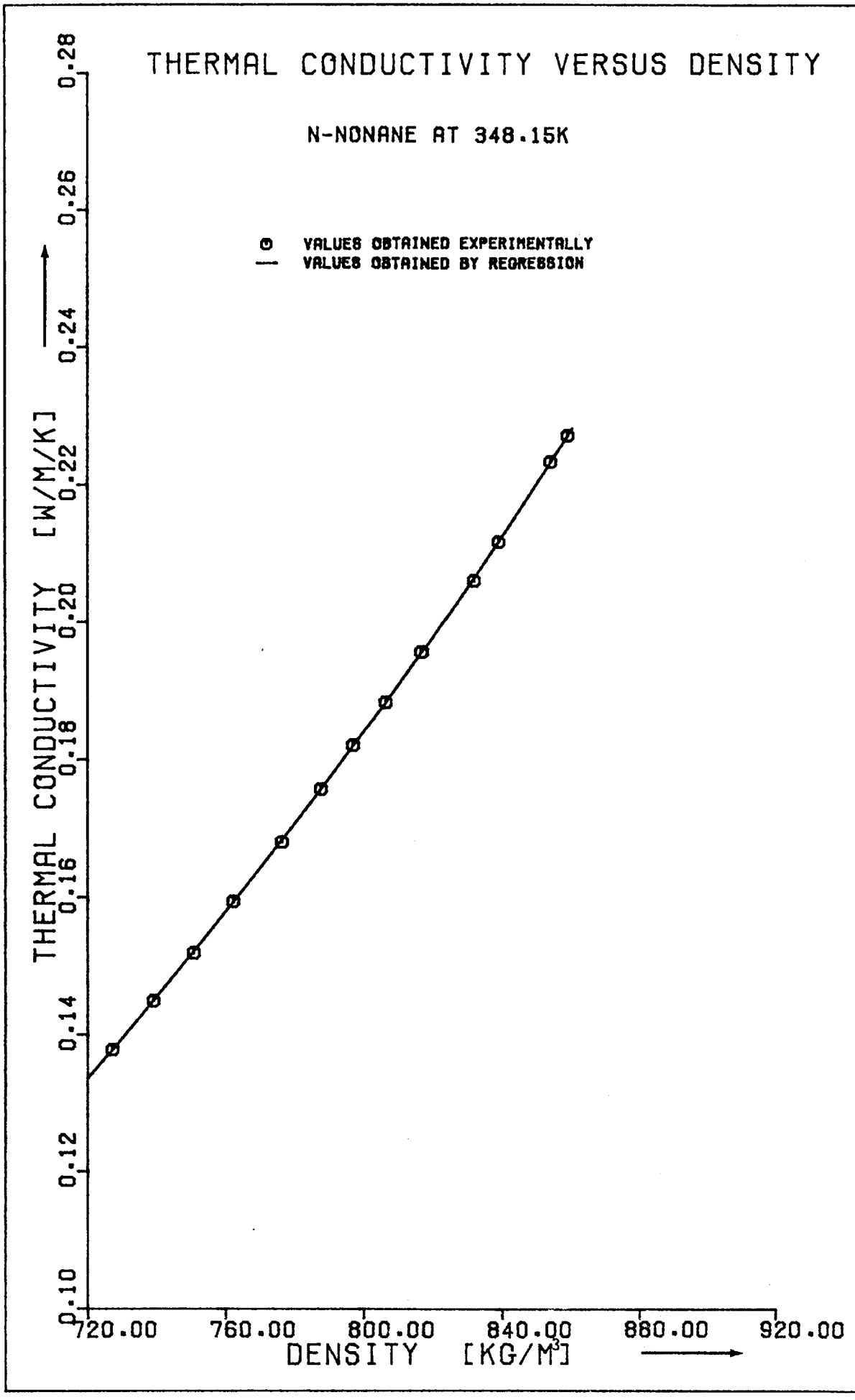
THERMAL CONDUCTIVITY VERSUS DENSITY
N-NONANE AT 348.15K
VALUES OBTAINED EXPERIMENTALLY
VALUES OBTAINED BY REGRESSION
THERMAL CONDUCTIVITY [W/M/K]
0.10
0.12
0.14
0.16
0.18
0.20
0.22
0.24
0.26
0.28
720.00
760.00
800.00
840.00
880.00
920.00
DENSITY [KG/M3]

Fig. (5.14)

Table 5.15 Thermal Conductivity Versus Density
N-Nonane at T_n = 363.15K

p	T_o	ρ_o	T_r	ρ_r	$\left(\frac{\partial\lambda}{\partial T}\right)_\rho$	$\lambda_{app}(T_r, \rho_r)$	$\lambda_{app}(T_n, \rho_r)$	$\lambda(T_n, \rho_r)$
MPa	K	kg/m^3	K	kg/m^3	$W/m/K^2$ $\times 10^{-4}$	W/m/K	W/m/K	W/m/K
53.7	360.507	713.9	364.241	711.8	1.04	0.1347	0.1346	0.1308
75.8	360.510	727.8	364.075	726.0	1.17	0.1429	0.1428	0.1389
103.8	360.583	742.7	363.977	741.1	1.28	0.1526	0.1525	0.1484
127.6	360.535	753.9	363.815	752.4	1.35	0.1588	0.1587	0.1545
159.4	360.537	766.9	363.676	765.6	1.43	0.1669	0.1668	0.1624
187.7	360.550	777.3	363.558	776.1	1.49	0.1742	0.1741	0.1696
211.8	360.560	785.3	363.2485	784.3	1.55	0.1789	0.1789	0.1742
213.3	360.533	785.8	363.426	784.7	1.55	0.1801	0.1800	0.1754
249.6	360.539	796.9	363.362	795.9	1.62	0.1872	0.1872	0.1824
304.4	360.557	811.9	363.192	811.0	1.74	0.1980	0.1980	0.1931
403.7	360.557	835.1	362.974	834.4	1.97	0.2156	0.2157	0.2105
425.4	360.523	839.7	362.891	839.0	2.02	0.2191	0.2192	0.2139
503.3	360.578	854.7	362.895	854.0	2.23	0.2308	0.2309	0.2255

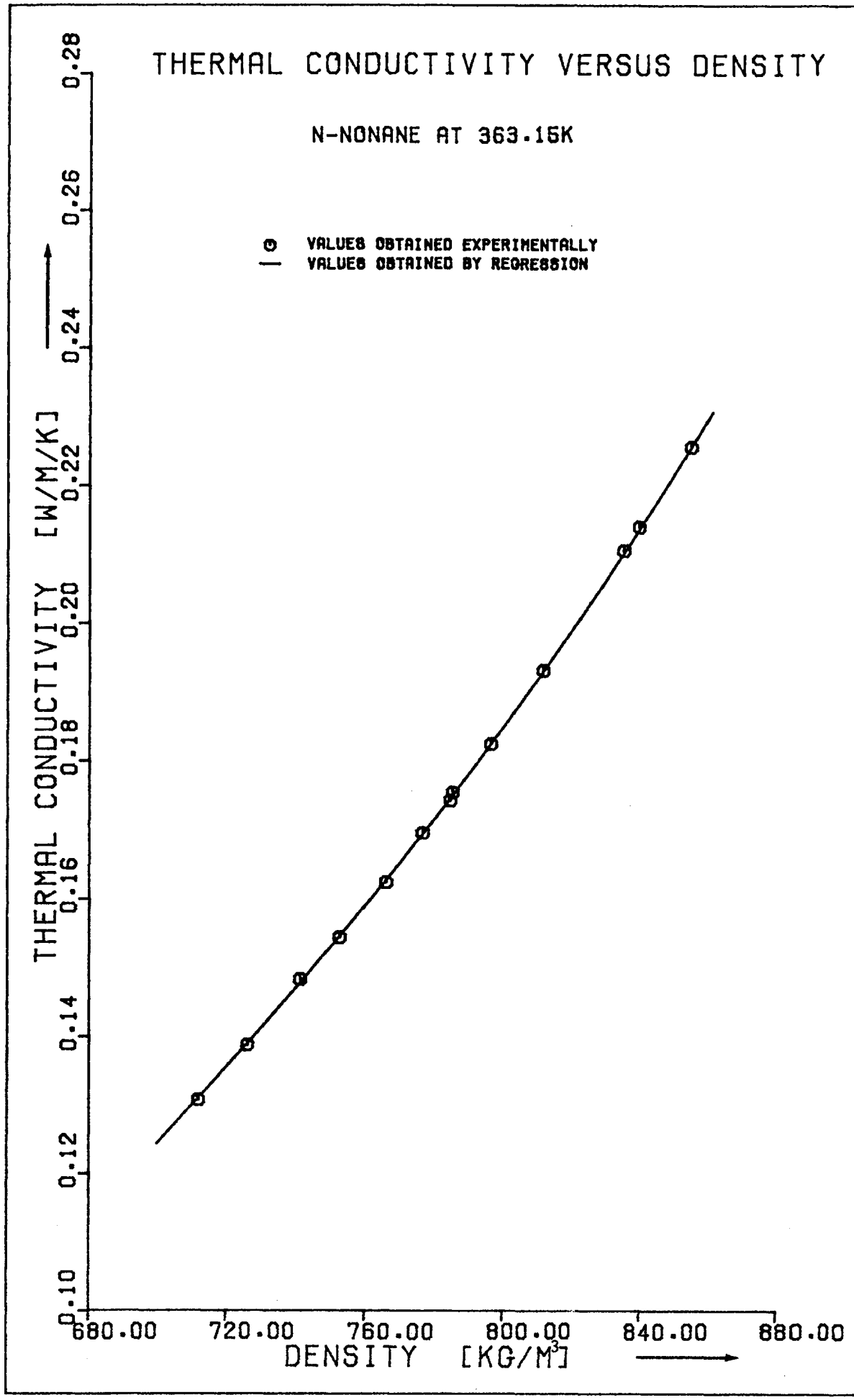
THERMAL CONDUCTIVITY VERSUS DENSITY
N-NONANE AT 363.15K
VALUES OBTAINED EXPERIMENTALLY
VALUES OBTAINED BY REGRESSION
THERMAL CONDUCTIVITY [W/M/K]
0.10
0.12
0.14
0.16
0.18
0.20
0.22
0.24
0.26
0.28
680.00
720.00
760.00
800.00
840.00
880.00
DENSITY [KG/M3]

Fig. (5.16)

Table 5.17 Thermal Conductivity Versus Density
N-Undecane at T_n = 308.15K

P	T_o	ρ_o	T_r	ρ_r	$\left(\frac{\partial\lambda}{\partial T}\right)_\rho$	$\lambda_{app}(T_r, \rho_r)$	$\lambda_{app}(T_n, \rho_r)$	$\lambda(T_n, \rho_r)$
MPa	K	kg/m^3	K	kg/m^3	$W/m/K^2$ $\times 10^{-4}$	W/m/K	W/m/K	W/m/K
47.4	305.270	762.8	309.343	760.3	1.35	0.1478	0.1476	0.1450
64.3	305.284	771.4	309.192	769.2	1.40	0.1529	0.1527	0.1501
75.7	305.288	776.9	309.154	774.8	1.44	0.1559	0.1558	0.1531
97.9	305.305	786.6	309.113	784.6	1.50	0.1621	0.1620	0.1592
120.5	305.312	795.5	309.006	793.6	1.55	0.1675	0.1674	0.1645
137.0	305.308	801.6	308.898	799.8	1.59	0.1712	0.1711	0.1682
149.2	305.304	805.8	308.827	804.1	1.61	0.1742	0.1741	0.1712
169.4	305.303	812.4	308.729	810.8	1.64	0.1785	0.1784	0.1754
183.7	305.283	816.9	308.642	815.3	1.66	0.1820	0.1819	0.1789
211.8	305.306	825.0	308.612	823.5	1.69	0.1870	0.1869	0.1838
242.0	305.304	833.4	308.506	832.0	1.71	0.1927	0.1926	0.1895
274.1	305.311	841.2	308.417	839.9	1.71	0.1982	0.1981	0.1949
304.6	305.322	848.4	308.386	847.1	1.69	0.2034	0.2033	0.2001
343.5	305.249	856.9	308.261	855.7	1.65	0.2091	0.2090	0.2058
344.0	305.328	857.0	308.281	855.8	1.65	0.2094	0.2094	0.2061
382.7	305.321	865.0	308.211	863.9	1.60	0.2153	0.2153	0.2120

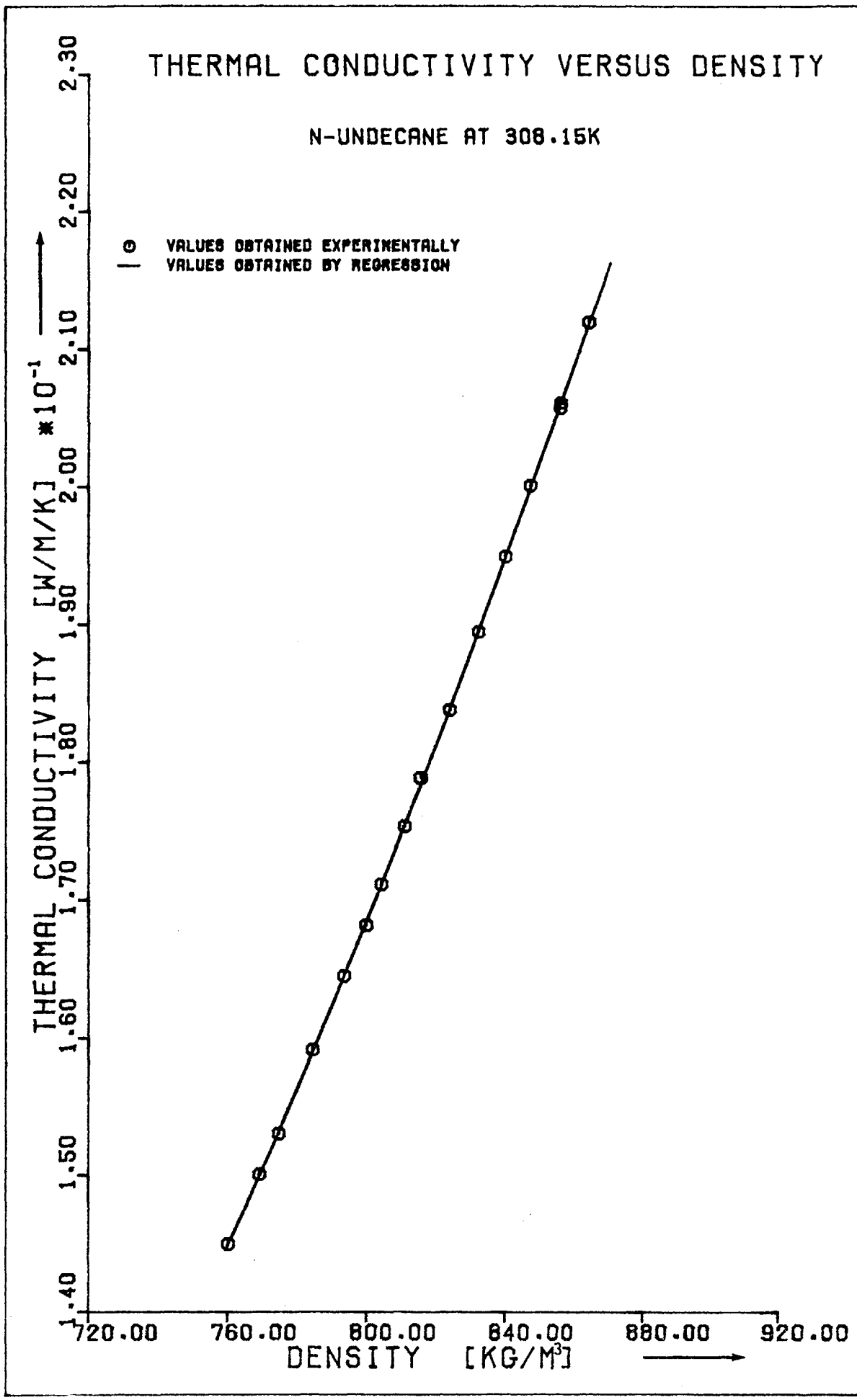
THERMAL CONDUCTIVITY VERSUS DENSITY
N-UNDECANE AT 308.15K
VALUES OBTAINED EXPERIMENTALLY
VALUES OBTAINED BY REGRESSION
THERMAL CONDUCTIVITY [W/M/K] *10⁻¹
2.30
2.20
2.10
2.00
1.90
1.80
1.70
1.60
1.50
1.40
720.00
760.00
800.00
840.00
880.00
920.00
DENSITY [KG/M³]

Fig. (5.18)

Table 5.19 Thermal Conductivity Versus Density
N-Undecane at T_n = 323.15K

p	T_o	ρ_o	T_r	ρ_r	$\left(\frac{\partial\lambda}{\partial T}\right)_\rho$	$\lambda_{app}(T_r, \rho_r)$	$\lambda_{app}(T_n, \rho_r)$	$\lambda(T_n, \rho_r)$
MPa	K	kg/m^3	K	kg/m^3	$W/m/K^2$ $\times 10^{-4}$	W/m/K	W/m/K	W/m/K
50.2	320.802	755.2	324.789	752.9	1.32	0.1465	0.1462	0.1433
50.3	320.797	755.3	324.819	753.0	1.32	0.1460	0.1458	0.1429
50.4	320.798	755.4	324.796	753.1	1.32	0.1458	0.1456	0.1427
72.3	320.804	766.9	324.661	764.8	1.38	0.1528	0.1526	0.1496
73.0	320.896	767.2	324.741	765.1	1.38	0.1527	0.1525	0.1495
93.4	320.860	776.7	324.554	774.8	1.44	0.1582	0.1580	0.1549
113.5	320.859	785.1	324.496	783.3	1.49	0.1634	0.1632	0.1600
133.4	320.865	792.8	324.375	791.2	1.54	0.1684	0.1682	0.1649
164.6	320.854	803.8	324.204	802.3	1.60	0.1762	0.1760	0.1726
186.2	320.894	810.2	324.174	809.4	1.64	0.1802	0.1800	0.1766
200.5	320.869	815.0	324.134	813.7	1.66	0.1835	0.1834	0.1799
239.1	320.899	825.8	324.055	824.6	1.69	0.1907	0.1905	0.1870
260.2	320.871	831.4	323.962	830.2	1.70	0.1946	0.1945	0.1909
285.5	320.853	837.7	323.873	836.6	1.71	0.1989	0.1987	0.1951
314.9	320.872	844.5	323.879	843.4	1.70	0.2039	0.2038	0.2001
325.3	320.874	846.9	323.860	845.8	1.69	0.2058	0.2057	0.2020
334.2	320.850	848.9	323.806	847.9	1.69	0.2070	0.2069	0.2031
364.4	320.857	855.5	323.682	854.5	1.66	0.2119	0.2118	0.2081
403.2	320.915	863.5	323.742	862.6	1.61	0.2175	0.2174	0.2136

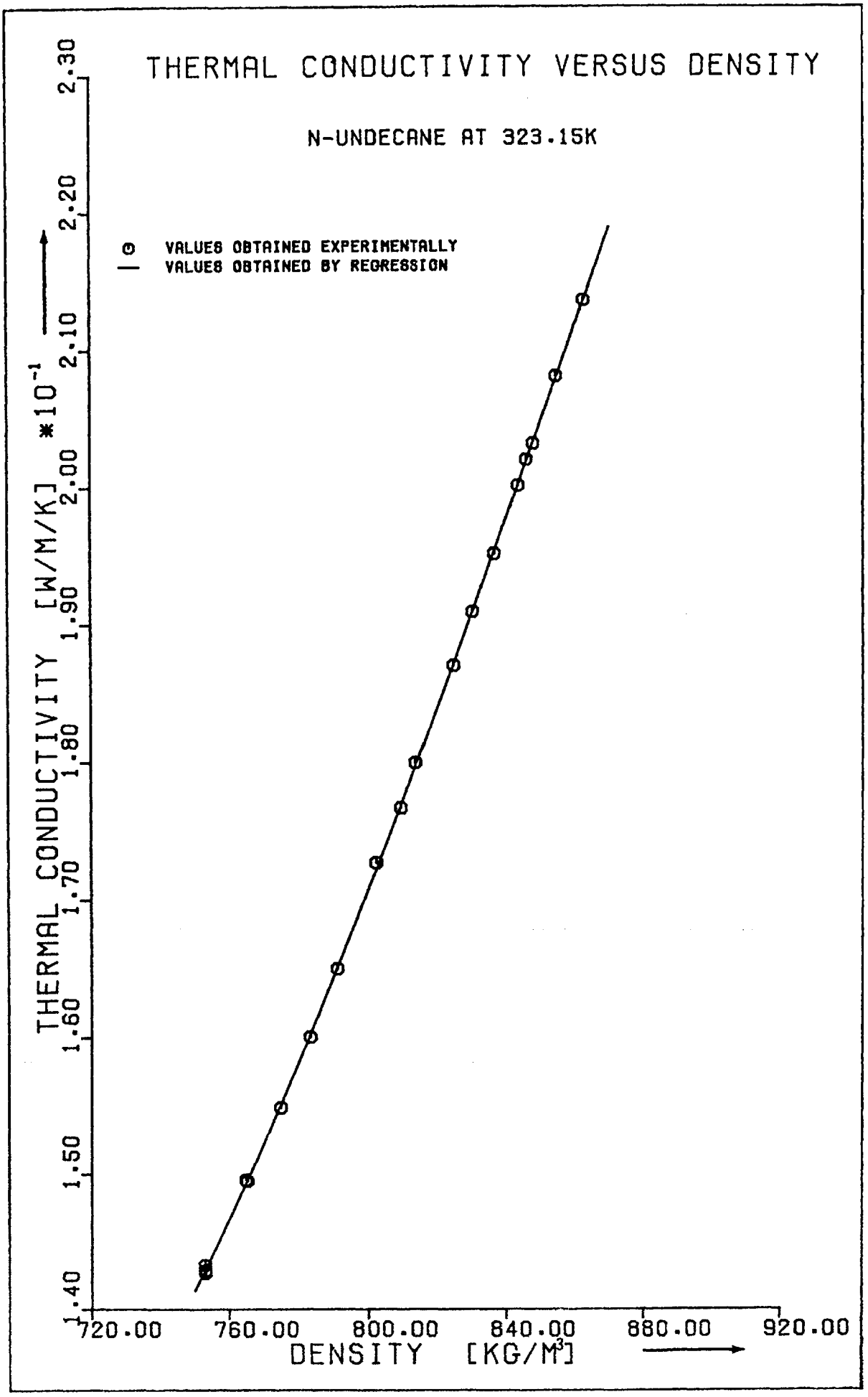
THERMAL CONDUCTIVITY VERSUS DENSITY
N-UNDECANE AT 323.15K
VALUES OBTAINED EXPERIMENTALLY
VALUES OBTAINED BY REGRESSION
THERMAL CONDUCTIVITY [W/M/K] *10⁻¹
1.40
1.50
1.60
1.70
1.80
1.90
2.00
2.10
2.20
2.30
720.00
760.00
800.00
840.00
880.00
920.00
DENSITY [KG/M³]

Fig. (5.20)

Table 5.21 Thermal Conductivity Versus Density
N-Undecane at T_n = 348.15K

P	T_o	ρ_o	T_r	ρ_r	$\left(\frac{\partial\lambda}{\partial T}\right)_\rho$	$\lambda_{app}(T_r, \rho_r)$	$\lambda_{app}(T_n, \rho_r)$	$\lambda(T_n, \rho_r)$
MPa	K	kg/m^3	K	kg/m^3	$W/m/K^2$ $\times 10^{-4}$	W/m/K	W/m/K	W/m/K
49.2	343.969	741.5	347.772	739.3	1.28	0.1408	0.1408	0.1374
49.6	343.804	741.8	347.785	739.6	1.28	0.1413	0.1414	0.1379
74.8	344.066	756.0	347.791	754.1	1.32	0.1497	0.1497	0.1461
96.5	344.097	766.7	347.734	764.9	1.38	0.558	0.1558	0.1521
116.8	344.050	775.6	347.562	774.1	1.43	0.1613	0.1614	0.1576
135.7	344.045	783.3	347.537	781.7	1.48	0.1654	0.1655	0.1616
137.2	344.001	783.9	347.475	782.4	1.48	0.1665	0.1666	0.1627
170.7	344.046	796.1	347.367	794.8	1.56	0.1742	0.1743	0.1703
195.3	344.042	804.2	347.330	802.9	1.61	0.1793	0.1794	0.1753
222.0	344.044	812.2	347.187	811.0	1.65	0.1848	0.1849	0.1807
252.1	344.067	820.7	347.121	819.6	1.68	0.1907	0.1909	0.1866
281.4	344.068	828.4	347.085	827.3	1.70	0.1956	0.1958	0.1915
301.2	344.095	833.2	347.078	832.2	1.71	0.1995	0.1997	0.1953
342.2	344.072	842.8	346.875	841.9	1.70	0.2065	0.2068	0.2023
371.6	344.068	849.4	346.721	848.6	1.69	0.2110	0.2113	0.2067
373.1	344.048	849.7	346.833	848.9	1.69	0.2113	0.2116	0.2070

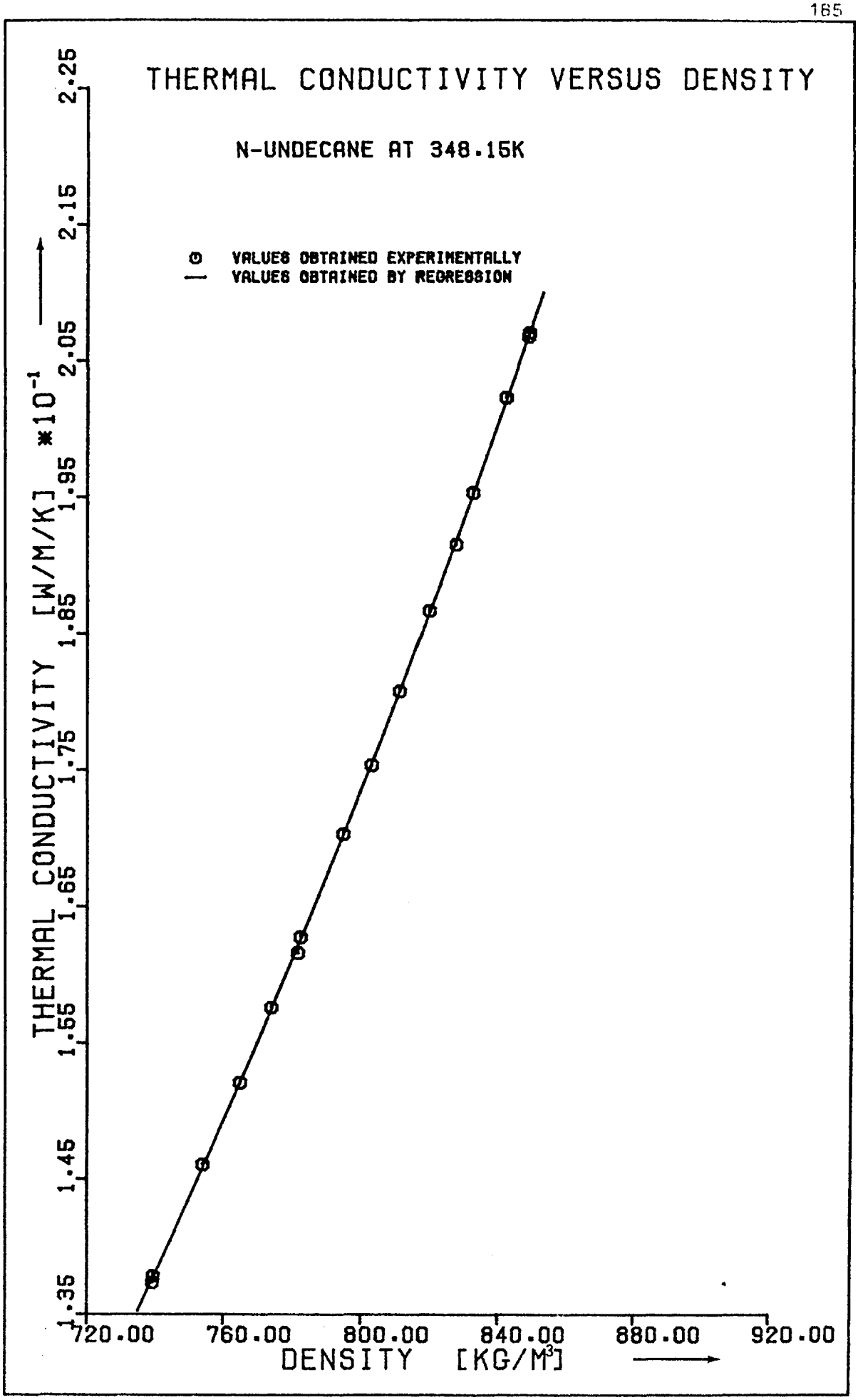
THERMAL CONDUCTIVITY VERSUS DENSITY
N-UNDECANE AT 348.15K
VALUES OBTAINED EXPERIMENTALLY
VALUES OBTAINED BY REGRESSION
THERMAL CONDUCTIVITY [W/M/K] *10⁻¹
1.35
1.45
1.55
1.65
1.75
1.85
1.95
2.05
2.15
2.25
720.00
760.00
800.00
840.00
880.00
920.00
DENSITY [KG/M³]

Fig. (5.22)

Results of the regression analysis to which the data were subjected

Table 5.23

Equation to which the data were fitted:-

$$1 = a_o\lambda + a_1(\rho - \rho^*) + a_2(\rho - \rho^*)^2 + a_3(\rho - \rho^*)^3$$

N-Alkane	Temperature [K]	ρ^* [kg/m^3]	a_o [mK/W]	a_1 [m^3/kg] $\times 10^{-3}$	a_2 [m^6/kg^2] $\times 10^{-6}$	a_3 [m^9/kg^3] $\times 10^{-9}$	Standard Deviation about regression line
N-Heptane	308.15	766.0	5.7723	-3.8380	-3.441	- 6.36	0.0012
	323.15	779.0	5.4300	-3.8413	-3.663	16.74	0.0007
	348.15	771.0	5.5145	-3.8840	-4.781	0.56	0.0011
N-Nonane	308.15	802.0	5.5751	-3.6568	-4.207	2.39	0.0008
	323.15	796.0	5.6194	-3.7662	-3.979	11.95	0.0011
	348.15	796.0	5.5106	-3.7321	-3.993	- 7.11	0.0010
	363.15	783.0	5.7504	-3.7783	-5.100	-10.60	0.0019
N-Undecane	308.15	814.0	5.6319	-3.6851	-4.318	12.53	0.0011
	323.15	806.0	5.7282	-3.7677	-5.025	30.11	0.0014
	348.15	806.0	5.6368	-3.6757	-5.034	- 5.57	0.0013

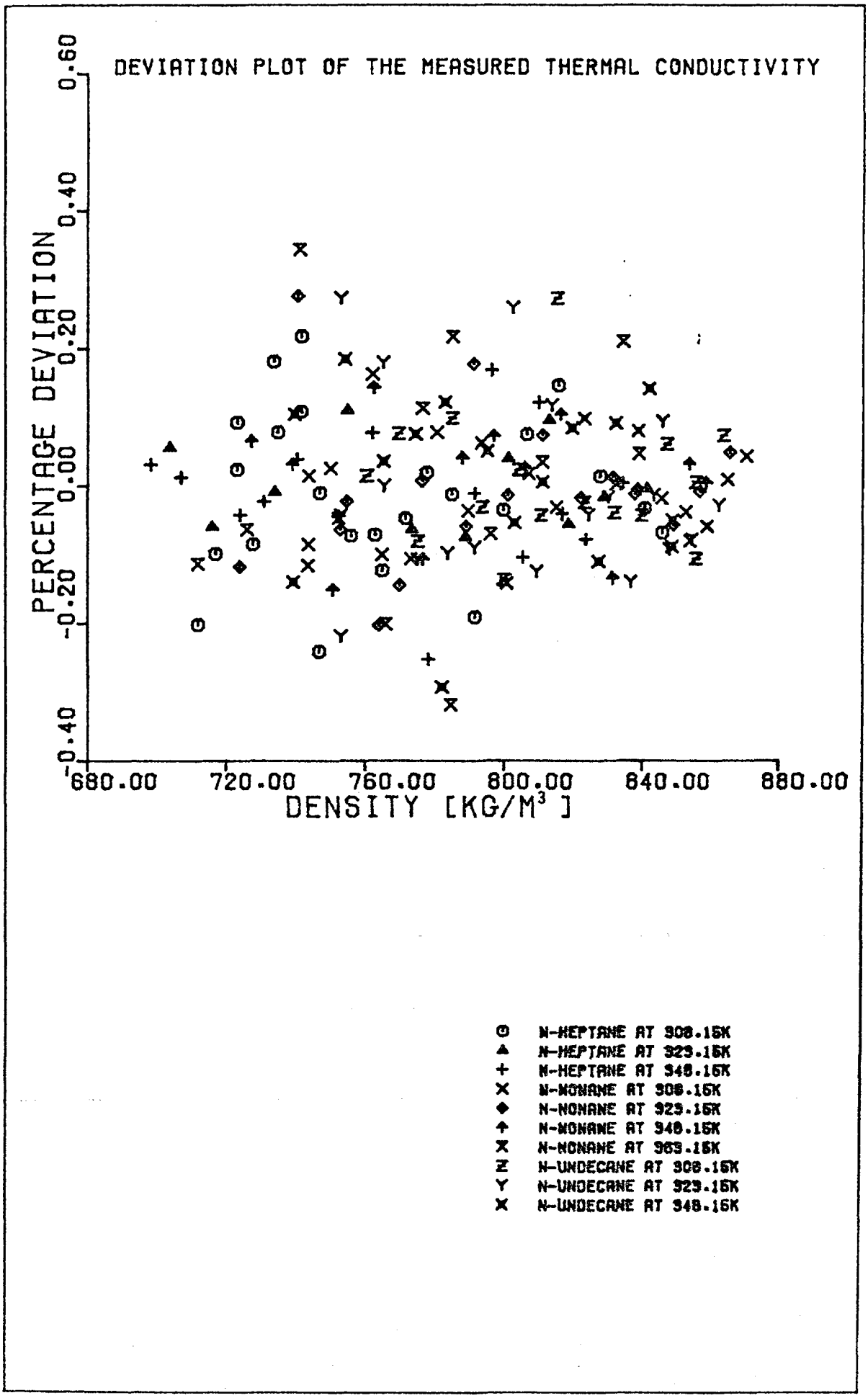

Fig. (5.24) Deviation of the measured thermal conductivity from its correlated value

5.3 Thermal Conductivity Versus Pressure

For most practical applications it is advantageous to have available the pressure dependence of the thermal conductivity of a liquid rather than its density dependence. For this reason, the thermal conductivity of n-Heptane, n-Nonane, and n-Undecane as a function of pressure is presented along the isotherms at which the measurements were performed. As for the density dependence, each set of results are presented both in tabular and graphical form. The results were fitted to polynomials of the form of equation (5.2) as explained in § 5.1 and the values of the coefficients a'_i pertaining to equation (5.2) are given in table (5.45) while the deviation plot of the measured thermal conductivity from their correlated values obtained using equation (5.2) is present in Fig. (5.46) at the end of the section. To reitterate the warning given in § 5.1, care must be used when extrapolating outside the pressure range using equation (5.2) as the equation has no physical significance and, strictly, is only valid within the pressure range over which measurements are performed.

Table 5.25 Thermal Conductivity Versus Pressure
N-Heptane at T_n = 308.15K

P	T_o	ρ_o	T_r	ρ_r	$\left(\frac{\partial\lambda}{\partial T}\right)_p$	$\lambda_{app}(T_r,P)$	$\lambda_{app}(T_n,P)$	$\lambda(T_n,P)$
MPa	K	kg/m^3	K	kg/m^3	$W/m/K^2$ $\times 10^{-5}$	W/m/K	W/m/K	W/m/K
52.4	306.344	713.7	309.500	711.8	-25.2	0.1406	0.1410	0.1390
61.6	307.274	718.6	310.360	716.8	-24.3	0.1440	0.1445	0.1425
71.5	306.356	724.7	309.319	723.0	-23.6	0.1479	0.1482	0.1461
71.5	306.351	724.7	309.318	723.0	-23.6	0.1480	0.1483	0.1462
80.9	306.271	729.2	310.220	727.6	-22.7	0.1507	0.1511	0.1491
91.6	306.353	735.0	309.242	733.5	-22.0	0.1548	0.1550	0.1529
95.3	307.307	736.3	310.225	734.7	-21.7	0.1554	0.1559	0.1538
108.8	306.360	742.9	309.193	741.4	-20.7	0.1597	0.1599	0.1577
109.1	306.377	743.0	309.190	741.6	-20.7	0.1600	0.1602	0.1580
121.5	306.352	748.4	309.127	747.0	-19.7	0.1631	0.1633	0.1611
122.1	307.281	748.2	310.003	746.8	-19.6	0.1627	0.1631	0.1609
142.9	306.346	757.0	309.993	755.8	-17.9	0.1687	0.1689	0.1666
162.0	307.267	763.7	309.863	762.5	-16.2	0.1733	0.1736	0.1713
167.6	307.276	765.7	309.829	764.6	-15.8	0.1746	0.1749	0.1726
187.2	307.278	772.4	309.855	771.3	-14.2	0.1793	0.1795	0.1772
205.5	307.274	778.3	309.794	777.2	-13.1	0.1834	0.1836	0.1813
229.6	307.315	785.6	309.780	784.6	-12.0	0.1885	0.1887	0.1863
253.5	307.289	792.4	310.066	791.3	-11.2	0.1928	0.1930	0.1906
284.1	307.273	800.6	309.601	799.7	-10.4	0.1990	0.1992	0.1967
310.9	307.280	807.2	309.535	806.4	-10.0	0.2041	0.2043	0.2017
350.5	307.278	816.5	309.492	815.7	- 9.0	0.2110	0.2112	0.2086
405.8	307.283	828.6	309.421	827.8	- 7.1	0.2198	0.2199	0.2173
472.0	307.273	841.5	309.345	840.8	- 4.7	0.2297	0.2297	0.2270
499.6	307.282	846.5	309.307	845.8	- 3.9	0.2335	0.2336	0.2308

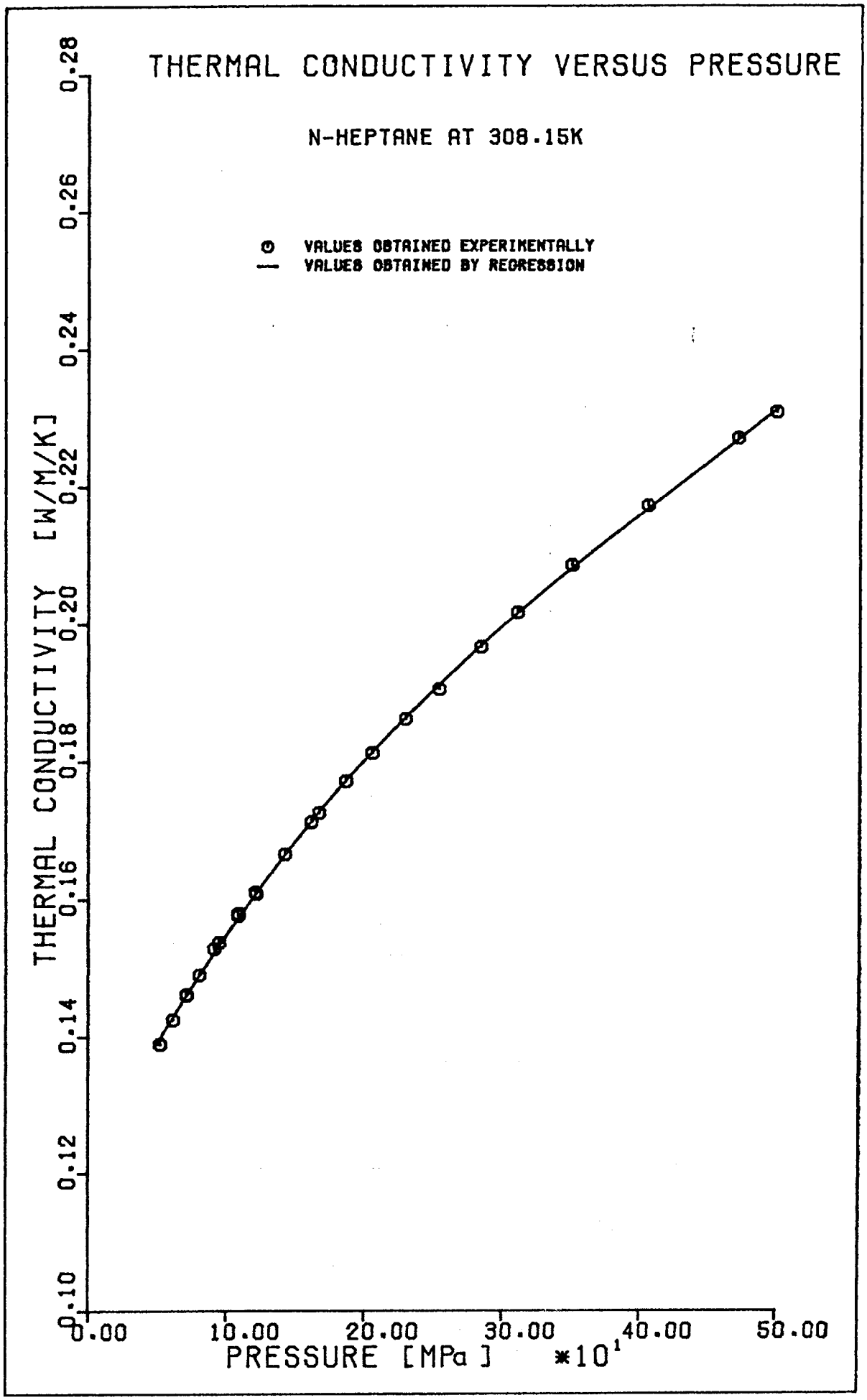
THERMAL CONDUCTIVITY VERSUS PRESSURE
N-HEPTANE AT 308.15K
VALUES OBTAINED EXPERIMENTALLY
VALUES OBTAINED BY REGRESSION
THERMAL CONDUCTIVITY [W/M/K]
0.10
0.12
0.14
0.16
0.18
0.20
0.22
0.24
0.26
0.28
0.00
10.00
20.00
30.00
40.00
50.00
PRESSURE [MPa] *10¹

Fig. (5.26)

Table 5.27 Thermal Conductivity Versus Pressure
N-Heptane at T_n = 323.15K

p	T_o	ρ_o	T_r	ρ_r	$\left(\frac{\partial\lambda}{\partial T}\right)_p$	$\lambda_{app}(T_r,p)$	$\lambda_{app}(T_n,p)$	$\lambda(T_n,p)$
MPa	K	kg/m^3	K	kg/m^3	$W/m/K^2$ $\times10^{-5}$	W/m/K	W/m/K	W/m/K
53.2	320.897	705.4	324.028	703.5	-19.8	0.1383	0.1385	0.1362
73.5	320.895	717.6	323.889	715.9	-20.2	0.1454	0.1455	0.1431
108.4	320.917	735.3	323.749	733.9	-19.6	0.1565	0.1566	0.1541
157.6	320.950	755.9	323.609	754.7	-17.3	0.1703	0.1703	0.1677
210.2	320.956	774.1	323.392	773.1	-14.2	0.1827	0.1827	0.1799
262.3	320.948	789.4	323.283	788.5	-11.4	0.1937	0.1937	0.1908
310.7	320.953	801.7	323.204	801.0	- 8.7	0.2031	0.2031	0.2001
360.8	320.955	813.7	323.112	812.9	- 6.2	0.2120	0.2120	0.2089
386.5	320.931	819.4	323.068	818.7	- 5.2	0.2161	0.2160	0.2130
435.7	320.946	829.7	323.046	829.0	- 3.7	0.2239	0.2239	0.2208
499.9	320.951	842.0	322.951	841.3	- 2.2	0.2333	0.2333	0.2301

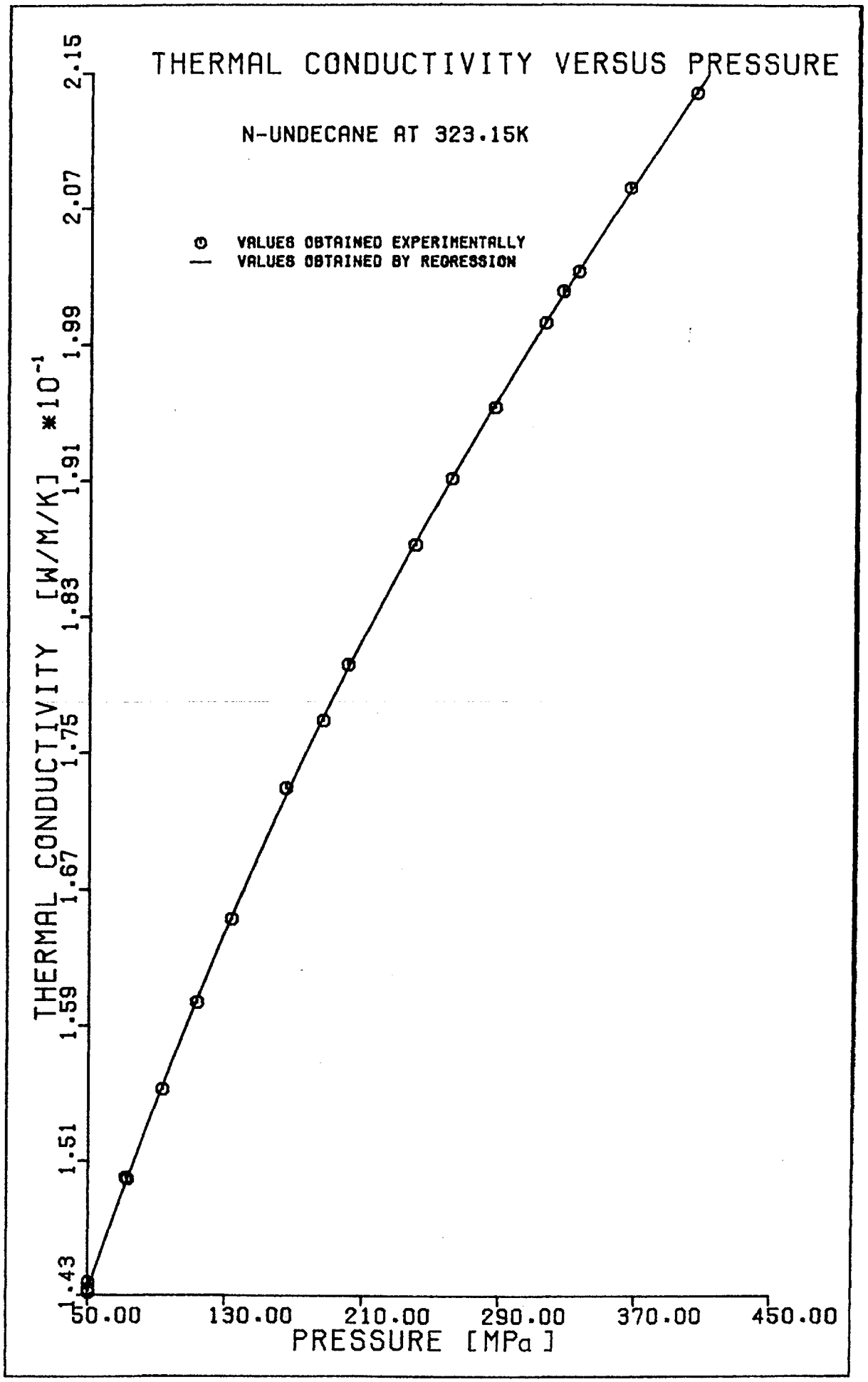
THERMAL CONDUCTIVITY VERSUS PRESSURE
N-UNDECANE AT 323.15K
VALUES OBTAINED EXPERIMENTALLY
VALUES OBTAINED BY REGRESSION
THERMAL CONDUCTIVITY [W/M/K] *10⁻¹
2.15
2.07
1.99
1.91
1.83
1.75
1.67
1.59
1.51
1.43
50.00
130.00
210.00
290.00
370.00
450.00
PRESSURE [MPa]

Fig. (5.42)

Table 5.29 Thermal Conductivity Versus Pressure
N-Heptane at T_n = 348.15K

p	T_o	ρ_o	T_r	ρ_r	$\left(\frac{\partial\lambda}{\partial T}\right)_p$	$\lambda_{app}(T_r,p)$	$\lambda_{app}(T_n,p)$	$\lambda(T_n,p)$
MPa	K	kg/m^3	K	kg/m^3	$W/m/K^2$ $\times 10^{-5}$	W/m/K	W/m/K	W/m/K
65.1	343.479	699.8	346.512	698.1	-18.5	0.1371	0.1368	0.1341
79.1	343.503	708.5	346.464	706.9	-18.7	0.1424	0.1421	0.1393
111.2	343.481	725.4	346.246	724.0	-18.3	0.1528	0.1525	0.1495
125.3	343.420	732.1	346.113	730.8	-17.9	0.1572	0.1568	0.1538
146.7	343.438	741.4	346.071	740.3	-17.1	0.1635	0.1631	0.1601
176.9	343.201	753.4	345.766	752.3	-15.9	0.1713	0.1710	0.1678
203.6	343.459	762.7	345.894	761.7	-14.6	0.1780	0.1777	0.1744
254.8	343.441	778.7	345.775	777.8	-11.7	0.1888	0.1885	0.1851
303.4	343.447	792.0	345.696	791.2	- 9.0	0.1990	0.1988	0.1953
322.2	343.212	796.8	345.370	796.1	- 8.1	0.2029	0.2028	0.1992
360.3	343.219	806.0	345.453	805.3	- 6.5	0.2095	0.2093	0.2057
380.4	343.220	810.6	345.324	809.9	- 5.7	0.2134	0.2133	0.2096
411.9	343.204	817.5	345.364	816.9	- 4.7	0.2186	0.2185	0.2147
443.9	343.235	824.2	345.185	823.6	- 3.8	0.2238	0.2237	0.2200
499.2	343.228	834.7	345.138	834.2	- 3.0	0.2325	0.2324	0.2286

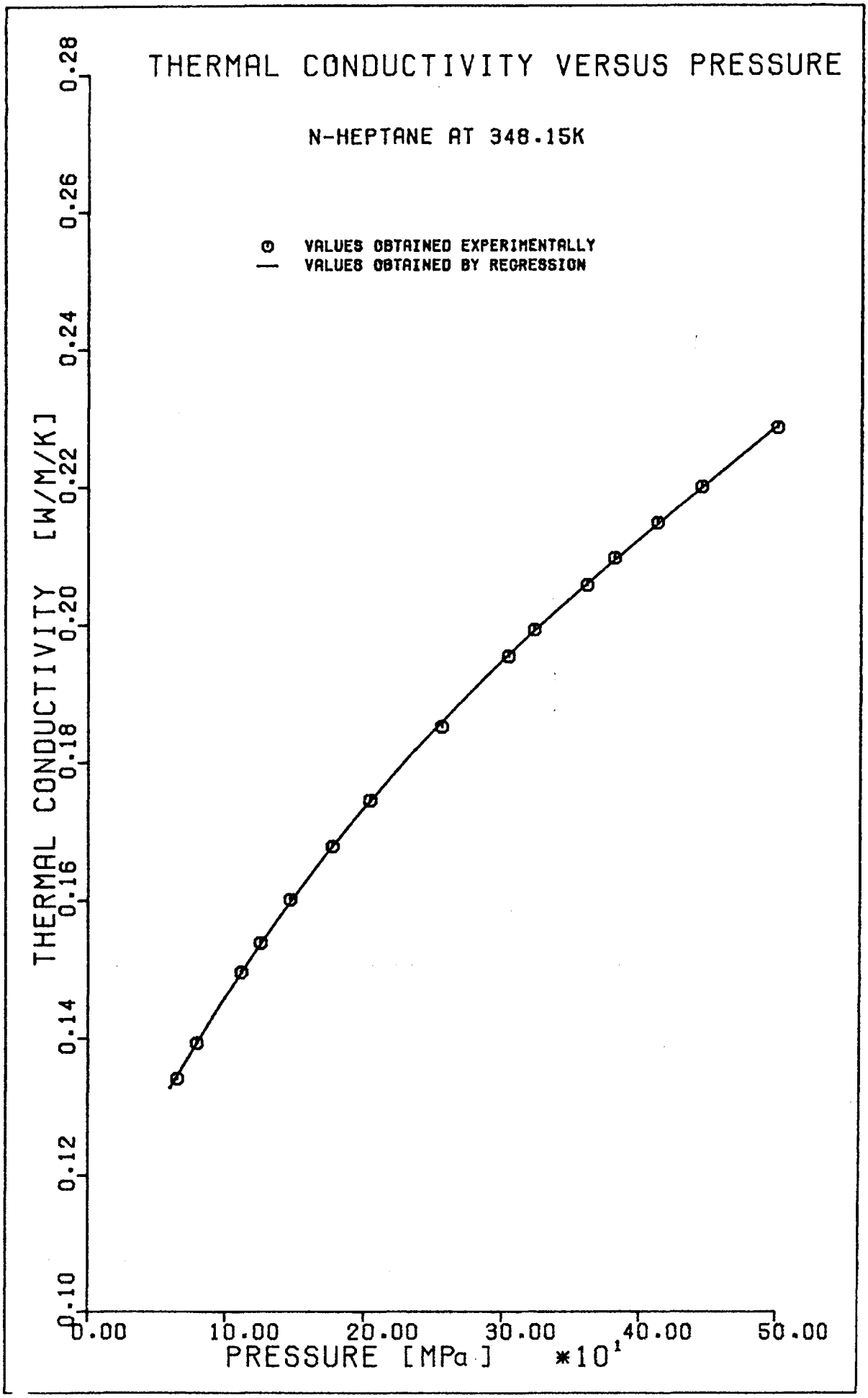
THERMAL CONDUCTIVITY VERSUS PRESSURE
N-HEPTANE AT 348.15K
VALUES OBTAINED EXPERIMENTALLY
VALUES OBTAINED BY REGRESSION
THERMAL CONDUCTIVITY [W/M/K]
0.10
0.12
0.14
0.16
0.18
0.20
0.22
0.24
0.26
0.28
0.00
10.00
20.00
30.00
40.00
50.00
PRESSURE [MPa] *10¹

Fig. (5.30)

Table 5.31 Thermal Conductivity Versus Pressure
N-Nonane at T_n = 308.15K

p	T_o	ρ_o	T_r	ρ_r	$\left(\frac{\partial\lambda}{\partial T}\right)_p$	$\lambda_{app}(T_r,p)$	$\lambda_{app}(T_n,p)$	$\lambda(T_n,p)$
MPa	K	kg/m^3	K	kg/m^3	$W/m/K^2$ $\times 10^{-5}$	W/m/K	W/m/K	W/m/K
51.6	304.145	745.3	307.137	743.5	-20.7	0.1460	0.1458	0.1432
51.8	304.129	745.4	307.164	743.6	-20.6	0.1461	0.1459	0.1433
52.0	304.110	745.5	307.196	743.7	-20.6	0.1463	0.1461	0.1435
63.5	304.086	751.7	307.081	750.0	-19.6	0.1499	0.1497	0.1471
87.1	304.116	763.3	306.977	761.8	-17.8	0.1571	0.1569	0.1541
92.9	304.093	766.0	306.911	764.5	-17.4	0.1583	0.1581	0.1553
112.5	304.081	774.2	306.875	772.8	-16.3	0.1633	0.1631	0.1603
130.9	304.123	781.4	306.781	780.1	-15.3	0.1682	0.1680	0.1651
156.3	304.122	790.6	306.714	789.3	-14.1	0.1738	0.1736	0.1706
167.5	304.122	794.3	306.702	793.1	-13.5	0.1764	0.1762	0.1733
190.6	304.136	801.7	306.735	800.6	-12.5	0.1809	0.1807	0.1777
211.9	304.135	808.1	306.665	807.0	-11.9	0.1856	0.1854	0.1823
241.0	304.132	816.2	306.596	815.2	-11.2	0.1909	0.1907	0.1876
271.6	304.145	824.2	306.610	823.2	-10.5	0.1967	0.1966	0.1934
309.2	304.130	833.3	306.475	832.4	- 9.6	0.2029	0.2027	0.1995
337.0	304.112	839.6	306.368	838.7	- 8.7	0.2075	0.2074	0.2041
369.2	304.118	846.6	306.348	845.7	- 7.3	0.2123	0.2122	0.2089
403.9	304.118	853.7	306.337	852.8	- 5.4	0.2175	0.2174	0.2140
435.5	304.107	859.7	306.153	859.0	- 3.4	0.2219	0.2219	0.2185
468.5	304.127	865.7	306.176	865.0	- 1.0	0.2266	0.2266	0.2231
500.1	304.147	871.2	306.120	870.5	- 0.2	0.2308	0.2308	0.2273

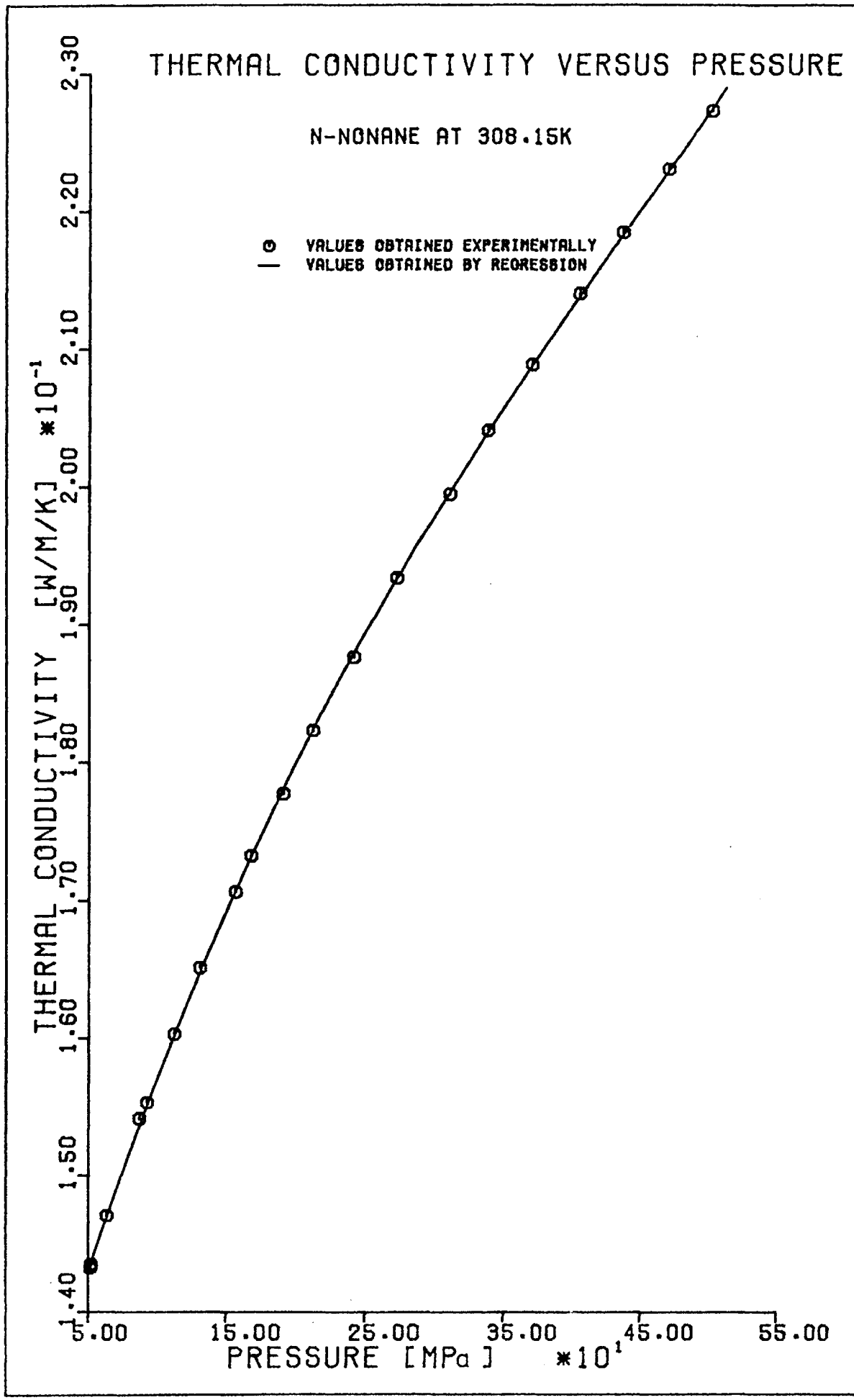
THERMAL CONDUCTIVITY VERSUS PRESSURE
N-NONANE AT 308.15K
VALUES OBTAINED EXPERIMENTALLY
VALUES OBTAINED BY REGRESSION
THERMAL CONDUCTIVITY [W/M/K] *10⁻¹
1.40
1.50
1.60
1.70
1.80
1.90
2.00
2.10
2.20
2.30
5.00
15.00
25.00
35.00
45.00
55.00
PRESSURE [MPa] *10¹

Fig. (5.32)

Table 5.33 Thermal Conductivity Versus Pressure
N-Nonane at T_n = 323.15K

P	T_o	ρ_o	T_r	ρ_r	$\left(\frac{\partial\lambda}{\partial T}\right)_p$	$\lambda_{app}(T_r,P)$	$\lambda_{app}(T_n,P)$	$\lambda(T_n,P)$
MPa	K	kg/m^3	K	kg/m^3	$W/m/K^2$ $\times10^{-5}$	W/m/K	W/m/K	W/m/K
35.3	319.685	725.8	322.858	723.8	-22.5	0.1367	0.1366	0.1338
62.3	319.677	742.2	322.685	740.5	-19.7	0.1466	0.1465	0.1436
85.4	319.698	754.2	322.447	752.8	-17.9	0.1534	0.1533	0.1502
89.6	319.682	756.2	322.591	754.7	-17.6	0.1546	0.1545	0.1515
109.7	319.711	765.1	322.523	763.7	-16.5	0.1598	0.1597	0.1566
123.0	319.685	770.8	322.420	769.5	-15.6	0.1636	0.1635	0.1603
139.3	319.713	777.2	322.423	775.9	-14.7	0.1679	0.1678	0.1645
174.8	319.725	789.8	322.281	788.7	-13.0	0.1762	0.1761	0.1728
181.0	319.690	791.9	322.216	790.8	-12.7	0.1780	0.1779	0.1745
213.8	319.714	802.0	322.229	801.0	-11.3	0.1846	0.1845	0.1811
249.1	319.714	811.9	322.105	811.0	- 9.9	0.1917	0.1916	0.1880
292.4	319.714	823.1	321.958	822.3	- 8.2	0.1994	0.1993	0.1957
331.2	319.702	832.2	321.949	831.4	- 6.6	0.2059	0.2058	0.2022
360.1	319.665	838.7	321.862	837.9	- 5.4	0.2105	0.2105	0.2067
412.5	319.710	849.8	321.792	849.1	- 3.1	0.2186	0.2185	0.2147
452.4	319.696	857.6	321.750	856.9	- 1.3	0.2245	0.2244	0.2206
500.5	319.698	866.4	321.712	865.7	- 0.2	0.2311	0.2311	0.2272

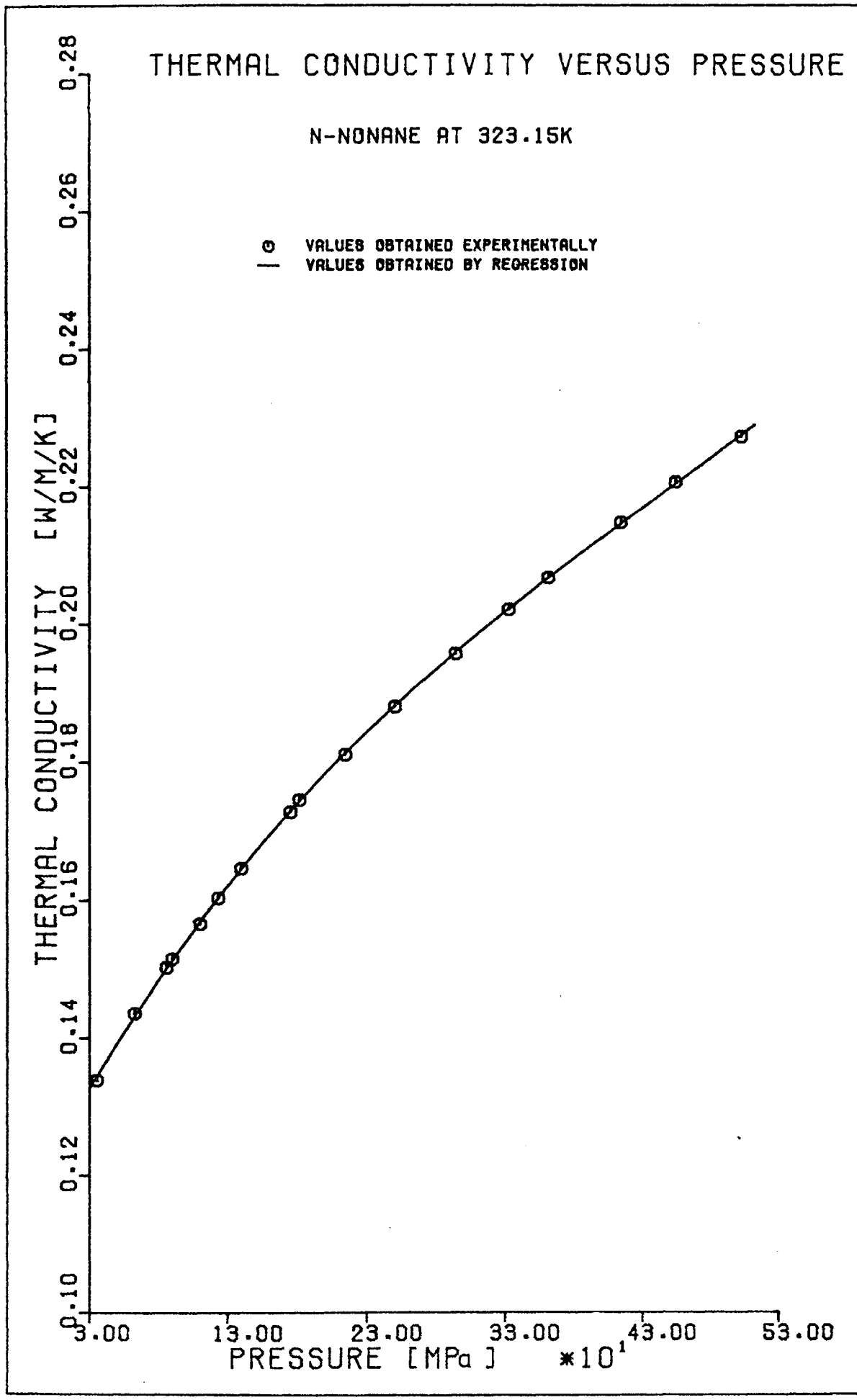
THERMAL CONDUCTIVITY VERSUS PRESSURE
N-NONANE AT 323.15K
VALUES OBTAINED EXPERIMENTALLY
VALUES OBTAINED BY REGRESSION
THERMAL CONDUCTIVITY [W/M/K]
0.10
0.12
0.14
0.16
0.18
0.20
0.22
0.24
0.26
0.28
3.00
13.00
23.00
33.00
43.00
53.00
PRESSURE [MPa] *10¹

Fig. (5.34)

Table 5.35 Thermal Conductivity Versus Pressure
N-Nonane at T_n = 348.15K

P	T_o	ρ_o	T_r	ρ_r	$\left(\frac{\partial\lambda}{\partial T}\right)_p$	$\lambda_{app}(T_r,P)$	$\lambda_{app}(T_n,P)$	$\lambda(T_n,P)$
MPa	K	kg/m^3	K	kg/m^3	$W/m/K^2$ $\times10^{-5}$	W/m/K	W/m/K	W/m/K
63.2	344.129	729.1	347.744	727.1	-30.0	0.1413	0.1411	0.1377
83.8	344.159	740.7	347.649	739.0	-24.1	0.1485	0.1484	0.1448
107.3	344.175	752.3	347.520	750.7	-19.5	0.1556	0.1555	0.1517
134.5	344.172	764.1	347.396	762.1	-15.8	0.1632	0.1631	0.1592
169.1	344.192	777.4	347.267	776.1	-12.6	0.1719	0.1718	0.1678
202.1	344.169	788.6	347.156	787.5	-10.6	0.1797	0.1796	0.1755
232.3	344.179	797.8	347.060	796.7	- 9.1	0.1861	0.1860	0.1818
264.2	344.184	806.9	346.951	805.9	- 7.8	0.1924	0.1924	0.1880
303.7	344.188	817.2	346.882	816.3	- 6.6	0.1999	0.1998	0.1954
367.7	344.181	832.2	346.946	831.4	- 5.2	0.2104	0.2103	0.2058
400.2	344.184	839.3	346.669	838.6	- 4.7	0.2160	0.2159	0.2113
475.6	344.165	854.4	346.491	853.7	- 4.1	0.2277	0.2277	0.2229
502.7	344.136	859.4	346.491	858.7	- 4.0	0.2315	0.2315	0.2267

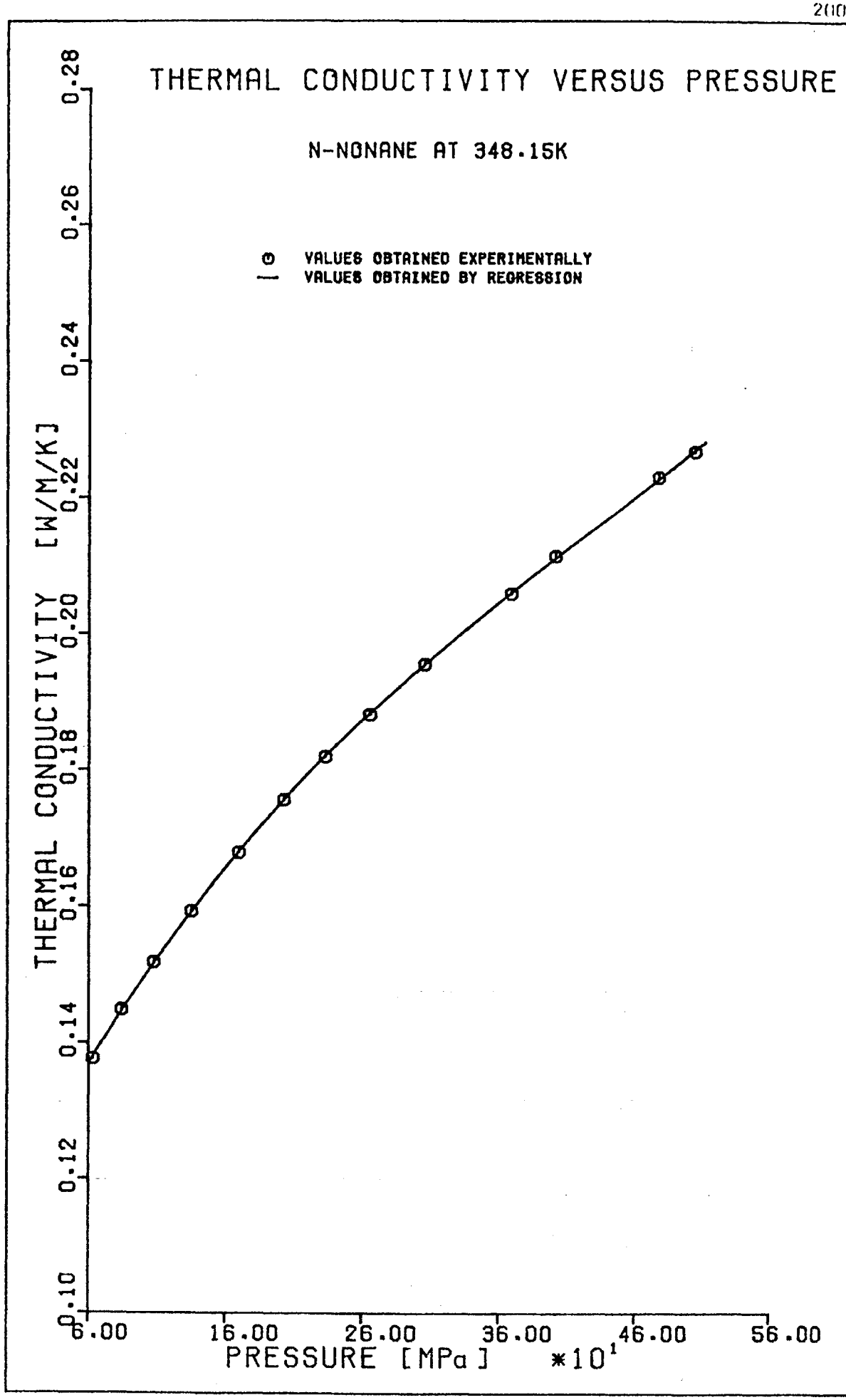
THERMAL CONDUCTIVITY VERSUS PRESSURE
N-NONANE AT 348.15K
VALUES OBTAINED EXPERIMENTALLY
VALUES OBTAINED BY REGRESSION
THERMAL CONDUCTIVITY [W/M/K]
0.10
0.12
0.14
0.16
0.18
0.20
0.22
0.24
0.26
0.28
6.00
16.00
26.00
36.00
46.00
56.00
PRESSURE [MPa] *10^1

Fig. (5.36)

Table 5.37 Thermal Conductivity Versus Pressure
N-Nonane at T_n = 363.15K

P	T_o	ρ_o	T_r	ρ_r	$\left(\frac{\partial\lambda}{\partial T}\right)_p$	$\lambda_{app}(T_r,P)$	$\lambda_{app}(T_n,P)$	$\lambda(T_n,P)$
MPa	K	kg/m^3	K	kg/m^3	$W/m/K^2$ $\times10^{-5}$	W/m/K	W/m/K	W/m/K
53.7	360.507	713.9	364.241	711.8	-21.4	0.1347	0.1349	0.1312
75.8	360.510	727.8	364.075	726.0	-18.3	0.1429	0.1431	0.1391
103.8	360.583	742.7	363.977	741.1	-15.6	0.1526	0.1527	0.1486
127.6	360.535	753.9	363.815	752.4	-13.9	0.1588	0.1589	0.1547
159.4	360.537	766.9	363.676	765.6	-12.1	0.1669	0.1670	0.1625
187.7	360.550	777.3	363.558	776.1	-10.8	0.1742	0.1742	0.1697
211.8	360.560	785.3	363.248	784.3	- 9.8	0.1789	0.1789	0.1743
213.3	360.533	785.8	363.426	784.7	- 9.8	0.1801	0.1801	0.1755
249.6	360.539	796.9	363.362	795.9	- 8.3	0.1872	0.1872	0.1824
304.4	360.557	811.9	363.192	811.0	- 6.3	0.1980	0.1980	0.1931
403.7	360.557	835.1	362.974	834.4	- 3.3	0.2156	0.2156	0.2104
425.4	360.523	839.7	362.891	839.0	- 2.8	0.2191	0.2191	0.2138
503.3	367.578	854.7	362.895	854.0	- 1.4	0.2308	0.2308	0.2254

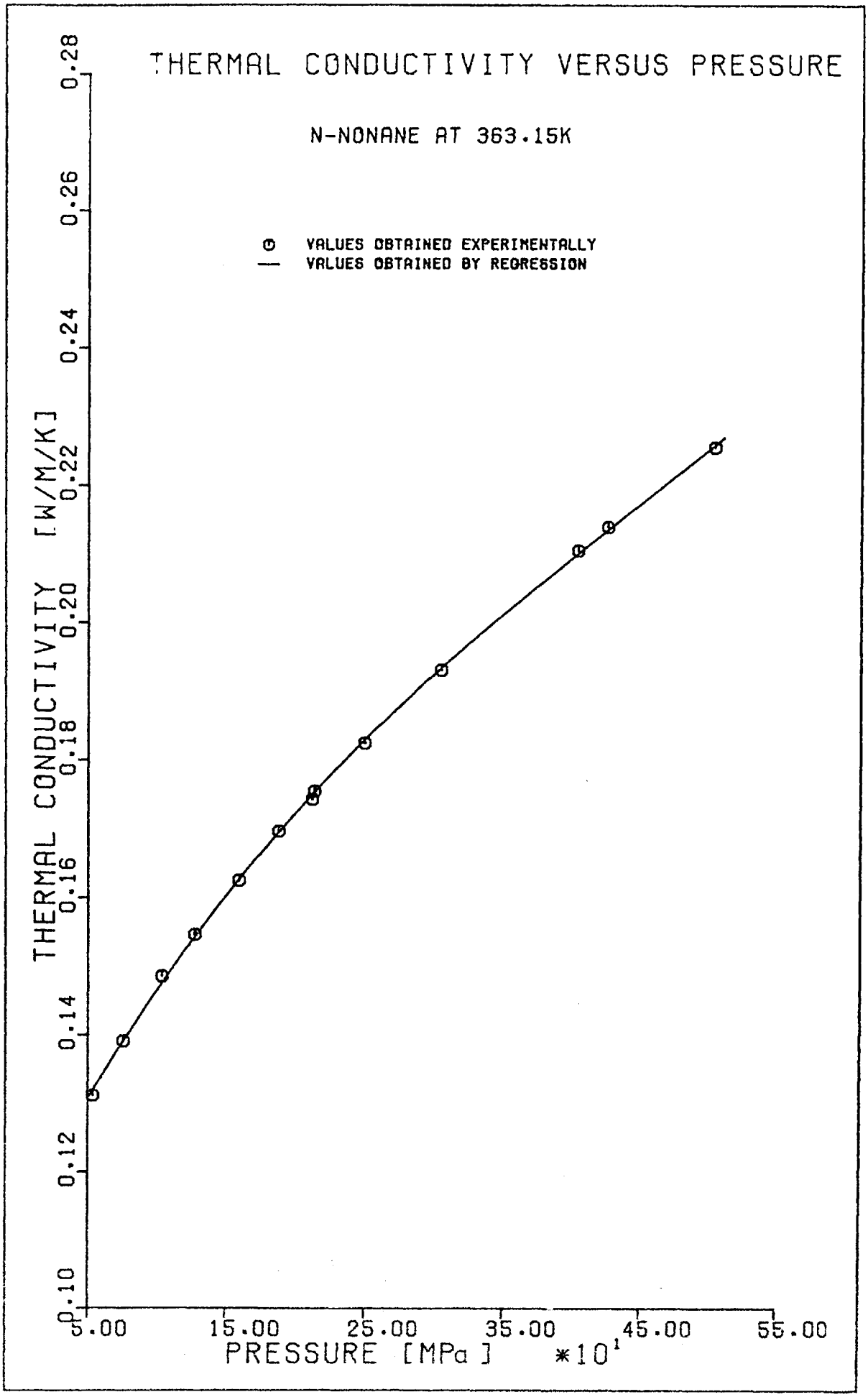
THERMAL CONDUCTIVITY VERSUS PRESSURE
N-NONANE AT 363.15K
VALUES OBTAINED EXPERIMENTALLY
VALUES OBTAINED BY REGRESSION
THERMAL CONDUCTIVITY [W/M/K]
0.10
0.12
0.14
0.16
0.18
0.20
0.22
0.24
0.26
0.28
5.00
15.00
25.00
35.00
45.00
55.00
PRESSURE [MPa] *10¹

Table 5.39 Thermal Conductivity Versus Pressure
N-Undecane at T_n = 308.15

p	T_o	ρ_o	T_r	ρ_r	$\left(\frac{\partial\lambda}{\partial T}\right)_p$	$\lambda_{app}(T_r,P)$	$\lambda_{app}(T_n,P)$	$\lambda(T_n,P)$
MPa	K	kg/m^3	K	kg/m^3	$W/m/K^2$ $\times10^{-5}$	W/m/K	W/m/K	W/m/K
47.4	305.270	762.8	309.343	760.3	-19.1	0.1478	0.1480	0.1454
64.3	305.284	771.4	309.192	769.2	-18.2	0.1529	0.1531	0.1504
75.7	305.288	776.9	309.154	774.8	-17.4	0.1559	0.1559	0.1532
97.9	305.305	786.6	309.113	784.6	-16.3	0.1627	0.1623	0.1595
120.5	305.312	795.5	309.006	793.6	-15.4	0.1675	0.1676	0.1648
137.0	305.308	801.6	308.898	799.8	-14.7	0.1712	0.1713	0.1684
149.2	305.304	805.8	308.827	804.1	-14.3	0.1742	0.1743	0.1714
169.4	305.303	812.4	308.729	810.8	-13.7	0.1785	0.1785	0.1756
183.7	305.283	816.9	308.642	815.3	-13.2	0.1820	0.1820	0.1790
211.8	305.306	825.0	308.612	823.5	-12.7	0.1870	0.1870	0.1839
242.0	305.304	833.4	308.506	832.0	-12.3	0.1927	0.1927	0.1896
274.1	305.311	841.2	308.417	839.9	-12.0	0.1982	0.1982	0.1950
304.6	305.322	848.4	308.386	847.1	-11.9	0.2034	0.2034	0.2002
343.5	305.249	856.9	308.261	855.7	-11.5	0.2091	0.2091	0.2058
344.0	305.328	857.0	308.281	855.8	-11.5	0.2094	0.2094	0.2061
382.7	305.321	865.0	308.211	863.9	-10.7	0.2153	0.2153	0.2120

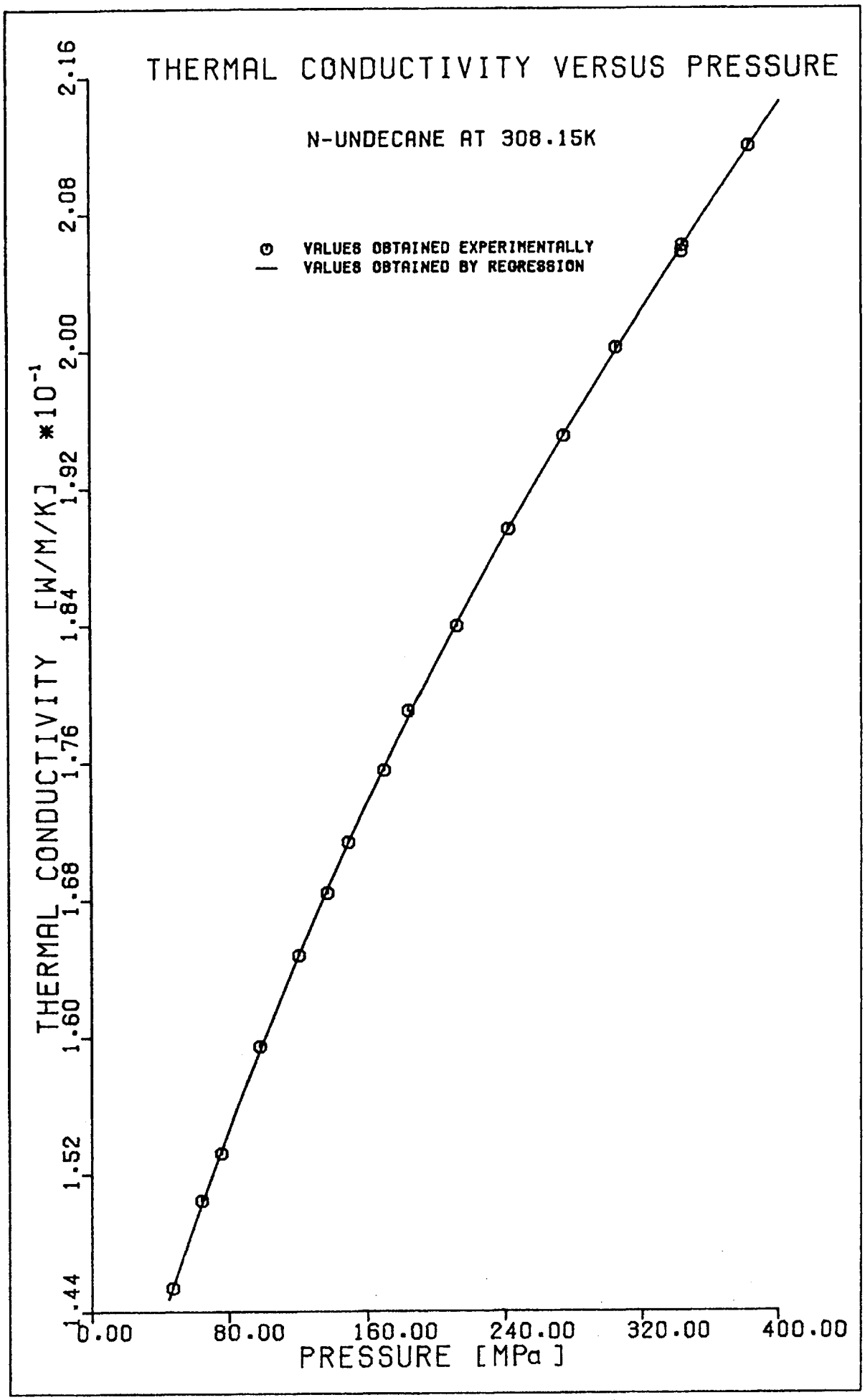
THERMAL CONDUCTIVITY VERSUS PRESSURE
N-UNDECANE AT 308.15K
VALUES OBTAINED EXPERIMENTALLY
VALUES OBTAINED BY REGRESSION
THERMAL CONDUCTIVITY [W/M/K] *10⁻¹
1.44
1.52
1.60
1.68
1.76
1.84
1.92
2.00
2.08
2.16
0.00
80.00
160.00
240.00
320.00
400.00
PRESSURE [MPa]

Fig. (5.40)

Table 5.41 Thermal Conductivity Versus Pressure
N-Undecane at T_n = 323.15K

P	T_o	ρ_o	T_r	ρ_r	$\left(\frac{\partial\lambda}{\partial T}\right)_\rho$	$\lambda_{app}(T_r,P)$	$\lambda_{app}(T_n,P)$	$\lambda(T_n,P)$
MPa	K	kg/m^3	K	kg/m^3	$W/m/K^2$ $\times 10^{-5}$	W/m/K	W/m/K	W/m/K
50.2	320.802	755.2	324.789	752.9	-16.6	0.1465	0.1467	0.1438
50.3	320.797	755.3	324.819	753.0	-16.6	0.1460	0.1463	0.1434
50.4	320.798	755.4	324.796	753.1	-16.6	0.1458	0.1461	0.1432
72.3	320.804	766.9	324.661	764.8	-15.9	0.1528	0.1531	0.1500
73.0	320.896	767.2	324.741	765.1	-15.9	0.1527	0.1530	0.1500
93.4	320.860	776.7	324.554	774.8	-15.0	0.1582	0.1584	0.1553
113.5	320.859	785.1	324.496	783.3	-14.2	0.1634	0.1636	0.1604
133.4	320.865	792.8	324.375	791.2	-13.4	0.1684	0.1685	0.1653
164.5	320.854	803.8	324.204	802.3	-12.2	0.1762	0.1763	0.1729
186.2	320.894	810.7	324.174	809.4	-11.2	0.1802	0.1803	0.1769
200.5	320.869	815.0	324.134	813.7	-10.7	0.1835	0.1836	0.1802
239.1	320.899	825.8	324.055	824.6	- 9.7	0.1907	0.1907	0.1872
260.2	320.871	831.4	323.962	830.2	- 9.2	0.1946	0.1947	0.1911
285.5	320.853	837.7	323.873	836.6	- 8.8	0.1989	0.1989	0.1953
314.9	320.872	844.5	323.879	843.4	- 8.4	0.2039	0.2040	0.2003
325.3	320.874	846.9	323.860	845.8	- 8.3	0.2058	0.2058	0.2021
334.2	320.850	848.9	323.806	847.9	- 8.1	0.2070	0.2070	0.2033
364.4	320.857	855.5	323.682	854.5	- 7.8	0.2119	0.2120	0.2082
403.2	320.915	863.5	323.742	862.6	- 7.4	0.2175	0.2176	0.2138

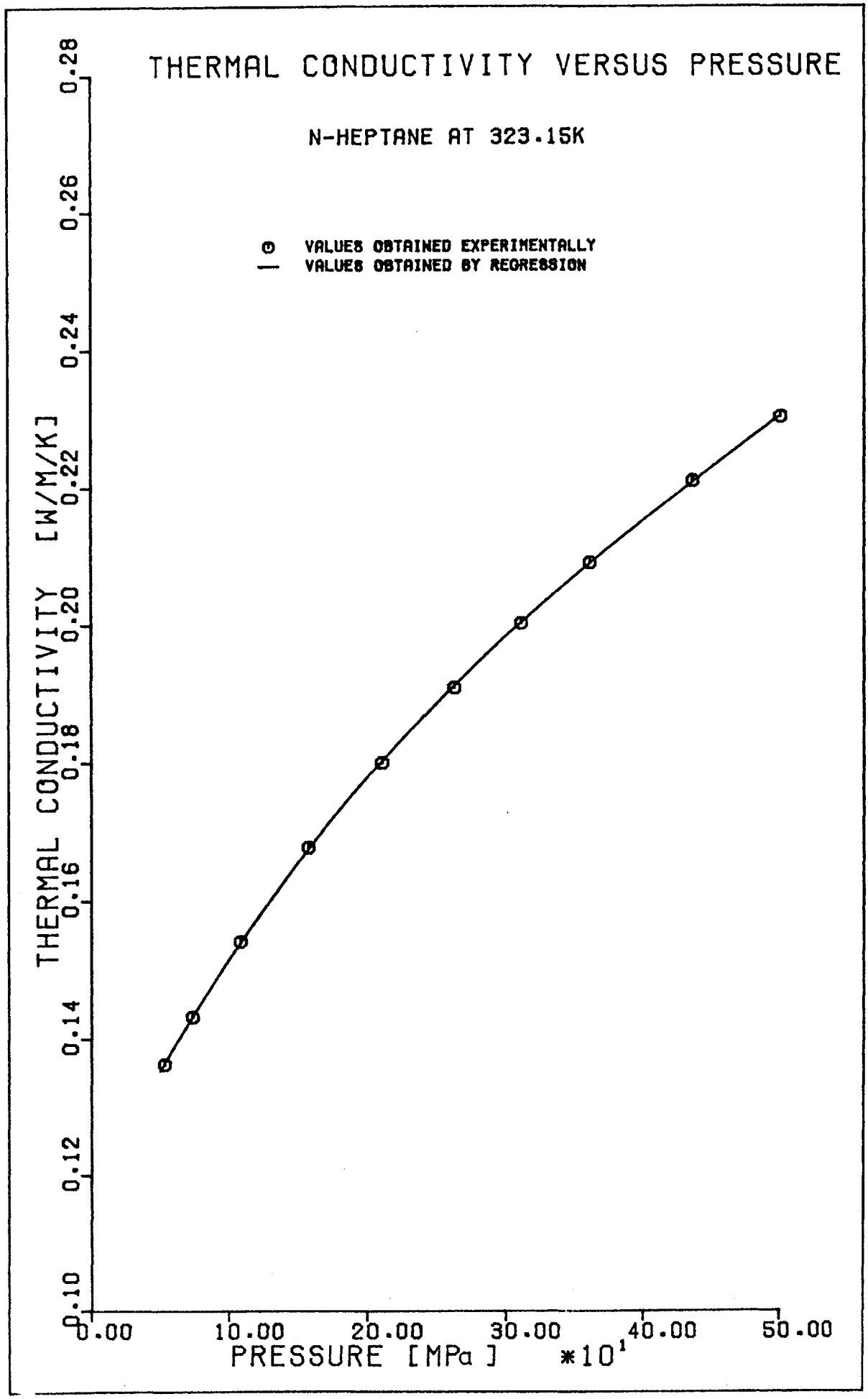
THERMAL CONDUCTIVITY VERSUS PRESSURE
N-HEPTANE AT 323.15K
VALUES OBTAINED EXPERIMENTALLY
VALUES OBTAINED BY REGRESSION
THERMAL CONDUCTIVITY [W/M/K]
0.10
0.12
0.14
0.16
0.18
0.20
0.22
0.24
0.26
0.28
0.00
10.00
20.00
30.00
40.00
50.00
PRESSURE [MPa] *10¹

Fig. (5.28)

Table 5.43 Thermal Conductivity Versus Pressure
N-Undecane at T_n = 348.15K

P	T_o	ρ_o	T_r	ρ_r	$\left(\frac{\partial\lambda}{\partial T}\right)_\rho$	$\lambda_{app}(T_r,P)$	$\lambda_{app}(T_n,P)$	$\lambda(T_n,P)$
MPa	K	kg/m^3	K	kg/m^3	$W/m/K^2$ $\times10^{-5}$	W/m/K	W/m/K	W/m/K
49.2	343.969	741.5	347.772	739.3	-16.5	0.1408	0.1407	0.1372
49.6	343.804	741.8	347.785	739.6	-16.5	0.1413	0.1413	0.1378
74.8	344.066	756.0	347.791	754.1	-15.5	0.1497	0.1496	0.1460
96.5	344.097	766.7	347.734	764.9	-14.2	0.1558	0.1557	0.1519
116.8	344.050	775.6	347.562	774.1	-13.1	0.1613	0.1612	0.1574
135.7	344.045	783.3	347.537	781.7	-12.0	0.1654	0.1654	0.1615
137.2	344.001	783.9	347.475	782.4	-12.0	0.1665	0.1665	0.1625
170.7	344.046	796.1	347.367	794.8	-10.3	0.1742	0.1741	0.1701
195.3	344.042	804.2	347.330	802.9	- 9.1	0.1793	0.1792	0.1751
222.0	344.044	812.2	347.187	811.0	- 8.0	0.1848	0.1847	0.1805
252.1	344.067	820.7	347.121	819.6	- 6.9	0.1907	0.1907	0.1864
281.4	344.068	828.4	348.085	827.3	- 5.9	0.1956	0.1956	0.1912
301.2	344.095	833.2	347.078	832.2	- 5.3	0.1995	0.1994	0.1950
342.2	344.072	842.8	346.875	841.9	- 4.6	0.2065	0.2065	0.2020
371.6	344.068	849.4	346.721	848.6	- 4.1	0.2110	0.2110	0.2064
373.1	344.048	849.7	346.833	848.9	- 4.1	0.2113	0.2113	0.2067

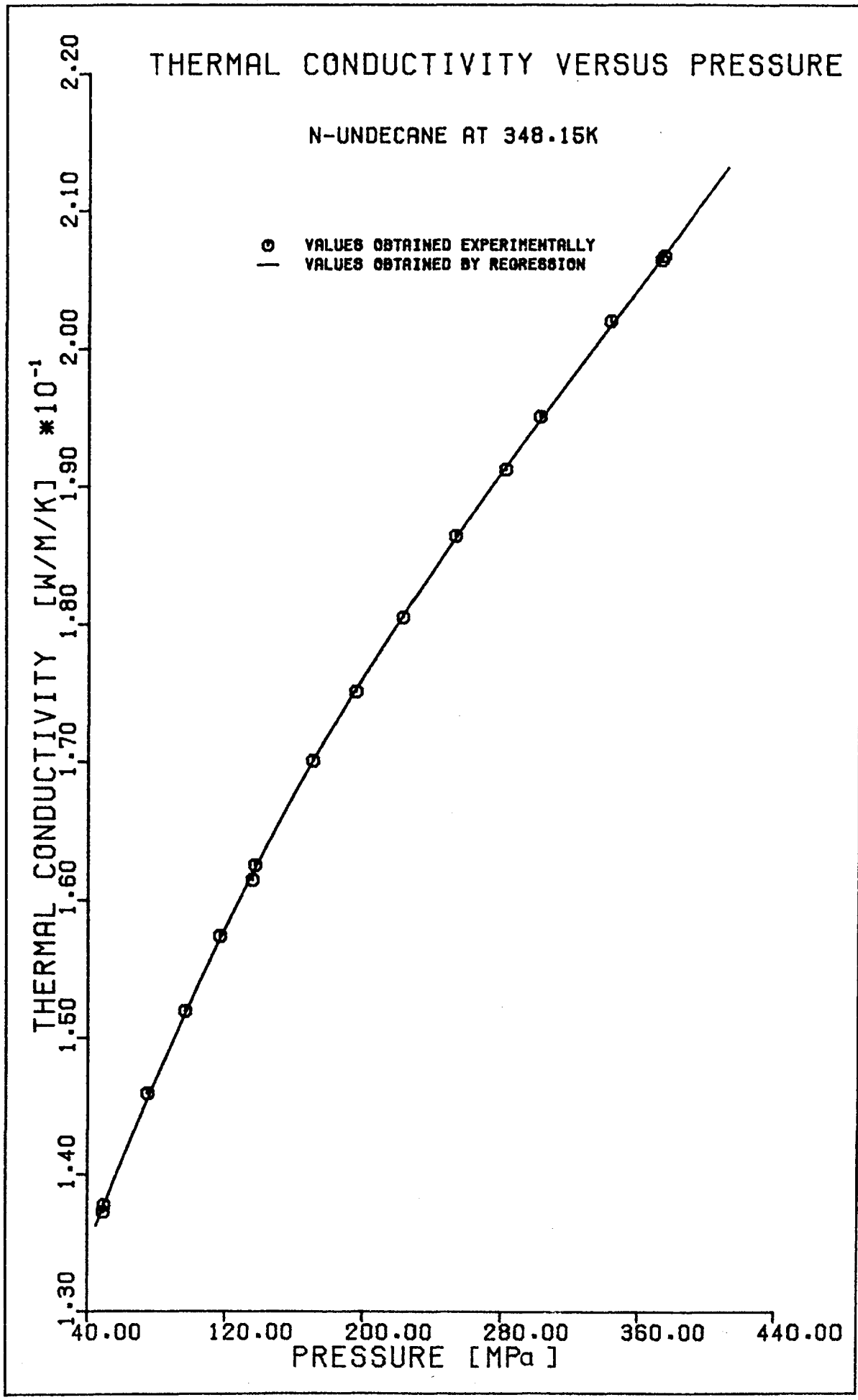
THERMAL CONDUCTIVITY VERSUS PRESSURE
N-UNDECANE AT 348.15K
VALUES OBTAINED EXPERIMENTALLY
VALUES OBTAINED BY REGRESSION
THERMAL CONDUCTIVITY [W/M/K] *10⁻¹
1.30
1.40
1.50
1.60
1.70
1.80
1.90
2.00
2.10
2.20
40.00
120.00
200.00
280.00
360.00
440.00
PRESSURE [MPa]

Fig. (5.44)

Results of the regression analysis to which the data were subjected

Table 5.45

Equation to which the data were fitted:-

$$1 = a'_0\lambda + a'_1(P-P^*) + a'_2(P-P^*)^2 + a'_3(P-P^*)^3$$

N-Alkane	Temperature [K]	P* [MPa]	a'_0 [mK/W]	a'_1 [MPa^{-1}] $\times 10^{-3}$	a'_2 [MPa^{-2}] $\times 10^{-6}$	a'_3 [MPa^{-3}] $\times 10^{-9}$	Standard Deviation about regression line
N-Heptane	308.15	194.0	5.5893	-1.2530	1.697	-2.37	0.0022
	323.15	247.0	5.3186	-1.0949	1.294	-1.87	0.0011
	348.15	259.0	5.3569	-1.1183	1.256	-2.13	0.0017
N-Nonane	308.15	224.0	5.4126	-1.0335	1.203	-1.81	0.0013
	323.15	224.0	5.4547	-1.0824	1.357	-2.14	0.0016
	348.15	254.0	5.3697	-1.0413	1.219	-2.26	0.0012
	363.15	232.0	5.5771	-1.1696	1.370	-2.13	0.0033
N-Undecane	308.15	197.0	5.5167	-1.0739	1.308	-2.31	0.0011
	323.15	196.0	5.5845	-1.1280	1.336	-2.01	0.0013
	348.15	198.0	5.6862	-1.1622	1.498	-3.45	0.0016

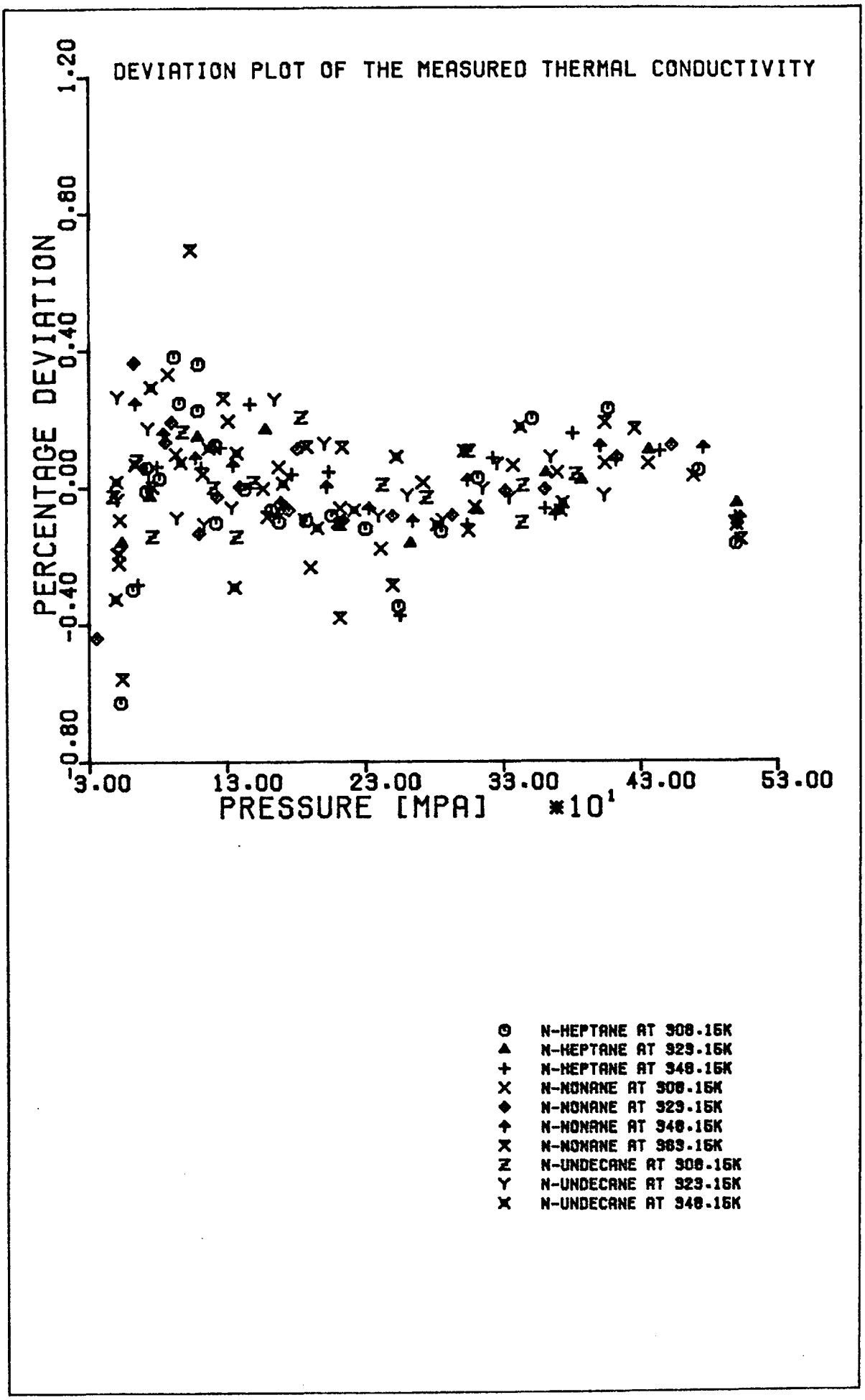

Fig. (5.46) Deviation of the measured thermal conductivity from its correlated value.

5.4 Comparison of Results

A literature survey on the thermal conductivity of the n-Alkanes studied in this work reveals two major difficulties. Firstly, there are very little data available on the thermal conductivity of these n-Alkanes at elevated pressures and those data that are available are subject to large errors, ± 5% at best.

During preliminary work on n-Heptane, when testing the apparatus, measurements were performed to determine the thermal conductivity of n-Heptane under its saturation vapour pressure. The results of the measurements performed at the saturation vapour pressure were not included in the tables in § 5.2 and § 5.3 because they were preliminary and their accuracy was considered inferior to that of the remainder of results. It is estimated that these results have a probable error of about ± 0.8%. Furthermore, these early measurements were also carried out at a temperature of approximately 6K from any nominal temperature for the main body of the results. However, for the purposes of a comparison with earlier results, which have most often been performed under these conditions, the accuracy is more than sufficient because it is still superior to that of the other available data.

In table 5.47 the thermal conductivity of n-Heptane obtained from these measurements performed by other investigators is compared with the saturated vapour measurements obtained on n-Heptane. The thermal conductivity is corrected in each case to its value at 308.15K using the temperature coefficient reported by the particular investigator or where this is unavailable a temperature coefficient of -3.00×10^{-4} W/mK^2 is assumed. Only measurements reported since 1960 are considered (in chronological order) as earlier work is considered to be too inaccurate.

The values of the thermal conductivity of n-Heptane reported in Table 5.47 show a scatter of more than 20% which is surprising since a substantial number of investigators estimate their absolute accuracy to be within a few percent. All the measurements with the notable

exception of those performed by Kastorgrev et al [104] and by Ganiev [103] predict values for the thermal conductivity of n-Heptane which are significantly in excess of those reported in the present work. The reasons for the inconsistency are many but there are a number which stand out above the rest. The first, and the major cause of unaccounted inaccuracy in measurements, is convection. In the present apparatus it can be shown that, by increasing the duration of a run from less than one second to only four seconds, convection can be induced in the test fluid. The thermal conductivity thus measured in the presence of convection can be greater, by 3%, than that measured in its absence thus indicating the importance of convection. A great number of methods used by the investigators in Table 5.47 employed steady state techniques which for the reasons enumerated previously in § 1.24 and & 2.31 are thought to be plagued by effects due to convection and thus produce inferior results. Relative measurements are not preferred as they immediately incurr the errors related to the reference fluid used and the method used to measure the physical properties of this reference fluid. Of the remaining observations which were performed using transient non-relative techniques, the majority of methods involved the duration of an experiment being insufficiently short to render negligible the effects of convection.

Of all the observations presented in Table 5.47 the only measurement known not to have suffered the drawbacks mentioned above is that by Castro [85] . Because the accuracy originally claimed by Castro is comparable with that ascribed to the present results, the discrepancy between the two results of about 3.5% requires some comment. Firstly, the measurements of Castro were carried out before the effects of the different resistances per unit length of the two wires were appreciated. If account is taken of these effects Castro's results are decreased by 0.7% [113] . Secondly, inadequate compensation was made for the effect of radiative heat transfer in Castro's and other investigators' measurements on radiation absorbing, reemitting liquids because an analysis of the type given in chapter 3 was, until now, unavailable. In the case of the measurement performed by Castro, because of the

Thermal Conductivity of N-Heptane
under its saturated vapour pressure at 308.15K

Table 5.47

	Investigator(s) Year, reference	Temperature at which measurements were performed [K]	Temperature Coefficient $\left[\frac{W/m/K^2}{\times 10^{-4}}\right]$	Thermal Conductivity @ 308.15K [W/m/K]
+	Present Work	314.45	-3.00	0.1165
+	Present Work	316.30	-3.00	0.1162
+	Castro (1976) [85]	308.18	-2.82	0.1206
+	Powell et al (1972) [97]	303.15	-3.00	0.1280
+	Naziev et al (1971) [98]	293.15	-2.65	0.1269
*	Mukhamedzyanov et al (1971) [99]	298.15	-3.15	0.1205
*	Brykov et al (1970) [100]	293.15	-3.51	0.1206
	Kerimov et al (1970) [101]	299.15	-0.96	0.1222
	Pittman (1968) [102]	333.15	-2.97	0.1352
*	Ganiev (1968) [103]	293.15	-2.40	0.1044
*	Rastorguev et al (1968) [104]	293.15	-3.10	0.1164
R+	Mallan (1968) [105]	298.15	-2.27	0.1199
+	Abas Zade (1967) [106]	290.15	-2.75	0.1281
R+	Jobst (1964) [107]	298.15	-3.45	0.1281
*	Akhmedov (1963) [108]	293.15	-4.10	0.1208
*	Mukhamedzyanov et al (1963) [109]	309.15	-2.86	0.1239
+	Golubev et al (1961) [110]	293.15	-2.57	0.1303
*	Vilim (1960) [111]	293.15	-3.00	0.1315

\+ Transient Method
* Steady State Method
R Relative Measurement

high temperature rise of the wire used ($\approx$10K), the apparent thermal conductivity is estimated to be approximately 2.5 - 3.0% higher than the true thermal conductivity. On application of these two corrections the thermal conductivities as measured by the author and by Castro agree to within the experimental uncertainties within the two measurements.

There are unfortunately no reliable measurements available for the thermal conductivity of n-Undecane and very few measurements for the thermal conductivities of n-Heptane and n-Nonane, within the temperature range of this work and at elevated pressures. Most of what is available on n-Heptane and n-Nonane only extends from atmospheric pressure up to about 50 MPa, when the present measurements began. Figures (5.48) and (5.49) compare the correlated pressure dependence of the thermal conductivities of n-Heptane and n-Nonane with the few independent measurements which are available. The thermal conductivity versus pressure relationships quoted for the present work are equation (5.2) with the relevant coefficients as given in Table 5.45 and the values quoted from the work of other investigators have, where necessary, been obtained by interpolating their data.

As was expected, for the reasons given earlier, it has been found that the thermal conductivity measurements performed by other investigators produce values which are, in general, a few percent higher than those found in the present work.

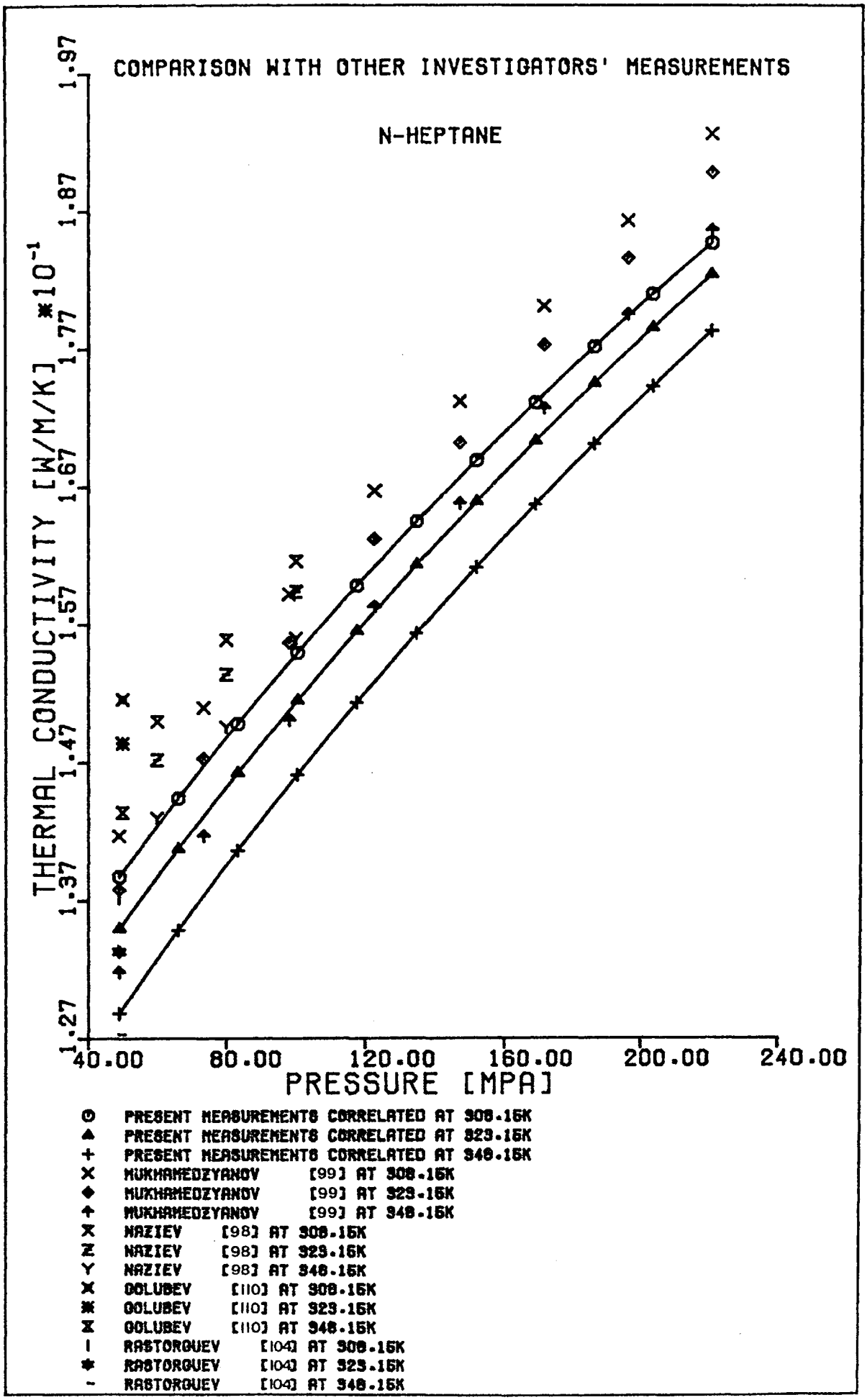
COMPARISON WITH OTHER INVESTIGATORS' MEASUREMENTS
N-HEPTANE
THERMAL CONDUCTIVITY [W/M/K] *10⁻¹
1.27
1.37
1.47
1.57
1.67
1.77
1.87
1.97
40.00
80.00
120.00
160.00
200.00
240.00
PRESSURE [MPA]
PRESENT MEASUREMENTS CORRELATED AT 308.15K
PRESENT MEASUREMENTS CORRELATED AT 323.15K
PRESENT MEASUREMENTS CORRELATED AT 348.15K
MUKHAMEDZYANOV [99] AT 308.15K
MUKHAMEDZYANOV [99] AT 323.15K
MUKHAMEDZYANOV [99] AT 348.15K
NAZIEV [98] AT 308.15K
NAZIEV [98] AT 323.15K
NAZIEV [98] AT 348.15K
GOLUBEV [110] AT 308.15K
GOLUBEV [110] AT 323.15K
GOLUBEV [110] AT 348.15K
RASTORGUEV [104] AT 308.15K
RASTORGUEV [104] AT 323.15K
RASTORGUEV [104] AT 348.15K

Fig. (5.48)

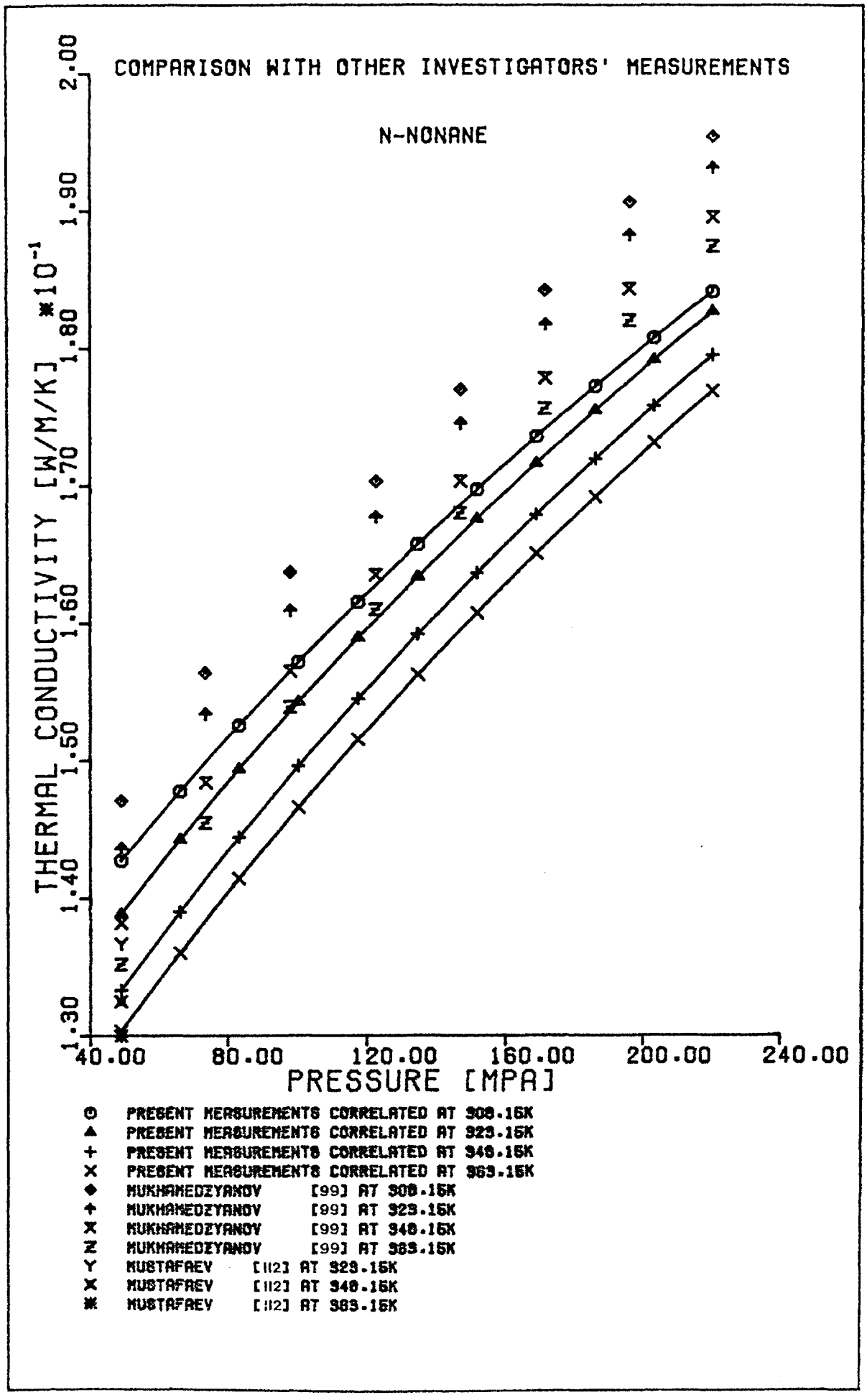
COMPARISON WITH OTHER INVESTIGATORS' MEASUREMENTS
N-NONANE
THERMAL CONDUCTIVITY [W/M/K] *10⁻¹
PRESSURE [MPA]
1.30
1.40
1.50
1.60
1.70
1.80
1.90
2.00
40.00
80.00
120.00
160.00
200.00
240.00
PRESENT MEASUREMENTS CORRELATED AT 308.15K
PRESENT MEASUREMENTS CORRELATED AT 323.15K
PRESENT MEASUREMENTS CORRELATED AT 348.15K
PRESENT MEASUREMENTS CORRELATED AT 363.15K
MUKHAMEDZYANOV [99] AT 308.15K
MUKHAMEDZYANOV [99] AT 323.15K
MUKHAMEDZYANOV [99] AT 348.15K
MUKHAMEDZYANOV [99] AT 363.15K
MUSTAFAEV [112] AT 323.15K
MUSTAFAEV [112] AT 348.15K
MUSTAFAEV [112] AT 383.15K

Fig. (5.49)

CHAPTER 6

Conclusions

6.1 Introduction

This chapter summarises the results and conclusions that can be drawn from the work undertaken and described in the previous chapters. It can broadly be separated into two sections. The first section is concerned with the work described in chapter 3 on radiative heat transfer and its effects on the transient hot wire method of measuring liquid conductivities. The second section is concerned with the use that can be made of the data presented in chapter 5 in relation to the pressure and density dependence of the thermal conductivity of liquid n-Alkanes as well as the practical application of these data.

6.2 Conclusions drawn from the work on radiative heat transfer

There has for a long time been controversy over the implication of the radiative heat transfer which is inherent in the transient hot wire technique of measuring thermal conductivities. There have been claims that the effects on the measured thermal conductivity were larger for participating media than transparent media [71,72,73] and there have also been claims to the contrary [114] . In chapter 3 of this work the problem of simultaneous conductive and radiative heat transfer, as is applicable to the transient hot wire apparatus, is formally presented and using certain consistent approximations was solved numerically. This problem was solved in order to determine the effect this additional mechanism of heat transfer had on the thermal conductivity of n-Heptane, n-Nonane, and n-Undecane as measured on the transient hot wire apparatus described in chapter 4.

As a result of this work it has been shown that were the effect ignored, errors of as much as 2.8% would have been incurred in the measured

thermal conductivity of these fairly weakly absorbing media ($K \approx 1000$) even at moderate temperatures ($T \approx 360K$). It has also been found that the error incurred is proportional to T_o^3, ΔT, and K which is consistent with previously held but until now not fully substantiated views [77,115] . It has also been shown, (see fig. (3.15) that increasing the duration of a measurement on a transient hot wire apparatus increases the error due to radiative heat transfer in the measurement. Furthermore, as fig. (3.15) is smooth and also almost linear in the region near zero time, this adds weight to the previously held view [53] that were it somehow possible to extrapolate the measured thermal conductivity as obtained from transient hot wire apparati back to zero time, then the absolute thermal conductivity would be recovered. This conclusion, although believed to be valid, required justification because the same assumption was unjustifiably used for the effect of convection on the measured thermal conductivity and has since been found to be invalid. In this context, it is now known that the dependence of the ratio of the true and apparent thermal conductivity, λ / λ_{capp}

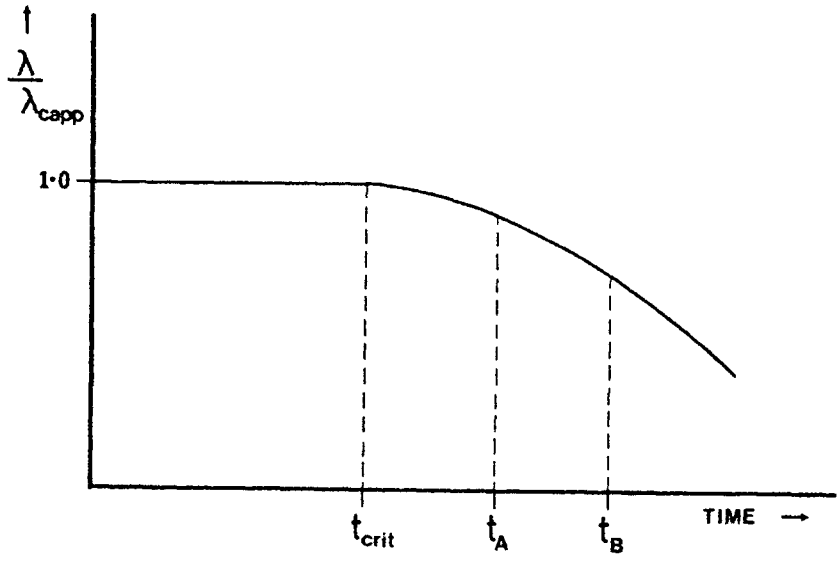

Fig. (6.1)

(λ_{capp} is the thermal conductivity measured without accounting for the effects of convection) on the duration of an experiment has the form shown in fig. (6.1)

When using experimental durations significantly longer than t_{crit} it is immediately apparent that the measured thermal conductivity will be in excess of its absolute value. If, for example, the measurement apparatus were operated between durations t_A and t_B then a linear extrapolation back to zero time would not yield the true thermal conductivity. This is not the case with the effects of radiative heat transfer (c.f. fig. (3.15)) and for the present measurements a linear extrapolation of the apparent thermal conductivity back to zero time would indeed recover the absolute thermal conductivity. In the absence of a satisfactory method for performing this extrapolation, § 3.44 describes an approximate method based on a radiation defect, ξ, for calculating the required correction to the apparent thermal conductivity. The radiation defect is calculated at the extreme ends of the thermal conductivity range over which measurements are performed and linearly interpolated within the range.

Far from the work carried out on simultaneous conductive and radiative heat transfer being an end in itself, it in fact indicates a number of areas which require further investigation. Firstly, although the precision of the thermal conductivity measurements performed in this work is estimated as $\pm$ 0.2%, the accuracy is only estimated as between $\pm$ 0.1% and $\pm$ 0.8%. The difference between the precision and accuracy is primarily due to the uncertainty in the test fluids' optical properties and specific heat capacities as used to calculate the radiation defects. This, therefore, exposes the need for an investigation into the temperature and pressure dependence of these quantities. Secondly, although a numerical solution to obtain the excess temperature rise due to radiation, δT_R,*** has been found and reported in this work, the computational effort required for sufficient accuracy is very large and necessitates a treatment different in approach and less desirable to that adopted for the other temperature corrections discussed in § 2.33. It would therefore be of great benefit if an approximate analytical treatment

***(This quantity is always negative but has been defined so as to be consistent with the other temperature corrections.)

of the problem were developed or if a reliable method of extrapolating the apparent thermal conductivity back to zero time were found. There is therefore room for improvement in this direction.

Finally, before leaving the topic of radiative heat transfer, it should be mentioned that there has been a recommendation put forward [114] that Dimethyl phthalate be used as a thermal conductivity calibration and test material because it has a high mean extinction coefficient, K, ($\approx$10,000 m^{-1}). The present work together with other work recently published [77,115] although not in complete agreement on all topics, unanimously conclude that a material which has a relatively large thermal conductivity and is as nearly transparent to infra-red radiation as is possible be used as a standard. This conclusion has been arrived at because the effect of radiative heat transfer on the measured thermal conductivity of strong radiation absorbing liquids is greater than that on weakly absorbing liquids, all other factors being the same. Thus the error incurred in measuring the thermal conductivity of a liquid possessing a high mean extinction coefficient will be greater than that incurred when performing measurements on a liquid possessing a lower mean extinction coefficient. It is therefore proposed to measure the thermal conductivity of carbon disulphide [116] which possesses a relatively small mean extinction coefficient ($\approx$650 m^{-1}) with a view to establishing this as a calibration and test material.

6.3 The Pressure and Density Dependence of the Thermal Conductivities of n-Alkanes

At present rigorous theories for the thermal conductivity of a liquid, of the type adopted by Zwanzig, Kirkwood and Oppenheim [117], are insufficiently advanced to enable reliable prediction of the absolute thermal conductivity of the liquid hydrocarbons that have been investigated in this work. We must, therefore, turn to less rigorous theories. Unfortunately, comparison with the most advanced approximate theories [85] results in poor agreement (errors of $\pm$ 50%)

between theoretically predicted and measured values for the thermal conductivities of n-Heptane, n-Octane, and n-Decane at atmospheric pressure and at temperatures between 290 and 330K.

As the development of the theory, required to enable the prediction of the absolute thermal conductivities of the liquids investigated, is beyond the scope of this work, we must look towards the approximate theories in order to at least be able to predict the pressure and density dependence of other n-Alkanes similar to those investigated. The problem of pressure and density dependence of the thermal conductivity of a liquid has been investigated by Kamal & McLaughlin [118]. Using the harmonic oscillator model, they found that the pressure and density dependence of the thermal conductivity could be expressed as:-

$$\frac{1}{\lambda}\left(\frac{\partial\lambda}{\partial P}\right)_T = \beta_T\left[1 - \left(\frac{\partial\nu}{\partial v}\right)_T\right] \qquad \text{.....(6.1)}$$

and:-

$$\frac{1}{\lambda}\left(\frac{\partial\lambda}{\partial v}\right)_T = -\frac{1}{v}\left[\frac{1}{3} - \left(\frac{\partial\nu}{\partial v}\right)_T\right] \qquad \text{.....(6.2)}$$

where in equations (6.1) and (6.2) ν is the frequency of oscillation of a molecule within its cell, v is the molar volume and β_T is the isothermal compressibility. McLaughlin [113] has shown that for a number of liquids $1/\lambda\,(\partial\lambda/\partial P)_T$ is linear in the isothermal compressibility and $-1/\lambda\,(\partial\lambda/\partial v)_T$ is linear in the reciprocal of the molar volume. It therefore seems sensible to examine these quantities for the liquids investigated in this work. Using the equations to which the data were fitted in chapter 5 viz:-

$$1 = a_o\lambda + a_1(\rho-\rho^*) + a_2(\rho-\rho^*)^2 + a_3(\rho-\rho^*)^3 \qquad \text{.....(6.3)}$$

and:-

$$1 = a_o'\lambda + a_1'(p-p^*) + a_2'(p-p^*)^2 + a_3'(p-p^*)^3 \qquad \text{.....(6.4)}$$

we find from equations (6.3) and (6.4) that:-

$$\frac{\rho}{\lambda}\left(\frac{\partial\lambda}{\partial\rho}\right)_T = -\frac{\left[a_1 + 2a_2(\rho-\rho^*) + 3a_3(\rho-\rho^*)^2\right]}{\left[1 - a_1(\rho-\rho^*) - a_2(\rho-\rho^*)^2 - a_3(\rho-\rho^*)^3\right]} \qquad \ldots\ldots\ldots\ldots(6.5)$$

and that:-

$$\frac{K_T}{\lambda}\left(\frac{\partial\lambda}{\partial P}\right)_T = \frac{-K_T\left[a_1' + a_2'(P-P^*) + a_3'(P-P^*)^2\right]}{\left[1 - a_1'(P-P^*) - a_2'(P-P^*)^2 - a_3'(P-P^*)^3\right]} \qquad \ldots\ldots\ldots\ldots(6.6)$$

where in equation (6.6) K_T is the bulk modulus and is defined as:-

$$K_T = \frac{1}{\beta_T} = \rho\left(\frac{\partial P}{\partial\rho}\right)_T \qquad \ldots\ldots\ldots\ldots\ldots\ldots\ldots\ldots\ldots\ldots(6.7)$$

It is further evident that the right hand side of both equations (6.5) and (6.6) should be identical to each other since by definition:-

$$\frac{\rho}{\lambda}\left(\frac{\partial\lambda}{\partial\rho}\right)_T = \frac{K_T}{\lambda}\left(\frac{\partial\lambda}{\partial P}\right)_T \qquad \ldots\ldots\ldots\ldots\ldots\ldots\ldots\ldots\ldots\ldots(6.8)$$

Figures (6.2) and (6.3) show plots of $\frac{\rho}{\lambda}\left(\frac{\partial\lambda}{\partial\rho}\right)_T$ versus ρ and $\frac{K_T}{\lambda}\left(\frac{\partial\lambda}{\partial P}\right)_T$ versus P for the liquids investigated.

With regard to the curves obtained in fig. (6.2) it must be pointed out that too much emphasis should not be placed on the shape of individual curves. It would be wrong because to a large extent the shape of a curve depends upon the magnitude and sign of the specific coefficient, a_3, used in equation (6.3). From the results of the regression analyses described in § 5.1 it has been found that for all the liquids and at all the temperatures investigated the value of the standard deviation in the coefficient, a_3, as obtained for a specific liquid at a single temperature, is comparable with the absolute value of the coefficient. What is significant, however, is

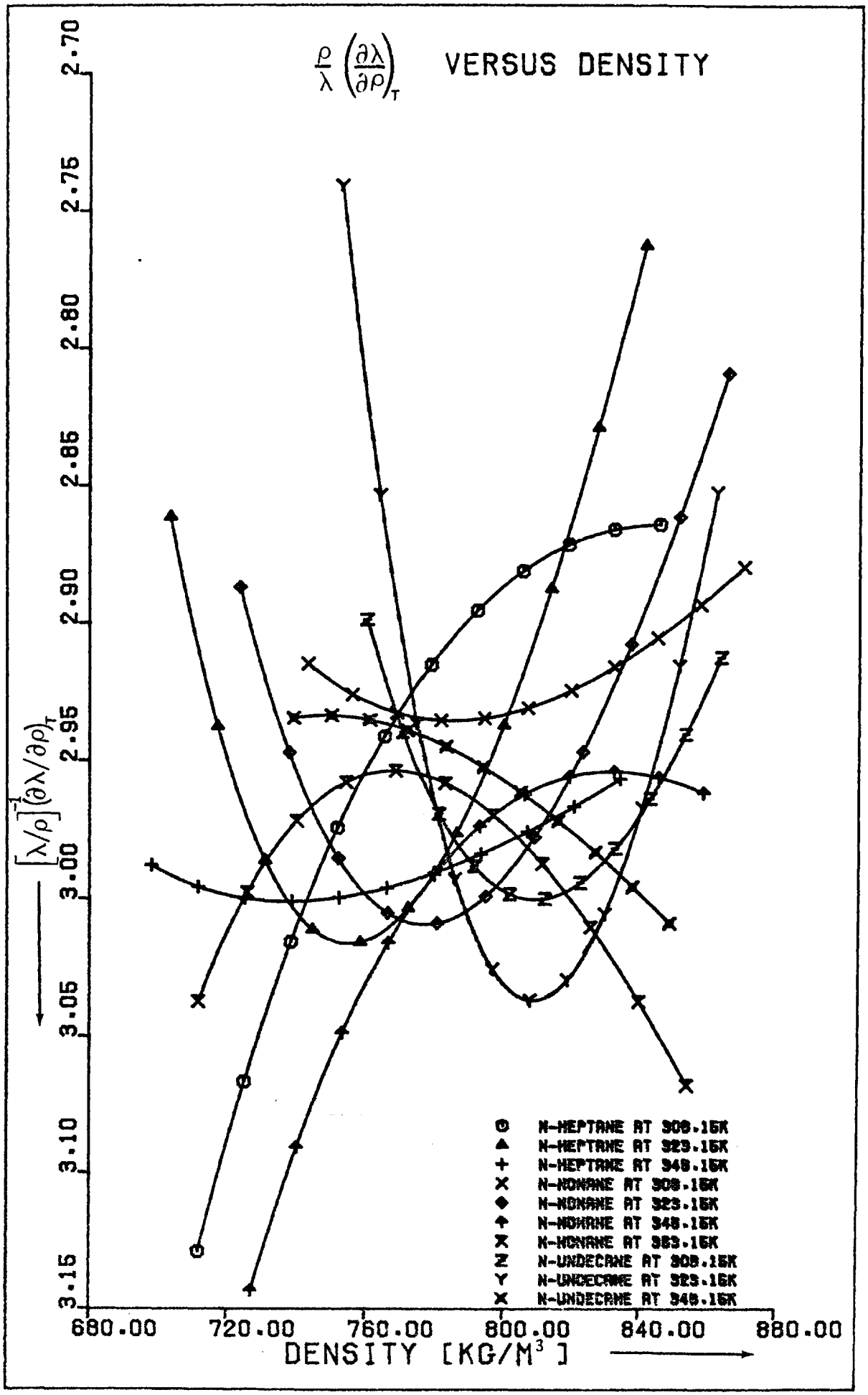
$\frac{\rho}{\lambda}\left(\frac{\partial\lambda}{\partial\rho}\right)_T$ VERSUS DENSITY
$[\lambda/\rho]^{-1}(\partial\lambda/\partial\rho)_T$
2.70
2.75
2.80
2.85
2.90
2.95
3.00
3.05
3.10
3.15
680.00
720.00
760.00
800.00
840.00
880.00
DENSITY [KG/M^3]
N-HEPTANE AT 308.15K
N-HEPTANE AT 323.15K
N-HEPTANE AT 348.15K
N-NONANE AT 308.15K
N-NONANE AT 323.15K
N-NONANE AT 348.15K
N-NONANE AT 383.15K
N-UNDECANE AT 308.15K
N-UNDECANE AT 323.15K
N-UNDECANE AT 348.15K

Fig. (6.2)

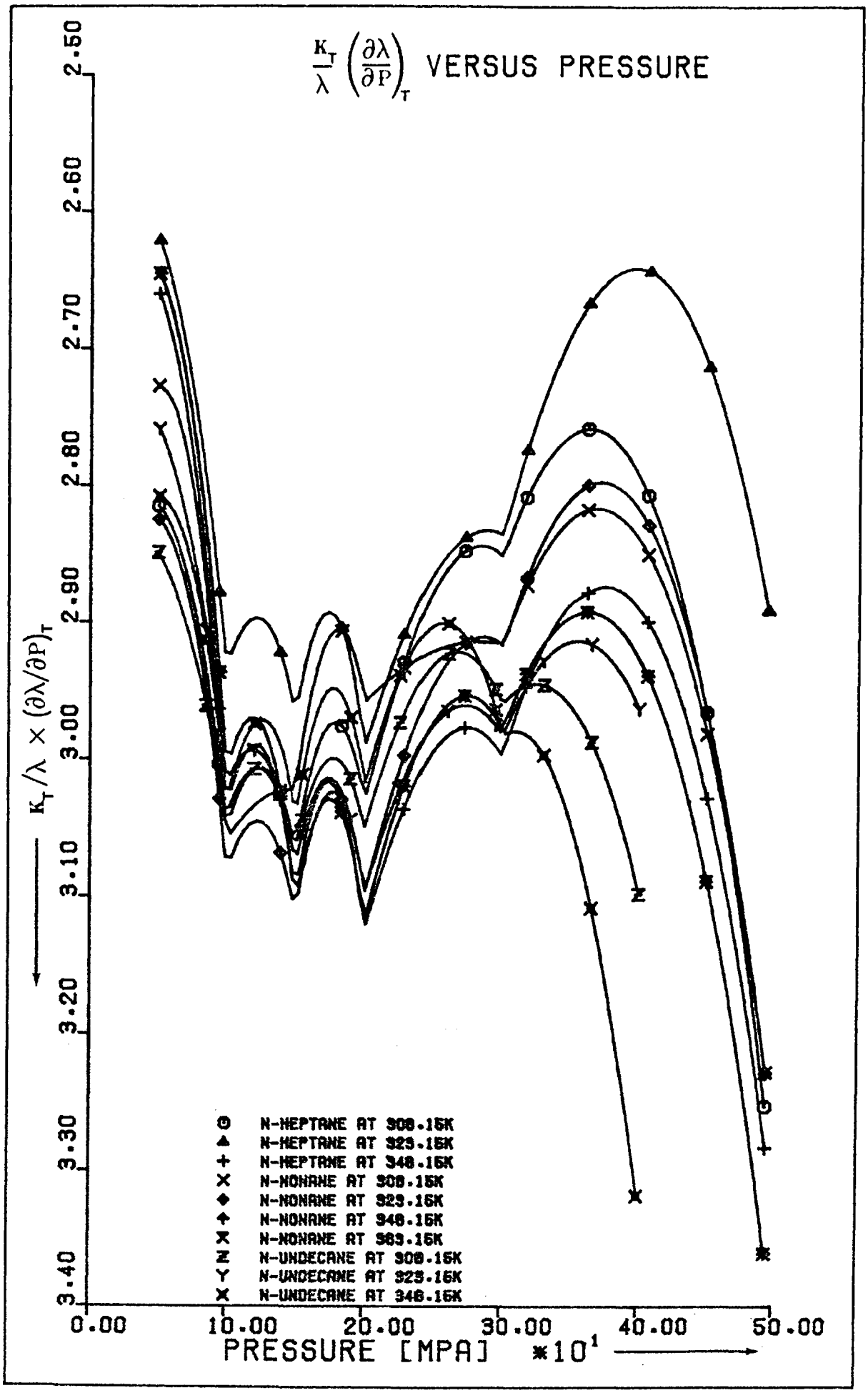
$\frac{K_T}{\lambda}\left(\frac{\partial\lambda}{\partial P}\right)_T$ VERSUS PRESSURE
$K_T/\lambda \times (\partial\lambda/\partial P)_T$
2.50
2.60
2.70
2.80
2.90
3.00
3.10
3.20
3.30
3.40
0.00
10.00
20.00
30.00
40.00
50.00
PRESSURE [MPA] *10^1
N-HEPTANE AT 308.15K
N-HEPTANE AT 323.15K
N-HEPTANE AT 348.15K
N-NONANE AT 308.15K
N-NONANE AT 323.15K
N-NONANE AT 348.15K
N-NONANE AT 383.15K
N-UNDECANE AT 308.15K
N-UNDECANE AT 323.15K
N-UNDECANE AT 348.15K

Fig. (6.7)

that the value of $\frac{\rho}{\lambda}\left(\frac{\partial\lambda}{\partial\rho}\right)_T$ has a mean of approximately 2.96 and the maximum deviation from this value is approximately 7% for all the fluids investigated over a fairly large temperature and density range.

The results plotted in fig. (6.3) are believed to be subject to larger errors than those plotted in fig. (6.2) so explaining the $\pm$ 14% deviation in $K_T/\lambda\ (\partial\lambda/\partial P)_T$ about 2.96. There are two reasons for this, firstly, equation (6.4) describing the pressure dependence of the thermal conductivity, is not able to represent the thermal conductivity versus pressure data given in chapter 3 as well as equation (6.3) is able to represent the thermal conductivity versus density data (c.f. figs. (5.24) and (5.46)). Secondly, the value of the bulk modulus, K_T, is obtained by differentiating the density versus pressure data given in appendix 3 thus incurring further error.

From figures (6.2) and (6.3) we see that the value of $\frac{\rho}{\lambda}\left(\frac{\partial\lambda}{\partial\rho}\right)_T$ is almost constant and independent of temperature. We may therefore write:-

$$\frac{\rho}{\lambda}\left(\frac{\partial\lambda}{\partial\rho}\right) \approx 2.96 \qquad \text{.....(6.9)}$$

and on integrating we find that:-

$$\text{Ln}\,\lambda = 2.97\ \text{Ln}\,\rho + C \qquad \text{.....(6.10)}$$

where the value of C in equation (6.10) is dependent upon both the temperature and the n-Alkane under consideration. If equation (6.10) were obeyed exactly for the n-Alkanes, a plot of $\text{Ln}\,\lambda$ versus $\text{Ln}\,\rho$ for each of the test liquids at each temperature at which observations were performed, would result in a set of parallel straight lines of slope 2.96. It would also be possible to superimpose all the lines by shifting them in the $\text{Ln}\,\lambda$ and $\text{Ln}\,\rho$ axes without changing their slope.

In order to examine the applicability of equation (6.10) with a view to perhaps using this equation to extrapolate thermal conductivity versus density data, the value of C in equation (6.10) has been defined as being equal to zero for n-Heptane at 308.15K. We are therefore using the experimentally obtained $Ln\lambda$ versus $Ln\rho$ line for n-Heptane at 308.15K as a reference. This line was chosen as the reference because in the present work more experiments were performed on n-Heptane at 308.15K than on any other of the test liquids at any other temperature. Also the accuracy of the experiments performed along this isotherm is thought to be greater than along the other isotherms because the correction due to radiation is smallest for these measurements (see fig. (3.16))thus incurring the smallest error from this source.

The lines $Ln\lambda$ versus $Ln\rho$ for the other n-Alkanes and temperatures were reduced to that of n-Heptane at 308.15K using a computer program. The program sought to minimise the squares of the deviations of the measurements forming each of these lines, $Ln\lambda$ versus $Ln\rho$, from the corresponding line for n-Heptane at 308.15K by merely applying shifts in the $Ln\lambda$ and $Ln\rho$ directions without altering the shape of the individual lines. The result of this is that we obtain a line of a reduced thermal conductivity, λ/λ', versus a reduced density, ρ/ρ', for each n-Alkane at each temperature. It should be noted that if the reference line and the line requiring reduction are parallel or indeed almost parallel the values of ρ' and λ' thus obtained will in general not be unique.

The values of λ' and ρ' thus obtained from the above analysis are given in Table 6.4 and the plot of $Ln(\lambda/\lambda')$ versus $Ln(\rho/\rho')$ for the n-Alkanes studied at each temperature is given in fig. (6.5). It can be seen that the lines plotted in fig. (6.5) do indeed superimpose one another and the single line $Ln(\lambda/\lambda')$ versus $Ln(\rho/\rho')$ thus obtained appears to be linear. Fig. (6.6) is a deviation plot for the reduced thermal conductivities, as obtained from each of the measurements, and for convenience they have been plotted against the reduced thermal conductivity which is merely the thermal

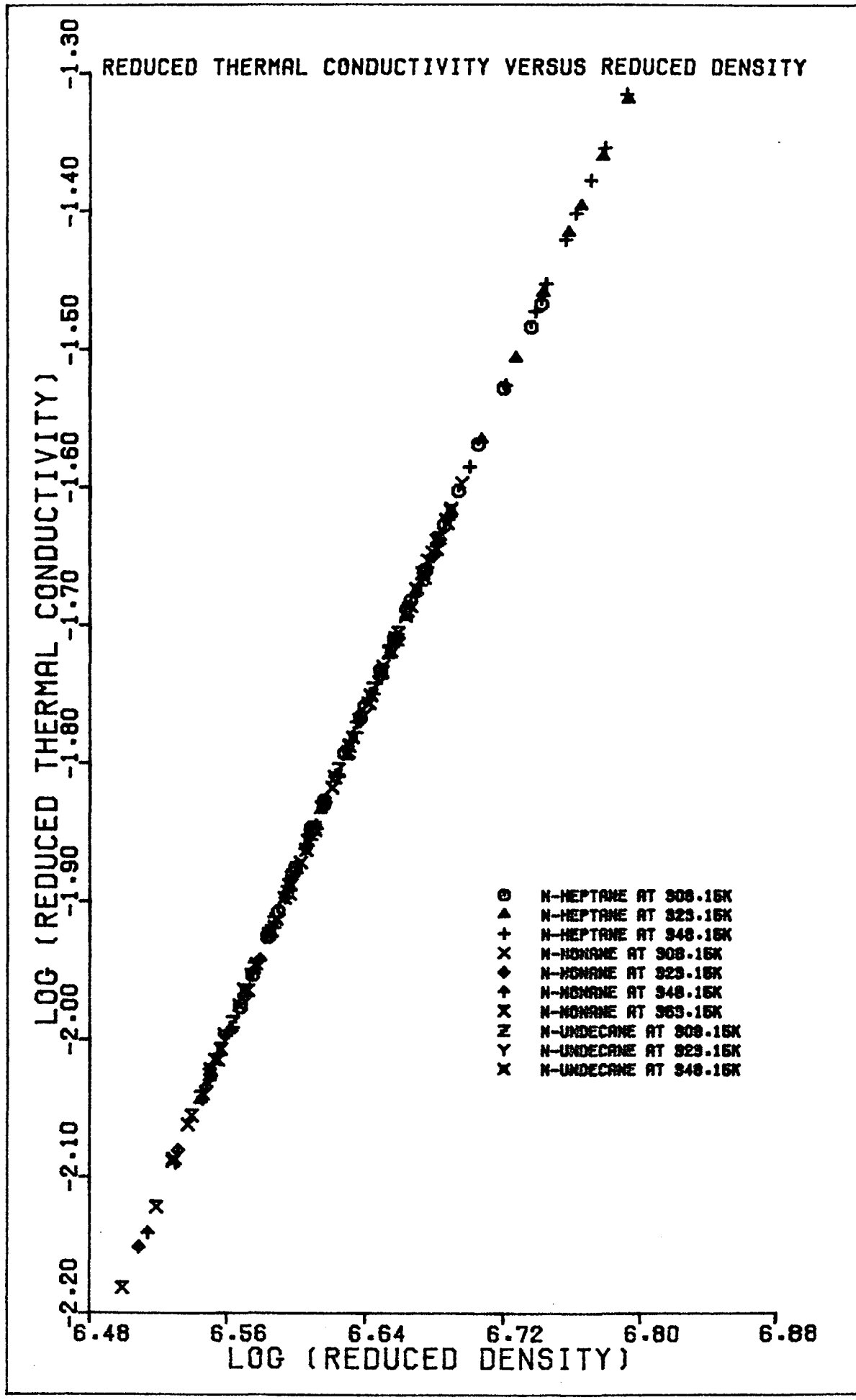
REDUCED THERMAL CONDUCTIVITY VERSUS REDUCED DENSITY
LOG (REDUCED THERMAL CONDUCTIVITY)
-1.30
-1.40
-1.50
-1.60
-1.70
-1.80
-1.90
-2.00
-2.10
-2.20
6.48
6.56
6.64
6.72
6.80
6.88
LOG (REDUCED DENSITY)
N-HEPTANE AT 308.15K
N-HEPTANE AT 323.15K
N-HEPTANE AT 348.15K
N-NONANE AT 308.15K
N-NONANE AT 323.15K
N-NONANE AT 348.15K
N-NONANE AT 363.15K
N-UNDECANE AT 308.15K
N-UNDECANE AT 323.15K
N-UNDECANE AT 348.15K

Fig. (6.5)

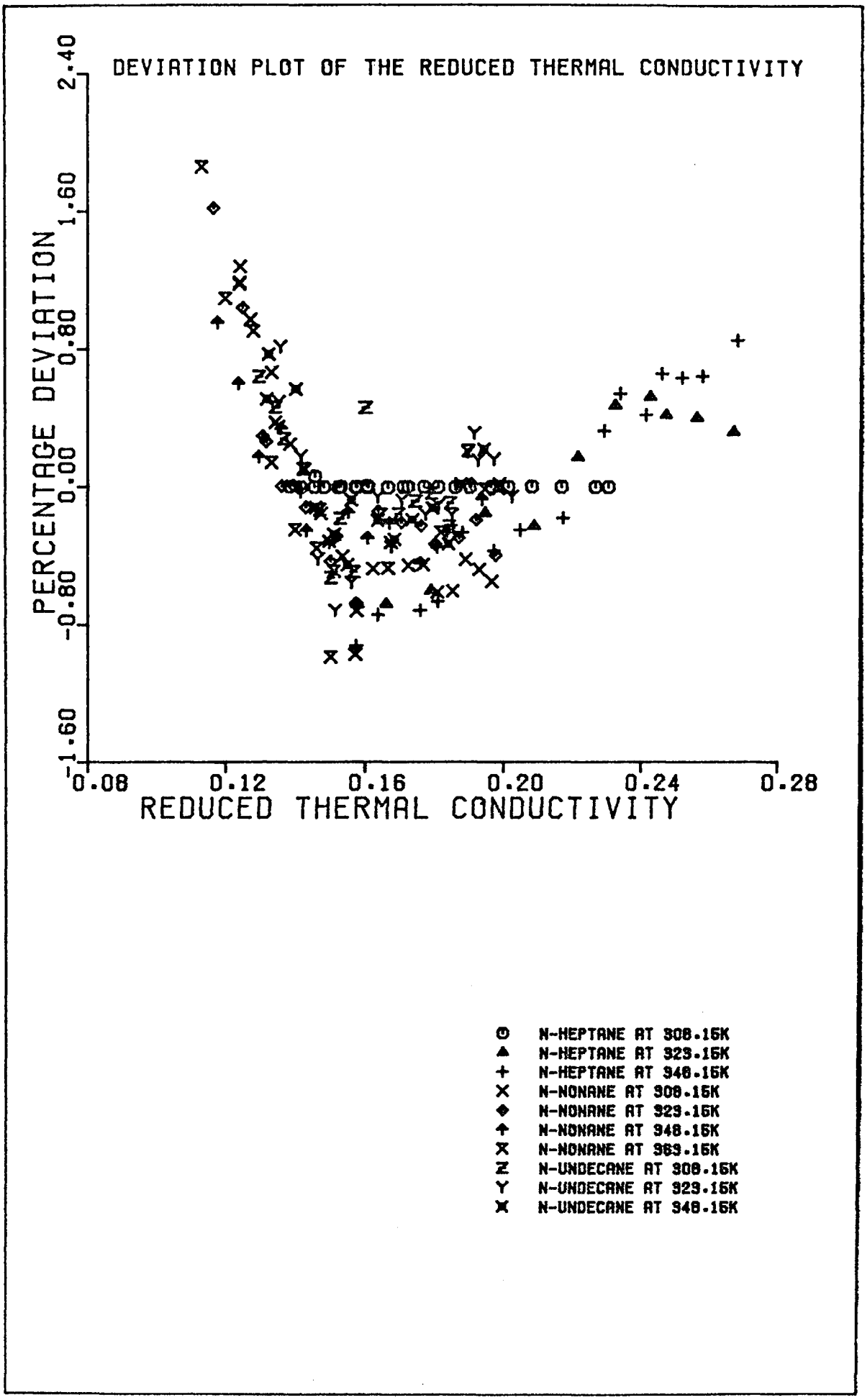
DEVIATION PLOT OF THE REDUCED THERMAL CONDUCTIVITY
PERCENTAGE DEVIATION
2.40
1.60
0.80
0.00
-0.80
-1.60
0.08
0.12
0.16
0.20
0.24
0.28
REDUCED THERMAL CONDUCTIVITY
N-HEPTANE AT 308.15K
N-HEPTANE AT 323.15K
N-HEPTANE AT 348.15K
N-NONANE AT 308.15K
N-NONANE AT 323.15K
N-NONANE AT 348.15K
N-NONANE AT 363.15K
N-UNDECANE AT 308.15K
N-UNDECANE AT 323.15K
N-UNDECANE AT 348.15K

Fig. (6.6)

conductivity of n-Heptane at 308.15K. It can be seen from Fig. (6.6) that within the thermal conductivity range in which measurements on n-Heptane were performed the deviations are largely within the expected accuracy of the individual measurements and that the deviations

n-Alkane	Temperature [K]	λ' [w/m/K]	ρ' [kg/m^3]
n-Heptane	308.15	1.0000	1.0000
n-Heptane	323.15	0.8610	0.9459
n-Heptane	348.15	0.8545	0.9383
n-Nonane	308.15	1.1589	1.0861
n-Nonane	323.15	1.1509	1.0787
n-Nonane	348.15	1.1727	1.0783
n-Nonane	363.15	1.1593	1.0711
n-Undecane	308.15	1.1175	1.0933
n-Undecane	323.15	1.0551	1.0675
n-Undecane	348.15	1.0413	1.0572

Table (6.4)

are significantly larger outside this range. The reason for this is that in the absence of any other information, equation (6.3) has been used to extrapolate for the thermal conductivity of n-Heptane outside the range in which measurements were performed and, as expected, equation (6.3) seems to be unsuited to this application.

Because of the shape of the plot shown in fig. (6.5) the experimental data , $Ln(\lambda/\lambda')$ versus $Ln(\rho/\rho')$, were fitted to a straight line:-

$$Ln(\lambda/\lambda') = A\, Ln(\rho/\rho') + B \qquad \text{.....(6.11)}$$

and the results of such a fit, including the values of the coefficients A and B, are presented in Table (6.7) below.

Coefficient	Value	Standard Deviation of Coefficient	T-Ratio
A	2.95986	0.00289	1025
B	-21.4137	0.0191	-1118
The standard deviation of $Ln(\lambda/\lambda')$ about the regression line = 0.00233			

Table (6.7) Results of the Regression Analysis

In addition to the results presented in Table (6.7) it is significant that the maximum deviation in any of the data about the regression line was $\pm$ 0.68% in the reduced thermal conductivity. In view of this information and because the accuracy of the data is estimated as being between $\pm$ 0.5% and $\pm$ 0.8% it would be difficult to justify the inclusion of higher order terms in equation (6.11).

It now appears as if we have in our possession a powerful tool for extrapolating odd numbered n-Alkane thermal conductivity data. In order to test the method we have made use of the results obtained for the thermal conductivity of n-Heptane at 308.15K and at atmospheric pressure as were measured during preliminary work on the apparatus described earlier. For the reasons given in § 5.4 these results were not used in the present work and therefore could not have influenced the values obtained for the coefficients A and B in equation (6.11).

During the preliminary work just referred to, the thermal conductivity of n-Heptane at atmospheric pressure and 308.15K was found to be 0.1164 W/m/K $\pm$ 9×10^{-4} W/m/K. Using equation (6.3), with the relevant values of a_i and ρ^* for n-Heptane at 308.15K, we find that the value obtained for the thermal conductivity of n-Heptane at atmospheric pressure (ρ = 671.26 kg/m^3) is 0.1147 W/m/K. This value is 1.5% from the measured value and furthermore as expected was outside the error bounds estimated for the measurement. On the other hand, using equation (6.11) to predict the value of the thermal conductivity of n-Heptane at 308.15K and at atmospheric pressure we obtain the predicted value as being 0.1168 W/m/K. This value is remarkably close to the measured value, well within the accuracy of the measurement and adds weight to the belief that equation (6.11) is suitable for extrapolating thermal conductivity data.

Why the odd numbered n-Alkanes investigated obey the relationship given by equation (6.11) so closely is as yet unknown as is the reason for the coefficient A being independent of both the chain

length of these n-Alkanes and the temperature. It would be wrong to expect the thermal conductivity of even numbered n-Alkanes to behave in an identical manner to that of the odd numbered members of the series but it is thought that a relationship similar to equation (6.11) may be found upon their examination.

At present it seems that it is possible to predict to within a few percent the thermal conductivity of any liquid, odd numbered member of the n-Alkane family merely by having available one reference value for its liquid thermal conductivity at the same temperature at which the prediction is required. Furthermore it has been shown [85] that the thermal conductivity of a liquid n-Alkane under its saturation vapour pressure obeys the relationship:-

$$\lambda(T) = \lambda(273.15) - D[T-273.15] \qquad \text{.....(6.12)}$$

where D in equation (6.12) is constant over a substantial temperature range. It therefore follows that if the reference thermal conductivity is known under saturation vapour pressure conditions, which is in practice the most likely pressure condition at which a value is known, then the above condition of the temperatures being the same is not necessary, provided the value of D is known.

In conclusion, two additional facts emerge as a result of the data presented in chapter 5. Firstly, within the thermodynamic range investigated, the isothermal pressure derivative of the thermal conductivity, $\left(\frac{\partial\lambda}{\partial P}\right)_T$, is negative for the n-Alkanes investigated. Secondly, and what has received far less publicity, is that it can also be seen that the isothermal density derivative of the thermal conductivity, $\left(\frac{\partial\lambda}{\partial\rho}\right)_T$, is positive.

APPENDICES

APPENDIX 1

A11 Derivation of $dQ_{dV_i \rightarrow dV_k}$

Consider the heat transferred from volume element dV_i to a parallelepiped dV_k with area dA_k normal to the direction of r. (see fig. (A1)

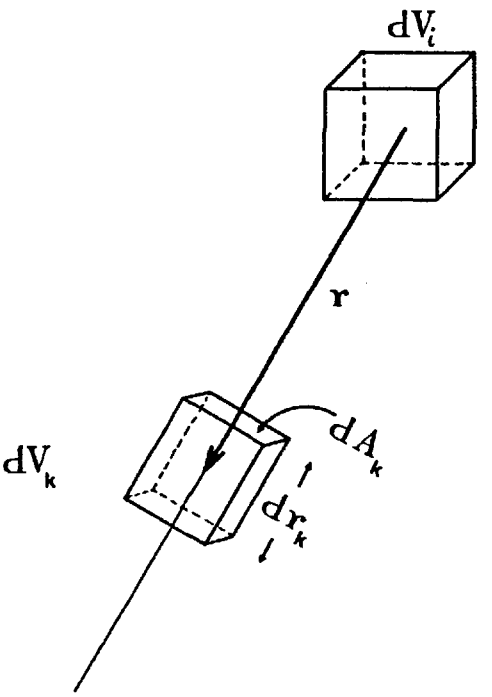

Fig. (A1) Heat transfer between fluid volume elements

We therefore find $dQ_{dV_i \rightarrow dV_k}$ as:-

$$dQ_{dV_i \rightarrow dV_k} dV_i = \underbrace{4K_i E_i \, dV_i}_{\text{emission by dV in 4 steradians}} \times \underbrace{\frac{dA_k}{4\pi r^2} \tau(r)}_{\text{fraction crossing } dA_k} \times \underbrace{K_k dr_k}_{\text{fraction absorbed}} \quad \ldots\ldots(A1)$$

Therefore:-

$$dQ_{dV_i \rightarrow dV_k} = \frac{K_i K_k E_i \, \tau(r) dV_k}{\pi r^2} \quad \ldots\ldots\ldots\ldots\ldots\ldots(A2)$$

Since any arbitrary volume dV_j can be made up of a number of parallepipes dV_k, the equation is general for any volume element dV_j and therefore:-

$$dQ_{dV_i \rightarrow dV_j} = K_i K_j E_i \tau(r) dV_j / \pi r^2 \qquad \text{.....(A3)}$$

A12 Integration coordinates transformation (Spherical to Cylindrical)

Consider two points $P_i(r_i, \psi_i, z_i)$ and $P_j(r_j, \psi_j, z_j)$ situated within the annulus formed by two infinite cylinders of radius r_1 and r_2 (see fig. (A2)). Defining a spherical polar coordinate system about point P_i as shown in the figure, it is now possible to describe point P_j in terms of this coordinate system, i.e.:-

$$P_j = P_j(r, \vartheta, \varphi) \qquad \text{.....(A4)}$$

where in terms of the cylindrical polar coordinate system we find that:-

$$r = \sqrt{r_j^2 + r_i^2 - 2r_i r_j \cos(\psi_j - \psi_i) + (z_j - z_i)^2} \qquad \text{...(A5)}$$

also that:-

$$\cos\vartheta = \frac{r_j \cos(\psi_j - \psi_i) - r_i}{r} \qquad \text{.....(A6)}$$

and:-

$$\sin\varphi = \frac{z_j - z_i}{\sqrt{r_j^2 \sin^2(\psi_j - \psi_i) + (z_j - z_i)^2}} \qquad \text{.....(A7)}$$

Applying a shift in the cylindrical, vertical and azimuthal coordinates such that:-

$$Z = z_j - z_i \qquad \text{.....(A8)}$$

and:-

$$\Phi = \psi_j - \psi_i \qquad \text{.....(A9)}$$

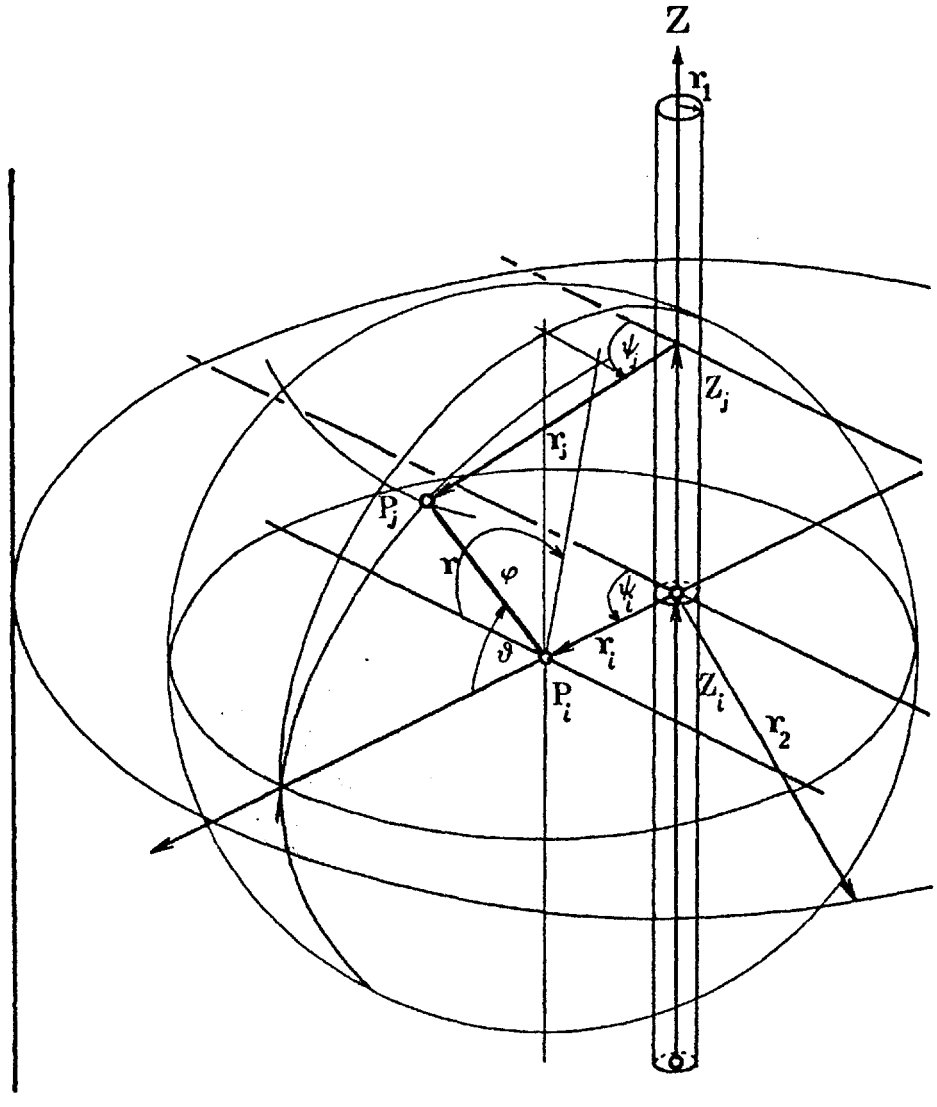

Fig. (A2) Definition of the spherical polar coordinate system about P_i.

we obtain from (A5), (A6) and (A7)

$$r = \sqrt{r_j^2 + r_i^2 - r_j r_i \cos\Phi + Z^2} \qquad \text{.....(A10)}$$

$$\cos\vartheta = \frac{r_j \cos\Phi - r_j}{r} \qquad \text{.....(A11)}$$

and:-

$$\sin\varphi = \frac{Z}{\sqrt{r_j^2 \sin^2\Phi + Z^2}} \qquad \text{.....(A12)}$$

Suppose now we wish to evaluate an integral, I, where:-

$$I = \int_V f(r,\vartheta,\varphi)\,dV \qquad \text{.....(A13)}$$

which in spherical polar coordinates is:-

$$I = \iiint_V f(r,\vartheta,\varphi)\sin\vartheta\, d\vartheta\, d\varphi\, dr \qquad \text{.....(A14)}$$

and if desired this may now be integrated in the cylindrical polar coordinate system as:-

$$I = \iiint_V f(r_j,\Phi,Z)\sin\vartheta\, \frac{\partial(r,\vartheta,\varphi)}{\partial(r_j,\Phi,Z)}\, dr_j\, d\Phi\, dZ \qquad \text{.....(A15)}$$

The jacobian in equation (A15) is evaluated using equations(A5) to (A7) and we find that:-

$$\frac{\partial(r,\vartheta,\varphi)}{\partial(r_j,\Phi,Z)} = \begin{vmatrix} \frac{\partial r}{\partial r_j} & \frac{\partial r}{\partial\Phi} & \frac{\partial r}{\partial Z} \\ \frac{\partial\vartheta}{\partial r_j} & \frac{\partial\vartheta}{\partial\Phi} & \frac{\partial\vartheta}{\partial Z} \\ \frac{\partial\varphi}{\partial r_j} & \frac{\partial\varphi}{\partial\Phi} & \frac{\partial\varphi}{\partial Z} \end{vmatrix} \qquad \text{.....(A16)}$$

$$= \begin{vmatrix} \cos\vartheta_j & \frac{r_i r_j \sin\Phi}{r} & \frac{Z}{r} \\ \frac{-(\cos\Phi \operatorname{cosec}\vartheta - \cot\vartheta\cos\vartheta_j)}{r} & \frac{r_j \sin\Phi (r\operatorname{cosec}\vartheta + r_i \cot\vartheta)}{r^2} & \frac{Z\cot\vartheta}{r^2} \\ -\frac{Z\sin\Phi}{(r_j^2\sin^2\Phi + Z^2)} & -\frac{Z r_j \cos\Phi}{r_j^2\sin^2\Phi + Z^2} & \frac{r_j \sin\Phi}{r_j^2\sin\Phi + Z^2} \end{vmatrix}$$

.....(A17)

$$= \frac{r_j}{\sqrt{(r_j^2 + r_i^2 - 2r_i r_j\cos\Phi + Z^2)(r_j^2\sin\Phi + Z^2)}} \quad \text{.....(A18)}$$

and therefore:-

$$I = \iiint \frac{f(r_j, \Phi, Z)\, r_j dr_j d\Phi dZ}{(r_j^2 + r_i^2 - 2r_j r_i \cos\Phi + Z^2)} \quad \text{.....(A19)}$$

N.B. Cos ϑ_j in equation (A17) is defined as:-

$$\cos\vartheta_j = \frac{r_j - r_i\cos\Phi}{r}$$

APPENDIX 2

A21 Gauge Calibration

The gauges used for measuring the pressure within the autoclave were calibrated against a dead weight tester. The dead weight tester which is described elsewhere [93] is accurate to better than 1 MPa at 700 MPa and has been calibrated by the National Engineering Laboratory.

The effective area of the piston A_p is given by:-

$$A_{pT} = A_p(a + b\Delta T) \qquad \text{.....(A20)}$$

where:-

$$A_p = A_o(a + aP) \qquad \text{.....(A21)}$$

$$\Delta T = T - 293.15 \qquad \text{.....(A22)}$$

and:-

$$A_o = 3.227477 \times 10^{-6}\ m^2 \pm 1.29 \times 10^{-10}\ m^2 \qquad \text{.....(A23)}$$

$$a = 2.973 \times 10^{-6}\ MPa^{-1} \pm 1.45 \times 10^{-7}\ MPa^{-1} \qquad \text{.....(A24)}$$

$$b \approx 23 \times 10^{-6}\ K^{-1} \qquad \text{.....(A25)}$$

The Pressure, P is then found as:-

$$P = \frac{Mg}{A_{pT}} \qquad \text{.....(A26)}$$

where M is the mass of the piston, carrier and weights.

Temperature [^{o}C]	Gauge No. 2 [Bars]	Gauge No. 5 [PSig]	Gauge No.10 [ATM]	M [kg]	Absolute Pressure [MPa]
19.5	666	800	1020	22.31585	67.9
19.5	955	1030	14450	31.97360	97.3
19.4	1244	1390	18750	41.61470	126.6
19.4	1534	1680	22900	51.28095	156.0
19.5	1827	1980	27300	61.00005	185.5
19.6	2117	2240	31650	70.61095	214.7
19.5	2407	2490		80.23315	243.9
19.7	2700	2800		89.89325	273.2
19.6	2992	3080		99.54040	302.5
18.8	3286	3330		109.16680	331.7
19.8	3578	3620		118.78980	360.9
19.7	3874	3900		128.45180	390.2
19.7	4168	4160		138.06325	419.4
19.7	4466	4420		147.70490	448.6
19.7	4762	4720		157.35160	477.9
19.8	5064	5000		167.08395	507.5
18.8	5351	5320		176.70065	536.6
20.1	5627	5550		186.36505	565.8
20.2		5800		194.17085	589.5
19.9		6100		203.79785	618.7
19.9		6300		210.46480	638.9
19.9		6460		217.13165	659.1
20.0		6600		223.79845	679.2
19.3		6780		230.46545	699.4

Fig. (A3) Gauge Calibration

The calibration of the gauges used in the pressure system are given in fig. (A3) and the pressure inside the autoclave is determined from the gauge readings by interpolating the calibration data.

A22 Pressurisation Procedure (see fig. 4.3)

The procedure for pressurising the autoclave follows. It is assumed that the system is initially at atmospheric pressure with all the valves open and that all the air has been bled from the tubing.

1. Close valves (3) and (13).
2. Pump up the system to 10 MPa using pump (12). This ensures the piston in the intensifier is fully pumped back.
3. Close valve (7) .
4. Continue pumping using (12) until the system reaches 200 MPa.
5. Isolate the low pressure side by closing valve (9) .
6. Continue the pressurisation by pumping (8) on the low pressure side of the intensifier (6) until the piston reaches the end of its stroke.
7. Isolate the autoclave by closing valve (4) .
8. Open valve (7) slowly reducing the pressure on the low pressure side of the intensifier. This drops the pressure between valves (4) and (9) to below 10 MPa.
9. Open valve (9) and pump back the intensifier piston using (12).
10. Continue the procedure from step 2. until the desired pressure is achieved. The pressure in the autoclave can usually be raised to 700 MPa during the second stroke of the intensifier.
11. During experiments valve (4) is shut to isolate the autoclave from the rest of the system.

A23 Calibration of the Platinum Resistance Thermometer

The thermometer used to measure the absolute equilibrium temperature, T_o, of the test fluid and oil bath, prior to measurement, consists of a class 1 platinum wire element whose resistance is measured to $\pm$ 0.0005 Ohms by a Smith Difference Bridge (Cambridge Instruments Co.). The element, model no. 8130 0031 has a 100 Ohms nominal resistance and its resistance, temperature characteristics are guaranteed by the

manufacturer to conform to the equation:-

$$W(T-273.15) = W(273.15)(1+A_1(T-273.15)+B_1(T-273.15)^2) \quad \ldots\ldots(A27)$$

where:-

$$A_1 = 3.90784 \times 10^{-3}\ K^{-1} \quad \ldots\ldots\ldots\ldots\ldots\ldots(A28)$$

$$B_1 = -5.78408 \times 10^{-7}\ K^{-7} \quad \ldots\ldots\ldots\ldots\ldots\ldots(A29)$$

sufficiently to enable temperature measurement (within the temperature range of interest) to within $\pm$ 0.001K.

In order to use the thermometer to measure temperature, the resistance of the element at 273.15K, W(273.15), is required. In order to perform the calibration, the resistance of the element, used in the four terminal mode, was measured at 273.160K. The calibration was performed using a water triple point cell which was itself calibrated by the National Physical Laboratory, England [94] and found to be accurate to within $\pm$ 0.0003K. The resistance of the element at 273.16K, was found to be 99.9737 Ohms results in the value of W(273.15) being 99.9698 Ohms.

The equilibrium temperature, T_o, can, with the above information be determined by measuring the resistance of the platinum wire element, immersed in the oil bath. The measured temperature, T_o, thus obtained is estimated to be accurate to $\pm$ 0.01K.

A24 The Temperature Coefficient of Resistance of the Platinum Wire.

A241 Applicability of the calculated Temperature Coefficient of Resistance.

In order to be able to use the values A and B, as given by equations (4.2) and (4.3), to calculate the pseudo linear temperature coefficient of resistance of the 7 μm platinum wire at atmospheric pressure and under no tensile stress, $\alpha'(T_o,0,0)$,(as defined by equation (4.12)) we must ascertain whether the coefficient thus predicted for pure

platinum is sufficiently close to the true coefficient of resistance of the 7 μm wire. This was achieved by measuring the resistances of two samples of the 7 μm platinum wire at several temperatures under atmospheric pressure conditions and under no axial tension. The ratio of the resistance of a wire at each temperature divided by its resistance at the lowest temperature is calculated for the two samples at each of the temperatures. These ratios are compared with the corresponding ratios obtained from measurement of the resistances of an NPL calibrated platinum resistance thermometer under the same conditions.

The resistances of the wires were measured using a 30 Hz a.c. bridge (Automatic Systems Laboratories) which is accurate to $\pm$ 2 x 10^{-4} Ohms and the resistance of the resistance thermometer was measured using a Smith Bridge no. 3, type 41623 (H. Tinsely & Co.). The results of the investigation are given in table (A4) and reveal that the resistance ratios for the two wire samples and the platinum resistance thermometer differ by less than 0.01%, so justifying the use of the values of A and B for pure platinum in the calculation of $\alpha'(T_o,0,0)$.

	Resistances			Resistance Ratios		
Temperature [K]	Pt Resistance Thermometer [Ohm]	Long Wire [Ohm]	Short Wire [Ohm]	Pt Resistance Thermometer	Long Wire	Short Wire
308.45	29.3472	352.9677	190.0153	1.0000	1.0000	1.0000
318.60	30.3651	468.6722	196.3722	1.0347	1.0347	1.0345
323.69	30.8880	476.8148	200.0012	1.0525	1.0526	1.0525

Table A4 The Platinum Wire Calibration

A242 The Effect of Hydrostatic Pressure

Because the measurement cell is to be used under conditions of elevated pressure, it is necessary to account for the pressure dependence on the temperature coefficient of resistance. Unfortunately, information on the direct pressure dependence of the temperature coefficient of resistance is unavailable so we must make use of the available information to estimate the effect. This has been achieved by making use of the available hydrostatic pressure dependence of the electrical resistance of platinum over the temperature range within which measurements were performed [93] .

Fig. (A5) shows the pressure dependence of the electrical resistance of a segment of platinum wire at temperatures, T_1 and T_2 (T_2 T_1). Pressure, P_o, corresponds to atmospheric pressure and pressure, P_1, to some elevated pressure. Knowing the resistance, Ω_1, of the segment of wire at position ① on the diagram, we are able to calculate, Ω_2, using $\alpha'(T_1,0,0)$ as defined by equation (4.12). Using the available information on the pressure dependence of the electrical resistance of platinum [93] we can also calculate Ω_3 and Ω_4 at the elevated pressure and thus $\alpha'(T_1,0,P)$.

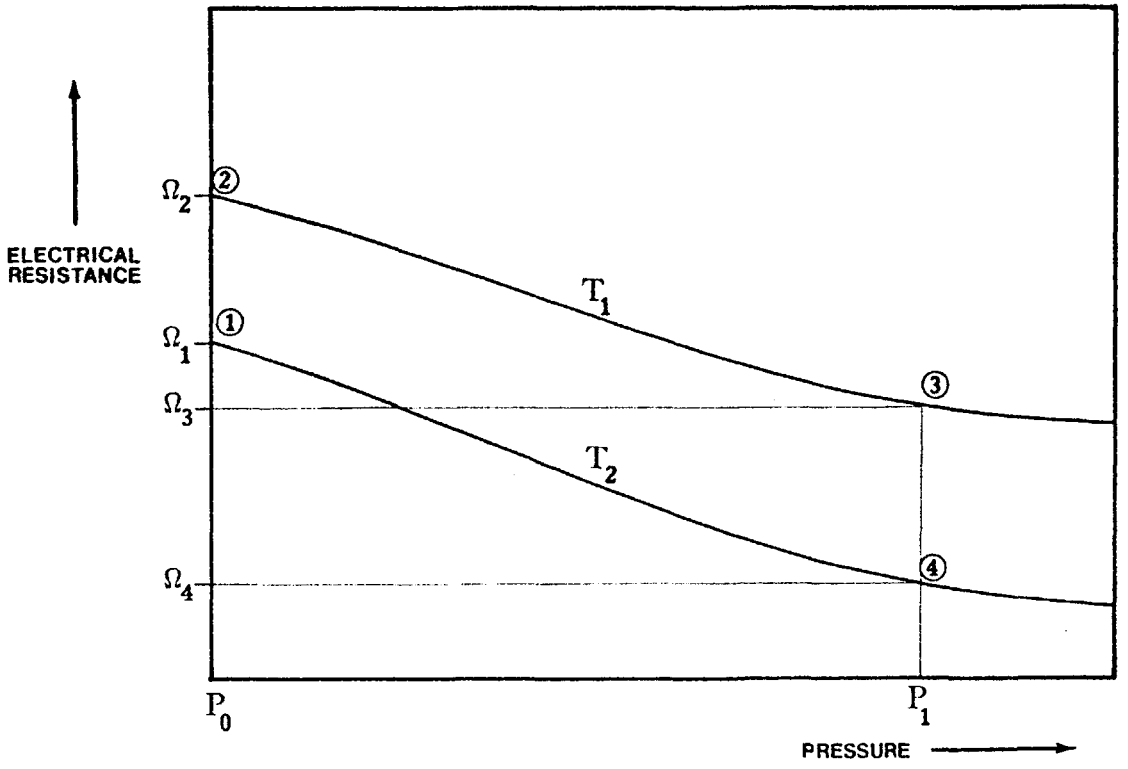

Fig. (A5) Pressure dependence of the resistance of the platinum wire.

Using the above procedure, it has been found that within the temperature range in which measurements were performed, the pressure dependence of the temperature coefficient of resistance can adequately ($\pm$ 0.02%) can be represented as:-

$$\alpha'(T,0,P) = \alpha'(T,0,0)(1 + \epsilon_p P) \qquad \text{.....(A30)}$$

where:-

$$\epsilon_p = 1.6 \times 10^{-6} \ \text{MPa}^{-1} \qquad \text{.....(A31)}$$

The applicability of equation (A30) has been supported through observation of the pressure dependence of the equilibrium resistance, $W_{lso}(T_o)$, as measured during experiments to determine the thermal conductivity of N-Nonane at 308.15K and 323.15K. The resistance values of W_{lso} were corrected to the nominal temperatures 304.1K and 319.7K respectively assuming the temperature coefficient to be independent of both temperature and pressure. This caused an insignificant error in the resistances because the correction to the nominal temperature occurred over a maximum of 0.1K. The resistance, $W_{lso}(304.1)$ versus pressure is presented in Table (A6) and $W_{lso}(319.7)$ versus pressure in Table (A7). Column, 3, in Table (A6) gives the values of the resistance $W'_{lso}(319.7)$ as calculated from $W_{lso}(304.1)$ using equation (A30) and column 4 gives the value of $W''_{lso}(319.7)$ as obtained by interpolating the values of $W_{lso}(319.7)$ given in Table (A7).

The values of W_{lso} as given in Tables (A6) and (A7) are thought to be correct to only $\pm$ 0.1K as the bridge (see § 4.41) which was used in its manual mode to obtain W_{lso} was not designed to measure absolute resistances but resistance differences. However, it is seen that the values of $W'_{lso}(319.7)$ as given in colum 3 and $W''_{lso}(319.7)$ in column 4 of Table (A6) agree to within the accuracy of their measurement.

Pressure [MPa]	W_{lso}(304.1) [Ohms]	W'_{lso}(319.7) [Ohms]	W''_{lso}(319.7) [Ohms]
51.6	271.80	286.68	286.81
51.8	271.77	286.65	286.80
52.0	271.75	281.63	286.80
63.5	271.64	286.51	286.66
87.1	271.61	286.47	286.56
92.9	271.55	286.41	286.52
112.5	271.40	286.26	286.39
130.9	271.37	286.23	286.31
156.3	271.25	286.10	286.19
167.5	271.15	285.99	286.16
190.6	271.00	285.84	285.99
211.9	270.90	285.73	285.82
241.0	270.78	285.61	285.68
271.6	270.58	285.39	285.54
309.2	270.39	285.20	285.33
337.0	270.32	285.12	285.16
369.2	269.15	284.95	284.99
403.9	269.92	284.71	284.74
435.3	269.84	284.62	284.64
468.5	269.61	284.38	284.48
500.1	269.49	284.25	284.32

Table (A6) Pressure variation of W_{lso} @ 304.1K and the calculated value at 319.7K.

Pressure [MPa]	W_{lso}(319.7) [Ohms]
35.3	286.86
62.3	286.77
85.4	286.58
89.6	286.55
109.7	286.39
123.0	286.36
139.3	286.25
174.8	286.14
181.0	286.06
213.8	285.81
249.1	285.65
292.4	285.44
331.2	285.19
360.1	285.05
412.5	284.74
452.4	284.56
500.5	284.31

Table (A7) Pressure variation of W_{lso} @ 319.7K

APPENDIX 3

This appendix contains the relevant physical and optical properties of the hydrocarbons whose thermal conductivities were measured, as well as the required physical properties of the materials used in the construction of the measurement cells.

A31 The Physical Properties of the Liquids Investigated

The density versus pressure data for the n-Alkanes investigated in this work were taken from a paper by Doolittle [120]. Tables A8, A9, and A10 contain those data taken from this source that were found relevant to this work and these data were estimated to be accurate in the reported densities to within ± 0.2%.

N-Heptane				
Pressure	Density			
[MPa]	@303.15K [kg/m^3]	@323.15K [kg/m^3]	@373.15K [kg/m^3]	@423.15K [kg/m^3]
0	675.31	658.29	612.56	558.75
5	680.32	664.23	621.47	573.82
10	684.93	669.48	629.68	585.75
20	693.34	678.98	642.63	605.66
30	700.97	687.38	653.60	619.81
50	714.24	701.95	671.73	642.10
100	740.63	730.19	705.02	680.87
150	761.21	751.93	729.55	708.67
200	778.33	769.94	749.34	730.89
300	806.26	798.40	780.70	764.29
500	847.96	841.26	825.76	812.68

Table A8 Density versus Pressure data for n-Heptane

Pressure	Density			
[MPa]	@303.15K [kg/m^3]	@323.15K [kg/m^3]	@373.15K [kg/m^3]	@423.15K [kg/m^3]
0	709.93	694.40	653.60	609.35
5	714.18	699.11	660.63	620.19
10	718.34	703.73	666.53	629.37
20	725.90	712.20	677.87	643.29
30	732.82	719.84	687.66	655.91
50	744.99	733.08	704.08	676.13
100	769.53	759.24	734.81	712.05
150	788.83	779.55	757.86	738.03
200	805.02	796.43	776.58	758.63
300	831.60	823.66	806.52	791.39
500	871.46	865.20	850.41	837.82

Table A9 Density versus Pressure data for n-Nonane

Pressure	Density			
[MPa]	@303.15K [kg/m^3]	@323.15K [kg/m^3]	@373.15K [kg/m^3]	@423.15K [kg/m^3]
0	732.82	717.98	680.00	639.63
5	736.81	722.39	686.06	648.59
10	740.58	726.64	691.23	656.34
20	747.61	734.38	701.51	668.67
30	753.98	741.40	710.43	680.18
50	765.40	753.75	725.58	698.91
100	788.58	778.39	754.60	732.76
150	807.10	797.77	776.58	757.75
200	822.64	813.94	794.53	777.06
300	848.25	840.27	823.45	809.85
500	886.84	880.98	866.55	855.51

Table A10 Density versus Pressure data for n-Undecane

The specific heat capacities of the investigated n-Alkanes are not known to great accuracy and have been taken as being independent of pressure and temperature. The values of the specific heat capacities of n-Heptane, n-Nonane, and n-Undecane used in this work are those obtained at 30°C and at atmospheric pressure [129] which are approximately 2.23, 2.20 and 2.21 kJ/kg/K respectively.

A32 The Physical, Electrical, and Mechanical Properties of Platinum

Table A11 contains the physical, electrical and mechanical properties of the 7 μm platinum wire which was used as a heat source in the transient hot wire measurement cell.

λ	=	67.05 W/m/K
ρ	=	2137 kg/m^3
C_p	=	131.3 J/kg/K
ν	=	Poissons ratio $\approx$ 0.35
ϵ_{2s}	=	$\frac{1}{w}\frac{\partial w}{\partial S}$ = 2.77 x 10^{-7} MPa^{-1}
ϵ_p	=	$\frac{1}{w}\frac{\partial w}{\partial P}$ = 1.6 x 10^{-6} MPa^{-1}
S_y	=	yield stress $\approx$ 150 MPa^{-1}

Table A11 Physical Electrical and Mechanical Properties of Platinum.

A33 Optical Properties

The mean extinction coefficient as used in the analysis presented in chapter 3 is defined as:-

$$K = -\frac{1}{L} \text{Ln} \frac{\int_0^\infty \left(\frac{I_\omega}{I_\omega^\circ}\right) E_\omega d\omega}{\int_0^\infty E_\omega d\omega} \quad ** \qquad \text{.....(A32)}$$

**The symbol, ω, has been used to define wave length so as to avoid confusion with the thermal conductivity, λ.

where in equation (A32) I_ω^o is the intensity of the radiant energy of wave length ω at position l=0 and I_ω is the intensity at l=L. This is distinct from the Planck mean extinction coefficient, K_p, as defined by:-

$$K_p = \frac{\int_0^\infty K_\omega E_\omega d\omega}{\int_0^\infty E_\omega d\omega} \qquad \text{.....(A33)}$$

where:-

$$K_\omega = -\frac{1}{L} \text{Ln}\left(\frac{I_\omega}{I_\omega^o}\right) \qquad \text{.....(A34)}$$

although it is expected that when performing measurements on liquids, these two extinction coefficients will have similar values. The reason for using equation (A32) as the definition of the mean extinction coefficient is to maintain consistency with the way in which the coefficient is used in chapter 3.

The values of the mean extinction coefficients and refractive indices for n-Heptane, n-Nonane and n-Undecane are given in Table A12.

n-Alkane	Extinction Coefficient @ 300K $[m^{-1}]$	Refractive Index @ 393.15K
n-Heptane	1070	1.385
n-Nonane	1120	1.405
n-Undecane	1150	1.418

Table A12 Optical properties of n-Heptane, n-Nonane, and n-Undecane.

Finally for the present work the emissivity of platinum ϵ_{pt} is taken to be equal to its absorbtivity, α_{pt}, and is assumed to be constant such that:-

$$\epsilon = \epsilon_{pt} = \alpha_{pt} = 0.037 \qquad \text{.....(A35)}$$

S Y M B O L S

a	Wire radius
a_i	Mechanical quadrature abscissa
A_a	Surface area of the wire
A_b	Surface area of the cell
b	Cell radius
C	Exponent of Euler's Constant
C_p	Specific heat capacity at constant pressure
E	Emissive power
E_i	Exponential integral
Eu	Eucken Factor
E	Accuracy of a measurement
F_{AB}	View Factor
g	Gravitational Constant
g_1	An impirical factor proportional to the mean free path of a molecule
g_υ	υ^{th} zero of the zeroth order Bessel function of the first kind
H_j	Mechanical Quadrature weighting coefficient
I	Radiant Intensity
J_o	Zeroth order Bessel function of the first kind
J_1	First order Bessel function of the first kind
k	Thermal diffusivity
K	Extinction Coefficient
L	A characteristic length
L_i	Lagrange Polynomial
M	Molecular weight
n	Refractive index
P	Pressure
P_m	m^{th} degree polynomial
$\{P_r\}$	Prandtl Number
q	Heat flux per unit length of emitter
Q	Heat flux
$\tilde{Q}_{V\rightarrow dV_i}$	Linearised radiative heat flux gradient
$\tilde{Q}_{V\rightarrow dA_i}$	Linearised radiative heat flux

r	Radius
R	Reduced radius
$\tilde{R}$	Fraction of incident radiation that is reflected
s	Spatial coordinate
S	Tensile stress
t	Time
T	Absolute temperature
V_r	Velocity in the radial direction
V_z	Velocity in the vertical direction
V	Voltage
V	Volume
W	Resistance
Y	Young's modulus of elasticity
Y_o	Zeroth order Bessel function of the second kind
Y_1	First order Bessel function of the second kind
z	Vertical direction
Z	Shifted vertical coordinate

GREEK SYMBOLS

α	Absorbtivity
α'	Pseudo linear temperature coefficient of resistance
β	$\frac{T}{\rho}\left(\frac{\partial \rho}{\partial T}\right)_p$
γ	Euler's Constant
δT	Temperature correction
ΔT	Temperature rise
ϵ	Emissivity
η	Kinematic viscosity
Θ	Normalised, reduced temperature
λ	Thermal Conductivity
λ_r	Radiation contribution to the apparent thermal conductivity
Λ	Mean free path of a molecule
μ	Viscosity
ν	Poissons ratio
Θ	Reduced temperature

ξ	Radiation defect
π	3.141592654....
ρ	Density
σ	Stefan Boltzman Constant
$\bar{\sigma}$	Mean resistance per unit length
τ	Fraction of electromagnetic radiation that is transmitted
ω	Wave length

S U B S C R I P T S

app	Apparent thermal conductivity
cc	Composite cylinders correction
FP	Correction due to variable fluid proportions
i	Conditions at point P_i in volume element dV_i
id	Ideal conditions
j	Conditions at point P_j in volume element dV_j
l	Long wire
ls	Difference between the long and short wires
mm	Mathematical model
n	Nominal value
NS	Numerical solution
o	Equilibrium conditions
OB	Outer boundary correction
P	Pressure
Pr	Precision
r	In the radial direction
r	Reference conditions
R	Due to radiation heat transfer
s	Short wire
Visc	Correction due to viscous dissipation
w	Wire conditions
z	In the vertical direction
1	Condition at the surface of the emitter
2	Condition at the surface of the cell walls

S U P E R S C R I P T S

o	Zero density
(o)	Zeroth itteration
(1)	First itteration
(2)	Second itteration

REFERENCES

1 Murray, J., Nicholson, W., Proc.Roy.Soc.(LON), 1 , (1800), 105.
2 Nicholson, W., Nicholson, J., Proc. Roy.Soc.(LON), 5 , (1802), 197.
3 Rumford, B., Nicholson, J., Proc.Roy.Soc.(LON), 14 , (1806), 353.
4 Thomson, T., Nicholson, J., Proc.Roy.Soc.(LON), 223 , (1923), 284.
5 Biot, J.B., Bibliotheque Brittanique, 27 , (1904), 310.
6 Depretz, M., Pogg.Ann., 46 , (1839), 340.
7 Paalzov, A., Pogg.Ann., 134 , (1868), 678.
8 Guthrie, R., Phil.Mag., 37 , (1869), 468.
9 Beetz, C., Wied.Ann.,7 , (1879), 435.
10 Berget, A., Compt.Rend., 105 , (1887), 224.
11 Christiansen, C., Wien.Ann., 14 , (1881), 23.
12 Hennerberg, H., Ann. Physik, 146 , (1889).
13 Jager, G., Wien.Ber., 99 , (1890), 245.
14 Jakob, M., Ann. Phys., 63 , (1920), 537.
15 Bates, K.O., Ind.Eng.Chem., 25 , (1933), 431.
16 Bates, K.O., Ind.Eng.Chem., 28 , (1936), 494.
17 Sakiadis, B.C., Coates, J., Engineering Experimental Station,Loisiana State Univ.Bulletin, 34(1952),35(1953),45(1954),48(1954).
18 Sakiadis, B.C., Coates, J., A.I. Chem.E. Journal, 1 , (1955), 275.
19 Michels, A., Botzen, A., Physica, 18 , (1952), 605.
20 Michels, A., Sengers, J.V., Van der Gulik, P.S., Physica, 28,(1962),1201.
21 Fritz, W., Poltz, H., Int.J.Ht.Mass Trans., 5 , (1962), 307.
22 Bridgman, P.W., Poc.Am.Acad.Arts and Sci., 59, (1923), 141.
23 Riedel, L., Chemie Ingenieur Technik, 13 , (1951), 321.
24 Schmidt, E., Sellschop, W., Forschg. Gebeite Ingenieurw., 3 ,(1932),277.
25 Sellschop, W., Forschg. Gebiete Ingenieurw., 5 , (1934), 162.
26 Kraussold, H., Forschg. Gebiete Ingenieurw., 58 , (1934), 186.
27 Schmidt, R.J., Milverton, S.W., Proc.Roy.Soc.(LON), A152 ,(1935),586.
28 Ziebland, H., Burton, J.T.A., Brit.J.Appl.Phys., 6 ,(1955), 416.
29 Ziebland, H., Burton, J.T.A., Brit.J.Appl.Phys., 9 ,(1958), 52.
30 Ziebland, H., Burton, J.T.A., Int.J.Ht.Mass Trans., 1 , (1960), 242.
31 Ziebland, H., Needham, D.P., Int.J.Ht.Mass Trans., 8 ,(1965), 1387.
32 Schleirmache, H., Wied.Ann., 34 , (1888), 623.
33 Taylor, W.J., Johnston, H.L., J.Chem.Phys., 14(4) , (1946), 219.
34 Goldschmidt, R., Physik.Z., 12 , (1911), 417.
35 Blackwell, J.H., Can.J.Phys.,34 , (1956), 412.
36 Riedel, L., Chemie Ing. Technik, 23 , (1951), 321.
37 Schrok, V.E., Starkman, E.S., Rev.Sci.Inst., 29(7), (1958), 625.
38 Richter, G.N., Sage, B.H., Ind.Eng.Chem.Chem.Eng.Data Series 2(1) (1957),61.
39 Leidenfrost, W., Paper presented at Thermal Cond. Conf. Gatlingburg, Tennesee, (1963).
40 Kestin, J., Ro, S.T., Wakeham, W.A., J.Chem.Phys., 56 ,(1972),4036.
41 Assael,M., Ph.D. Thesis, Imp.Col. Univ. of London,(1980), 19.
42 Ibid page 11.
43 Carslaw, H.S., Jaeger, J.C., Conduction of heat in solids, 2nd Edition, Oxford Univ. Press (1959), 261.
44 Stalhane, B., Pyk, S., Tecknish Tidskrift, 61 , (1931), 389.

45 Pfriem, H., V.D.I.Z., 82 , (1938), 71.
46 Weishaupt, J., Forschung Gebiete Ingenieurw., 11 , (1940), 20.
47 Van der Held, E.F.M., Van Drunen, F.G., Physica, 15 , (1949), 865.
48 Van der Held, E.F.M., Hardebal, J., Kalshaven, J., Physica, 19 , (1953), 208.
49 Gillam, D.G., Romben, L., Nissen, H.E., Lamm, O., Acta Chemica Scandinavica, 9 , (1955), 641.
50 Hill, R.A.W., Proc.Roy.Soc.(LON),A239 , (1957), 476.
51 Turnbull, A.G., Australian J. Appl. Sci., 12 , (1961), 30.
52 Horrocks, J.K., McLaughlin, E., Proc.Roy.Soc., A273, (1963), 259.
53 Pittman, J.F.T., Thesis submitted to Chem.Eng. Dept. Imperial College, Univ. of London, (1968).
54 Kandiyoti, R., Ph.D. Thesis submitted to Chem.Eng.Dept. Imperial College, Univ. of London (1969).
55 Haarman, J.W., Thesis Technische Hayeschool Delft Netherlands, (1969).
56 De Groot, J.J., Kestin, J., Sookiazian, H., Physica, 75,(1974), 454.
57 Healy, J.J., De Groot, J.J., Kestin, J., Physica, 82C , (1976), 392.
58 Kestin, J., Wakeham, W.A., Physica, 92A , (1978), 102.
59 Castro, C.A.N., Wakeham, W.A., Proc. 1st Nat. Con. Pure & Applied Mathematics(LISBON) (1974).
60 Danilov, G., Refrigeration Technology (Russian), 22 , (1951).
61 Petruchov, B., Ragulin, N., Refrigeration Technology, 22 , (1951).
62 Golubev, I.F., Teplocnergetika, 10(12), (1963), 78.
63 Carslaw, H.S., Jäeger, J.C., Conduction of heat in solids 2nd Edition, Oxford Univ. Press London (1959), 338.
64 Smoluckowski, M., Ann.Phys.Chem., 35 , (1911), 983.
65 Smoluckowski, M., Phil.Mag., 21 , (1911), 11.
66 Goldstein, R.T., Briggs, D.G., J.Ht.Transfer ASME, C86 ,(1964), 490.
67 Fischer, J., Ann.Phys., 34 , (1939), 669.
68 Haarman, J.H., Physica, 52 , (1971), 605.
69 Blackwell, J.H., Can.J.Phys., 34 , (1917), 437.
70 Leidenfrost, W., Paper to Thermal Cond. Conf. Gatlingburg, Tennesee, (1963).
71 Poltz, H., Int.J.Ht.Mass.Trans., 8 , (1965), 515.
72 Ibid page 609.
73 Poltz, H., Jugel, R., Int.J.Ht.Mass Trans., 10 ,(1967), 1075.
74 Diessler, R.G., J.Ht.Trans. Trans. ASME, 86 , (1960), 240.
75 Grief, R., Clapper, G.P., Appl.Sci.Res., (15)A.
76 Rosseland, S., Astrophysik und Atom-Theoretisches Grundlage, Springer Verlag Berlin, 41 , (1931).
77 Saito, A., Mani, N., Venart, J.E.S., Poner no. 76-CSME/CSChE-6, 16th National Heat Transfer Conference, St. Louis, MO. (1976).
78 Hottel, H.C., Sarofim, A.F., Radiative Transfer, (McGraw Hill) (1967), 256.
79 Lowan,Davids,Levenson, Bull.Amer.Math.Soc., 48 , (1942), 739.
80 Liskovets, O.A., The Method of Lines (Eng. Translation) J. Diff.Eqs., 1 , (1965), 1308.
81 Gear, C.W., Comm. of the ACM, 14(3), (March 1971), 176.
82 Hindmarsh Lawrence Liverpore Laboratory report, UCID-30001 Rev.2 (1972).
83 Curtis, A.B., Reid, J.K., AERE-R-6844, Harwell, (1971).
84 Menashe, J., Progress Report, Imperial College, August 1978.
85 Castro, C.A.N., Ph.D. Thesis submitted to the University of Lisbon,(1977)
86 International Practical Temperature Scale of 1968 (NPL)(HMSO Lond,1968)

87 International Practical Temperature Scale of 1976 (NPL) Revised ed. (HMSO Lond.1976).
88 Property of Fluids Internal Report No. 144,(NEL East Kilbride 1976).
89 Property of Fluids Internal Report No. 145,(NEL East Kilbride 1976).
90 Olsen, F.C.W., Schultz, O.T., Ind.Eng.Chem. 34 , (1942), 874.
91 Assael, M., Dix, M., Lucas, A.,Wakeham, W.A., Faraday Soc. (1980)
92 International Critical Tables, Washbone, E.W., Ed.,(McGraw Hill) VI , (1929), 136.
93 Harlow, A., Ph.D. Thesis, submitted to Imperial College, Univ. of London, (1967).
94 National Physical Laboratory Report, TPC.S.I./SST.56, (1976).
95 Menashe, J., Wakeham, W.A., Ber.Bunsenges.Physik.Chem. (To be published 1981).
96 Wurflinger, A., Schneider, G.M., Ber Bunsenges.Physik.Chem., 77 , (1973), 121.
97 Powell, R.W., Groot, H., Int.J.Ht.Mass Trans.,15 , (1972), 360.
98 Naziev, Ya.M., Nurberdyev, A.A., Abasov, A.A., Chem.Techn., 23(12) (1971), 738.
99 Mukhamedzyanov, I.Kh., Mukhamedzyanov, G.Kh., Usmanov, A.G., (Russian) Trudy Kazan Khim.Tekhnol.In-ta, 47 , (1971), 22.
100 Brykov, V.P., Mukhamedzyanov, G.Kh., Usmanov, A.G., (Russian) Inzh-fiz.Zh., 18(1), (1970), 82.
101 Kerimov, A.M., El'darov, F.G., El'darov, V.S., (Russian) Izv.vyssh. ucheb.Zaved., Neft' i Gaz, 13(1), (1970), 77.
102 Pittman, J.F.T., Ph.D. Thesis submitted to Imperial College, Univ. of London, (1968).
103 Ganiev, Yu.A., Teplo.Svoistva Zhidk;Mater.Vses.Teplofiz.Konf.Svoistva. Veshch.Vys.Temp., 3rd, (1968), 95.
104 Rastorguev, Yu.L., Bogatov, G.F., Grigor'ev, B.A., Izv.vyssh.ucheb. Zaved.,Neft'i Gaz., 11(12), (1968), 59.
105 Mallan, G.M., Ph.D. Thesis submitted to University of South California, Los Angeles, U.S.A., (1968).
106 Abas-Zade, A.K., Guseinov, K.D., Ukr.fiz.Zh., 12(1), (1967), 34.
107 Jobst, W., Ph.D. Thesis submitted to Techn.Hoch.Zurich, (1964).
108 Akhmedov, A.G., Azerb.neft.Khoz., 42(4), (1963), 41.
109 Mukhamedzyanov, G.Kh., Usmanov, A.G., Tarzimanov, A.A., (Russian) Izv.vyssh.ucheb.Zaved.Neft'i Gaz, 6(9), (1963), 75.
110 Golubev, I.F., Naziev, Ya.M., Trudy Energ.Inst.AN.Azerb.SSR, 15 (1962), 84.
111 Vilim, O., Collection Czech.Chem.Commun., 25 , (1960), 993.
112 Mustafaev, R.A., (Russian) Izv.vyssh,ucheb.Zaved.,Neft'i Gaz, 15(5), (1972), 36 & 64.
113 Castro, C.A.N., University of Lisbon, Private Communication,(1980).
114 McLaughlin, E., Chem.Rev., 64 , (1964), 389.
115 Ziebland, H., International Union of Pure and Applied Chemistry, Sub-Commission I 4.1, (1977).
116 Saito, A., Venart, J.E.S., Paper submitted to the 6th Int.Heat Trans. Conference, Toronto, (1978).
117 Wakeham, W.A., Imperial College, London, Private Communication, (1980).
118 Zwanzig, R.W., Kirkwood, J.G., Oppenheim, I., Alder, B.J., J.Chem.Phys., 22 , (1954), 783.
119 Kamal, I., McLaughlin, E., Trans.Faraday Soc., 60 , (1964), 809.
120 Doolittle, Q.K., Journal of Chemical Engineering data, 9, No.2, (April 1964), 275.

121 Palmer, G., Industrial & Engineering Chemistry, 48 No.1, (1948), 89.
122 Jamieson, D.T., Irving, J.B., Tudhope, J.S., Liquid Thermal Conductivity data survey to 1973 (Edinburgh,HMSO 1973).
123 Castro, C.A.N., Caldo, J.C.G., Wakeham, W.A., Dise, M., J. Phys.E., 9 , (1976), 1073.
124 Castro, C.A.N., Caldo, J.C.G., Wakeham, W.A., Proceedings of the Seventh Symposium on Thermophysical Properties ASME, (1977), 730.